Natural and perturbed dynamics about Trojan bodies

PhD candidate:

Marta Ceccaroni

Advanced Space Concepts Laboratory
Department of Mechanical and Aerospace Engineering
University of Strathclyde

A.Y. 2012-2013

This thesis is the result of the authors original research. It has been composed by the author and has not been previously submitted for examination which has led to the award of a degree.

The author: 

Date: 27th November 2012

Abstract

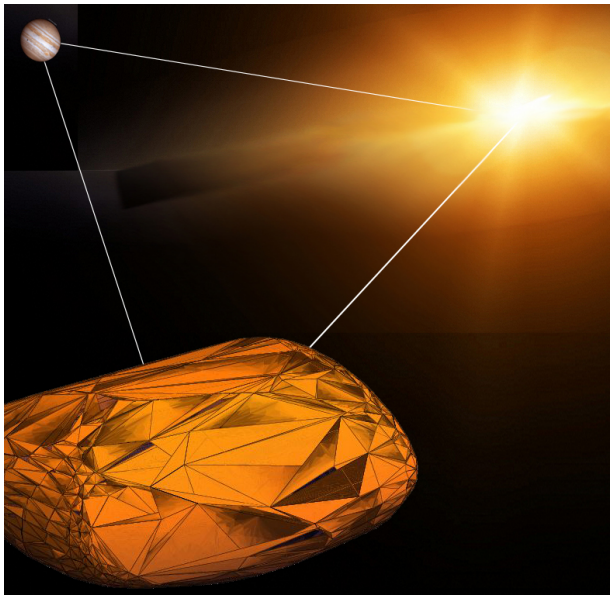

This thesis analyses the dynamics of a massless spacecraft (or point mass) around an inhomogeneous Trojan body in a system composed of three primaries lying on a plane at the vertexes of an equilateral triangle, with their mutual positions fixed over the course of the motion. This configuration will here be referred to as "Lagrangian" or "equilateral triangle", implicitly meaning that the three primaries lie on a common plane. To this end two suitable models are identified to represent the system, depending on the distance from the primary. The first model, adopted for use close to the asteroid, where the dynamics is dominated by this sole body, is the Restricted Two Body Problem. In this model the inhomogeneities of the asteroid are taken into account as they have a dominant effect on the dynamics of the spacecraft. This model will therefore be referred to as the Inhomogeneous R2BP. The second model is the Lagrangian Circular Restricted Four Body Problem (CR4BP), with the primaries lying on the same plane, which is adopted far from the asteroid[1], where the gravitational perturbations of the

[1]Note that by "far from the asteroid" is meant that the point mass is at a significant distance from the body such that the gravitational influence of the Sun and Jupiter is far greater than the influence of the inhomogeneities in the gravitational field of the body, but still close enough to the body for scientific and observational purposes.

Sun and Jupiter are dominant while the inhomogeneities of the asteroid are negligible. Low-thrust propulsion perturbations are incorporated into this model. The possibility to determine the range of validity of each model using an application of a Weak Stability Boundary (WSB) theory, a relatively novel approach to dynamics for designing low-energy transfers, is investigated and applied.

A completely new, analytical definition of the Weak Stability Boundary, coherent with the previous algorithmic definitions, is thus developed in this work for the first time. The existing (algorithmic) WSB theory, previously always treated numerically and mainly applied to Circular Restricted Three Body Problems (CR3BP), is here rebuilt from an analytical point of view and extended to the Lagrangian CR4BP. Moreover some topological properties of the WSB are introduced and applied, leading to analytical estimations of the set of stable orbits around the small primary. An estimation of the range of validity of the models is thus derived, which is based on the region of stable orbits.

The dynamics in a Restricted Two Body Problem incorporating the shape/density inhomogeneities of the body, is analysed, suitable for modelling the spacecraft dynamics inside the estimated reference region. The irregular gravitational potential is formulated using spherical harmonics, the coefficients describing the physical properties of the body. An analytical, arbitrary degree, perturbation theory[2], assuming the spherical harmonics of the body as known, is derived. This result generalizes to arbitrary degree the previous closed form (i.e. valid for every eccentricity) perturbation theories which are usually limited to second degree (namely to the inclusion of two spherical harmonics coefficients).
The theory here developed, double averaging the system by means of two canonic Lie transformations, leads to an integrable, arbitrarily accurate approximation of the system whose explicit second order Hamiltonian formulation, derived in closed form, is thus stated. From this theory an analytic method for determining initial conditions for frozen orbits around any irregular body is derived for the first time. Such Frozen orbits are orbits with no secular perturbations in the inclination, argument of pericentre, and eccentricity.
Results are shown for a major Jupiter Trojan: 624-Hektor. As the spherical harmonics of this Trojan are unknown and not present in any previous literature, a method is here applied, which deduces these coefficients from a three dimensional polyhedric model of the body, assuming a constant density.

[2]It must be noted that this theory is general, namely valid to study the dynamics in every Two Body Problem with an inhomogeneous gravitational field (i.e. it is not restricted to systems in the Lagrangian configuration)

Finally the dynamics of the Lagrangian CR4PB is studied, for modelling the system outside the estimated reference boundary. The natural equilibria and Lyapunov stability of the linearized system are analysed. A study of the changes in the topology of the linearly stable zone for different conceivable masses of the Trojan is shown in this work for the first time. Low-thrust propulsion perturbations, in all previous literature confined to two and three body problems, are here incorporated into the four bodies system examined, enabling the generation of surfaces of artificial equilibria. Applications are shown for the main example of Lagrangian configuration in the Solar system, the Sun-Jupiter-Trojan-spacecraft system. Numerical simulations for 624-Hektor confirm the validity of the model once its real tadpole orbit around the triangular point is taken into account.

Acknowledgments

This thesis collects the outputs of a three year PhD course at the Advanced Space Concepts Laboratory of the University of Strathclyde, Glasgow. My research project has been funded by the Glasgow Research Partnership in Engineering (GPRe). Moreover the European Space Agency (ESA) funded my position as a research associate at the University of Strathclyde for the work on "Analytical Perturbative Theories of Motion in Highly Inhomogeneous Gravitational field" which forms a major part of this thesis.

A serious (and huge) thanks goes to my supervisor, prof. James Biggs, for the patience, the comprehension, the guidance, the encouraging... but mainly for all the times he had to tidy up my brain (and there have been many)...
it was a pleasure to work with you, James.

***

To that moment that unleashed the geek in me, when it all started, a long long time ago....
To Colle, in summer and in winter
To the synergic vegetable garden, for the thousand things it represents for me
To Skype, oh yes Skype...
Well, to the Mc Donald's and Lord Todd free wireless, sorry for stealing your electricity
To the "moment of panic" technique on the ryanair flights and never ending stories about flights I have collected
To duck and the low flow of my shower: in the end it was fun
To "Maths? Certainly not from me!", the spoken and the unspoken ones
To the Saturday bread bakery and the sense of power and satisfaction it gives
To the electrical mokas, both the "fired" and the "unstolen", for bringing people together like only the coffee breaks can do
To the befy, while waiting her to be back
To the chicchirichis and snmps
To each of the 25 little presents in the advent calendars
Somehow to you, despite all

To my tender wad of hair I miss every day and always will...

...

To "sorry daaaaaarling I need to swear", for cheering me up a priori

To "Checco, give daddy his demonstration back"...that was fun too

To Hektor (Ettore), the only Trojan lost in the Greek camp...

To the Weegies, the native and the adoptive ones, for teaching me what kind ("KEIND") really means

And to Scotland, a place that I call home

To the Hairy Cooo

(I might sound selfish but) to the fire in the James Weir and whatever started it: my life would have been much different without you...

Contents

Chapter 1

Introduction

1.1 Research Background and Motivations

In 1772 the French mathematician and astronomer Joseph-Louis Lagrange [1] predicted that a small body could be trapped in the orbit of a larger one around the Sun, if the three masses were located at the vertexes of an equilateral triangle and their mutual positions being maintained over the course of the motion. Those positions, now bearing the symbols L_4 and L_5, are two of five so-called Lagrange points (the others were defined earlier by Euler). Although Lagrange thought his equilateral triangle solutions were of no great practical significance it was later realised that the Sun, Jupiter and a group of asteroids, now called Trojans, formed such a configuration. It was not until 1906 that the first object trapped at either of such points was found: the asteroid 588-Achilles at the L_4 point in the Sun-Jupiter system. Since then many more asteroids were found both at the Sun-Jupiter L_4 and L_5, each named, by convention, after a hero of the Trojan War from Greek mythology, hence the origin of the term 'Trojan asteroids'[1]. Other Trojans since then have been discovered, which share the orbits of Mars and Neptune around the Sun. Moreover two of Saturn's moons, Tethys and Dione, have Trojan moons. In 2011 a team from Athabasca University, Canada [2] announced the discovery of the first known Earth's Trojan, somewhat less romantically named 2010 TK7. However, since the Earth Trojans are so hard to spot, it's likely that there are a lot more of them. As such asteroids provide the perfect base for interplanetary missions beyond the Earth-Moon system [3], their discovery renewed and highlighted again the importance of dynamical studies on the Lagrange configuration of the Restricted Four Body Problem, still largely unexplored.

The Trojan asteroids of Jupiter, in particular, lie at the crux of several of the most

[1] Heroes of the Greek camp are clustered at L_4 (Agamemnon, Odysseus, Ajax, Menelaus) and those of Troy at L_5 (Priamus, Troilus, and so on); only two early discoveries, the Greek Patroclus and the Trojan Hektor, were, in fact, assigned to the wrong camps.

interesting issues regarding the formation and evolution of the Solar System. Jupiters companion asteroids, indeed, hold the potential to unlock the answers to fundamental questions about planetary migration, the late heavy bombardment, the formation of the jovian system, the origin and evolution of transneptunian objects (TNOs) and many more. Despite a population comparable in number to the main asteroid belt, they remain poorly understood [4]. What we know about these asteroids is based on observations of these objects as point sources, by spectrometric analysis or by analogy with objects believed to be similar. Spacecraft investigation of this Trojan population has been recognized as a 'New Frontiers goal' already in the Decadal Survey in 2002 [5] and, most importantly, the technical feasibility for any of these mission architectures is well within our capabilities at the present time. Dedicated missions will revolutionize our current understanding of these bodies, by a comprehension of the solar system as a whole. Getting in orbit around any of these bodies could already provide valuable initial reconnaissance, including a view of surface composition, geology, and density, which, refined at each revolution, would finally provide an arbitrarily accurate global picture of the properties of such asteroid, which are necessary to any study aiming to unlock the answers to fundamental questions about the early stages of the solar system. To this end orbits with good stability properties would be needed. Among these frozen orbits might represent a major candidate as, being periodic except for the precession of the argument of nodes, they can be seen as a first generalization of periodic orbits and might therefore be suitable for such physical characterization and detection missions.

To get information on the density of the body, for example, it is possible to compare the actual dynamics due to the experienced gravitational field with the one predicted using a model built assuming a constant density, like for example measuring the divergence from the predicted a frozen orbit. To this end an accurate description of the dynamics of a point mass in an inhomogeneous gravity field is necessary. The main difficulty here lies in the fact that typically such bodies feature shapes and density distributions more irregular than those of planets. Such irregularities break symmetries and require more complicated analytical expressions for their description, increasing noticeably the mathematical difficulties involved in such studies. These obstacles are maximized in the case of bodies such as asteroids and comets, where shapes and density distributions are highly irregular and often unknown. Furthermore asteroids are at the centre of a number of recent advanced mission concepts. Asteroid deflection missions have been studied by ESA and are being discussed for some time now in the scientific community. Further asteroid sample return missions are being considered and human missions to asteroids have entered the agenda of space agencies.

Due to the relevance of the scientific equipment needed onboard, such future inter-

planetary missions will aim to maximize the payload by lowering the propellant mass fraction within reasonable transfer times. A sensitive reduction could be achieved by either exploiting the chaotic dynamics arising in an n-body context or by including low thrust propulsion technologies into the system [6]. Over the last 20 years an attempt has been made to take advantage of the gravitational fields through the Weak Stability Boundaries, a method for designing fuel efficient space missions, which reduces the use of propellent with a direct impact on the onboard payload [7]. The WSB is a complicated zone of the phase space where ballistic (i.e. natural) capture occurs. Although it has been extensively studied since the 90's its nature and associated sensitive dynamics has not been well understood yet, and a full, analytical and topological understanding of this set and its properties is still missing.

Primary electric low thrust propulsion, instead, is a widely accepted method for station-keeping and final orbit insertion of commercial satellites. NASA, JAXA, and ESA have already used this type of propulsion for several science missions. Low thrust propulsion enables a range of new, potential applications for several scientific fields like space physics, human exploration, asteroid observation, material retrieval and many more, by seeking families of novel, exploitable, non-Keplerian orbits.The concept of counter-acting gravity through a thrust vector was apparently first proposed by Dusek in 1966 [95], who noted that a spacecraft could be held in an artificial equilibrium at some distance from a natural libration point if the difference in gravitation and centripetal force (gravity gradient) were compensated for by continuous low thrust propulsion [96]. The use of continuous thrust can be applied in all directions including perpendicular to the flight direction, which forces the spacecraft out of a natural orbit into a displaced, non-Keplerian orbit: such kind of orbits have a wide range of potential applications. The setting, thus far, for such analysis has been confined to include low-thrust propulsion systems in the two and three body problems but is extended here to a four body problem.

1.2 Research Objectives and Aims

The overall objective of this research project is to use mathematical tools such as stability analysis for dynamical systems, non linear and high order analysis, normal forms, Lie series, chaos theory and exploit the Weak Stability Boundaries, to seek interesting families of orbits close to the smaller primary of a Sun-Planet-Trojan like system. The investigation thus aims to find natural orbits (e.g. frozen orbits) close to the body and new families of artificial, non-Keplerian orbits (e.g. generated by the use of constant low thrust) to be exploited for many possible science applications. Results are shown for the Sun-Jupiter-Trojan-spacecraft system, with particular emphasis on the asteroid

624-Hektor, a major Jupiter Trojan.

***

• The range of validity of the two models

As the system is modelled in two different ways, depending on the distance from the primary, the range of validity of each model is investigated. The estimation is carried out by exploiting some topological properties of the set of the stable orbits around the smaller body whose boundary is, by definition, the so called WSB. To study such properties an analytical definition of the WSB is needed, therefore, in this work, a completely new analytic WSB theory, coherent with the previous algorithmic ones, is introduced and developed for the first time.

This part of the thesis is therefore focused on:

◇ providing an exhaustive background on the Weak Stability Boundary theories, including the evolution and generalizations of the concept and the analysis of its deficiencies.

◇ formulating a new, analytic definition of the WSB, compatible with the previous algorithmic and numerical definitions, but such that it enables topological properties of the WSB to be deduced.

◇ investigating the possibility of using this new WSB theory to determine the range of validity of the two models used to represent the system.

◇ deriving an estimation of the range of applicability of the two models for the Sun-Jupiter-Hektor-spacecraft system.

***

• Inhomogeneous restricted two body model

Within the identified reference region, the research analyses the dynamics of a Restricted Two Body model (Fig. 1.1) which incorporates the shape/density inhomogeneities of the body. Generalising previous results, which only included two spherical harmonics (the coefficients describing the inhomogeneities of the body), an arbitrary degree spherical harmonics representation for the inhomogeneous potential is here used.

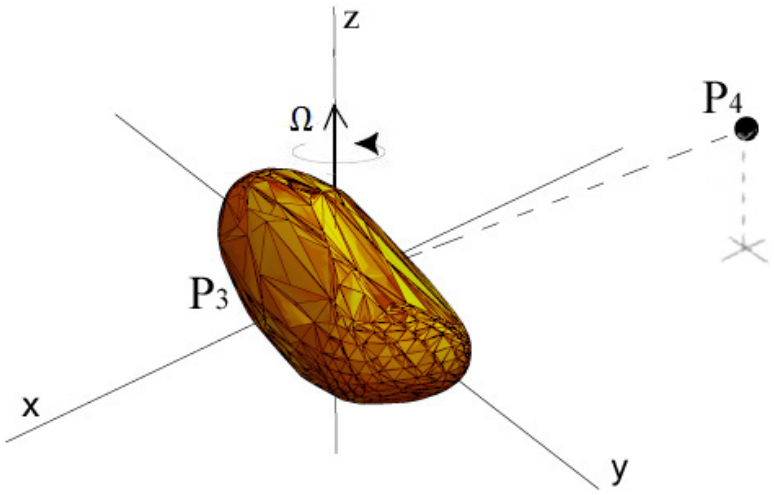

Figure 1.1: The inhomogeneous restricted two body model (adopted inside the estimated region)

Following the usual Lie series approach, a completely analytical, perturbative method is, n this work, developed completely in closed form and based on an arbitrarily accurate model of the massive body, thus describing the dynamics around the body in an arbitrarily accurate way.
This section is focussed on:

◇ defining the state of art of orbital dynamics in inhomogeneous gravitational fields, including an explanation of the usual techniques used to handle the problems.

◇ building an analytical perturbative theory of motion for inhomogeneous gravitational fields which generalizes previous results to arbitrary degree (in the spherical harmonics) and second order, by means of Lie transformations.

◇ constructing a novel, general method to find interesting families of orbits around inhomogeneous bodies.

◇ applying the methodology developed to the Trojan 624-Hektor, suitable for possible future science and observational mission applications.

***

• **Lagrangian (low-thrust) circular restricted four-body model**
Outwith the identified reference region, where the gravitational influence of the Sun

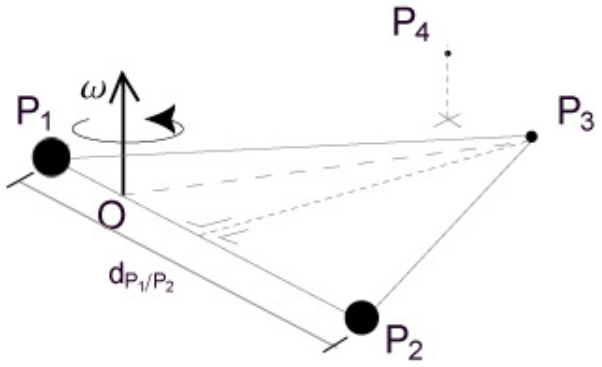

Figure 1.2: The Lagrangian circular restricted four-body model (adopted outside the estimated region)

and Jupiter are dominant perturbations, the Lagrangian Circular Restricted Four Body model is applied (see Fig. 1.2). In this setting low-thrust propulsion technologies, in previous literature only appearing in two and three body models, are incorporated, to study the dynamics of the model both in its natural and artificial (i.e. low thrust perturbed) state.
This part of the work focusses on:

◇ providing a general picture of the studies on the Lagrangian CR4BP, also including recent results and advances of low thrust propulsion systems in two and three body problems.

◇ identifying and applying mathematical techniques, classically used in low thrust two and three body problems, that have the potential to be applied to the Lagrangian low thrust four body problem.

◇ applying the methodology found to the Sun-Jupiter-Trojan-spacecraft system to seek surfaces of artificial equilibrium points and new non-Keplerian orbits for useful for many applications.

◇ testing the robustness of this novel results for the real Sun-Jupiter-Hektor-spacecraft system (i.e. using observed data for the orbits of the planets studied)

1.3 Contributions of This Research

1.3.1 Novelties

Some of the novelties contained in this thesis are listed hereafter. It must be noted that the Sun-Planet-Trojan-spacecraft system is itself a novel system to be studied.

• Previous studies on the WSB were based on the definition formulated in [8] for Earth-Moon-spacecraft CR3BP, then corrected/generalized in [9]. Existing definitions in the literature are all based on an algorithm therefore allowing only numerical studies on the WSB for specific cases to be undertaken and thus no general mathematical property of such a set can be obtained for them.
What's new:

◇ This work provides a new, analytic definition of the WSB for the CR3BP which is coherent with the known algorithmic definitions.

◇ It generalizes the definition of the WSB to the equilateral triangle, CR4BP.

◇ It investigates some topological properties of the "stable region" (near to the smaller primary) whose boundary is, by definition, the WSB.

◇ It provides an analytical and numerical estimation of the stable zone.

Reference also to [10], [11], and [12].

***

• Analytical perturbative studies on inhomogeneous gravitational fields carried out in closed form (i.e. without expanding in power series of the eccentricity) are mainly limited to second degree potentials (i.e. they only account for the ellipticity and oblateness terms). In these the resulting, double averaged, Hamiltonian depends on the sole argument of pericenter, which does not hold, in general, when including more spherical harmonics coefficients.
What's new:

◇ This research derives, in the close vicinity of the small body (i.e. inside the estimated stability boundary), the inhomogeneous gravitational potential in polar-nodal variables, accounting arbitrary degree spherical harmonics coefficients.

◇ It states the explicit analytical formulation for the averaged, first order, arbitrary degree Hamiltonian of any inhomogeneous gravitational field found in closed-form (i.e. valid for every eccentricity).

◇ It provides a method for determining initial conditions for frozen orbits around any irregular body by prescribing the inclination and eccentricity of the desired orbit.

◇ It implements the algorithm to find the spherical harmonics coefficients from the shape of the asteroid assuming a constant density, to find the harmonics of 624-Hektor.

Reference also to [13], [14], [15] and [16].

***

Existing literature on the Lagrangian CR4BP are contemporary to the published works collected in this thesis. They are mainly focussed on determining the number of equilibrium points depending on the mass distribution of the primaries and on numerical determination of families of orbits. None of the previous works considers that there are no asteroids in the exact L_4 or L_5 position and that they all move on tadpole orbits around such points.
What's new:

◇ This work incorporates low thrust perturbations in the Lagrangian CR4BP to generate surfaces of artificial equilibria and displaced non Keplerian orbits;

◇ It studies the topological changes of the linearly stable zone with variations in the Trojan mass.

◇ It identifies novel, artificial, non-Keplerian orbits both for mathematical interest as well as for potential future mission applications.

◇ It finds useful applications to such orbits and tests the validity of the model for a real case, i.e. considering the real tadpole orbit of the asteroid 624-Hektor around the triangular equilibrium point.

Reference also to [17], [18], and [19].

1.3.2 Publications and Outputs

All the results collected in this thesis have been published as journal papers, although, as they are general, the applications here shown may differ from the ones in the papers, in order to give homogeneity to the work. Moreover other results, contained in the conference papers listed below, complete and widen the ones contained in this thesis but have not been included here as they where beyond the scope of this work.

• On Weak Stability Boundaries and applications:

Journal publication(s):

◇ April 2012: Ceccaroni, M., Biggs, J. D., Biasco, L.: "Analytic estimates and topological properties of the weak stability boundary"; Celestial Mechanics and Dynamical Astronomy (2012) 114:124 DOI 10.1007/s10569-012-9419-x.

http://www.springerlink.com/content/728265144j86524h/

Conference publication(s):

◇ June 2011: Ceccaroni, M., Biggs, J. D., Biasco, L.:"Some Analytic Estimates of the Weak Stability Boundary", New Trends in Astrodynamics and Applications VI, New York.

◇ June 2011: Ceccaroni, M., Biggs, J. D., Biasco, L.:"The Weak Stability Boundary in the Sun-Jupiter-Trojan-spacecraft four body problem", New Trends in Astrodynamics and Applications VI, New York.

***

• On inhomogeneous Restricted Two Body Problem and applications:

Journal publication(s):

◇ February 2013: Ceccaroni, M., Biggs, J. D.: "Analytic perturbative theories in highly inhomogeneous gravitational fields." Icarus, in press

http://dx.doi.org/10.1016/j.icarus.2013.01.007

◇ December 2012: Ceccaroni, M., Biscani, F., Biggs, J. D.: "Analytical

method for perturbed frozen orbit around an Asteroid in highly inhomogeneous gravitational fields: a first approach" Solar System Research, in press.

Conference publication(s):
◇ October 2012: Ceccaroni, M., Biscani, F., Biggs, J. D.: "Analytical Perturbative method for frozen orbits around the asteroid 433-Eros"; IAC2010 - International Astronautical Congress - (Naples).

◇ September 2012: Ceccaroni, M., Biscani, F., Biggs, J. D.:"Analytical method for perturbed frozen orbits around an Asteroid in highly inhomogeneous gravitational fields"; Analytical methods for celestial mechanics, St.Petersburg.

◇ September 2011-January 2012: Ceccaroni, M., Biscani, F., Biggs, J. D.: Ariadna Study "Analytical perturbative theories of motion in highly inhomogeneous gravitational fields (11-5201)".
http://www.esa.int/gsp/ACT/doc/ARI/ARI%20Study%20Report/ACT-RPT-1205_Analytical_perturbative_theories_motion_inhomogeneous_%20gravitational_fields.pdf

***

• On low-thrust Lagrangian Circular Restricted Four Body Problem and applications:

Journal publication(s):
◇ November 2011: Ceccaroni, M., Biggs, J. D.:"Low-thrust propulsion in a coplanar circular restricted four body problem"; Celestial Mechanics and Dynamical Astronomy, Volume 112, Issue 2 (2012), Page 191-219. DOI: 10.1007/s10569-011-9391-x.
http://www.springerlink.com/content/728265144j86524h/

Conference publication(s):
◇ October 2011: Ceccaroni, M., Biggs, J. D.:"Nonlinearly stable equilibria in the Sun-Jupiter-Trojan-Spacecraft four body problem"; IAC2011 - International Astronautical Congress - (Cape Town).
http://www.iafastro.net/iac/archive/browse/IAC-11/C1/4/11300/

◇ September/ October 2010: Ceccaroni, M., Biggs, J. D.:"Extension of low thrust propulsion to the Autonomous Coplanar Circular Restricted Four Body problem with application to Future Trojan Asteroids Missions",

IAC2010 - International Astronautical Congress - (Prague).
http://www.iafastro.net/iac/browse/IAC-10/C1/1/

1.4 Thesis Structure

This thesis is organized as follows:
Chapter 1 provides a global picture of this thesis by stressing the motivations, objectives, aims and key questions addressed by the research project. Moreover it provides a summary of the work highlighting the main results and novelties. Finally it includes a list of the outcomes and publications related to this thesis work.

Chapter 2 sets the starting point of the analysis by introducing both the dynamical systems which are used to model the problem. These are here formulated in terms of Hamiltonian equations of motion. In this chapter both the systems are expressed for different sets of variables which will be useful for the analysis contained in the following chapters. Sections 2.1 and 2.2 formulate the Hamiltonian of the two models proposed: the equilateral triangle CR4BP and the inhomogeneous R2BP, in different sets of variables including the Delaunay variables, which will be key for both the models. Section 2.3 constructs the inhomogeneous potential for the second model, by means of spherical harmonics.

Chapter 3 in this chapter the range of applicability of the two models, the inhomogeneous Restricted Two Body Problem and the Lagrangian CR4BP, is estimated as an application of the WSB. Section 3.3 contains the existing definitions of WSB and an analysis of the main problems affecting such definitions; moreover it includes a completely new, analytical definition of the WSB and a comparison with previous algorithmic definitions of WSB from the literature. In Section 3.4 some topological properties are derived and discussed as enabled by the new definition of WSB here formulated. In section 3.5 the symplectic Delaunay coordinates, unusual for the WSB theories, are used to rewrite the problem. It results that the Delaunay coordinates are suitable for estimating analytically the WSB and, consequently, the range of validity of the two models.

Chapter 4 analyses the inhomogeneous R2BP. Inside the set of the stable orbits around the smaller primary, estimated in chapter 3, the dynamics is assumed to be dominated by the sole smaller body. However, within this region, the inhomogeneities of the grav-

itational field can't be neglected. In Section 4.3 and 4.4 the hamiltonian describing the system is transformed by means of two lie transformations, the relegation and the normalisation, which enable to find suitable changes of coordinates to reduce the initial non integrable Hamiltonian of the system into an integrable one plus a negligible, perturbative remainder of higher degree. In addition, an explicit analytical formulation for the relegated, Hamiltonian in any inhomogeneous gravitational field is derived in closed-form, generalised to second order, arbitrary degree. Section 4.5 develops a new method for determining initial conditions for frozen orbits around any irregular body by simply prescribing the desired inclination and eccentricity of the orbit. Results are shown in Section 4.6 for the Trojan asteroid 624-Hektor.

Chapter 5 introduces the Lagrangian (low-thrust) circular restricted four-body model. Outside the estimated region of stable orbits, the perturbations due to the gravitational effects of the Sun and Jupiter dominate the dynamics. Furthermore, the effect of the inhomogeneous gravitational field of the body becomes negligible relative to these gravitational perturbations. Sections 5.3 and 5.4 analyse the natural dynamics of the system (i.e. without the use of low thrust), focusing on the equilibrium points of the system and the stability analysis. Sections 5.5 e 5.6 incorporates, for the first time in a four body problem, low thrust perturbations into the model. The artificial dynamics of the system is thus studied, showing the surfaces of artificial equilibria created by the inclusion of low thrust. In Section 5.7 and 5.8 new, artificial, stable orbits are found, maintainable using constant low thrust and without the need for any state feedback control. Section 5.9 tests the methodology developed in the previous Sections, considering the full, observed dynamics of the real jovian Trojan 624-Hektor.

Chapter 2

Hamiltonian dynamics about Trojan asteroids

The aim of this thesis is to analyse the dynamics of a point mass around an inhomogeneous Trojan body in a system with three primaries lying at the vertexes of an equilateral triangle. To start such analysis it is necessary to introduce both the dynamical systems which will be used in the next chapters to model the problem. The Hamiltonian formulation of these dynamical models is necessary for setting the base of the analysis that will be carried on in the remainder of this thesis. In this chapter the Hamiltonians describing the two models proposed are formulated within different frames of reference and for various sets of coordinates which will then be recalled in the next chapters.

The equilateral triangle CR4BP will be first introduced, as it sets the base for both the estimation of the range of validity of the two models through the use of the WSB contained in Chapter 3, and the analysis of the dynamics relatively far from the asteroid which is contained in Chapter 5. In order to set the most suitable system of reference for such estimates and analysis, several intermediate systems of reference (e.g. inertial, rotating, barycentric, asteroid centered) and sets of coordinates (e.g. polar, Whittaker, Delaunay variables) will be introduced and the corresponding transformations to obtain them described. Then the inhomogeneous R2B dynamical model will be introduced as well, which sets the starting point of the analysis contained in Chapter 4. Again it will be described using the Hamiltonian formalism and through a series of intermediate systems of reference and sets of variables. Finally, at the end of the Chapter, the inhomogeneous potential used for this model, will also be constructed by means of spherical harmonics, the coefficients usually adopted to describe the shape/density inhomogeneities of a massive body.

2.1 The system

The system is initially derived as follows: let be P_1, P_2 and P_3 the three primaries and P_4 the point mass, with corresponding masses m_1, m_2, m_3 and m_4 (assumed to be infinitesimal and thus called a Restricted model) such that: $0 < m_4 << m_3 << m_2 \leq m_1$.
Set the three masses in the equilateral triangle configuration, where the position of P_3 corresponds to one of the triangular Lagrangian points in [20].
This configuration is well known to be stable if the masses of the three planets satisfy the condition (see [21] , [22], [23] and [24])

$$\frac{m_1m_2+m_1m_3+m_2m_3}{(m_1+m_2+m_3)^2} < \frac{1}{27}, \tag{2.1}$$

that is:

$$27(m_1m_2 + m_1m_3 + m_2m_3) - (m_1 + m_2 + m_3)^2 < 0. \tag{2.2}$$

As it is assumed that $m_3 \leq m_2$ and the left term of this inequality is monotonically increasing in m_3, $\forall m_3 \in (0, m_2)$, the left term is maximized for $m_3 = m_2$, thus, to obtain the most restrictive condition possible, independently from m_3, it is set (just for the following estimation) $m_3 = m_2$, obtaining:

$$27(m_1m_2+m_1m_3+m_2m_3)-(m_1+m_2+m_3)^2 < 27(2m_1m_2+m_2^2)-(m_1+2m_2)^2 \quad \forall m_1, m_2 \tag{2.3}$$

Therefore the stability condition becomes:

$$-m_1^2 + 50m_1m_2 + 23m_2^2 < 0 \tag{2.4}$$

(more restrictive then the previous), that rearranged is:

$$\frac{m_1}{m_2} > 25 + 18\sqrt{2}. \tag{2.5}$$

In addition, the mass of the Asteroid is taken to be small enough not to influence the motion of P_1 and P_2, therefore the center of rotation of the three primaries coincides with the barycenter O of the two main primaries. The three bodies will thus rotate anticlockwise on circular orbits around it with constant angular velocity perpendicular to the plane containing the primaries $\boldsymbol{\omega}$.
The system just described is shown in Figure 1.2.

2.2 The Hamiltonian of the equilateral triangle CR4BP

The first model to be used in this thesis is the equilateral CR4BP, which will be used both in estimating the range of validity of the two models (Chapter 3) and in the analysis of the dynamics of the problem contained in Chapter 5.
In this scaled units of measure for mass and distance will be used, normalized with the sum of the masses of P_1 and P_2 and their distance $d_{P1/P2}$ respectively. Therefore, in nondimensional units, it is set

$$\begin{aligned} 1 - M &= m_{1scaled} = \tfrac{m_1}{m_1+m_2}, \\ M &= m_{2scaled} = \tfrac{m_2}{m_1+m_2}, \\ m &= m_{3scaled} = \tfrac{m_3}{m_1+m_2}, \\ \mathcal{M} &= m_{4scaled} = \tfrac{m_4}{m_1+m_2} \simeq 0. \end{aligned} \tag{2.6}$$

Moreover it results $d_{P1/P2} = d_{P1/P2_{scaled}} = 1$.
Finally the unit of time is scaled $t = t_{scaled} = \sqrt{\frac{\mathcal{G}(m_1+m_2)}{d^3_{P1/P2}}}t$, where $\mathcal{G}$ is the universal gravitational constant $\mathcal{G} = 6.67428 \times 10^{-11} \frac{m^3}{kg \cdot s^2}$, such that the gravitational constant in nondimensional unit is $\mathcal{G}_{scaled} = 1$. Moreover, by Kepler's *third Law* for a circular orbit,

> "The square of the orbital period of a planet is directly proportional to the cube of the semi-major axis of its orbit",

the period of revolution of P_1 and P_2 around each other is $\mathcal{T} = 2\pi\sqrt{\frac{d^3_{P1/P2}}{\mathcal{G}(m_1m_2)}}$ which, in nondimensional units, is $\mathcal{T}_{scaled} = 2\pi$. Moreover notice that, in nondimensional it results: $|\boldsymbol{\omega}_{scaled}| = \frac{2\pi}{\mathcal{T}_{scaled}} = 1$.

2.2.1 Barycentric, fixed, inertial reference frame

A fixed inertial frame (**F0**) is taken, which is centered in the center of rotation O of the planets, where the x/y plane contains the three bodies and the x axes passes through P_1 and P_2 at time $t = 0$. This implies $\boldsymbol{\omega} = [0, 0, 1]$ (in the scaled units) and that the initial position of the primaries is

$$P_1 = (-M, 0, 0),$$

$$P_2 = (1 - M, 0, 0)$$

and, in order to form an equilateral triangle,

$$P_3 = (L_x, L_y, 0) = (\frac{1}{2} - M, \frac{\sqrt{3}}{2}, 0).$$

Notice that, as it will be shown later, in a rotating system of reference, centered in the barycenter O of P_1 and P_2 and rotating with the same angular velocity of the primaries $\boldsymbol{\omega} = [0, 0, 1]$ (in the scaled units), the primaries will keep their positions as fixed over the course of the motion and the system would become autonomous (i.e. time independent).

The motions of P_1, P_2 and P_3 are, respectively,

$$\begin{aligned} &M[\cos(t+\pi), \sin(t+\pi), 0], \\ &(1-M)[\cos t, \sin t, 0], \\ &\sqrt{1-M+M^2}[\cos(t+\tau_0), \sin(t+\tau_0), 0], \end{aligned} \tag{2.7}$$

with the primaries starting, for $t = 0$, respectively at

$$\begin{aligned} &[-M, 0, 0] \\ &[1-M, 0, 0] \\ &\sqrt{1-M+M^2}[\cos(\tau_0), \sin(\tau_0), 0] = [\tfrac{1}{2} - M, \tfrac{\sqrt{3}}{2}]. \end{aligned} \tag{2.8}$$

Note that, before including low thrust into the system (see Chapter 5), the spacecraft moves on the plane containing the primaries, therefore the third motion decouples and the system can be considered planar. This system is represented in Fig. 2.1, where, for simplicity of representation, the figure shows only the plane of revolution of the bodies.

Let $\mathbf{q} = [q_x, q_y, q_z]$ be the position vector of the point mass P in the barycentric inertial frame of reference (**F0**). By Newton's Second *Law of Motion*:

> "The rate of change of momentum is proportional to the force and is in same direction as that force"

and *Gravitational Law*:

> "Any two bodies attract one another with a force proportional to the product of their masses and inversely proportional to the square of distance between them",

the equations of motion of the point mass, in (**F0**), are:

$$\mathcal{M}\ddot{\mathbf{q}} = -\frac{\partial U(\mathbf{q})}{\partial \mathbf{q}}, \tag{2.9}$$

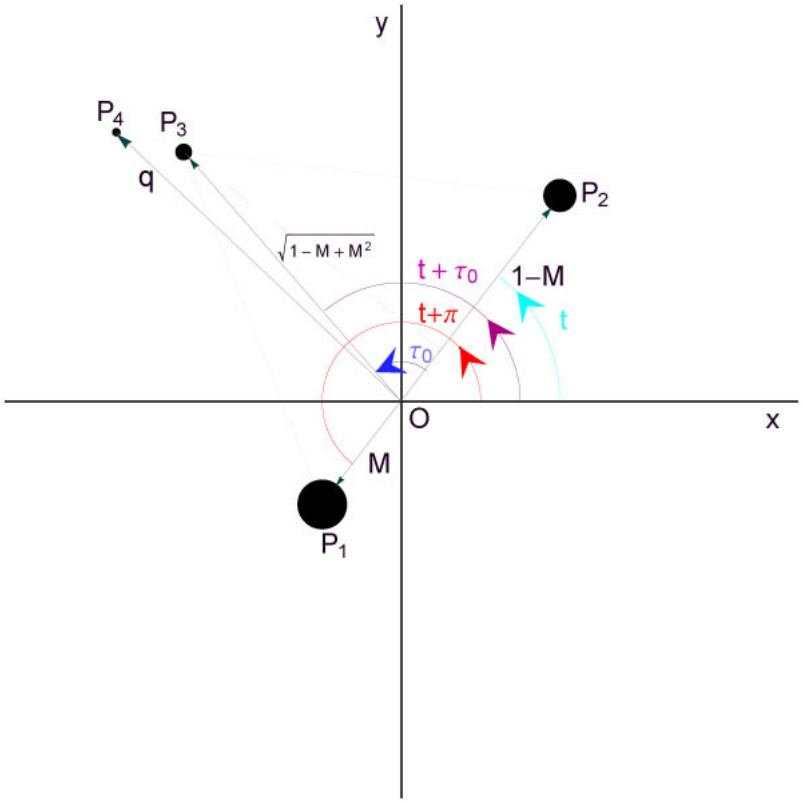

Figure 2.1: F0) Barycentric, fixed, inertial reference frame

where $U(\mathbf{q})$ is the *potential energy* of the point mass:

$$\begin{aligned} U(\mathbf{q}) = &-\frac{\mathcal{M}(1-M)}{|\mathbf{q}-M[\cos(t+\pi),\sin(t+\pi),0]|} \\ &-\frac{\mathcal{M}M}{|\mathbf{q}-(1-M)[\cos t,\sin t,0]|} \\ &-\frac{\mathcal{M}m}{|\mathbf{q}-\sqrt{1-M+M^2}[\cos(t+\tau_0),\sin(t+\tau_0),0]|}, \end{aligned} \tag{2.10}$$

with

$$\tau_0 = \arcsin\frac{\sqrt{3}}{2\sqrt{1-M+M^2}}. \tag{2.11}$$

The *kinetic energy* of the spacecraft is:

$$T(\dot{\mathbf{q}}) = \frac{1}{2}\mathcal{M}|\dot{\mathbf{q}}|^2, \tag{2.12}$$

thus the *Lagrangian* of the body, given by the difference between kinetic and potential energies, is:

$$\mathcal{L}(\mathbf{q},\dot{\mathbf{q}}) := T(\dot{\mathbf{q}}) - U(\mathbf{q}). \tag{2.13}$$

The conjugate momenta $\mathbf{p} = [p_x, p_y, p_z]$ of $\mathbf{q}$ is found by:

$$\mathbf{p} = \frac{\partial \mathcal{L}(\mathbf{q}, \dot{\mathbf{q}})}{\partial \dot{\mathbf{q}}} = \mathcal{M}\dot{\mathbf{q}}, \tag{2.14}$$

thus, by the Euler−Lagrange equations:

$$\begin{aligned} \dot{\mathbf{p}} &= \tfrac{d}{dt}\left(\tfrac{\partial \mathcal{L}(\mathbf{q},\dot{\mathbf{q}})}{\partial \dot{\mathbf{q}}}\right) \\ &= \tfrac{\partial \mathcal{L}(\mathbf{q},\dot{\mathbf{q}})}{\partial \mathbf{q}} \\ &= -\tfrac{\partial U(\mathbf{q})}{\partial \mathbf{q}}. \end{aligned} \tag{2.15}$$

The *Hamiltonian* of the body is then the Legendre transform of the Lagrangian with respect to $\dot{\mathbf{q}}$, namely:

$$\begin{aligned} H(\mathbf{q}, \mathbf{p}) &:= \sup_{\boldsymbol{\eta} \in \mathbb{R}^3} \{p.\boldsymbol{\eta} - \mathcal{L}(\boldsymbol{\eta}, \mathbf{p})\} \\ &= \mathbf{p}.\dot{\mathbf{q}} - \mathcal{L}(\mathbf{q}, \mathbf{p}) \\ &= \tfrac{1}{\mathcal{M}}\mathbf{p}.\mathbf{p} - T(\mathbf{p}) + U(\mathbf{q}) \\ &= T(\mathbf{p}) + U(\mathbf{q}) \\ &= \tfrac{1}{2\mathcal{M}}|\mathbf{p}|^2 + U(\mathbf{q}), \end{aligned} \tag{2.16}$$

where the . indicates the scalar product between two vectors.
The equations of motion can therefore be obtained by the system:

$$\begin{cases} \dot{\mathbf{q}} = \frac{\partial H(\mathbf{q},\mathbf{p})}{\partial \mathbf{p}} = \frac{\mathbf{p}}{\mathcal{M}} \\ \dot{\mathbf{p}} = -\frac{\partial H(\mathbf{q},\mathbf{p})}{\partial \mathbf{q}} = -\frac{\partial U(\mathbf{q})}{\partial \mathbf{q}}. \end{cases} \tag{2.17}$$

The momenta are now scaled to introduce the free mass parameter μ:

$$\begin{cases} \mathbf{q}' = \mathbf{q} \\ \mathbf{p}' = \frac{\mathcal{M}\mathbf{p}}{\mu}. \end{cases} \tag{2.18}$$

This is a symplectic transformation of coefficient $\frac{\mathcal{M}}{\mu}$, and therefore, to make it canonic, the resulting Hamiltonian in the new coordinates must be divided by a factor $\frac{\mathcal{M}}{\mu}$:

$$\begin{aligned} H'(\mathbf{p}', \mathbf{q}') &= \tfrac{\mathcal{M}}{\mu} H(\mathbf{p}', \mathbf{q}') \\ &= \tfrac{1}{2\mu}|\mathbf{p}'|^2 + U'(\mathbf{q}), \end{aligned} \tag{2.19}$$

with

$$\begin{aligned} U'(\mathbf{q}) = &-\tfrac{\mu(1-M)}{|\mathbf{q}-M[\cos(t+\pi),\sin(t+\pi),0]|} \\ &-\tfrac{\mu M}{|\mathbf{q}-(1-M)[\cos t,\sin t,0]|} \\ &-\tfrac{\mu m}{|\mathbf{q}-\sqrt{1-M+M^2}[\cos(t+\tau_0),\sin(t+\tau_0),0]|}. \end{aligned} \tag{2.20}$$

To simplify notations hereafter the primes will be dropped.

2.2.2 Trojan centered, (non−inertial) reference frame, with axes parallel to the inertial

The motions are now expressed in a Trojan centered (non−inertial) frame (**F1**) with the smaller primary at the origin and the other primaries moving with angular velocity $\boldsymbol{\omega} = [0, 0, 1]$ (in the scaled units) on a unitary circle around it and the axes of reference x', y' and z' parallel to the respective axes in (**F0**) $\forall t \geq 0$.
The motions of P_1 and P_2 are respectively:

$$\begin{aligned} &\left[\cos\left(t + \tfrac{4}{3}\pi\right), \sin\left(t + \tfrac{4}{3}\pi\right), 0\right] \\ &\left[\cos\left(t - \tfrac{\pi}{3}\right), \sin\left(t - \tfrac{\pi}{3}\right), 0\right], \end{aligned} \tag{2.21}$$

with their initial positions at the time $t = 0$:

$$\begin{aligned} \left[-\tfrac{1}{2}, -\tfrac{\sqrt{3}}{2}, 0\right] &= \left[\cos\left(\tfrac{4}{3}\pi\right), \sin\left(\tfrac{4}{3}\pi\right), 0\right] \\ \left[\tfrac{1}{2}, -\tfrac{\sqrt{3}}{2}, 0\right] &= \left[\cos\left(-\tfrac{\pi}{3}\right), \sin\left(-\tfrac{\pi}{3}\right), 0\right]. \end{aligned} \tag{2.22}$$

The system is represented in Fig. 2.2.
The new coordinates of the spacecraft are given by:

$$\mathbf{s} = \mathbf{q} - \sqrt{1 - M + M^2}[\cos(t + \tau_0), \sin(t + \tau_0), 0], \tag{2.23}$$

which implies

$$\dot{\mathbf{s}} = \dot{\mathbf{q}} - \sqrt{1 - M + M^2}[-\sin(t + \tau_0), \cos(t + \tau_0), 0], \tag{2.24}$$

and therefore

$$\begin{aligned} \mu\ddot{\mathbf{s}} &= \mu\ddot{\mathbf{q}} + \mu\sqrt{1 - M + M^2}[\cos(t + \tau_0), \sin(t + \tau_0), 0] \\ &= -\tfrac{\partial U_1(\mathbf{s})}{\partial \mathbf{s}} + \mu\sqrt{1 - M + M^2}[\cos(t + \tau_0), \sin(t + \tau_0), 0], \end{aligned} \tag{2.25}$$

with

$$U_1(\mathbf{s}) = -\tfrac{\mu(1-M)}{|\mathbf{s} - [\cos(t+\frac{4}{3}\pi), \sin(t+\frac{4}{3}\pi), 0]|} - \tfrac{\mu M}{|\mathbf{s} - [\cos(t-\frac{\pi}{3}), \sin(t-\frac{\pi}{3}), 0]|} - \tfrac{\mu m}{|\mathbf{s}|}. \tag{2.26}$$

Equation (2.25) is equivalent to the Hamiltonian system:

$$\begin{cases} \dot{\mathbf{s}} = \frac{\partial H_1(\mathbf{s}, \mathbf{S}; t)}{\partial \mathbf{S}} \\ \dot{\mathbf{S}} = -\frac{\partial H_1(\mathbf{s}, \mathbf{S}; t)}{\partial \mathbf{s}} \end{cases} \tag{2.27}$$

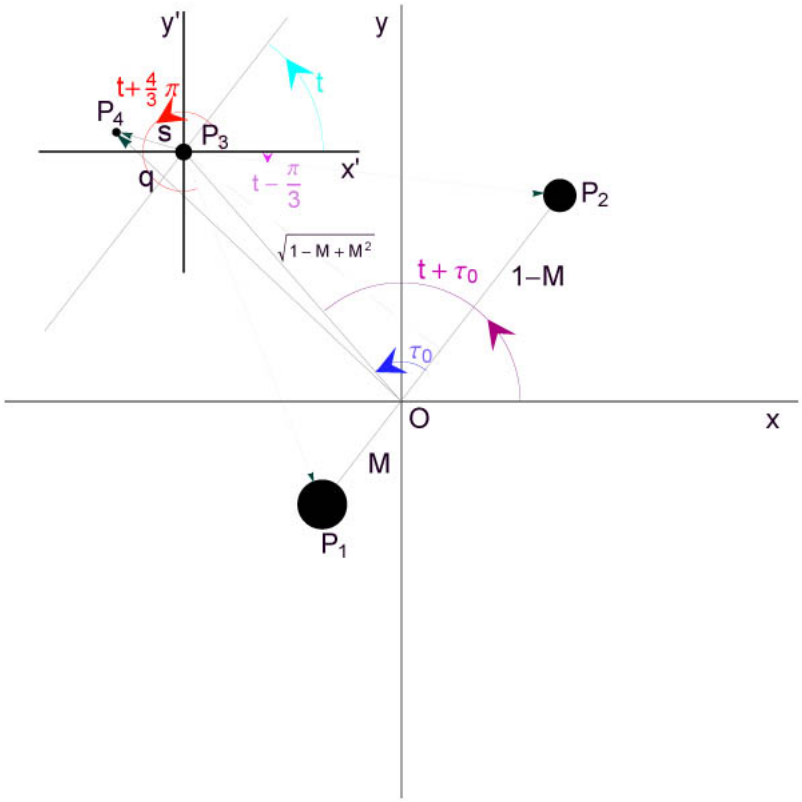

Figure 2.2: F1) Trojan centered, (not inertial) reference frame, with axes parallel to the inertial reference frame

with Hamiltonian

$$H_1(\mathbf{s},\mathbf{S};t) := \frac{1}{2\mu}|\mathbf{S}|^2 + U_1(\mathbf{s}) - \mu\sqrt{1-M+M^2}[\cos(t+\tau_0),\sin(t+\tau_0),0].\mathbf{s} \quad (2.28)$$

in the conjugated variables $\mathbf{S},\ \mathbf{s}\in\mathbb{R}^3$ with symplectic form $d\mathbf{S}\wedge d\mathbf{s}$.
The stability of the orbits in the WSB theory (see Chapter 3) is based on monitoring the sign of the *two-body Kepler energy*; this energy can heuristically be seen as the Hamiltonian $H_1^M(\mathbf{s},\mathbf{S})$ (in the Trojan centered frame) of the spacecraft due to the asteroid only, namely when the influence of the two main bodies is neglected.
Notice that the Trojan centered system of reference for the two body model would be inertial as the Trojan-spacecraft system would not be in rotation.

Definition 1 *(Two-Body Kepler energy)*
*In the Trojan centered frame (**F1**) defined above, with conjugate variables velocity-position* $(\boldsymbol{x},\boldsymbol{X})$*, the* two-body Kepler energy *of the P_4 with respect to the P_3 is defined as:*

$$H_1^M(\boldsymbol{s},\boldsymbol{S}) := \frac{|\boldsymbol{S}|^2}{2\mu} - \frac{\mu m}{|\boldsymbol{s}|}\,. \quad (2.29)$$

2.2.3 Trojan centered, rotating reference frame

The Trojan centered rotating system of reference (**F2**) is now considered, rotating anticlockwise with angular velocity $\boldsymbol{\omega} = [0, 0, 1]$. In this frame all the primaries are at rest, their positions coinciding $\forall t \geq 0$ with the initial positions as in (2.22). See Fig. 2.3. The change of coordinates is defined by the matrix:

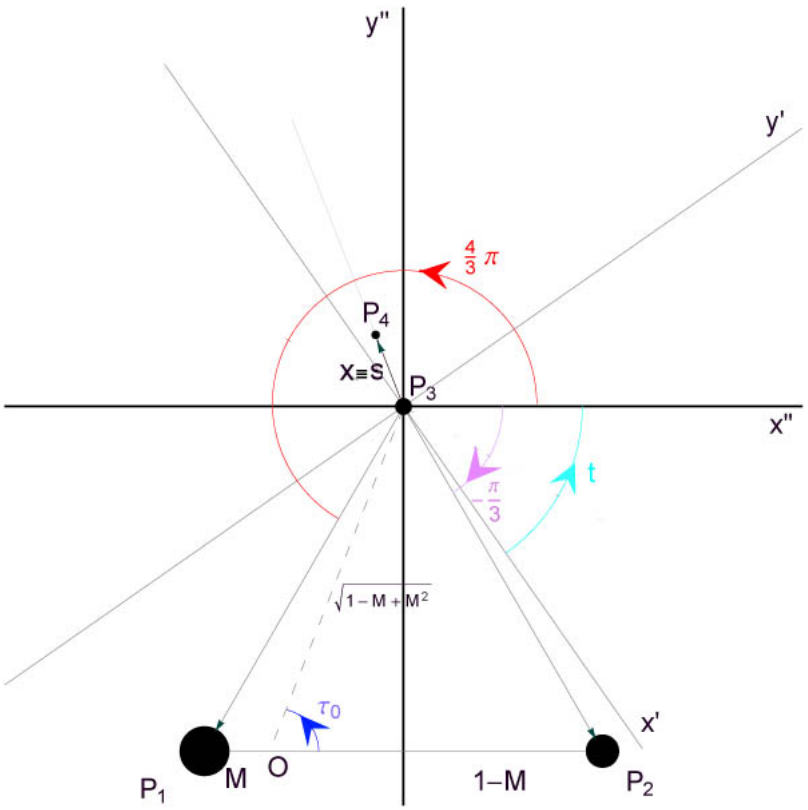

Figure 2.3: F2) Trojan centered, rotating ($\boldsymbol{\omega} = [0, 0, 1]$) reference frame

$$R(t) = \begin{pmatrix} \cos(t) & \sin(t) & 0 \\ -\sin(t) & \cos(t) & 0 \\ 0 & 0 & 1 \end{pmatrix}, \tag{2.30}$$

which defines the position vector of the spacecraft $\mathbf{x} = [x, y, z]$ in the rotating system as:

$$\mathbf{x} = R(t)\mathbf{s}. \tag{2.31}$$

Therefore:

$$\begin{cases} x = s_x \cos(t) + s_y \sin(t) \\ y = -s_x \sin(t) + s_y \cos(t) \\ z = s_z. \end{cases} \tag{2.32}$$

Differentiating with respect to time:

$$\begin{cases} \dot{x} = \dot{s}_x \cos(t) + \dot{s}_y \sin(t) - s_x \sin(t) + s_y \cos(t) \\ \dot{y} = -\dot{s}_x \sin(t) + \dot{s}_y \cos(t) - s_x \cos(t) - s_y \sin(t) \\ \dot{z} = \dot{s}_z. \end{cases} \tag{2.33}$$

Differentiating again with respect to time:

$$\begin{cases} \ddot{x} = \ddot{s}_x \cos(t) + \ddot{s}_y \sin(t) - 2\dot{s}_x \sin(t) + 2\dot{s}_y \cos(t) \\ \qquad -s_x \cos(t) - s_y \sin(t) \\ \ddot{y} = -\ddot{s}_x \sin(t) + \ddot{s}_y \cos(t) - 2\dot{s}_x \cos(t) - 2\dot{s}_y \sin(t) \\ \qquad +s_x \sin(t) - s_y \cos(t) \\ \ddot{z} = \ddot{s}_z. \end{cases} \tag{2.34}$$

In this system of reference the equations of motion in (2.25) becomes:

$$\begin{cases} \mu\ddot{x} = \mu x + 2\mu\dot{y} + \mu\ddot{s}_x \cos t + \mu\ddot{s}_y \sin t \\ \quad = \mu x + 2\mu\dot{y} - \frac{\partial U_2(\mathbf{x})}{\partial x} + \mu\sqrt{1 - M + M^2}\cos\tau_0 \\ \quad = \mu\left(x + (\frac{1}{2} - M)\right) + 2\mu\dot{y} - \frac{\partial U_2(\mathbf{x})}{\partial x} \\ \\ \mu\ddot{y} = \mu y - 2\mu\dot{x} - \mu\ddot{s}_x \sin t + \mu\ddot{s}_y \cos t \\ \quad = \mu y - 2\mu\dot{x} - \frac{\partial U_2(\mathbf{x})}{\partial y} + \mu\sqrt{1 - M + M^2}\sin\tau_0 \\ \quad = \mu\left(y + \frac{\sqrt{3}}{2}\right) - 2\mu\dot{x} - \frac{\partial U_2(\mathbf{x})}{\partial y} \\ \\ \mu\ddot{z} = \mu\ddot{s}_z \\ \quad = -\frac{\partial U_2(\mathbf{x})}{\partial z}, \end{cases} \tag{2.35}$$

with

$$U_2(\mathbf{x}) = -\frac{\mu(1-M)}{|\mathbf{x} - [\cos(\frac{4}{3}\pi), \sin(\frac{4}{3}\pi), 0]|} - \frac{\mu M}{|\mathbf{x} - [\cos(-\frac{\pi}{3}), \sin(-\frac{\pi}{3}), 0]|} - \frac{\mu m}{|\mathbf{x}|}. \tag{2.36}$$

Equation (2.35) is equivalent to the Hamiltonian system:

$$\begin{cases} \dot{\mathbf{x}} = \frac{\partial H_2(\mathbf{x}, \mathbf{X})}{\partial \mathbf{X}} \\ \dot{\mathbf{X}} = -\frac{\partial H_2(\mathbf{x}, \mathbf{X})}{\partial \mathbf{x}} \end{cases} \tag{2.37}$$

with Hamiltonian

$$H_2(\mathbf{x}, \mathbf{X}) := \frac{1}{2\mu}|\mathbf{X}|^2 - \mathbf{x} \times \mathbf{X} + U_2(\mathbf{x}) - \mu\sqrt{1 - M + M^2}[\cos(\tau_0), \sin(\tau_0), 0].\mathbf{x} \tag{2.38}$$

in the conjugated variables $\mathbf{X}$, $\mathbf{x} \in \mathbb{R}^3$ with symplectic form $d\mathbf{X} \wedge d\mathbf{x}$. In this system of reference the two-body Kepler energy remains unchanged as the Trojan-spacecraft system would not be in rotation (i.e. for the R2BP the systems of reference (**F1**) and

(**F2**) coincides).

$$H_2^M(\mathbf{x}, \mathbf{X}) := \frac{|\mathbf{X}|^2}{2\mu} - \frac{\mu m}{|\mathbf{x}|}\,. \tag{2.39}$$

2.2.4 The equilateral triangle CR4BP in polar coordinates

In the reference frame (**F2**) a canonic change of coordinates is performed, to pass to the polar coordinates (r, θ, R, Θ). As said before the natural motion of the spacecraft, before the inclusion of the low trust, can be considered as planar.
The symplectic transformation is given by:

$$\begin{aligned} &\mathbf{x} = r[\cos(\theta), \sin(\theta), 0] \\ &\mathbf{X} = [R\cos(\theta) - \tfrac{\Theta}{r}\sin(\theta), R\sin(\theta) + \tfrac{\Theta}{r}\cos(\theta), 0] \end{aligned} \tag{2.40}$$

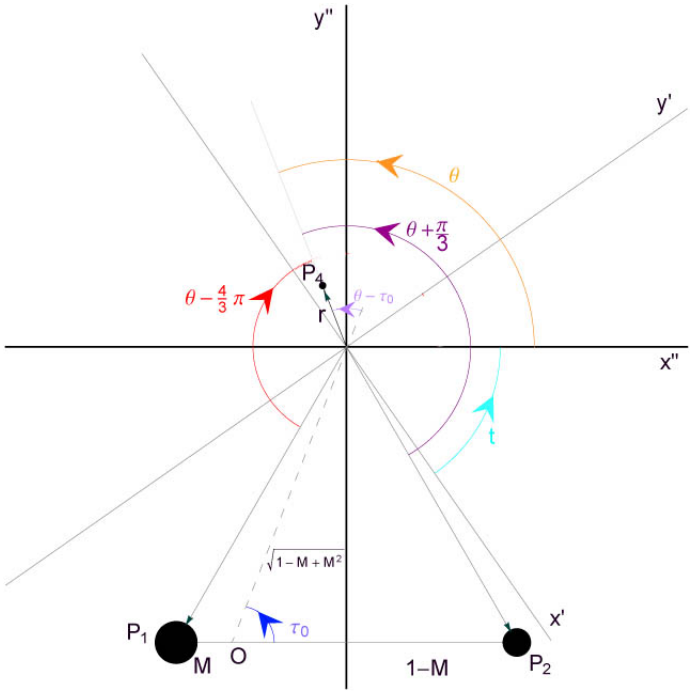

Figure 2.4: (**F2**), polar coordinates: the angle variables describing the system

The system is thus transformed into the autonomous system:

$$\begin{cases} \dot{r} = \frac{\partial H_3(r,\theta,R,\Theta)}{\partial R} \\ \dot{\theta} = \frac{\partial H_3(r,\theta,R,\Theta)}{\partial \Theta} \\ \dot{R} = -\frac{\partial H_3(r,\theta,R,\Theta)}{\partial r} \\ \dot{\Theta} = -\frac{\partial H_3(r,\theta,R,\Theta)}{\partial \theta} \end{cases} \tag{2.41}$$

with Hamiltonian

$$H_3(r,\theta,R,\Theta) := \frac{1}{2\mu}\left(R^2+\frac{\Theta^2}{r^2}\right) - \Theta + U_3(r,\theta,R,\Theta) - \mu\sqrt{1-M+M^2}r\cos(\theta-\tau_0), \tag{2.42}$$

with

$$U_3(r,\theta,R,\Theta) = -\frac{\mu(1-M)}{\sqrt{r^2+1-2r\cos(\theta-\frac{4}{3}\pi)}} - \frac{\mu M}{\sqrt{r^2+1-2r\cos(\theta+\frac{\pi}{3})}} - \frac{\mu m}{r}. \tag{2.43}$$

The two-Body Kepler energy becomes:

$$H_3^M(r,\theta,R,\Theta) := \frac{1}{2\mu}\left(R^2+\frac{\Theta^2}{r^2}\right) - \frac{\mu m}{r}\,. \tag{2.44}$$

2.2.5 The equilateral triangle CR4BP in Delaunay coordinates

The Delaunay coordinates are symplectic action-angle variables (ℓ, g, L, G), where the angles ℓ and g are conjugate to the actions L and G respectively, where

- ℓ is the *mean anomaly* measured from the pericenter;
- g is the argument of the pericenter;
- L is related to the major semi-axis, a, by $L = \mu\sqrt{ma}$
- G is the *total angular momentum* of the spacecraft with respect to the Asteroid (in the inertial frame), related to the eccentricity and the variable L by

$$e = \sqrt{1-\frac{G^2}{L^2}}; \tag{2.45}$$

Moreover the relation between the *True anomaly* f and the *Eccentric anomaly* u is defined as:

$$\tan\left(\frac{f}{2}\right) = \sqrt{\frac{1+e}{1-e}}\tan\left(\frac{u}{2}\right), \tag{2.46}$$

which, in particular, implies

$$r = a(1-e\cos u) = a\frac{1-e^2}{1+e\cos f}. \tag{2.47}$$

The change of coordinates from the polar variables to the Delaunay coordinates is generated by the function

$$S = G\theta + \int_{r_{min}}^{r}\sqrt{-\frac{G^2}{r^2}+2\frac{m\mu^2}{r}-\frac{\mu^4m^2}{L^2}}dr \tag{2.48}$$

with $r_{min} = a(1-e)$ by (2.47).
It is completely canonical as

$$d\ell \wedge dL + dg \wedge dG = dr \wedge dR + d\theta \wedge d\Theta. \tag{2.49}$$

Therefore:

$$\begin{aligned}
R &= \tfrac{\partial S}{\partial r} = \sqrt{-\tfrac{G^2}{r^2} + 2\tfrac{m\mu^2}{r} - \tfrac{\mu^4 m^2}{L^2}} \\
\Theta &= \tfrac{\partial S}{\partial \theta} = G \\
\ell &= \tfrac{\partial S}{\partial L} \\
&= \tfrac{\partial}{\partial L}\left(G\theta + \textstyle\int_{r_{min}}^{r} \sqrt{-\tfrac{G^2}{r^2} + 2\tfrac{m\mu^2}{r} - \tfrac{\mu^4 m^2}{L^2}}\, dr\right) \\
&= \textstyle\int_{r_{min}}^{r} \tfrac{\mu^4 m^2}{L^3 \sqrt{-\frac{G^2}{r^2} + 2\frac{m\mu^2}{r} - \frac{\mu^4 m^2}{L^2}}}\, dr \\
&= \textstyle\int_{r_{min}}^{r} \tfrac{(1-e\cos u)}{ae\sin u}\, dr \\
&= \textstyle\int_0^u (1 - e\cos u)\, du \\
&= u - e\sin u \\
g &= \tfrac{\partial S}{\partial G} \\
&= \tfrac{\partial}{\partial G}\left(G\theta + \textstyle\int_{r_{min}}^{r} \sqrt{-\tfrac{G^2}{r^2} + 2\tfrac{m\mu^2}{r} - \tfrac{\mu^4 m^2}{L^2}}\, dr\right) \\
&= \theta - \textstyle\int_{r_{min}}^{r} \tfrac{G}{r^2 \sqrt{-\frac{G^2}{r^2} + 2\frac{m\mu^2}{r} - \frac{\mu^4 m^2}{L^2}}}\, dr \\
&= \theta - \tfrac{G}{L}\textstyle\int_0^u \tfrac{1}{(1-e\cos u)}\, du \\
&= \theta - \tfrac{G}{L\sqrt{1-e^2}}\textstyle\int_0^f df \\
&= \theta - f,
\end{aligned} \tag{2.50}$$

where:

$$\begin{aligned}
\tfrac{dr}{du} &= ae\sin u \\
\tfrac{du}{d\ell} &= \tfrac{1}{1+e\cos u} \\
\tfrac{df}{d\ell} &= \tfrac{r^2}{a^2}\sqrt{1-e^2}
\end{aligned} \tag{2.51}$$

The system becomes:

$$\begin{cases}
\dot{\ell} = \frac{\partial H_4(\ell,g,L,G)}{\partial L} \\
\dot{g} = \frac{\partial H_4(\ell,g,L,G)}{\partial G} \\
\dot{L} = -\frac{\partial H_4(\ell,g,L,G)}{\partial \ell} \\
\dot{G} = -\frac{\partial H_4(\ell,g,L,G)}{\partial g}
\end{cases} \tag{2.52}$$

with Hamiltonian

$$H_4(\ell, g, L, G) := -\frac{\mu^3 m^2}{2L^2} - G + U_4(\ell, g, L, G) - \mu\sqrt{1 - M + M^2}\, r\cos(g + f - \tau_0), \tag{2.53}$$

with

$$U_4(\ell, g, L, G) = -\frac{\mu(1-M)}{\sqrt{r^2+1-2r\cos(g+f-\frac{4}{3}\pi)}} - \frac{\mu M}{\sqrt{r^2+1-2r\cos(g+f+\frac{\pi}{3})}}. \tag{2.54}$$

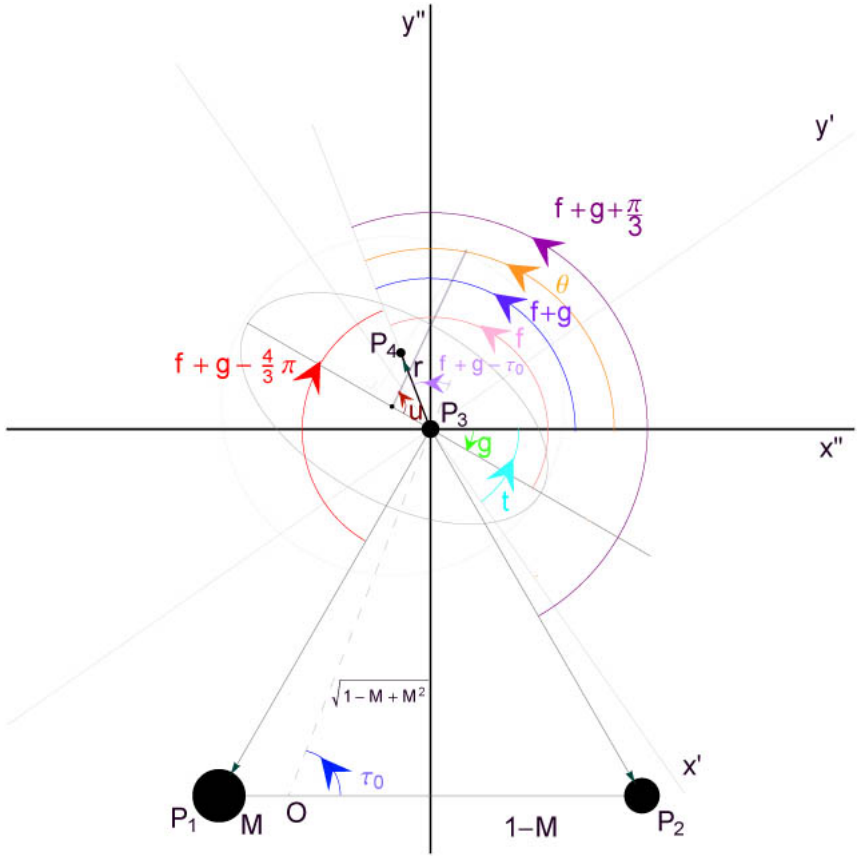

Figure 2.5: (**F2**) Delaunay coordinates: the angles describing the system

Finally, following the usual procedure for the Delaunay coordinates (see for example [25]), the free mass parameter μ is set to be equal to $m^{-\frac{2}{3}}$. This $m^{-\frac{2}{3}}$ is an effective mass scaling for the Hamiltonian system, and is therefore usually used to obtain the standard form of the integrable part of the Hamiltonian i.e. $-\frac{1}{2L^2}$. This yields:

$$H_4(\ell, g, L, G) := -\frac{1}{2L^2} - G + U_4(\ell, g, L, G) - m^{-\frac{2}{3}}\sqrt{1 - M + M^2}r\cos(g + f - \tau_0), \tag{2.55}$$

with

$$U_4(\ell, g, L, G) = -\frac{m^{-\frac{2}{3}}(1-M)}{\sqrt{r^2+1-2r\cos(g+f-\frac{4}{3}\pi)}} - \frac{m^{-\frac{2}{3}}M}{\sqrt{r^2+1-2r\cos(g+f+\frac{\pi}{3})}}. \tag{2.56}$$

In Delaunay variables, the two-Body Kepler energy $H_4^M(\ell, g, L, G)$ takes the form:

$$\begin{aligned} H_4^M(\ell, g, L, G) &= -\frac{\mu^3 m^2}{2L^2} \\ &= -\frac{1}{2L^2} \end{aligned} \tag{2.57}$$

Calling

$$
\begin{aligned}
\rho &= \sqrt{1-M+M^2}\, r\cos\left(g+f-\tau_0\right) \\
&= m^{\frac{1}{3}}L^2\left[\cos g\left(\left(\tfrac{1}{2}-M\right)(\cos u-e)+\tfrac{\sqrt{3}}{2}\sqrt{1-e^2}\sin u\right)\right. \\
&\quad \left.+\sin g\left(\tfrac{\sqrt{3}}{2}(\cos u-e)-\left(\tfrac{1}{2}-M\right)\sqrt{1-e^2}\sin u\right)\right] \\
\rho_1 &= r\cos\left(g+f-\tfrac{4}{3}\pi\right) \\
&= -m^{\frac{1}{3}}L^2\left[\cos g\left(\tfrac{1}{2}(\cos u-e)+\tfrac{\sqrt{3}}{2}\sqrt{1-e^2}\sin u\right)\right. \\
&\quad \left.+\sin g\left(-\tfrac{1}{2}\sqrt{1-e^2}\sin u+\tfrac{\sqrt{3}}{2}(\cos u-e)\right)\right] \\
\rho_2 &= r\cos\left(g+f+\tfrac{\pi}{3}\right) \\
&= m^{\frac{1}{3}}L^2\left[\cos g\left(\tfrac{1}{2}(\cos u-e)-\tfrac{\sqrt{3}}{2}\sqrt{1-e^2}\sin u\right)\right. \\
&\quad \left.+\sin g\left(-\tfrac{1}{2}\sqrt{1-e^2}\sin u-\tfrac{\sqrt{3}}{2}(\cos u-e)\right)\right]
\end{aligned}
\tag{2.58}
$$

The Hamiltonian (2.55) becomes:

$$
H^* = -\frac{1}{2L^2} - G - m^{-\frac{2}{3}}\rho - \frac{m^{-\frac{2}{3}}(1-M)}{\sqrt{r^2+1-2\rho_1}} - \frac{m^{-\frac{2}{3}}M}{\sqrt{r^2+1-2\rho_2}}. \tag{2.59}
$$

The equation of motions of the Hamiltonian (2.59) are:

$$
\begin{aligned}
\dot{\ell} &= \frac{dH_4}{dL} = \frac{dH^*}{dL} \\
&= \partial_L H^* + \partial_r H^*(\partial_L r + (\partial_u r\partial_e u + \partial_e r)\partial_L e) + \partial_\rho H^*(\partial_L\rho + (\partial_u\rho\partial_e u + \partial_e\rho)\partial_L e) \\
&\quad +\partial_{\rho_1} H^*(\partial_L\rho_1 + (\partial_u\rho_1\partial_e u + \partial_e\rho_1)\partial_L e) + \partial_{\rho_2} H^*(\partial_L\rho_2 + (\partial_u\rho_2\partial_e u + \partial_e\rho_2)\partial_L e) \\
\dot{g} &= \frac{dH_4}{dG} = \frac{dH^*}{dG} \\
&= \partial_G H^* + \partial_r H^*(\partial_u r\partial_e u + \partial_e r)\partial_G e + \partial_\rho H^*(\partial_u\rho\partial_e u + \partial_e\rho)\partial_G e \\
&\quad +\partial_{\rho_1} H^*(\partial_u\rho_1\partial_e u + \partial_e\rho_1)\partial_G e + \partial_{\rho_2} H^*(\partial_u\rho_2\partial_e u + \partial_e\rho_2)\partial_G e \\
\dot{L} &= -\frac{dH_4}{d\ell} = -\frac{dH^*}{d\ell} \\
&= -\partial_r H^*\partial_u r\partial_\ell u - \partial_\rho H^*\partial_u\rho\partial_\ell u - \partial_{\rho_1} H^*\partial_u\rho_1\partial_\ell u - \partial_{\rho_2} H^*\partial_u\rho_2\partial_\ell u \\
\dot{G} &= -\frac{dH_4}{dg} = -\frac{dH^*}{dg} \\
&= -\partial_\rho H^*\partial_g\rho - \partial_{\rho_1} H^*\partial_g\rho_1 - \partial_{\rho_2} H^*\partial_g\rho_2\,.
\end{aligned}
\tag{2.60}
$$

where

$$
\begin{aligned}
&\partial_L H^* = \tfrac{1}{L^3}\,, \\
&\partial_G H^* = -1\,, \\
&\partial_r H^* = \tfrac{m^{-\frac{2}{3}}(1-M)r}{(\sqrt{r^2+1-2\rho_1})^3} + \tfrac{m^{-\frac{2}{3}}Mr}{(\sqrt{r^2+1-2\rho_2})^3}\,, \\
&\partial_\rho H^* = -m^{-\frac{2}{3}}\,, \\
&\partial_{\rho_1} H^* = -m^{-\frac{2}{3}}(1-M)\left(\tfrac{1}{(\sqrt{r^2+1-2\rho_1})^3}\right)\,, \\
&\partial_{\rho_2} H^* = -m^{-\frac{2}{3}}M\left(\tfrac{1}{(\sqrt{r^2+1-2\rho_2})^3}\right)\,,
\end{aligned}
\tag{2.61}
$$

Moreover:

$$
\begin{aligned}
\partial_L r &= 2Lm^{\frac{1}{3}}(1-e\cos u)\\
\partial_u r &= eL^2m^{\frac{1}{3}}\sin u\\
\partial_e r &= -L^2m^{\frac{1}{3}}\cos u
\end{aligned}
$$

$$
\begin{aligned}
\partial_L\rho &= 2m^{\frac{1}{3}}L\left[\cos g\left((\tfrac{1}{2}-M)(\cos u-e)+\tfrac{\sqrt{3}}{2}\sqrt{1-e^2}\sin u\right)\right.\\
&\quad\left.+\sin g\left(\tfrac{\sqrt{3}}{2}(\cos u-e)-(\tfrac{1}{2}-M)\sqrt{1-e^2}\sin u\right)\right]\\
\partial_g\rho &= m^{\frac{1}{3}}L^2\left[-\sin g\left((\tfrac{1}{2}-M)(\cos u-e)+\tfrac{\sqrt{3}}{2}\sqrt{1-e^2}\sin u\right)\right.\\
&\quad\left.+\cos g\left(\tfrac{\sqrt{3}}{2}(\cos u-e)-(\tfrac{1}{2}-M)\sqrt{1-e^2}\sin u\right)\right]\\
\partial_u\rho &= m^{\frac{1}{3}}L^2\left[\cos g\left(-(\tfrac{1}{2}-M)\sin u+\tfrac{\sqrt{3}}{2}\sqrt{1-e^2}\cos u\right)\right.\\
&\quad\left.+\sin g\left(\tfrac{-\sqrt{3}}{2}\sin u-(\tfrac{1}{2}-M)\sqrt{1-e^2}\cos u\right)\right]\\
\partial_e\rho &= m^{\frac{1}{3}}L^2\left[\cos g\left(-(\tfrac{1}{2}-M)-\tfrac{\sqrt{3}}{2}\tfrac{e}{\sqrt{1-e^2}}\sin u\right)\right.\\
&\quad\left.+\sin g\left(\tfrac{-\sqrt{3}}{2}+(\tfrac{1}{2}-M)\tfrac{e}{\sqrt{1-e^2}}\sin u\right)\right]
\end{aligned}
$$

$$
\begin{aligned}
\partial_L\rho_1 &= 2m^{\frac{1}{3}}L\left[\cos g\left(-\tfrac{1}{2}(\cos u-e)-\tfrac{\sqrt{3}}{2}\sqrt{1-e^2}\sin u\right)\right.\\
&\quad\left.+\sin g\left(\tfrac{1}{2}\sqrt{1-e^2}\sin u-\tfrac{\sqrt{3}}{2}(\cos u-e)\right)\right]\\
\partial_g\rho_1 &= m^{\frac{1}{3}}L^2\left[-\sin g\left(-\tfrac{1}{2}(\cos u-e)-\tfrac{\sqrt{3}}{2}\sqrt{1-e^2}\sin u\right)\right.\\
&\quad\left.+\cos g\left(\tfrac{1}{2}\sqrt{1-e^2}\sin u-\tfrac{\sqrt{3}}{2}(\cos u-e)\right)\right]\\
\partial_u\rho_1 &= m^{\frac{1}{3}}L^2\left[\cos g\left(+\tfrac{1}{2}\sin u-\tfrac{\sqrt{3}}{2}\sqrt{1-e^2}\cos u\right)\right.\\
&\quad\left.+\sin g\left(\tfrac{1}{2}\sqrt{1-e^2}\cos u+\tfrac{\sqrt{3}}{2}\sin u\right)\right]\\
\partial_e\rho_1 &= m^{\frac{1}{3}}L^2\left[\cos g\left(\tfrac{1}{2}+\tfrac{\sqrt{3}}{2}\tfrac{e}{\sqrt{1-e^2}}\sin u\right)\right.\\
&\quad\left.+\sin g\left(-\tfrac{1}{2}\tfrac{e}{\sqrt{1-e^2}}\sin u+\tfrac{\sqrt{3}}{2}\right)\right]
\end{aligned}
\tag{2.62}
$$

$$
\begin{aligned}
\partial_L\rho_2 &= 2m^{\frac{1}{3}}L\left[\cos g\left(\tfrac{1}{2}(\cos u-e)-\tfrac{\sqrt{3}}{2}\sqrt{1-e^2}\sin u\right)\right.\\
&\quad\left.+\sin g\left(-\tfrac{1}{2}\sqrt{1-e^2}\sin u-\tfrac{\sqrt{3}}{2}(\cos u-e)\right)\right]\\
\partial_g\rho_2 &= m^{\frac{1}{3}}L^2\left[-\sin g\left(\tfrac{1}{2}(\cos u-e)-\tfrac{\sqrt{3}}{2}\sqrt{1-e^2}\sin u\right)\right.\\
&\quad\left.+\cos g\left(-\tfrac{1}{2}\sqrt{1-e^2}\sin u-\tfrac{\sqrt{3}}{2}(\cos u-e)\right)\right]\\
\partial_u\rho_2 &= m^{\frac{1}{3}}L^2\left[\cos g\left(-\tfrac{1}{2}\sin u-\tfrac{\sqrt{3}}{2}\sqrt{1-e^2}\cos u\right)\right.\\
&\quad\left.+\sin g\left(-\tfrac{1}{2}\sqrt{1-e^2}\cos u+\tfrac{\sqrt{3}}{2}\sin u\right)\right]\\
\partial_e\rho_2 &= m^{\frac{1}{3}}L^2\left[\cos g\left(-\tfrac{1}{2}+\tfrac{\sqrt{3}}{2}\tfrac{e}{\sqrt{1-e^2}}\sin u\right)\right.\\
&\quad\left.+\sin g\left(\tfrac{1}{2}\tfrac{e}{\sqrt{1-e^2}}\sin u+\tfrac{\sqrt{3}}{2}\right)\right]
\end{aligned}
$$

Furthermore, since $e = \sqrt{1-\frac{G^2}{L^2}}$ and $u = u(\ell, e)$ solves the Kepler equation $\ell = u - e\sin u$, it is found that

$$\begin{aligned}
&\partial_L e = \frac{G^2}{L^3\sqrt{1-\frac{G^2}{L^2}}} = \frac{(1-e^2)}{eL} \\
&\partial_G e = -\frac{G}{L^2\sqrt{1-\frac{G^2}{L^2}}} = -\frac{\sqrt{1-e^2}}{eL} \\
&\partial_e u = \sin u + e\cos u\ \partial_e u \Rightarrow \partial_e u = \tfrac{\sin u}{1-e\cos u} \\
&\partial_\ell u = 1 + e\cos u\ \partial_\ell u \quad \Rightarrow \partial_\ell u = \tfrac{1}{1-e\cos u}\,.
\end{aligned} \tag{2.63}$$

In conclusion:

$$\begin{aligned}
&\dot\ell = \partial_L H = \\
&\tfrac{1}{L^3} + \tfrac{L}{m^{\frac{1}{3}}}\left\{\left(-\tfrac{(1-M)}{(\sqrt{1-2\rho_1+r^2})^3}\right)\left[\cos(g-\tfrac{4}{3}\pi)\left(2\cos u - e - \tfrac{1}{e} - \tfrac{\sin^2 u(1-e^2)}{e(1-e\cos u)}\right)\right.\right. \\
&\qquad \left.+\sin(g-\tfrac{4}{3}\pi)\left(-\sqrt{1-e^2}\sin u(1+\tfrac{(1-e^2)\cos u}{e(1-e\cos u)})\right)\right] \\
&+\left(-\tfrac{M}{(\sqrt{1-2\rho_2+r^2})^3}\right)\left[\cos(g+\tfrac{1}{3}\pi)\left(2\cos u - e - \tfrac{1}{e} - \tfrac{\sin^2 u(1-e^2)}{e(1-e\cos u)}\right)\right. \\
&\qquad \left.+\sin(g+\tfrac{1}{3}\pi)\left(-\sqrt{1-e^2}\sin u(1+\tfrac{(1-e^2)\cos u}{e(1-e\cos u)})\right)\right] \\
&+\left(-\sqrt{1-M+M^2}\right)\left[\cos(g-\tau_0)\left(2\cos u - e - \tfrac{1}{e} - \tfrac{\sin^2 u(1-e^2)}{e(1-e\cos u)}\right)\right. \\
&\qquad \left.\left.+\sin(g-\tau_0)\left(-\sqrt{1-e^2}\sin u(1+\tfrac{(1-e^2)\cos u}{e(1-e\cos u)})\right)\right]\right\} \\
&+L^3\left(\tfrac{1-M}{(\sqrt{1-2\rho_1+r^2})^3} + \tfrac{M}{(\sqrt{1-2\rho_2+r^2})^3}\right)\left[3 - 3e\cos u + 2e^2\cos^2 u - \tfrac{1}{e}\cos u - e^2\right]
\end{aligned} \tag{2.64}$$

$$\begin{aligned}
&\dot g = \partial_G H = \\
&-1 + \tfrac{L}{m^{\frac{1}{3}}}\left\{\left(-\tfrac{1-M}{(\sqrt{1-2\rho_1+r^2})^3}\right)\left[\cos(g-\tfrac{4}{3}\pi)\left(\tfrac{\sqrt{1-e^2}}{e}(1+\tfrac{\sin^2 u}{(1-e\cos u)})\right)+\right.\right. \\
&\qquad \left.+\sin(g-\tfrac{4}{3}\pi)\sin u\left(\tfrac{-e+\cos u}{e(1-e\cos u)}\right)\right] \\
&+\left(-\tfrac{M}{(\sqrt{1-2\rho_2+r^2})^3}\right)\left[\cos(g+\tfrac{1}{3}\pi)\left(\tfrac{\sqrt{1-e^2}}{e}(1+\tfrac{\sin^2 u}{(1-e\cos u)})\right)+\right. \\
&\qquad \left.+\sin(g+\tfrac{1}{3}\pi)\sin u\left(\tfrac{-e+\cos u}{e(1-e\cos u)}\right)\right] \\
&+\left(-\sqrt{1-M+M^2}\right)\left[\cos(g-\tau_0)\left(\tfrac{\sqrt{1-e^2}}{e}(1+\tfrac{\sin^2 u}{(1-e\cos u)})\right)+\right. \\
&\qquad \left.\left.+\sin(g-\tau_0)\sin u\left(\tfrac{-e+\cos u}{e(1-e\cos u)}\right)\right]\right\} \\
&+L^3\left(\tfrac{1-M}{(\sqrt{1-2\rho_1+r^2})^3} + \tfrac{M}{(\sqrt{1-2\rho_2+r^2})^3}\right)\left[\tfrac{\sqrt{1-e^2}}{e}(\cos u - e)\right]
\end{aligned} \tag{2.65}$$

$$
\begin{aligned}
&\dot{L} = -\partial_\ell H = \\
&-\frac{L^2}{m^{\frac{1}{3}}}\left\{\left(\frac{1-M}{(\sqrt{1-2\rho_1+r^2})^3}\right)\left[\cos\left(g-\tfrac{4}{3}\pi\right)\left(\frac{\sin u}{1-e\cos u}\right)+\sin\left(g-\tfrac{4}{3}\pi\right)\left(\frac{\sqrt{1-e^2}\cos u}{1-e\cos u}\right)\right]\right. \\
&+\left(\frac{M}{(\sqrt{1-2\rho_2+r^2})^3}\right)\left[\cos\left(g+\tfrac{1}{3}\pi\right)\left(\frac{\sin u}{1-e\cos u}\right)+\sin\left(g+\tfrac{1}{3}\pi\right)\left(\frac{\sqrt{1-e^2}\cos u}{1-e\cos u}\right)\right] \\
&\left.+\left(\sqrt{1-M+M^2}\right)\left[\cos\left(g-\tau_0\right)\left(\frac{\sin u}{1-e\cos u}\right)+\sin\left(g-\tau_0\right)\left(\frac{\sqrt{1-e^2}\cos u}{1-e\cos u}\right)\right]\right\} \\
&\qquad -L^4\left(\frac{1-M}{(\sqrt{1-2\rho_1+r^2})^3}+\frac{M}{(\sqrt{1-2\rho_2+r^2})^3}\right)(e\sin u)\,.
\end{aligned}
\tag{2.66}
$$

$$
\begin{aligned}
&\dot{G} = -\partial_g H = \\
&-\frac{L^2}{m^{\frac{1}{3}}}\left\{\left(\frac{1-M}{(\sqrt{1-2\rho_1+r^2})^3}\right)\left(\sin\left(g-\tfrac{4}{3}\pi\right)(\cos u-e)+\cos\left(g-\tfrac{4}{3}\pi\right)\sqrt{1-e^2}\sin u\right)\right. \\
&+\left(\frac{M}{(\sqrt{1-2\rho_2+r^2})^3}\right)\left(\sin\left(g+\tfrac{1}{3}\pi\right)(\cos u-e)+\cos\left(g+\tfrac{1}{3}\pi\right)\sqrt{1-e^2}\sin u\right) \\
&\left.+\left(\sqrt{1-M+M^2}\right)\left(\sin\left(g-\tau_0\right)(\cos u-e)+\cos\left(g-\tau_0\right)\sqrt{1-e^2}\sin u\right)\right\}
\end{aligned}
\tag{2.67}
$$

Since G appears in the Hamiltonian vector field only through e, it is convenient to use e instead of G as the independent variable. Then the value of G is recovered by the formula

$$G = L\sqrt{1-e^2}\,.$$

The equation for $\dot{e}$ is:

$$
\begin{aligned}
&\dot{e} = \partial_L e\dot{L} + \partial_G e\dot{G} = \\
&-\frac{L}{m^{\frac{1}{3}}}\left\{\left(\frac{1-M}{(\sqrt{1-2\rho_1+r^2})^3}\right)\left[\cos\left(g-\tfrac{4}{3}\pi\right)\left(\frac{(1-e^2)\sin u\cos u}{1-e\cos u}\right)+\sin\left(g-\tfrac{4}{3}\pi\right)\frac{\sqrt{1-e^2}}{1-e\cos u}\right.\right. \\
&\qquad \left.\left(-2e\cos u+1+\cos^2 u\right)\right] \\
&+\left(\frac{M}{(\sqrt{1-2\rho_2+r^2})^3}\right)\left[\cos\left(g+\tfrac{1}{3}\pi\right)\left(\frac{(1-e^2)\sin u\cos u}{1-e\cos u}\right)+\sin\left(g+\tfrac{1}{3}\pi\right)\frac{\sqrt{1-e^2}}{1-e\cos u}\right. \\
&\qquad \left.\left(-2e\cos u+1+\cos^2 u\right)\right] \\
&+\left(\sqrt{1-M+M^2}\right)\left[\cos\left(g-\tau_0\right)\left(\frac{(1-e^2)\sin u\cos u}{1-e\cos u}\right)+\sin\left(g-\tau 0\right)\frac{\sqrt{1-e^2}}{1-e\cos u}\right. \\
&\qquad \left.\left.\left(-2e\cos u+1+\cos^2 u\right)\right]\right\} \\
&-L^3\left(\frac{1-M}{(\sqrt{1-2\rho_1+r^2})^3}+\frac{M}{(\sqrt{1-2\rho_2+r^2})^3}\right)\left((1-e^2)\sin u\right) \\
&=: w(L,e,\ell,g)\,.
\end{aligned}
\tag{2.68}
$$

In summary, in the variables (L,e,ℓ,g), the equation of motions are

$$\dot{L} = -\partial_\ell H\,,\quad \dot{e} = w\,,\quad \dot{\ell} = \partial_L H\,,\quad \dot{g} = \partial_G H\,. \tag{2.69}$$

2.3 The inhomogeneous restricted two body problem

In the close vicinity of the asteroid the system is modeled as a two body problem, which will be analysed in Chapter 4. Such dynamical model is here set and described for different systems of reference and sets of coordinates which are necessary for the analysis contained in the next chapters.
In this model an inhomogeneous primary body is considered, which rotates uniformly around its axes of greatest inertia with constant angular velocity $\mathbf{\Omega}$.
The units of measure will not be scaled, thus the mass of the body is m_3.

2.3.1 Trojan centered, fixed, inertial reference frame

It is set a fixed inertial frame (**F3**) with the origin coinciding with the center of mass of the Trojan and the third axis parallel to the axis of greatest inertia of the body such that $\mathbf{\Omega} = [0, 0, \Omega]$. Let $\mathbf{s} = [s_x, s_y, s_z]$ be the position vector of the point mass P in this system of reference.

$$\ddot{\mathbf{s}} = -\frac{\partial U_1^{2b}(\mathbf{s})}{\partial \mathbf{s}}, \tag{2.70}$$

where $U_1^{2b}(\mathbf{s})$ is the inhomogeneous potential of the irregular body which will be formulated in terms of the spherical harmonics coefficient in Section 2.4.
System (2.70) is equivalent to the Hamiltonian system:

$$\begin{cases} \dot{\mathbf{s}} = \frac{\partial H_1^{2b}(\mathbf{s},\mathbf{S})}{\partial \mathbf{S}} \\ \dot{\mathbf{S}} = -\frac{\partial H_1^{2b}(\mathbf{s},\mathbf{S})}{\partial \mathbf{s}} \end{cases} \tag{2.71}$$

with *Hamiltonian*:

$$H_1^{2b}(\mathbf{s}, \mathbf{S}) = \tfrac{1}{2}|\mathbf{S}|^2 + U_1^{2b}(\mathbf{s}). \tag{2.72}$$

The formulation of the inhomogeneous potential $U_1^{2b}(\mathbf{s})$ generated by the irregular Trojan body, will be discussed in the Section 2.4.

2.3.2 Trojan centered, rotating reference frame

The Trojan centered rotating system of reference (**F4**) is now considered, rotating anticlockwise with angular velocity $\mathbf{\Omega} = [0, 0, \Omega]$. The change of coordinates is given by the matrix:

$$R'(t) = \begin{pmatrix} \cos(\Omega t) & \sin(\Omega t) & 0 \\ -\sin(\Omega t) & \cos(\Omega t) & 0 \\ 0 & 0 & 1 \end{pmatrix}, \tag{2.73}$$

which defines the position vector of the spacecraft $\mathbf{x} = [x, y, z]$ in the rotating system as:

$$\mathbf{x} = R'(t)\mathbf{s}. \tag{2.74}$$

In this system of reference the equations of motion in (2.70) become:

$$\begin{cases} \ddot{x} = \Omega^2 x + 2\Omega\dot{y} + \ddot{s}_x \cos t + \ddot{s}_y \sin t \\ \quad = \Omega^2 x + 2\Omega\dot{y} - \frac{\partial U(\mathbf{x})}{\partial x} \\ \ddot{y} = \Omega^2 y - 2\Omega\dot{x} - \ddot{s}_x \sin t + \ddot{s}_y \cos t \\ \quad = \Omega^2 y - 2\Omega\dot{x} - \frac{\partial U(\mathbf{x})}{\partial y} \\ \ddot{z} = \ddot{s}_z \\ \quad = -\frac{\partial U(\mathbf{x})}{\partial z}, \end{cases} \tag{2.75}$$

Equation (2.75) is equivalent to the Hamiltonian system:

$$\begin{cases} \dot{\mathbf{x}} = \frac{\partial H_2^{2b}(\mathbf{x},\mathbf{X})}{\partial \mathbf{X}} \\ \dot{\mathbf{X}} = -\frac{\partial H_2^{2b}(\mathbf{x},\mathbf{X})}{\partial \mathbf{x}} \end{cases} \tag{2.76}$$

with Hamiltonian

$$H_2^{2b}(\mathbf{x}, \mathbf{X}) := \frac{1}{2}|\mathbf{X}|^2 - \Omega\mathbf{x} \times \mathbf{X} + U_2^{2b}(\mathbf{x}), \tag{2.77}$$

in the conjugated variables $\mathbf{X}$, $\mathbf{x} \in \mathbb{R}^3$ with symplectic form $d\mathbf{X} \wedge d\mathbf{x}$, where, again, the potential $U_2^{2b}(\mathbf{x})$ will be discussed in Section 2.4.

2.3.3 The R2BP in Polar-Nodal coordinates

It is convenient to express the Hamiltonian and the perturbing potential using the so called nodal-polar variables [26] so that it may easily be transformed to the Delaunay coordinates in the later chapters.

. This set of variables, will here be indicated as $(r, \theta, \nu, R, \Theta, N)$, where r, θ, and ν are respectively the distance of the spacecraft from origin of the axes, the angular distance of the spacecraft from the line of the ascending node on the orbital plane, and the argument of nodes (see Fig. 2.6), while R, Θ, and N are their respective conjugate momenta.

Remark that this model spacecraft can move around the Trojan in the three dimensions, therefore the four variables used before to describe the system in polar coordinates are not sufficient.

The transformation required is given in [27]:

$$\begin{aligned}
x &= r(\cos\theta\cos\nu - \sin\theta\cos I\sin\nu)\\
y &= r(\cos\theta\sin\nu + \sin\theta\cos I\cos\nu)\\
z &= r\sin\theta\sin I\\
X &= (R\cos\theta - \tfrac{\Theta}{r}\sin\theta)\cos\nu - (R\sin\theta + \tfrac{\Theta}{r}\cos\theta)\cos I\sin\nu\\
Y &= (R\cos\theta - \tfrac{\Theta}{r}\sin\theta)\sin\nu + (R\sin\theta + \tfrac{\Theta}{r}\cos\theta)\cos I\cos\nu\\
Z &= (R\sin\theta + \tfrac{\Theta}{r}\cos\theta)\sin I
\end{aligned} \tag{2.78}$$

with $N = |\Theta|\cos I$.

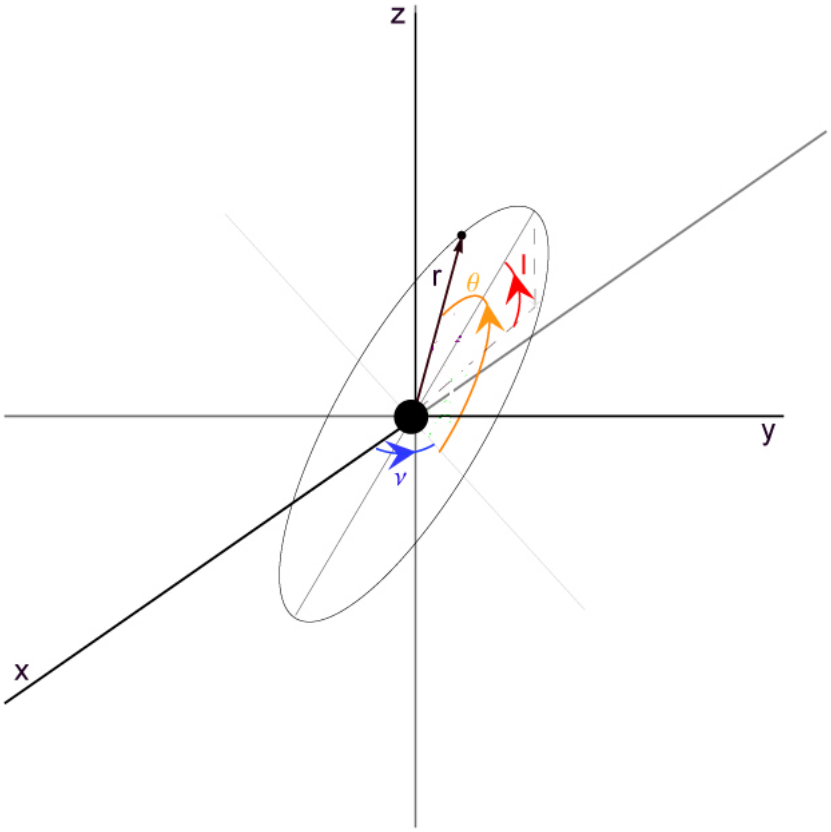

Figure 2.6: The Polar-Nodal angles

In these coordinates the Hamiltonian takes the form:

$$H_3^{2b}(r,\theta,\nu,R,\Theta,N) = \tfrac{1}{2}(R^2 + \tfrac{\Theta^2}{r^2}) - \Omega N + U_3^{2b}(r,\theta,\nu,\_,\Theta,N), \tag{2.79}$$

where $U_3^{2b}(r,\theta,\nu,\_,\Theta,N)$ is formulated in Section (2.4).

2.4 The gravitational potential

By Newton's Gravitational law the potential generated by a body of mass m_3 with **spherical symmetry** whose position vector is $\mathbf{x}_1$, on a particle set in $\mathbf{x}$ is given by:

$$U(\mathbf{x}) = -\frac{\mathcal{G}m_3}{|\mathbf{x}-\mathbf{x}_1|}, \tag{2.80}$$

which can be generalized for a discrete mass distribution of N masses $m_3^{(i)}$ whose position vector is $\mathbf{x}_i$, as the superimposition of the single potential of each mass:

$$U(\mathbf{x}) = -\sum_{i=1}^{N} \frac{\mathcal{G}m_3^{(i)}}{|\mathbf{x}-\mathbf{x}_i|} \tag{2.81}$$

An arbitrarily shaped body B of finite extension is now considered. The potential $U_2^{2b}(\mathbf{x})$ generated from such body, in the reference frame (**F4**) is firstly formulated. To this end denote with $\mathbf{x}' \in \mathbb{R}^3$ the position of the infinitesimal mass element dm_3 fixed in this reference frame.

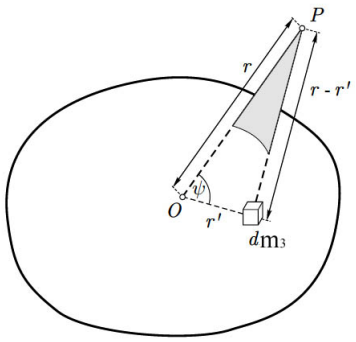

Figure 2.7: *The potential generated by an arbitrarily shaped body B is the integral over the volume the infinitesimal mass elements dm_3*

The gravity potential of such a continuous mass distribution on an external point P set in $\mathbf{x} \in \mathbb{R}^3$ can be obtained from (2.81) substituting the sum with an integral over the volume of the body, namely:

$$U(\mathbf{x}) = -\mathcal{G}\int_V \frac{\rho(\mathbf{x}')}{|\mathbf{x}-\mathbf{x}'|}dV \tag{2.82}$$

where $\rho(\mathbf{x}')$ is the density of the body and dV is the infinitesimal element of volume (i.e. $dm_3 = \rho(\mathbf{x}')dV$) and V is the volume of the body.
Notice that, to get back to (2.80) it is sufficient to impose the spherical symmetry property, that is the radial distribution of density $\rho(\hat{\mathbf{x}}) = \rho(-\hat{\mathbf{x}}), \quad \forall \hat{\mathbf{x}} \in B$.

With a few algebraic manipulations, calling $r = |\mathbf{x}|$ and $r' = |\mathbf{x}'|$, it can be shown that:

$$\begin{aligned} U(r, r', \psi) &= -\mathcal{G} \int_V \frac{\rho(\mathbf{x}')}{\sqrt{r^2 - 2\mathbf{x}\cdot\mathbf{x}' + r'^2}} dV \\ &= -\frac{\mathcal{G}}{r} \int_V \frac{\rho(\mathbf{x}')}{\sqrt{1 - 2\frac{r'}{r}\cos(\psi) + \left(\frac{r'}{r}\right)^2}} dV, \end{aligned} \tag{2.83}$$

where ψ is the colatitude of $\mathbf{x}'$ over $\mathbf{x}$ i.e. the angle between $\mathbf{x}$ and $\mathbf{x}'$.
Indicating with $P_n(\xi)$ the Legendre polynomial of degree n, the expansion

$$(1 - 2\xi\eta + \eta^2)^{-\frac{1}{2}} = \sum_{n=0}^{\infty} \eta^n P_n(\xi) \tag{2.84}$$

is now used, which can be demonstrated by the binomial theorem generalized for all exponents (other than only nonnegative integers).
Substituting $\xi = \cos(\psi)$ and $\eta = \frac{r'}{r}$ yields, for $\frac{r'}{r} < 1$ (ray of convergence of the series):

$$\frac{1}{\sqrt{1 - 2\frac{r'}{r}\cos(\psi) + \left(\frac{r'}{r}\right)^2}} = \sum_{n=0}^{\infty} \left(\frac{r'}{r}\right)^n P_n(\cos(\psi)). \tag{2.85}$$

Then, substituting into the potential (2.83), yields, for $\frac{r'}{r} < 1$:

$$U(r, \psi) = -\frac{\mathcal{G}}{r} \int_V \sum_{n=0}^{\infty} \left(\frac{r'}{r}\right)^n P_n(\cos(\psi))\rho(\mathbf{x}')dV. \tag{2.86}$$

The condition $\frac{r'}{r} < 1$ implies that the model is valid only outside the reference sphere that is the sphere circumscribing the asteroid.

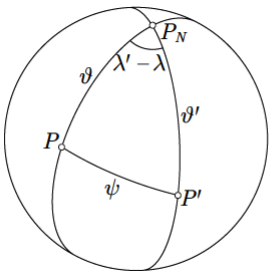

Figure 2.8: *The angle ψ can be expressed in terms of the* latitude δ *and* longitude λ

Expressing the angle ψ in terms of the *latitude* δ and *longitude* λ it is obtained that:

$$\cos\psi = \sin\delta\sin\delta' + \cos\delta\cos\delta'\cos(\lambda - \lambda') \tag{2.87}$$

and the generic Legendre Polynomial $P_n(\cos\psi)$ decomposes to:

$$P_n(\cos\psi) = \sum_{m=0}^{n} \left((2-\delta_{m,0}) \frac{(n-m)!}{(n+m)!} P_n^m(\sin\delta) P_n^m(\sin\delta') \cos\left(m(\lambda-\lambda')\right) \right) \tag{2.88}$$

(see [28]), where $P_n^m(x)$ is the associated Legendre function of degree n and order m and $\delta_{m,0}$ (different from the *latitude* δ) is the Kronecker delta that gives 1 if $m = 0$, and 0 elsewhere[1].
The potential becomes:

$$\begin{aligned} U(r,r',\delta,\lambda) = -\tfrac{\mathcal{G}}{r} \int_V \sum_{n=0}^{\infty} \left(\frac{r'}{r}\right)^n \sum_{m=0}^{n} \Bigg((2-\delta_{m,0}) \frac{(n-m)!}{(n+m)!} P_n^m(\sin\delta) P_n^m(\sin\delta') \cdot \\ \cdot \cos\left(m(\lambda-\lambda')\right) \Bigg) \rho(r',\delta',\lambda') dV \end{aligned} \tag{2.89}$$

Now, calling, $\forall 0 \le m \le n$:

$$\begin{aligned} C_{n,m} &= \tfrac{(2-\delta_{m,0})}{m_3} \tfrac{(n-m)!}{(n+m)!} \int_V \left(\frac{r'}{\alpha}\right)^n P_{n,m}(\sin\delta') \cos(m\lambda') \rho(r',\delta',\lambda') dV \\ S_{n,m} &= \tfrac{(2-\delta_{m,0})}{m_3} \tfrac{(n-m)!}{(n+m)!} \int_V \left(\frac{r'}{\alpha}\right)^n P_{n,m}(\sin\delta') \sin(m\lambda') \rho(r',\delta',\lambda') dV \end{aligned} \tag{2.90}$$

where α is a conventionally chosen reference radius and it has been used that $P_n^m = (-1)^m P_{n,m}$, to be consistent with [29]. Note that, in particular, the equations in (2.90) imply that:

$$\begin{aligned} &C_{0,0} = 1 \\ &C_{n,0} = \tfrac{1}{m_3} \int_V \left(\frac{r'}{\alpha}\right)^n P_n(\sin\delta') \rho(r',\delta',\lambda') dV \quad \forall n > 0 \\ &S_{n,0} = 0 \quad \forall n \ge 0 \end{aligned} \tag{2.91}$$

Moreover, as the origin of the system of reference is set in the center of mass of the asteroid, it can be demonstrated that the term $C_{1,0} = 0$.
The coefficients $C_{2,0}$ and $C_{2,2}$ express the "ellipticity" and "oblateness" of the body. Therefore it is found:

$$U(r,\delta,\lambda) = -\tfrac{\bar{M}}{r} \sum_{n=0}^{\infty} \left(\frac{\alpha}{r}\right)^n \sum_{m=0}^{n} (-1)^m \left(C_{n,m} \cos(m\lambda) + S_{n,m} \sin(m\lambda) \right) P_n^m(\sin\delta) \tag{2.92}$$

where $\bar{M} = \mathcal{G} m_3$.

[1] The index m must not be confused with any mass parameter.

Calling:

$$\begin{aligned}\bar{\mathcal{F}}^1_{n,m}(\lambda,\delta) &:= (-1)^m P_n^m(\sin\delta)\cos(m\lambda)\\ \bar{\mathcal{F}}^2_{n,m}(\lambda,\delta) &:= (-1)^m P_n^m(\sin\delta)\sin(m\lambda)\end{aligned}$$

where:

$$\begin{aligned}\bar{\mathcal{F}}^1_{n,m}(\lambda,\delta) &:= (-1)^m P_n^m(\sin\delta)\cos(m\lambda)\\ &= (\cos\delta)^m \tfrac{n!^2 m!^2}{2^n}\sum_{j=0}^{n}\sum_{\ell=\max\{0,j+m-n\}}^{\min\{j,m\}}\sum_{p=0}^{\lfloor\frac{m}{2}\rfloor}\Big((-1)^{j+\ell+p}\cdot\\ &\quad\cdot\tfrac{1}{(j)!(n-j)!\ell!(m-\ell)!(n-m-j+\ell)!(j-\ell)!(2p)!(m-2p)!}\cdot\\ &\quad\cdot(1+\sin\delta)^{n-m-j+\ell}(1-\sin\delta)^{j-\ell}\cos(\lambda)^{m-2p}\sin(\lambda)^{2p}\Big)\end{aligned} \tag{2.93}$$

$$\begin{aligned}\bar{\mathcal{F}}^2_{n,m}(\lambda,\delta) &:= (-1)^m P_n^m(\sin\delta)\sin(m\lambda)\\ &= (\cos\delta)^m \tfrac{n!^2 m!^2}{2^n}\sum_{j=0}^{n}\sum_{\ell=\max\{0,j+m-n\}}^{\min\{j,m\}}\sum_{p=0}^{\lfloor\frac{m-1}{2}\rfloor}\Big((-1)^{j+\ell+p}\cdot\\ &\quad\cdot\tfrac{1}{(j)!(n-j)!\ell!(m-\ell)!(n-m-j+\ell)!(j-\ell)!(2p+1)!(m-2p-1)!}\cdot\\ &\quad\cdot(1+\sin\delta)^{n-m-j+\ell}(1-\sin\delta)^{j-\ell}\cos(\lambda)^{m-2p-1}\sin(\lambda)^{2p+1}\Big),\end{aligned}$$

which can be demonstrated by: $\forall m\in\mathbb{N}$ the fact that:

$$\begin{aligned}\cos(mx) &= \sum_{p=0}^{\lfloor\frac{m}{2}\rfloor}\binom{m}{2p}(-1)^p\cos(x)^{m-2p}\sin(x)^{2p}\\ \sin(mx) &= \sum_{p=0}^{\lfloor\frac{m-1}{2}\rfloor}\binom{m}{2p+1}(-1)^p\cos(x)^{m-2p-1}\sin(x)^{2p+1}\end{aligned} \tag{2.94}$$

and

$$\begin{aligned}P_n^m(x) = (-1)^m(1-x^2)^{\frac{m}{2}}\tfrac{n!^2 m!^2}{2^n}\sum_{j=0}^{n}\sum_{\ell=\max\{0,j+m-n\}}^{\min\{j,m\}}&\Big((-1)^{j+\ell+p}\cdot\\ \cdot\tfrac{1}{(j)!(n-j)!\ell!(m-\ell)!(n-m-j+\ell)!(j-\ell)!}(1+x)^{n-m-j+\ell}&(1-x)^{j-\ell}\Big).\end{aligned} \tag{2.95}$$

The formulation for the potential, expressed in the reference frame (**F4**), to be substi-

tuted in (2.77), is thus obtained:

$$U_2^{2b}(\mathbf{x}) = U_2^{2b}(r,\delta,\lambda) = -\frac{\bar{M}}{r}\sum_{n=0}^{\infty}\left(\frac{\alpha}{r}\right)^n \sum_{m=0}^{n}\left(C_{n,m}\bar{\mathcal{F}}^1_{n,m}(\lambda,\delta) + S_{n,m}\bar{\mathcal{F}}^2_{n,m}(\lambda,\delta)\right) \tag{2.96}$$

in which the following relations must be considered:

$$\begin{aligned} r &= |\mathbf{x}| = \sqrt{x^2+y^2+z^2} \\ \cos\delta &= \frac{\sqrt{x^2+y^2}}{\sqrt{x^2+y^2+z^2}} \\ \sin\delta &= \frac{z}{\sqrt{x^2+y^2+z^2}} \\ \cos\lambda &= \frac{x}{\sqrt{x^2+y^2}} \\ \sin\lambda &= \frac{y}{\sqrt{x^2+y^2}} \end{aligned} \tag{2.97}$$

together with their inverse:

$$\begin{aligned} \sqrt{x^2+y^2} &= r\cos\delta \\ z &= r\sin\delta \\ x &= r\cos\delta\cos\lambda \\ y &= r\sin\lambda\cos\delta \end{aligned} \tag{2.98}$$

The potential is now expressed in the *Nodal-Polar* coordinates, by (2.78), which yields:

$$\begin{aligned} \mathcal{F}^1_{n,m}(I,\theta,\nu) = \tfrac{1}{2^n} m!^2 n!^2 \sum_{j=0}^{n}\sum_{\ell=\max\{0,j+m-n\}}^{\min\{j,m\}}\sum_{p=0}^{\lfloor\frac{m}{2}\rfloor}\Big((-1)^{j+\ell+p}\cdot \\ \cdot\left(\frac{1}{j!(n-j)!\ell!(m-\ell)!(n-m-j+\ell)!(j-\ell)!(2p)!(m-2p)!}\right)(1+\sin(\theta)\sin(I))^{n-m-j+\ell}\cdot \\ \cdot(1-\sin(\theta)\sin(I))^{j-\ell}(\cos(\theta)\cos\nu-\cos(I)\sin(\theta)\sin(\nu))^{m-2p}\cdot \\ \cdot(\cos(\theta)\sin(\nu)+\cos(I)\sin(\theta)\cos(\nu))^{2p}\Big) \end{aligned} \tag{2.99}$$

and

$$\begin{aligned}\mathcal{F}^2_{k,m}(I,\theta,\nu) = \tfrac{1}{2^n} m!^2 n!^2 \sum_{j=0}^{n} \sum_{\ell=\max\{0,j+m-n\}}^{\min\{j,m\}} \sum_{p=0}^{\lfloor \frac{m-1}{2} \rfloor} \Big((-1)^{j+\ell+p} \cdot \\ \cdot \Big(\tfrac{1}{j!(n-j)!\ell!(m-\ell)!(n-m-j+\ell)!(j-\ell)!(2p+1)!(m-2p-1)!} \Big) \cdot \\ \cdot (1+\sin(\theta)\sin(I))^{n-m-j+\ell} (1-\sin(\theta)\sin(I))^{j-\ell} \cdot \\ \cdot (\cos(\theta)\cos\nu - \cos(I)\sin(\theta)\sin(\nu))^{m-2p-1} \cdot \\ \cdot (\cos(\theta)\sin(\nu) + \cos(I)\sin(\theta)\cos(\nu))^{2p+1} \Big)\end{aligned} \tag{2.100}$$

where it should be noted that, in $\mathcal{F}^1_{n,m}(\lambda,\delta)$, the term $\left(\frac{1}{D}\right)^m$, with $D = \sqrt{\cos\theta^2 + \cos I^2 \sin\theta^2}$, arising from $\cos(\lambda)^{m-2p}\sin(\lambda)^{2p}$ in (2.93) cancels with the $(\cos\delta)^m = D^m$ in the same formula; analogously in $\mathcal{F}^2_{n,m}(\lambda,\delta)$, where $\left(\frac{1}{D}\right)^m$ arises from

$$\cos(\lambda)^{m-2p-1}\sin(\lambda)^{2p+1}.$$

The potential becomes:

$$U_3^{2b}(r,\theta,\nu,\_,\Theta,N) = -\tfrac{\bar{M}}{r}\sum_{n=0}^{\infty}\left(\frac{\alpha}{r}\right)^n \sum_{m=0}^{n}\left(C_{n,m}\mathcal{F}^1_{n,m}(I,\theta,\nu) + S_{n,m}\mathcal{F}^2_{n,m}(I,\theta,\nu)\right), \tag{2.101}$$

which has to be substituted into (2.79).

The same potential can also be derived using the addition formula for non scaled spherical harmonics [29] and Wigner's rotation theorem for non scaled spherical harmonics [30]. This derivation, see Appendix A, leads to:

$$\begin{aligned}\bar{U}(r,\theta,\nu,\_,\Theta,N) = -\sum_{n=0}^{\infty}\sum_{m=0}^{n}\sum_{j=-n}^{n}\sum_{t=\max\{0,j+m\}}^{\min\{n+m,n+j\}} ci^{2n+m+j-2t} si^{2t-m-j} \cdot \\ \cdot \tfrac{1}{r^{n+1}} \left(\mathcal{A}_{n,m,j,t}\cos(m\nu - j\theta) + \mathcal{B}_{n,m,j,t}\sin(m\nu - j\theta)\right),\end{aligned} \tag{2.102}$$

where

$$\begin{aligned} ci &:= ci(N,\Theta) = \cos\left(\tfrac{I}{2}\right) = \sqrt{\tfrac{1+\cos I}{2}} = \sqrt{\tfrac{1+\frac{N}{\Theta}}{2}} \\ si &:= si(N,\Theta) = \sin\left(\tfrac{I}{2}\right) = \sqrt{\tfrac{1-\cos I}{2}} = \sqrt{\tfrac{1-\frac{N}{\Theta}}{2}} \end{aligned} \tag{2.103}$$

and:

$$\begin{aligned}\mathcal{A}_{n,m,j,t} &= \bar{\mathcal{G}}_{n,m,j,t}\left(C_{n,m}\cos\left(\tfrac{\pi}{2}(j+m)\right) - S_{n,m}\sin\left(\tfrac{\pi}{2}(j+m)\right)\right)\\ \mathcal{B}_{n,m,j,t} &= \bar{\mathcal{G}}_{n,m,j,t}\left(C_{n,m}\sin\left(\tfrac{\pi}{2}(j+m)\right) + S_{n,m}\cos\left(\tfrac{\pi}{2}(j+m)\right)\right),\end{aligned} \tag{2.104}$$

and

$$\begin{aligned}\bar{\mathcal{G}}_{n,m,j,t} = (-1)^{m+3t-j+1}\bar{M}\alpha^n \tfrac{(n+m)!(n-j)!}{t!(n+j-t)!(n+m-t)!(t-m-j)!}(-1)^{\frac{n+j}{2}}\tfrac{1}{2^n}\tfrac{(n+j)!}{(\frac{n+j}{2})!(\frac{n-j}{2})!}\cdot\\ \cdot((n+j)_{mod_2}-1)\end{aligned} \tag{2.105}$$

where α is a conventionally chosen reference radius, usually taken as the radius of the circumscribing sphere of the small body and x_{mod_y} stands for the value of x modulus y, i.e. the integer reminder of the division of x by y, and where $C_{n,m}$ and $S_{n,m}$ as in (2.90).

This formulation can be shown to be completely equivalent to the one in (2.101) and will be used hereafter.

Chapter 3

The WSB and the range of validity of the two models

In this chapter the range of applicability of the two models, the inhomogeneous Restricted Two Body Problem and the Lagrangian CR4BP, is estimated as an application of the WSB. This is only a minor application of the theory concerning the WSB concept which is introduced and developed in this Chapter.

3.1 WSB: state of art

In January 1990 Japan's ISAS Institute launched a pair of small spacecraft linked together into an elliptic Earth orbit. The smaller one, called MUSES-B, detached and lost communication connections; it was supposed to go to the Moon and into lunar orbit using a Hohmann transfer. The larger craft, MUSES-A, still orbiting the Earth, was meant to send and collect communications to and from MUSES-B and perform scientific experiments while in Earth orbit. It was then desired by the ISAS Institute to try to get MUSES-A to the Moon as a replacement for MUSES-B, with a desired lunar periapsis radius at capture r equal to $r_{Moon} + 100km$. MUSES-A was never designed to go to the Moon, and therefore it had a very small ΔV capability of approximately 100 meters per second (m/s), far less than what is necessary to be placed into lunar orbit using an Hohmann transfer. A solution was found by Belbruno and Miller [31] at the Jet Propulsion Laboratory (JPL) in June 1990 to enable MUSES-A, renamed Hiten, to reach the Moon on a ballistic capture transfer to the region $\mathcal{W}$, thus named lunar Weak Stability Boundary. This transfer rescued the Japanese lunar mission; without it, there was not enough ΔV to get Hiten to the Moon by any other means. Since then low energy interplanetary transfers by means of WSB have been widely studied (see for example: [32], [33], [8] and [34]), particularly, arousing the interest in designing lunar trajectories ([35], [36], [37] and [38]) or to reach other systems of planets [39]. Many

different ways have been proposed for designing them ([40], [41], [42], [43]). All of these techniques for ballistic capture transfers used this "fuzzy" set, the WSB, upon arrival. Moreover, the Weak Stability Boundary theory has been applied to ESA's spacecraft SMART-1 in 2004 [44], in NASA's GRAIL mission in 2010 and will be applied again in ESA's BepiColombo mission to explore the planet Mercury [45].

There exist a wide range of descriptions of the WSB, which may (and sometimes may not) help to get a general idea of this Cantor-recalling set. Among them "*a generalization of the Lagrange points and a complicated region surrounding the Moon*[1]" [31], or "*a region in phase space supporting a special type of chaotic motion for special choices of elliptic initial conditions with respect to* m_2" [8]. Moreover "*a transition region between the gravitational capture and escape from the Moon in the phase space*" [46] which *"supports transitory behavior and the motion associated with this region is both unstable and chaotic in nature"* [47]. Independently from their utility in clarifying the concept of WSB, these descriptions highlight the complexity of its mathematical structure.

Edward Belbruno, in [8], was the first to formulate the algorithmic definition of WSB, presenting its geometry for the Earth-Moon-spacecraft CR3BP, planar case, in terms of the initial eccentricity, pericenter, altitude and Jacobi constant of the osculating orbit. Then García and Gómez in [9] provided a new definition, again algorithmic, which addressed all the inadequacies of the previous one (see Section 3.3.2), and gave numerical evidence of the shape of the WSB arising from their definition. Moreover they introduced a generalisation of this concept: the n^{th} WSB. This is obtained by monitoring the stability of a trajectory about the Moon after n-cycles, instead of 1 cycle as in [8], and collecting the n boundaries obtained. This generalized boundary has an interesting fractal appearance and, as conjectured in [48], may be related to the limit set resulting from the invariant manifolds of the Lyapunov orbits associated to L_1 and L_2 near the target planet. Such a connection was already suggested in the 1960's by Conley. He also conjectured the weak capture for the Earth-Moon-spacecraft R3BP, suggesting that the invariant manifold structure associated to the unstable collinear Lagrange points would have to somehow play a role, although he didn't provide any demonstration. If proved to be true, that would be a surprising result, providing a new approach for studying such limit sets in general, with a consequent number of promising applications to mission design and dynamical astronomy.

However, the nature of the weak stability boundary and its associated dynamics has not been well understood yet [47], meaning that to give any estimate on this complicated global limit set normally requires extensive numerical computations.

[1] As it is mainly applied to the Earth-Moon-Spacecraft CR3BP, the descriptions are usually referred to the Moon as the target body (m_2).

3.2 Introduction and main results

As, thus far, the existing definitions and theories on the WSB are all algorithmic and therefore can only be studied in a numerical way, no general, topological properties can be deduced by them. This implies, in particular, that the WSB, as it can be found in the literature, cannot be used for aim of this Chapter: apply the WSB to estimate analytically the range of the stable orbits. Indeed, to get this estimation, which will then be used in the next chapters as the estimation of the set of applicability of the two dynamical models proposed, an analytical definition of the WSB set is needed. To this end, in this thesis a completely new, analytical definition of the WSB, coherent with the previous algorithmic definitions, is built in Section 3. Moreover this theory, usually applied to the Earth-Moon-Spacecraft CR3BP, is here generalized, in view of the applications, to the Lagrangian autonomous, coplanar CR4BP, therefore representing a double step further in the development of this theory. However, setting the mass parameter of the smaller primary to zero, its usual setting, the CR3BP, can be obtained back. The new, analytical definition introduced in this thesis is then also compared with previous definitions of WSB from the literature, which highlights the improvements brought by the analytic definition. Furthermore, as such new definition is analytic, it allows for the first time some generic topological properties of the WSB to be deduced, which are here discussed as well. Then the symplectic Delaunay coordinates, unusual for the WSB theories (i.e. not used in the previous literature), are here used to rewrite the problem. It results that these coordinates are suitable for estimating analytically the WSB and, consequently, the range of validity of the two models[2]. The analytic estimates on the Hamiltonian vector field in Delaunay variables are enabled by the assumption that, if the spacecraft starts close enough to the smaller primary, then the mean anomaly is a so called "fast angle". As these estimates are based on the set of stable orbits around the smaller primary, they provide a highly accurate description of this region.

[2]For low values of the eccentricity good stability estimates can be obtained working with the usual polar coordinates. The range of applicability of the models will here be estimated for eccentricities $e_0 > \frac{1}{2}$ as these lead, in general, to worse estimates (i.e. to a smaller set in which the dynamics can be considered as dominated by the sole smaller primary). In this case the stability estimates deteriorate and polar coordinates are no longer convenient for analytic estimates.

3.3 Various definitions of the WSB

Three main definitions of Weak Stability Boundaries are introduced in this section. The first is the algorithmic definition given by Belbruno (see for example [8]). The second is the modified version given in [9], which corrects and completes the former, although it is still algorithmic. Finally the latter is a new, analytic definition of the WSB, followed by a topological analysis of it and a comparison with the previous definitions, which represents one of the novelties of this thesis. All these definitions are based on the concept of "ballistic capture", here presented as well, following the definition in [8]. Ballistic capture is based on monitoring the sign of Kepler's energy function of the target body-spacecraft system, for which, in Chapter 2, various formulations have been found, for different reference frames, all equivalent to the one given in [8].

3.3.1 Belbruno's definition of WSB

Consider a solution $\psi(t)$ of the Hamiltonians (2.28), (2.38) or (2.42). Note that it is not important to specify which one among $H_1(\mathbf{s}, \mathbf{S}; t)$, $H_2(\mathbf{x}, \mathbf{X})$ or $H_3(r, \theta, R, \Theta)$ is being considered since they are related by symplectic changes of variables. Obviously $H^M = H_i^M \ for\ some\ i = 1, 2, 3$, the two-body keplerian energy, must be intended in the same variables of the corresponding Hamiltonian.

Definition 2 *(Ballistic Capture)*
Given $0 < t_1 < \infty$. A Spacecraft is said to be ballistically captured by a primary in $t = t_1$ if

$$H^M(\psi(t_1)) \leq 0\,. \tag{3.1}$$

Definition 3 *(Osculating ellipse)*
*In the asteroid centered frame (**F1**) the* osculating ellipse*, is the orbit made by the spacecraft around the asteroid in the asteroid-spacecraft two-body system (i.e. neglecting the other two primaries) with negative energy. In it the asteroid is set in one of the foci of the ellipse. In other words it is like considering the motions of the Hamiltonian H^M when the energy is negative.*

Recalling the relation between the orbital elements of the osculating ellipse (see, e.g., [25] for details): the eccentricity e, the energy E, the major semi-axis a, the minimal r_{min} and maximal r_{max} distance from the asteroid (pericenter and apocenter respectively) are:

$$E = -\frac{\mu m}{2a}\,, \qquad r_{min} = a(1-e)\,, \qquad r_{max} = a(1+e)\,. \tag{3.2}$$

Definition 4 *((r_0, e_0, ϑ_0)-Test orbit)*
*In (**F2**) consider radial line l emanating from the asteroid (see Fig.3.1) and inclined of an angle $\vartheta_0 \in S^1$ with respect to the axis x', which is the axis passing through the asteroid and parallel to one joining the other two primaries (see Fig.2.1). Then the*

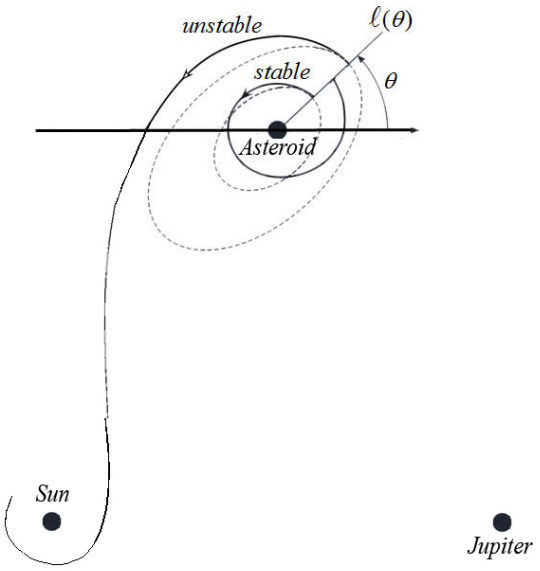

Figure 3.1: **Stable and unstable test-orbits**

((r_0, e_0, ϑ_0)-Test orbit) is the trajectory of the spacecraft which, at time $t = 0$:

- *departs from the line l at a distance $r_0 > 0$ from the Trojan*
- *is at the pericenter or at the apocenter of the osculating ellipse, i.e. its initial velocity vector is normal to the line l, pointing in the direct or retrograde direction*
- *with a fixed initial eccentricity[3] $e_0 \in [0, 1]$.*

Therefore the initial conditions in polar coordinates are (recalling (2.44) and (3.2)):

$$R(0) = 0\,, \quad \Theta(0) = \pm\mu\sqrt{mr_0(1 \pm e)}\,, \quad r(0) = r_0\,, \quad \theta(0) = \vartheta_0\,, \tag{3.3}$$

where in $\Theta(0)$ the first $\pm$ is $+$ in the direct direction and $-$ in the retrograde one and the second $\pm$ depends if one is at the pericenter or at the apocenter.

Definition 5 *(Stability)*
A test orbit is said to be stable about the asteroid if, after leaving l, makes a full cycle

[3]This implies that the two body Kepler energy is negative.

about the asteroid in a time $T > 0$ without going around any of the other two primaries (or crashing into it) and returns to a point on l with $H^M(\psi(T)) \leq 0$.

Definition 6 *(Instability)*
A test orbit is said to be unstable about the asteroid if:

- *it performs a full cycle around the asteroid without going around any of the other two primaries and returns to a point on l with $H^M > 0$*
- *the Spacecraft moves away from the asteroid towards any of the other two primaries and makes a full cycle about it or collides with it.*

The stability definition above corresponds to the ballistic capture with respect to the asteroid given in Definition 2 at time both 0 and T ("ballistic capture transfer"). The first condition of instability is called ballistic escape from the asteroid, while the second is called primary interchange escape.

For every fixed $(e, \theta) \in [0, 1] \times S^1$ Belbruno claims [8] that it is possible to find numerically a finite distance $r' = r'(e, \theta) > 0$ from the target planet such that a (r, e, θ)-test orbit is

$$\text{stable if } \; r < r'(e, \theta)\,, \qquad \text{unstable if } \; r > r'(e, \theta)\,. \tag{3.4}$$

Definition 7 *(Belbruno's WSB)*

$$\mathcal{W} := \left\{(r, e, \theta) \in \mathbb{R}^+ \times [0, 1] \times S^1 \;\text{ s.t. }\; r = r'(e, \theta)\right\}.$$

Note that $\mathcal{W}$ is a two dimensional stability transition region of position and velocity, which has two components corresponding to the direct and retrograde motions.

3.3.2 García-Gómez definition of WSB

García and Gómez, in [9], stress some lack of accuracy in Belbruno's definitions. One regards the definition of unstable orbits and the other the definition of the radius of the change of stability $r'(\theta, e)$.
More precisely, the latter arises from noticing that Definition 7 is not exhaustive of the complementary set of the Stable orbits as given in Definition 6. Therefore a more general definition of instability is adapted in [9], where is defined as unstable any orbit that does not fulfill the Stability criterion. On the other hand, they highlight that it is not clear how, for fixed values of θ and e there exists a unique finite distance $r'(\theta, e)$ defining the boundary between stable and unstable orbits. In fact it is shown in the paper that for each fixed inclination and eccentricity there are many changes from stability to instability and that the set of the stable points recalls a Cantor set.
Then, in [9], an extended definition of WSB is proposed:

Definition 8 *(García-Gómez WSB)*
$\forall (e,\theta) \in [0,2\pi] \times [0,1]$ *there exist a finite number of points (up to a certain precision)* $r_1^* = 0, r_2^* = r_2^*(e,\theta), ..., r_{2n}^* = r_{2n(e,\theta)}^*$ *such that if* r *belongs to*

$$S^*(e,\theta) := \bigcup_{1 \le j \le n} [r_{2j-1}^*, r_{2j}^*] \tag{3.5}$$

the motion of a (r,e,θ)*-test orbit is stable according to Definition 5 otherwise it is unstable. Then the WSB is defined as:*

$$\mathcal{W} := \left\{(r,e,\theta) \in \mathbb{R}^+ \times [0,1] \times S^1 \text{ s.t. } r \in \mathcal{W}(e,\theta)\right\} \quad \text{where} \quad \mathcal{W}(e,\theta) := \partial S^*(e,\theta) \subset \mathbb{R}^+ . \tag{3.6}$$

The number of points r_i^* and their values, varies with the values of θ and e, as well as with the precision of computation.

As $r_1^* = 0$, the radius $r_2^*(e,\theta)$, for each fixed θ and e, represents the bigger radius such that $\forall\, 0 < r < r_2^*(e,\theta)$, a (r,e,θ)-test orbit is stable. Therefore, $\forall \theta$, e fixed, $r_2^*(e,\theta)$ could be seen as a lower limit of the WSB. However, as the stability/instability of an orbit is determined in a purely numerical way, all these properties would be true only *limited to a certain precision*[4], which means that nothing prevents an unstable test orbit to be found in the stable interval $(0, r_2^*(e,\theta)]$, once the precision has been increased. In Section 3.5 some analytic estimates on $r_2^*(e,\theta)$ (i.e. with "infinite" precision) will be given.

3.3.3 The new analytical definition of WSB

Remark 1 *In the following the only component of the WSB to be considered will be the one generated by direct motions; analogous consideration for the retrograde motions are possible (leading to better stability estimates in Section 3.5).*

Interesting topological considerations on the WSB are possible if Definition 5 is modified by adding the request that the angular velocity $\dot{\vartheta}(T)$ of the test orbit (see Definition 4) at the time $T > 0$ of first return to the line l (after making a full cycle around the asteroid) is *strictly* positive, namely $\dot{\vartheta}(T) > 0$. This "transversality" condition is (sometimes) implicitly assumed by Belbruno and [9] and explicitly by Topputo [34].

[4]Note that Belbruno's definition of WSB is affected by the same dependence from the accuracy of the numerical evaluation

For $(e,\theta) \in [0,1] \times S^1$ it is set

$$S = S(e,\theta) \;:=\; \{r > 0 \;\; s.t. \;\; \text{the } (r,e,\theta)-\text{test orbit is stable according to Definition 5} \\ \text{and} \;\; \dot{\vartheta}(T) > 0\}\,. \tag{3.7}$$

Then the new, analytical definition of the WSB is:

Definition 9

$$\mathcal{W} := \big\{(r,e,\theta) \in \mathbb{R}^+ \times [0,1] \times S^1 \;\; \text{s.t.} \;\; r \in \mathcal{W}(e,\theta)\big\} \quad \text{where} \quad \mathcal{W}(e,\theta) := \partial S(e,\theta) \subset \mathbb{R}^+\,. \tag{3.8}$$

The relation between the analytic definition of the WSB and the previous ones, that are algorithmic in nature, is now investigated.
Given a $\delta > 0$ it is defined a subset $S_\delta(e,\theta)$ of $S(e,\theta)$, which is a "δ-approximation" of $S(e,\theta)$. By Proposition 1 $S(e,\theta)$ is the disjoint union of at most countable open intervals $I_j(e,\theta)$, $0 \le j < j(e,\theta)$ (where $j(e,\theta) \in \mathbb{N} \cup \{\infty\}$), with $I_0(e,\theta) = (0, r^*(e,\theta))$, plus at most a countable set of points. Therefore

$$\text{meas}\big(S(e,\theta)\big) = \sum_{0 \le j < j(e,\theta)} \text{meas}\big(I_j(e,\theta)\big)\,. \tag{3.9}$$

Then, there exists[5] $j_\delta < j(e,\theta)$ such that

$$S_\delta(e,\theta) := \bigcup_{0 \le j \le j_\delta} I_j(e,\theta) \subseteq S(e,\theta) \tag{3.10}$$

satisfies

$$\text{meas}\big(S_\delta(e,\theta)\big) \ge \text{meas}\big(S(e,\theta)\big) - \delta\,. \tag{3.11}$$

Consequently it can be defined a "δ-approximation" of the weak stability boundary setting

$$\mathcal{W}_\delta := \big\{(r,e,\theta) \in \mathbb{R}^+ \times [0,1] \times S^1 \;\; \text{s.t.} \;\; r \in \mathcal{W}_\delta(e,\theta)\big\} \quad \text{where} \quad \mathcal{W}_\delta(e,\theta) := \partial S_\delta(e,\theta)\,. \tag{3.12}$$

Remark 2 *If $\delta > 0$ is the "computational error" the sets $S^*(e,\theta)$ in (3.5) and $S_\delta(e,\theta)$ have the same form, being finite union of disjoint intervals[6]. The same holds for $\mathcal{W}, \mathcal{W}(e,\theta)$ in (3.6) and $\mathcal{W}_\delta, \mathcal{W}_\delta(e,\theta)$ above.*

[5] If $j(e,\theta) < \infty$ one can take $j_\delta = j(e,\theta) - 1$.

[6] The fact that the intervals in (3.5) contain their endpoints is irrelevant since it does not affect the boundary.

3.4 The topology of the WSB

The topology of the stable set $S(e,\theta)$ is firstly considered (recall (3.7)), initially showing that $S(e,\theta)$ is bounded.

Lemma 1 *If r_0 is large enough (independently from e and θ), a (r_0,e,θ)-test orbit is never stable, according to Definition 5. In particular, for every (e,θ) fixed, $S(e,\theta)$ is a bounded subset of $\mathbb{R}^+$.*

Proof Assume that[7] $r_0 \geq 10^4$. It is claimed that $\forall\, 0 \leq t \leq 4\pi$

$$\frac{r_0}{2} < r(t) < 2r_0\,, \qquad |\Theta(t)| < 30\mu r_0\,. \tag{3.13}$$

By the Hamilton's equation for the Hamiltonian $H_3(r,\theta,R,\Theta)$ in (2.42) it is found:

$$\dot\theta = \frac{\Theta}{\mu r^2} - 1\,, \quad |\dot\Theta| \leq \frac{2\mu r}{|r-1|^3} + \mu r\,, \quad |\ddot r| \leq \frac{\Theta^2}{\mu^2 r^3} + \frac{1}{r^2} + \frac{r+1}{|r-1|^3} + 1\,. \tag{3.14}$$

Let us prove (3.13) by contradiction. Assume that there exists $0 < T < 4\pi$ such that (3.13) holds $\forall\ 0 < t < T$ and does not hold for $t = T$. Then $\forall\, 0 < t < T$ it results

$$|\dot\Theta| \leq \mu(3 + 2r_0)\,, \quad |\ddot r| \leq \frac{8\Theta^2}{\mu^2 r_0^3} + \frac{4}{r_0^2} + 3. \tag{3.15}$$

Which yields

$$|\Theta(t)| \leq \Theta_0 + 4\pi\mu(3+2r_0) \overset{By(3.3)}{\leq} \mu\sqrt{2r_0} + 28\mu r_0 \leq 29\mu r_0\,, \tag{3.16}$$

and

$$|\ddot r| \leq \frac{7200}{r_0} + \frac{4}{r_0^2} + 3 \leq 4 \quad \Longrightarrow \quad |r(t) - r_0| \leq 4\frac{T^2}{2} \leq 32\pi^2 \leq \frac{r_0}{3} \tag{3.17}$$

$\forall\, 0 < t < T$. Then yields

$$|\Theta(T)| \leq 29\mu r_0\,, \quad |r(T) - r_0| \leq \frac{r_0}{3} \tag{3.18}$$

namely (3.13) still holds for $t = T$, which is a contradiction. Recollecting it has been proved (3.13).

By (3.14) it is found that $\forall\, 0 \leq t \leq 4\pi$

$$\dot\vartheta(t) \leq \frac{120}{r_0} - 1 \leq -\frac{1}{2}\,. \tag{3.19}$$

[7] Obviously no effort has been made in obtaining the best value of r_0, since the aim of this study is only in its existence.

This means that the orbit makes a clockwise turn around the origin in a time $0 < T_* \leq 4\pi$. In particular, since $r(t) \geq 5000$, it makes a clockwise turn around the three primaries, and therefore it is not stable (according to Definition 5).

Proposition 1 *For every $(e,\theta) \in (0,1) \times S^1$, $S(e,\theta)$ is a bounded set formed by at most a countable disjoint union of open intervals plus at most a countable set of points. Moreover there exists $r^*(e) > 0$ such that $S(e,\theta) \supset \big(0, r^*(e)\big)$.*

Proof

Fix $(e,\theta) \in (0,1) \times S^1$. If $\bar{r} \in S(e,\theta)$ the first time T of return on l after making a circle around the asteroid is an analytic function of r in an open neighborhood of $\bar{r}$.

Denoting $\psi(t;\bar{r}) = \psi(t;\bar{r},e,\theta)$ the flow of the $(\bar{r},e,\theta)$-test orbit. Let $\vartheta(t;\bar{r})$ be its ϑ-component. Indeed if $\bar{T}$ is the first time of return w.r.t. $\bar{r}$ then, *using the transversality condition*

$$\vartheta(\bar{T};\bar{r}) = \theta\,, \qquad \partial_T \vartheta(\bar{T};\bar{r}) = \dot{\vartheta}(\bar{T};\bar{r}) > 0 \tag{3.20}$$

and the implicit function theorem (in analytic class[8]) is applicable to the equation

$$\vartheta(T;r) = \theta\,. \tag{3.21}$$

Then an analytic function $T = T(r)$ is found such that $\vartheta(T(r);r) = \theta$ for every r in an open neighborhood of $\bar{r}$.

Define

$$S_{<0} = S_{<0}(e,\theta) := \{r \in S(e,\theta) \;\; s.t. \;\; H^M(\psi(T;r)) < 0\} \tag{3.22}$$

$$S_{=0} = S_{=0}(e,\theta) := \{r \in S(e,\theta) \;\; s.t. \;\; H^M(\psi(T;r)) = 0\}\,. \tag{3.23}$$

Obviously $S = S_{<0} \cup S_{=0}$.

Note that $S_{<0}$ is an open subset of $\mathbb{R}^+$. If $\bar{r} \in S_{<0}$, for every r in an open neighborhood of $\bar{r}$, $T(r)$ is well defined, $\dot{\vartheta}(T(r);r) > 0$ and $H(\psi(T(r);r)) < 0$ by continuity, since the Hamiltonian flow is a diffeomorphism.

The topology of $S_{=0}$ is more involved. Assume that $\bar{r} \in S_{=0}$. Still for every $r \in (\bar{r}-\epsilon, \bar{r}+\epsilon)$ (with ϵ small enough), $T(r)$ is well defined and $\dot{\vartheta}(T(r);r) > 0$ by continuity. Consider the analytic function

$$h(r) := H(\psi(T(r);r))\,. \tag{3.24}$$

Taking $r \in (\bar{r}-\epsilon, \bar{r}+\epsilon)$; then $r \in S_{=0}$ iff $h(r) = 0$. Since h is analytic, two cases are possible: h is identically zero on $(\bar{r}-\epsilon, \bar{r}+\epsilon)$ or there are at most a finite number of zeros in $[\bar{r}-\epsilon/2, \bar{r}+\epsilon/2]$. Consequently any point of $S_{=0}$ is an inner point or an isolated point. Since the number of isolated points of a subset of $\mathbb{R}$ is at most countable[9], $S_{=0}$

[8] Note that $\vartheta(T;r)$ is an analytic function of T and r, since the Hamiltonian flow is analytic.

[9] Since it can be covered by a union of disjoint open intervals.

is an open set plus, at most, a countable set of points. The same holds for S.

Note that, by standard measure theory arguments, any open subset of $\mathbb{R}^+$ is formed by at most a countable disjoint union of open intervals (with at most one unbounded interval).

It will be proved later (see Corollary[10] 1) that, if r is small enough (uniformly on e and θ), then $r \in S_{<0}$. Moreover S is bounded by Lemma 1. The proof of Proposition 1 is now completed.

Remark 3 *It is conceivable that for some e, θ the set $S(e, \theta)$ does possess isolated points, however to prove it is not straightforward.*

3.5 Analytic estimates on the stable zone around the Trojan

As the aim of this chapter is to estimate the range of applicability of the two models which will be analysed later, as an application of the WSB, a realistic, analytic estimate from below on r^*, as defined in Proposition 1, will, in this section, be derived. This, being an estimation of the set of the stable orbits, will therefore be used as an estimation of the set in which the dynamics can be modeled using the sole Trojan, and neglecting the gravitational influence of the other two primaries.
For low values of the eccentricity good stability estimates can be obtained working with the usual polar coordinates (see the reference frame (**F2**)). However, in view of the applications (i.e. determining the range of validity of the inhomogeneous R2BP), we will focus on the eccentricities $e_0 > \frac{1}{2}$ as they lead to smaller estimations of the stable set. In this case the stability estimates deteriorate, moreover polar coordinates are not convenient for analytic estimates anymore. Thus symplectic Delaunay coordinates are thus used, which are suitable for analytic estimates in the relatively large eccentricity regimes. Therefore some analytic estimates on the Hamiltonian vector field in Delaunay variables (see Lemma 2) are found, using the assumption that, if the spacecraft starts quite close to the Trojan, then the "mean anomaly" is a so called "fast angle". This means that the Spacecraft actually comes back to the starting line l in a time of first return T which is quite short, allowing to estimate the variation of all the other variables over one revolution. Such estimates allow the formulation of the stability properties stated in Proposition 2, which leads to the desired estimate from below on $r^*(e)$ contained in Corollary 1.

The system in the Delaunay coordinates has already been derived in (2.55), with the corresponding two body keplerian energy (2.57).

[10] Actually in Corollary 1 the only case considered is when the eccentricity is larger than 1/2, as the case of eccentricity smaller than 1/2 is simpler (see Remark 4).

Notice that, by construction, Delaunay variables describe only motions with $H^M < 0$. This is not a problem here. As a matter of fact the aim of the next sections of this chapter is to show (analytically) that orbits starting sufficiently close to the Trojan are stable according to Definition 5.

By the fact that $L = \mu\sqrt{ma}$ and (2.47) it is found that:

$$r = a(1 - e\cos u) = m^{\frac{1}{3}}L^2(1 - e\cos u) \tag{3.25}$$

and therefore, by (2.57):

$$H^M = -\frac{m^{\frac{1}{3}}(1 - e\cos u)}{2r}\,, \tag{3.26}$$

which at the pericenter, namely when $f = u = \ell = 0$, is

$$H^M = -\frac{m^{\frac{1}{3}}(1 - e)}{2r}\,, \tag{3.27}$$

which differs from the one usually adopted by Belbruno $H^M = -\frac{m(1-e)}{2r}$ by a positive mass factor $m^{\frac{2}{3}}$, but, as the interest of this study is focused on the sign of this function, here the two are essentially equivalent.

By (2.50) the angle ϑ as function of the Delaunay variables is

$$\vartheta = f + g\,, \tag{3.28}$$

since $f+g$ is the angle between the Trojan-Spacecraft and the axes passing through the asteroid and parallel to the line connecting the two main primaries (see Figure (2.5)). In the rotating frame (**F2**) an orbit $(r(t), \vartheta(t))$ of the Spacecraft starting at time $t = t_0$ *makes an (anti-clockwise) circle around the Trojan* in a time $T > 0$ if

$$\int_{t_0}^{t_0+T} \frac{d}{dt}\vartheta \; dt = \int_{t_0}^{t_0+T} \frac{d}{dt}(f + g) \; dt = 2\pi. \tag{3.29}$$

A (r_0, e_0, ϑ_0)-test orbit (see Definition 4) in Delaunay variables has:

1) $f(0) = 0$ or π (pericenter or apocenter) $\overset{(2.46)}{\Longrightarrow}$ $u(0) = 0$ or π $\overset{(2.50)}{\Longrightarrow}$ $\ell(0) = 0$ or π

2) $\vartheta(0) = \vartheta_0$, (starting on the line l with inclination ϑ_0) $\overset{(2.50)}{\Longrightarrow}$ $g(0) = \vartheta_0$ or $\vartheta_0 + \pi$

3) $r(0) = r_0$ (starting at a distance r_0 from the Trojan)
$\overset{(3.25)}{\Longrightarrow}$ $L(0) = \sqrt{\frac{r_0 m^{-1/3}}{(1 \mp e_0)}}$

4) $e(0) = e_0$ (starting with eccentricity e_0) $\overset{(2.45)}{\Longrightarrow}$ $G(0) = \pm L(0)\sqrt{1 - e_0^2}$ (+/− for direct/retrograde direction).

Recollecting a (r_0, e_0, ϑ_0)-test orbit has initial data

$$\begin{aligned} L(0) &= \sqrt{r_0 m^{-1/3}/(1 \mp e_0)} \ \ (-/+ \text{ for pericenter/apocenter}) , \\ G(0) &= \pm\sqrt{r_0 m^{-1/3}(1 \pm e_0)} \ \ (+/- \text{ for direct/retrograde and pericenter/apocenter}) , \\ \ell(0) &= 0 \text{ or } \pi \ \ (\text{pericenter or apocenter}) , \\ \vartheta(0) &= \vartheta_0 \end{aligned} \tag{3.30}$$

(recall also (3.3)).

For some fixed

$$0 < L_{max} , \quad 1/2 \leq e_{min} < e_{max} < 1 , \tag{3.31}$$

satisfying

$$r_{max} := m^{1/3} L_{max}^2 (1 + e_{max}) < 1 , \tag{3.32}$$

we set

$$\Omega := \left\{ (L, e, \ell, g) \ \ | \ \ L \in (0; L_{max}) , \quad e \in (e_{min}; e_{max}) , \ \ell , \ g \in \mathbb{T}^1 \right\} . \tag{3.33}$$

Notice that, by (3.25), in Ω

$$0 < r < r_{max} < 1 . \tag{3.34}$$

Remark 4 *In view of applications it is assumed*

$$e_{min} \geq 1/2. \tag{3.35}$$

However it is possible to prove that better estimates can be obtained for smaller values of the eccentricity.

Let us define

$$S_0 := \inf_{\Omega} \partial_L H , \quad S_1 := - \inf_{\Omega} \partial_G H , \quad S_2 := \sup_{\Omega} |\partial_\ell H| , \quad S_3 := \sup_{\Omega} |w| . \tag{3.36}$$

The next Lemma contains some analytic estimates on S_0, S_1, S_2, S_3 in terms of L_{max}, e_{min}, e_{max} (defined in (3.31)).

Lemma 2 *It results*

$$S_0 \geq \tilde{S}_0 , \quad \sup_{\Omega} |1 + \partial_G H| \leq \tilde{S}_1 \implies S_1 \leq 1 + \tilde{S}_1 , \quad S_2 \leq \tilde{S}_2 , \quad S_3 \leq \tilde{S}_3 , \tag{3.37}$$

where

$$\begin{aligned}\tilde{S}_0 &:= \frac{1}{L_{max}^3} - \frac{L_{max}}{m^{\frac{1}{3}}}\sqrt{1-M+M^2}\left(\frac{1}{(1-r_{max})^3}-1\right)\frac{(1+e_{min})^2}{e_{min}} \\ &\quad -L_{max}^3\left(\frac{1}{(1-r_{max})^3}\right)\frac{(1+e_{max})^3}{e_{max}}\,, \end{aligned} \tag{3.38}$$

$$\tilde{S}_1 := \frac{L_{max}}{m^{\frac{1}{3}}}\sqrt{1-M+M^2}\left(\frac{1}{(1-r_{max})^3}-1\right)\frac{\sqrt{3+2e_{min}-e_{min}^2}}{e_{min}} \tag{3.39}$$

$$+L_{max}^3\frac{1}{(1-r_{max})^3}\frac{\sqrt{1-e_{min}^2}}{e_{min}}(1+e_{min}) \tag{3.40}$$

$$\tilde{S}_2 := \frac{L_{max}^2}{m^{\frac{1}{3}}}\sqrt{1-M+M^2}\left(\frac{1}{(1-r_{max})^3}-1\right)\sqrt{\frac{1+e_{max}}{1-e_{max}}}+\frac{L_{max}^4}{(1-r_{max})^3}e_{max} \tag{3.41}$$

$$\tilde{S}_3 := \frac{L_{max}}{m^{\frac{1}{3}}}\sqrt{1-M+M^2}\left(\frac{1}{(1-r_{max})^3}-1\right)2\sqrt{1-e_{min}^2}+\frac{L_{max}^3}{(1-r_{max})^3}(1-e_{min}^2) \tag{3.42}$$

Proof
Calling:

$$\begin{aligned} A &= \left(2\cos u - e - \tfrac{1}{e} - \tfrac{\sin^2 u(1-e^2)}{e(1-e\cos u)}\right) \\ B &= \left(-\sqrt{1-e^2}\sin u(1+\tfrac{(1-e^2)\cos u}{e(1-e\cos u)})\right) \end{aligned} \tag{3.43}$$

$$
\begin{aligned}
&\min_{\Omega} \partial_L H \\
&\geq \tfrac{1}{L_{max}^3} - \tfrac{L_{max}}{m^{\frac{1}{3}}} \max_{\Omega} \left\{ \left| \left(-\frac{(1-M)}{(\sqrt{1-2\rho_1+r^2})^3} \right) \left[A\cos\left(g-\frac{4}{3}\pi\right) + B\sin\left(g-\frac{4}{3}\pi\right) \right] \right.\right. \\
&+ \left(-\tfrac{M}{(\sqrt{1-2\rho_2+r^2})^3} \right) \left[A\cos\left(g+\tfrac{1}{3}\pi\right) + B\sin\left(g+\tfrac{1}{3}\pi\right) B \right] \\
&\left.\left. + \left(-\sqrt{1-M+M^2} \right) \left[A\cos(g-\tau_0) + B\sin(g-\tau_0) \right] \right| \right\} \\
&- L_{max}^3 \max_{\Omega} \left\{ \left| \frac{1-M}{(\sqrt{1-2\rho_1+r^2})^3} + \frac{M}{(\sqrt{1-2\rho_2+r^2})^3} \right| \right\} \cdot \\
&\cdot \max_{e\in[e_{min},e_{max}],u\in[0,2\pi]} \left\{ \left| 3 - 3e\cos u + 2e^2\cos^2 u - \frac{1}{e}\cos u - e^2 \right| \right\} \\
&\geq \tfrac{1}{L_{max}^3} - \tfrac{L_{max}}{m^{\frac{1}{3}}} \max_{\Omega} \left\{ \left| \cos g \left[\left(-A\frac{1}{2} + B\frac{\sqrt{3}}{2} \right) \left(1 - \frac{1}{(\sqrt{1-2\rho_1+r^2})^3} \right) \right.\right.\right. \\
&+ M \left((A\tfrac{1}{2} - B\tfrac{\sqrt{3}}{2}) \left(1 - \tfrac{1}{(\sqrt{1-2\rho_2+r^2})^3} \right) + (\tfrac{1}{2}A + B\tfrac{\sqrt{3}}{2}) \left(1 - \tfrac{1}{(\sqrt{1-2\rho_2+r^2})^3} \right) \right) \Big] \\
&+ \sin g \left[\left(-B\tfrac{1}{2} - A\tfrac{\sqrt{3}}{2} \right) \left(1 - \tfrac{1}{(\sqrt{1-2\rho_1+r^2})^3} \right) \right. \\
&\left.\left.\left. + M \left((B\tfrac{1}{2} + A\tfrac{\sqrt{3}}{2}) \left(1 - \tfrac{1}{(\sqrt{1-2\rho_2+r^2})^3} \right) + (\tfrac{1}{2}B - A\tfrac{\sqrt{3}}{2}) \left(1 - \tfrac{1}{(\sqrt{1-2\rho_2+r^2})^3} \right) \right) \right] \right| \right\} \\
&- L_{max}^3 \max_{\Omega} \left\{ \left| \frac{1-M}{(\sqrt{1-2\rho_1+r^2})^3} + \frac{M}{(\sqrt{1-2\rho_2+r^2})^3} \right| \right\} \cdot \\
&\cdot \max_{e\in[e_{min},e_{max}],u\in[0,2\pi]} \left\{ \left| 3 - 3e\cos u + 2e^2\cos^2 u - \frac{1}{e}\cos u - e^2 \right| \right\} \\
&\geq \tfrac{1}{L_{max}^3} - \tfrac{L_{max}}{m^{\frac{1}{3}}} \sqrt{1-M+M^2} \left(\tfrac{1}{(1-r_{max})^3} - 1 \right) \max_{e\in[e_{min},e_{max}],u\in[0,2\pi]} \left\{ \sqrt{A^2+B^2} \right\} \\
&+ L_{max}^3 \left(\tfrac{1}{(1-r_{max})^3} \right) \max_{e\in[e_{min},e_{max}],u\in[0,2\pi]} \left\{ \left| 3 - 3e\cos u + 2e^2\cos^2 u - \frac{1}{e}\cos u - e^2 \right| \right\} \\
&\geq \tfrac{1}{L_{max}^3} - \tfrac{L_{max}}{m^{\frac{1}{3}}} \sqrt{1-M+M^2} \left(\tfrac{1}{(1-r_{max})^3} - 1 \right) \max_{e\in[e_{min},e_{max}],u\in[0,2\pi]} \left\{ \left(\frac{1}{4e^2(1-e\cos u)} \right.\right. \\
&\qquad \left.\left. \left(10 + 22e^2 + 8e^4 - 3e(7+13e^2)\cos u + 6(-1+3e^2+2e^4) \cdot \right.\right.\right. \\
&\qquad \left.\left.\left. \cdot \cos(2u) + (e - e^3 - 4e^5)\cos(3u)\right)\right)^{\frac{1}{2}} \right\} \\
&+ L_{max}^3 \left(\tfrac{1}{(1-r_{max})^3} \right) \max_{e\in[e_{min},e_{max}]} \left\{ \frac{(1+e)^3}{e} \right\} \\
&\geq \tfrac{1}{L_{max}^3} - \tfrac{L_{max}}{m^{\frac{1}{3}}} \sqrt{1-M+M^2} \left(\tfrac{1}{(1-r_{max})^3} - 1 \right) \max_{u\in[0,2\pi]} \left\{ \left| \left(\frac{1}{4e_{min}^2(1-e_{min}\cos u)} \right.\right.\right. \\
&\qquad \left.\left. \left(10 + 22e_{min}^2 + 8e_{min}^4 - 3e_{min}(7+13e_{min}^2)\cos u + 6(-1+3e_{min}^2+2e_{min}^4) \cdot \right.\right.\right. \\
&\qquad \left.\left.\left. \cdot \cos(2u) + (e_{min} - e_{min}^3 - 4e_{min}^5)\cos(3u)\right)\right)^{\frac{1}{2}} \right| \right\} \\
&+ L_{max}^3 \left(\tfrac{1}{(1-r_{max})^3} \right) \max_{e\in[e_{min},e_{max}]} \left\{ \frac{(1+e)^3}{e} \right\}
\end{aligned}
\tag{3.44}
$$

where it has been used that

$$
\max_{g\in[0,2\pi]} (A\cos g + B\sin g) = \sqrt{A^2+B^2} \tag{3.45}
$$

and it has been noted that, by (3.35), the function

$$\Big(\tfrac{1}{4e^2(1-e\cos u)}\left(10+22e^2+8e^4-3e(7+13e^2)\cos u+6(-1+3e^2+2e^4)\cos(2u)+\right.$$
$$\left.+(e-e^3-4e^5)\cos(3u)\right)\Big)^{\frac{1}{2}}$$

reaches its maximum in $u=\pi$ leading to the decreasing function $(1+e)^2/e$.

The function

$$\left|3-3e\cos u+2e^2\cos^2 u-\frac{1}{e}\cos u-e^2\right|$$

has two relative maxima in $u=0$ and $u=\pi$ $\forall e\in(0,1]$, $u\in[0,2\pi]$; therefore the absolute maximum is reached for $u=\pi$. Finally $(1+e)^3/e$ is increasing by (3.35). This proves (3.38).

Analogously, Calling:

$$\begin{aligned} A &= \left(\tfrac{\sqrt{1-e^2}}{e}(1+\tfrac{\sin^2 u}{(1-e\cos u)})\right) \\ B &= \sin u\left(\tfrac{-e+\cos u}{e(1-e\cos u)}\right) \end{aligned} \tag{3.46}$$

It results:

$$
\begin{aligned}
&\sup_\Omega |1+\partial_G H| \\
&\leq \tfrac{L_{max}}{m^{\frac{1}{3}}} \max_\Omega \left\{ \left| \left\{ \left(-\frac{1-M}{(\sqrt{1-2\rho_1+r^2})^3} \right) \left[A\cos(g-\frac{4}{3}\pi) + B\sin(g-\frac{4}{3}\pi) \right] \right.\right. \\
&+ \left(-\tfrac{M}{(\sqrt{1-2\rho_2+r^2})^3} \right) \left[A\cos(g+\tfrac{1}{3}\pi) + B\sin(g+\tfrac{1}{3}\pi) \right] \\
&\left.\left. + \left(-\sqrt{1-M+M^2} \right) \left[A\cos(g-\tau_0) + B\sin(g-\tau_0) \right] \right\} \right| \Bigg\} \\
&+ L^3_{max} \max_\Omega \left\{ \left| \left(\frac{1-M}{(\sqrt{1-2\rho_1+r^2})^3} + \frac{M}{(\sqrt{1-2\rho_2+r^2})^3} \right) \right| \right\} \cdot \\
&\cdot \max_\Omega \left\{ \left| \left[\frac{\sqrt{1-e^2}}{e} (\cos u - e) \right] \right| \right\} \\
&\leq \tfrac{L_{max}}{m^{\frac{1}{3}}} \max_\Omega \left\{ \left| \left[-\frac{A}{2} \left((1-2M) - \frac{1-M}{(\sqrt{1-2\rho_1+r^2})^3} + \frac{M}{(\sqrt{1-2\rho_2+r^2})^3} \right) \right.\right. \right. \\
&+ \tfrac{\sqrt{3}}{2} B \left(1 - \tfrac{1-M}{(\sqrt{1-2\rho_1+r^2})^3} - \tfrac{M}{(\sqrt{1-2\rho_2+r^2})^3} \right) \Bigg] \cos g \\
&\left[-\tfrac{B}{2} \left((1-2M) - \tfrac{1-M}{(\sqrt{1-2\rho_1+r^2})^3} + \tfrac{M}{(\sqrt{1-2\rho_2+r^2})^3} \right) \right. \\
&\left.\left. - \tfrac{\sqrt{3}}{2} A \left(1 - \tfrac{1-M}{(\sqrt{1-2\rho_1+r^2})^3} - \tfrac{M}{(\sqrt{1-2\rho_2+r^2})^3} \right) \right] \sin g \right| \Bigg\} \\
&+ L^3_{max} \left(\tfrac{1}{(1-r_{max})^3} \right) \max_{e\in[e_{min},e_{max}]} \tfrac{\sqrt{1-e^2}}{e}(1+e) \\
&\overset{(3.45)}{\leq} \tfrac{L_{max}}{m^{\frac{1}{3}}} \sqrt{1-M+M^2} \left(\frac{1}{(1-r_{max})^3} - 1 \right) \max_{e\in[e_{min},e_{max}],u\in[0,2\pi]} \sqrt{f_1(e,\cos u)} \\
&+ L^3_{max} \left(\tfrac{1}{(1-r_{max})^3} \right) \tfrac{\sqrt{1-e^2_{min}}}{e_{min}} (1+e_{min}) \\
&\leq \tfrac{L_{max}}{m^{\frac{1}{3}}} \sqrt{1-M+M^2} \left(\frac{1}{(1-r_{max})^3} - 1 \right) \max_{u\in[0,2\pi]} \sqrt{f_1(e_{min},\cos u)} \\
&+ L^3_{max} \left(\tfrac{1}{(1-r_{max})^3} \right) \tfrac{\sqrt{1-e^2_{min}}}{e_{min}} (1+e_{min})
\end{aligned}
\tag{3.47}
$$

where

$$f_1(e,x) := \frac{1}{e^2(1-ex)} \left(4 - 3e^2 - (2e-e^3)x - (3-2e^2)x^2 + ex^3 \right)$$

and it has been used that $f_1(e,\cos u)$ is monotone decreasing in the eccentricity $\forall u \in [0,2\pi]$. Since

$$f_1(e,x) = \frac{1}{e^2(1-ex)} \left(3 - 2e^2 - ex - (3-2e^2)x^2 + ex^3 \right) + \frac{1-e^2}{e^2} = f_2(e,x) + \frac{1-e^2}{e^2}$$

where

$$f_2(e,x) := \frac{(1-x^2)(3-2e^2-x)}{e^2(1-ex)}\,.$$

Note that, for $|x| \leq 1$, f_2 is a positive function which attains maximum for $0 \leq x \leq 1$. For $0 \leq x \leq 1$ the term $1-x^2$ is decreasing, while $(3-2e^2-x)/(1-ex)$ is increasing.

A rough estimate of this value is obtained the first term in $x = 0$ and the second one in $x = 1$, getting $2(1 + e)/e^2$. Recollecting yields

$$0 \leq f_1(e, x) \leq \frac{3 + 2e - e^2}{e^2} \leq \frac{3 + 2e_{min} - e_{min}^2}{e_{min}^2}$$

Finally it has been used that the function $\sqrt{1 - e^2}(1 - e)/e$ is monotone decreasing.

By (2.66), calling

$$\begin{aligned} A &= \left(\tfrac{\sin u}{1 - e\cos u}\right) \\ B &= \left(\tfrac{\sqrt{1-e^2}\cos u}{1 - e\cos u}\right) \end{aligned} \tag{3.48}$$

$$\begin{aligned}
&\sup_\Omega |\partial_\ell H| \leq \tfrac{L_{max}^2}{m^{\frac{1}{3}}} \max_\Omega \left\{ \left| \left(\frac{1 - M}{(\sqrt{1 - 2\rho_1 + r^2})^3} \right) \left[A\cos\left(g - \frac{4}{3}\pi\right) + B\sin\left(g - \frac{4}{3}\pi\right) \right] \right.\right. \\
&+ \left(\tfrac{M}{(\sqrt{1-2\rho_2+r^2})^3} \right) \left[A\cos\left(g + \tfrac{1}{3}\pi\right) + B\sin\left(g + \tfrac{1}{3}\pi\right) \right] \\
&\left.\left. + \left(\sqrt{1 - M + M^2} \right) \left[A\cos(g - \tau_0) + B\sin(g - \tau_0) \right] \right| \right\} \\
&+ L_{max}^4 \max_\Omega \left\{ \left| \frac{1 - M}{(\sqrt{1 - 2\rho_1 + r^2})^3} + \frac{M}{(\sqrt{1 - 2\rho_2 + r^2})^3} \right| \right\} \max_\Omega \{|e\sin u|\} \\
&\leq \tfrac{L_{max}^2}{m^{\frac{1}{3}}} \max_\Omega \left\{ \left| \left[\frac{A}{2} \left((1 - 2M) - \frac{1 - M}{(\sqrt{1 - 2\rho_1 + r^2})^3} + \frac{M}{(\sqrt{1 - 2\rho_2 + r^2})^3} \right) \right.\right. \right. \\
&- \tfrac{\sqrt{3}}{2} B \left(1 - \tfrac{1-M}{(\sqrt{1-2\rho_1+r^2})^3} - \tfrac{M}{(\sqrt{1-2\rho_2+r^2})^3} \right) \Big] \cos g \\
&+ \left[\tfrac{B}{2} \left((1 - 2M) - \tfrac{1-M}{(\sqrt{1-2\rho_1+r^2})^3} + \tfrac{M}{(\sqrt{1-2\rho_2+r^2})^3} \right) \right. \\
&\left.\left.\left. + \tfrac{\sqrt{3}}{2} A \left(1 - \tfrac{1-M}{(\sqrt{1-2\rho_1+r^2})^3} - \tfrac{M}{(\sqrt{1-2\rho_2+r^2})^3} \right) \right] \sin g \right| \right\} \\
&+ L_{max}^4 \tfrac{1}{(1-r_{max})^3} e_{max} \\
&\leq \tfrac{L_{max}^2}{m^{\frac{1}{3}}} \sqrt{1 - M + M^2} \left(-1 + \tfrac{1}{(1-r_{max})^3} \right) \sqrt{\tfrac{1+e_{max}}{1-e_{max}}} + L_{max}^4 \tfrac{1}{(1-r_{max})^3} e_{max}
\end{aligned} \tag{3.49}$$

where in the last inequality it has been used (3.45) and the fact that

$$\frac{1 + e\cos u}{(1 - e\cos u)} \leq \frac{1 + e_{max}}{1 - e_{max}}.$$

Then (3.41) follows.

We conclude estimating w in (2.68), calling:

$$\begin{aligned} A &= \left(\tfrac{(1-e^2)\sin u\cos u}{1 - e\cos u}\right) \\ B &= \tfrac{\sqrt{1-e^2}}{1 - e\cos u}\left(-2e\cos u + 1 + \cos^2 u\right) \end{aligned} \tag{3.50}$$

$$
\begin{aligned}
&\sup_\Omega |w| \le \tfrac{L_{max}}{m^{\frac{1}{3}}} \max_\Omega \left\{ \left| \left(\frac{1-M}{(\sqrt{1-2\rho_1+r^2})^3} \right) \left[A\cos(g-\frac{4}{3}\pi) + B\sin(g-\frac{4}{3}\pi) \right] \right.\right. \\
&+ \left(\tfrac{M}{(\sqrt{1-2\rho_2+r^2})^3} \right) \left[A\cos(g+\tfrac{1}{3}\pi) + B\sin(g+\tfrac{1}{3}\pi) \right] \\
&\left.\left. + \left(\sqrt{1-M+M^2} \right) \left[A\cos(g-\tau_0) + B\sin(g-\tau_0) \right] \right| \right\} \\
&+ L_{max}^3 \max_\Omega \left\{ \left| \left(\frac{1-M}{(\sqrt{1-2\rho_1+r^2})^3} + \frac{M}{(\sqrt{1-2\rho_2+r^2})^3} \right) \right| \right\} \max_\Omega \left\{ \left| (1-e^2)\sin u \right| \right\} \\
&\le \tfrac{L_{max}}{m^{\frac{1}{3}}} \max_\Omega \left\{ \left| \left[\frac{A}{2} \left((1-2M) - \frac{1-M}{(\sqrt{1-2\rho_1+r^2})^3} + \frac{M}{(\sqrt{1-2\rho_2+r^2})^3} \right) \right.\right. \right. \\
&- \tfrac{\sqrt{3}}{2} B \left(1 - \tfrac{1-M}{(\sqrt{1-2\rho_1+r^2})^3} - \tfrac{M}{(\sqrt{1-2\rho_2+r^2})^3} \right) \Big] \cos g \\
&+ \left[\tfrac{B}{2} \left((1-2M) - \tfrac{1-M}{(\sqrt{1-2\rho_1+r^2})^3} + \tfrac{M}{(\sqrt{1-2\rho_2+r^2})^3} \right) \right. \\
&\left.\left.\left. + \tfrac{\sqrt{3}}{2} A \left(1 - \tfrac{1-M}{(\sqrt{1-2\rho_1+r^2})^3} - \tfrac{M}{(\sqrt{1-2\rho_2+r^2})^3} \right) \right] \sin g \right| \right\} \\
&+ L_{max}^3 \tfrac{1}{(1-r_{max})^3} (1-e_{min}^2) \\
&\le \tfrac{L_{max}}{m^{\frac{1}{3}}} \sqrt{1-M+M^2} \left(1 - \tfrac{1}{(1-r_{max})^3} \right) 2\sqrt{1-e_{min}^2} + L_{max}^3 \tfrac{1}{(1-r_{max})^3} (1-e_{min}^2)
\end{aligned}
\tag{3.51}
$$

where in the last inequality it has been used (3.45) and the fact that

$$
\frac{10 - 15e\cos u + 6\cos 2u - e\cos 3u}{(1-e\cos u)} \le 16\,.
$$

Note that

$$
\tilde{S}_0 \to \infty\,, \qquad \tilde{S}_1\,,\ \tilde{S}_2/L_{max}\,,\ \tilde{S}_3\ \to 0\,, \quad \text{as}\ \ L_{max}\ \to\ 0\,. \tag{3.52}
$$

In the following it is assumed that

$$
\inf_\Omega \partial_L H = S_0 > 0\,, \quad -S_1 = \inf_\Omega \partial_G H \le \sup_\Omega \partial_G H \le 0\,, \quad S_0 \ge 5S_1\,, \tag{3.53}
$$

$$
S_2\tilde{T} < L_{max}\,, \qquad 2S_3\tilde{T} < e_{max} - e_{min} \quad \text{where} \quad \tilde{T} = 2\pi/(S_0 - S_1)\,. \tag{3.54}
$$

Note that from (3.52) these conditions can always be assumed if L_{max} is small enough.

Then it can be chosen

$$
\begin{aligned}
&0 < \tilde{L}_{max} := L_{max} - S_2\tilde{T} < L_{max}\,, \\
&e_{min} < \tilde{e}_{min} := e_{min} + S_3\tilde{T} < \tilde{e}_{max} := e_{max} - S_3\tilde{T} < e_{max}
\end{aligned}
\tag{3.55}
$$

and set

$$\tilde{\Omega} := \left\{ (L, e, \ell, g) \;\; | \;\; L \in (0, \tilde{L}_{max}] \,, \quad e \in [\tilde{e}_{min}, \tilde{e}_{max}] \,, \; \ell \,, \, g \in \mathbb{T}^1 \right\} . \tag{3.56}$$

Lemma 3 *Assuming* (3.53) *and* (3.54). *Then*

$$(L(0), e(0), \ell(0), g(0)) \in \tilde{\Omega} \quad \Longrightarrow \quad (L(t), e(t), \ell(t), g(t)) \in \Omega \,, \quad \forall \, t \in [0, \tilde{T}] \,.$$

Proof Assume by contradiction that $\exists \, T_* \in (0, \tilde{T})$ such that $(L(t), e(t), \ell(t), g(t)) \in \Omega$ for every $t \in [0, T_*)$, but $(L(T_*), e(T_*), \ell(T_*), g(T_*)) \notin \Omega$. Then (at least) one of the following equalities occurs:

$$L(T_*) = L_{max} \,, \quad e(T_*) = e_{min} \,, \quad e(T_*) = e_{max} \,.$$

But this is in contradiction with (3.55) from (2.69), (3.53) and (3.54), proving the Lemma.

Proposition 2 *Assume* (3.53) *and* (3.54). *A* (r_0, e_0, θ_0)*-test orbit with*

$$0 < r_0 < r^* := m^{1/3} \tilde{L}_{max}^2 (1 - \tilde{e}_{max}) \,, \qquad e_0 \in (\tilde{e}_{min}, \tilde{e}_{max}) \tag{3.57}$$

is stable according to Definition 5. In particular:

i) $r(t) < 1$ *for every* $t \in [0, \tilde{T}]$, *namely it cannot go around the any of the other two primaries or crash into it up to time* $\tilde{T}$

ii) there exists $0 < T \leq \tilde{T}$ *such that*

$$\int_0^T \dot{f} + \dot{g} = 2\pi \,, \tag{3.58}$$

namely the orbit makes a circle around the Trojan in time T.

Moreover

$$\dot{\vartheta}(T) = \dot{f}(T) + \dot{g}(T) > 0 \,.$$

Remark 5 *In the proposition above the worst case is considered, which is when the test orbit starts at pericenter (see the minus sign in equation (3.57) and recall (3.30)). Better estimates hold for the apocenter case (in particular replace* $1 - \tilde{e}_{max}$ *with* $1 + \tilde{e}_{min}$ *in formula (3.57)).*

Proof. Let us first note that, by (3.25) and (3.57) the test orbits starts in $\tilde{\Omega}$. Then, by Lemma 3, it remains in Ω for every $t \in [0, \tilde{T}]$. In particular, by (3.34), $r(t) < 1$ for every $t \in [0, \tilde{T}]$.

Consider only the case $\ell(0) = 0$, the case $\ell(0) = \pi$ being analogous, then there

exists $0 < T_* \le \bar{T}$ such that

$$\int_0^{T_*} \dot{\ell} + \dot{g} = 2\pi \qquad \text{and} \qquad 2\pi \le \int_0^{T_*} \dot{\ell} \le 3\pi\,. \tag{3.59}$$

Since $\dot{\ell} + \dot{g} \ge S_0 - S_1 > 0$ the existence of (a unique) $0 < T_* \le \bar{T}$ satisfying the equality in (3.59) follows. Also the first inequality in (3.59) is trivial since $\dot{g} \le 0$. It remains to prove that $\int_0^{T_*} \dot{\ell} \le 3\pi$. Assume by contradiction that $\int_0^{T_*} \dot{\ell} > 3\pi$. Then

$$2\pi = \int_0^{T_*} \dot{\ell} + \dot{g} > 3\pi - S_1 T_* \ge 3\pi - S_1 \bar{T} \ge 2\pi \tag{3.60}$$

since $S_0 \ge 3S_1$. This proves (3.59).

Note that the solution $u = u(\ell)$ of the Kepler equation (2.50) and $f = f(u)$ in (2.46) satisfy $u(n\pi) = n\pi = f(n\pi)$

$$f(u) \ge u\,, \quad u(\ell) \ge \ell \quad \text{when} \quad u, \ell \in [0, \pi] + 2n\mathbb{Z}\,. \tag{3.61}$$

In particular $f(u(\ell)) \ge \ell$ for $\ell \in [0, \pi] + 2n\mathbb{Z}$. Since by (3.59) $\ell(T_*) \in [2\pi, 3\pi]$ it results $f(T_*) = f(u(\ell(T_*))) \ge \ell(T_*)$. Then, since $f(0) = f(u(\ell(0))) = f(u(0)) = 0$,

$$\int_0^{T_*} \dot{f} + \dot{g} = f(T_*) + \int_0^{T_*} \dot{g} \ge \ell(T_*) + \int_0^{T_*} \dot{g} = \int_0^{T_*} \dot{\ell} + \dot{g} = 2\pi\,. \tag{3.62}$$

The existence of T in (3.58) follows by continuity.

Using (2.50) and (2.46) and denoting $u^t := u(\ell(t))$, $f^t := f(u^t)$ it is computed for $0 \le t \le T$

$$\begin{aligned} \dot{f}(t) &= \frac{df}{du}(u^t)\frac{du}{d\ell}\big(l(t)\big)\dot{\ell}(t) \\ &= \left(1 + \frac{1+e}{1-e}\tan^2(u^t/2)\right)^{-1} \sqrt{\frac{1+e}{1-e}}\frac{1}{\cos^2(u^t/2)}\frac{1}{1-e\cos u^t}\dot{\ell}(t) \\ &= \big(1 + \tan^2(f^t/2)\big)^{-1} \sqrt{\frac{1+e}{1-e}}\frac{1}{\cos^2(u^t/2)}\frac{1}{1-e\cos u^t}\dot{\ell}(t) > 0\,. \end{aligned} \tag{3.63}$$

Denoting $f_* := f(T) - 2\pi$ it yields $0 \le f_* \le \pi/2$. Indeed $0 \le f_*$ follows since $\dot{f} > 0$. On the other hand (3.58) implies that

$$f_* = -\int_0^T \dot{g} \le S_1 T \le 2\pi \frac{S_1}{S_0 - S_1} \overset{S_0 \ge 5S_1}{\le} \frac{\pi}{2}\,. \tag{3.64}$$

Noting that $u_* := u(T) - 2\pi$ satisfies $0 \le u_* \le f_* \le \pi/2$ (recall (3.61)), by (3.63) it results

$$\dot{f}(T) > \big(1 + \tan^2(f_*/2)\big)^{-1} \dot{\ell}(T) \ge \dot{\ell}(T)/2 \ge S_0/2\,. \tag{3.65}$$

Then

$$\dot{f}(T) + \dot{g}(T) \geq S_0/2 - S_1 \geq 3S_1/2 > 0\,. \tag{3.66}$$

The proposition is proved.

Corollary 1 *Choose*

$$0 < \tilde{L}_{max} < L_{max}\,, \qquad \frac{1}{2} \leq e_{min} < \tilde{e}_{min} < \tilde{e}_{max} < e_{max} \leq 1 \tag{3.67}$$

satisfying (3.32)*,* (3.53)*,* (3.54) *and* (3.55)*.*

Then

$$S(e,\theta) \supset (0, r^*) \qquad \forall\, e \in (\tilde{e}_{min}, \tilde{e}_{max}) \quad \forall\, \theta \in S^1\,, \tag{3.68}$$

where r^* *was defined in* (3.57)*.*

3.5.1 An example

The value of $r^*(e)$ is now explicitly evaluated, in view of the applications contained in the next chapter, for relatively high eccentricities, i.e. when $e > \frac{1}{2}$.

The parameters satisfying the hypotheses of Corollary 1 must now be chosen. Two different ways to proceed are now adopted. The former is analytic and uses Lemma 2 to estimate S_i, $i = 0, 1, 2, 3$ in (3.37). The latter is the numerical estimation of the function over a defined set, and is obtained using a basic numerical constrained global optimization (e.g. the one provided by an algebraic manipulators like Mathematica) to estimate the $\sup_\Omega$ and $\inf_\Omega$ in (3.37).

In the first case it must be noted that the conditions

$$\begin{aligned} &\tilde{S}_0 > 0\,, \quad \tilde{S}_1 < 1\,, \quad \tilde{S}_0 \geq 5(\tilde{S}_1 + 1) \\ &\tilde{S}_2 \bar{T} < L_{max}\,, \quad 2\tilde{S}_3 \bar{T} < e_{max} - e_{min} \;\text{ with }\; \bar{T} := 2\pi/(\tilde{S}_0 - \tilde{S}_1 - 1) \end{aligned} \tag{3.69}$$

imply (3.53)-(3.54), from (3.37) and $\bar{T} \geq \tilde{T}$.
Taking

$$\tilde{L}_{max} = 0.3\,, \quad \tilde{e}_{min} = 0.54\,, \quad \tilde{e}_{max} = 0.97\,,$$

which implies, by (3.32):

$$r_{max} := 0.0000339673$$

yields

$$\begin{aligned} &\tilde{S}_0 = 36.1237\,, \quad \tilde{S}_1 = 0.639735\,, \quad \tilde{S}_2 = 0.395622\,, \quad \tilde{S}_3 = 0.287628 \\ &\bar{T} = 0.177071\,. \end{aligned}$$

Then (3.32) and (3.69) are satisfied. By (3.55)

$$\tilde{L}_{max} = 0.229947\,, \quad \tilde{e}_{min} = 0.590931\,, \quad \tilde{e}_{max} = 0.919069\,,$$

meaning that the set of the stable orbits for the range $e_0 \in [\tilde{e}_{min}, \tilde{e}_{max}]$ is being considered. for which, by (3.57), it results

$$r^*(e_0) = 8.19828 \times 10^{-7} = 638.097km \tag{3.70}$$

The value of r^* can also be confirmed numerically S_0, S_1, S_2, S_3 in (3.36), e.g. by Mathematica. Moreover the estimations obtained will improve the analytical result obtained above as they are numerical and obtained without the uniform $(g,\, u)$ estimation of the maximum/minimum contained in Lemma 2. Taking

$$L_{max} := 0.3\,, \quad e_{min} := 0.54\,, \quad e_{max} := 0.97$$

yields

$$S_0 = 37.0163\,, \quad S_1 = 1.11659\,, \quad S_2 = 0.0166893\,, \quad S_3 = 0.102606\,, \quad \tilde{T} = 0.17502\,.$$

Then (3.32), (3.53) and (3.54) are satisfied. By (3.55)

$$\tilde{L}_{max} = 0.297079\,, \quad \tilde{e}_{min} = 0.557958\,, \quad \tilde{e}_{max} = 0.952042\,,$$

meaning that the set of the stable orbits for the range $e_0 \in [\tilde{e}_{min}, \tilde{e}_{max}]$ is being considered. for which, by (3.57), it results

$$r^*(e_0) = 8.10881 \times 10^{-7} = 631.133km \tag{3.71}$$

3.6 Summary

The formulation of an analytical definition of the WSB enables the possibility to study the topological properties of this complicate set, key for future space missions although still largely unknown. The comparison with the existing algorithmic definitions confirms the validity of the new definition and enables the possibility to exploit previous results to get directions of research for new analytical studies. Moreover such definition has here been generalized to the autonomous coplanar CR4BP. Key topological properties of the set of the stable orbits have been discussed, from which the properties of the WSB, frontier of this set, can be directly deduced. In particular it has been demonstrated that the set of the stable orbits is bounded, is a disjoint union of at most countable open intervals plus an at most a countable set of points and that $\forall e \in [0, 1]$ fixed and that

there exist a radius $r^*(e) > 0$ such that all the orbits generated by a radius smaller than r^* are stable. Analytical estimates of the radius r^* have therefore be deduced using the Delaunay coordinates. This general procedure has been here applied, in view of the applications, to estimate the zone of the stable orbits with relatively high eccentricities (i.e. $e_0 > \frac{1}{2}$), around the asteroid 624-Hektor, a major Jupiter Trojan. The estimated $r^* = 631,133km$ can be seen both as an estimation of the region formed by the sole stable orbits or as an estimation of the WSB.

Chapter 4

Analysis of the inhomogeneous R2BP

In the previous chapter a method has been produced, which analytically estimates the set of the stable orbits around the smaller primary by fixing a range of initial eccentricities and semimajor axes for the orbit. Inside this estimated region dynamics is assumed to be dominated by the sole smaller body. However, within this region, the inhomogeneities of the gravitational field influence the motion of the orbiting spacecraft and must therefore be included in the modelling. The inhomogeneous R2BP is thus adopted to model the dynamics of the system inside the reference domain. It must be noted that such a model and the perturbative theory here developed are general (i.e. can be applied to every inhomogeneous body), although, in this thesis, they are applied to a Trojan object.

4.1 State of art

Analytical studies on the effects of the inhomogeneous potential on the dynamics around a planet is a classical subject of research in the context of celestial mechanics. The two body problem including the perturbation due to the bulge of the planet, namely the J_2 or "oblateness" effect, has been extensively studied since Brouwer's analysis [55] on the main problem of the artificial satellite. Generalizations of Brouwer's approach can be found in [56], [57], [58] and [59], each pushing previous studies to higher orders, but still avoiding series expansions. In recent years this type of research has gained importance for future planned missions of spacecraft to the moon and to other asteroids in addition to asteroid deflection missions such as the European Space Agency's "Don Quijote" concept [60], in which, after arriving to the target asteroid and be inserted into an orbit around it, an orbiter spacecraft, called Sancho, will measure with great accuracy its position, shape, mass, and gravity field for several months before and after

the impact of the other spacecraft (the Impactor), named Hidalgo.
Research undertaken in this area are mainly focused on the effect of the Earth's inhomogeneous gravitational field on the motion of natural and artificial satellites, that is, artificial satellite theory for small and moderate eccentricities [61]. More recent studies have researched the effects on motion of the inhomogeneous gravitational field of other solar system bodies, including the Trojans [62] and other asteroids [63]. The analysis of the spacecraft's motion about these bodies is particularly challenging as they typically feature shapes and density distributions more irregular than those of planets. Such irregularities break symmetries and require more complicated analytical expressions for their description, which increases the complexity involved in such studies. Numerical methods are today widely used ([64], [65] and [66]) to study the trajectories of objects orbiting specific irregular bodies [67] or for finding stability criteria [68]. In these works the entire potential containing the spherical harmonics coefficients is usually placed at first order, assumption that will be used in this thesis as well. Disadvantages of these methods are that they can be highly computational and require a complete re-design for each different body. Analytical methods, by contrast, have the potential to rapidly identify useful, natural motions for general bodies with inhomogeneous gravitational fields. Furthermore, they can provide a full dynamical picture of the motion around irregular bodies that can be used to search and study particular classes of useful orbits. Finally, while a numerical integration usually provides high accuracy and even may gain in computation time, only an analytical theory can provide a complete, deep insight into the nature of the perturbation [54]. Current analytical methods are only used in a limited and semi-numerical way like in [69] and [70], meaning that analytical expansions constitute the first step in such studies, which are then typically carried out from a numerical standpoint [71]. The main drawbacks of these methods are that their application in the case of highly inhomogeneous bodies requires extensive symbolic computations involving algebraic manipulations, and that they are usually restricted to a certain range of eccentricities due to series convergence. Analytical studies on inhomogeneous gravitational fields have been, so far, limited to low degree gravity fields [27], [50], [63], thus restricting the results to a class of bodies for which the dynamics is dominated by a few coefficients (e.g. oblateness or ellipticity). In [64] a theory for the tesseral problem for low altitude satellites based on Deprit's relegation algorithm is developed, with the purpose of producing ephemeris of the satellites motion. In [72] near-circular orbits in a model that included both the third bodys gravity and J_2 are studied. In addition, in [73], the authors studied the orbital dynamics about oblate planetary satellites using the rigorous averaging method which is applied in this thesis. The effect of the coefficient J_3 is then added in [74]. Finally the planar elliptic restricted three-body problem including the J_2 and J_3 coefficients, can be found in [75], which uses a Deprit's perturbation method that allow to build a doubly averaged Hamiltonian

and to provide the transformation between osculating and mean initial conditions.

4.2 Introduction and main results

The aim of this Chapter is to apply Deprit's and Palacián's theory [27] for constructing closed form (i.e. without using series expansion in the eccentricity) normalization of perturbed two body problems, to study the motion of a spacecraft around any (shape/density) inhomogeneous body for the so called "fast rotating case".
While the "slow rotation" case has been previously studied in depth, by the direct application of a Lie transformation called the Delaunay Normalisation[49], which averages the Hamiltonian with respect to the fast angle, thus reducing the number of variables, this usual technique cannot be directly applied to the complementary "fast rotating case". This is due to the presence of the argument of node that appears in the Coriolis term of the Hamiltonian describing the system in this case. The addition of this term in the Lie derivative, indeed, prevents the conventional computation of the Lie transform generator [50]. However another Lie transformations method, Palacian's closed form relegation algorithm [51], can be applied first, which "relegates" the action of the argument of node to a negligible remainder, thus allowing the application of the Delaunay Normalization. This Lie transformation, the Delaunay normalisation, constructed following Palácian's and Deprit's method for Lie transformations [53], is thus be applied to further reduce the number of variables of the Hamiltonian describing the system.
Therefore in this chapter this two existing theories for averaging perturbed Hamiltonians are here applied for the first time to the perturbed dynamics describing this problem, for the "fast rotating case", to obtain the explicit formulation of the double averaged (by means of Lie transformation) Hamiltonian, generalized, with respect to previous results ([27], [71]) to second order, arbitrary degree, gravitational fields.
Assuming that the planetary body is in uniform rotation around its axis of greatest inertia, the potential generated by the inhomogeneous gravitational field has been derived, following the classical procedure, in the rotating polar nodal variables [26], convenient for the necessary transformation to Delaunay coordinates. This potential takes into account an arbitrary number of spherical harmonic coefficients thus providing a dynamical model based on an arbitrarily accurate approximation of the inhomogeneous body. Spherical harmonics are divided between zonal and tesseral harmonics, coefficients respectively independent and dependent from the longitude, therefore zonal are invariant under the rotation through a particular fixed axis [29]. In this work, both zonal and tesseral harmonics are be taken into account. Note that the perturbation theories which take into account longitude-dependent tesseral coefficients of the spherical harmonics, i.e. involving the rotation of the planet, are, in general, more complex

than the theories which include only the zonal harmonics, the reason being that the tesseral problem is formulated by means of a three degree of freedom autonomous Hamiltonian, whereas the zonal problem is represented as a system of two degrees of freedom. Then through the application of two different Lie transformations, suitable changes of coordinates are here explicitly found, which reduce the initial non integrable Hamiltonian of the system into an integrable one plus a negligible, perturbative remainder of higher degree. The explicit analytical formulation for the relegated, first and second order, arbitrary degree Hamiltonian, for relatively high altitude motion, in any inhomogeneous gravitational field is, in this work, derived in closed-form for the first time. Furthermore, in this thesis novel applications for the algorithm built are found and presented, which include a method for determining initial conditions for frozen orbits around any irregular body by simply prescribing the desired inclination and eccentricity of the orbit. The method obtained is used to find interesting orbits for space mission applications such as frozen orbits. Frozen orbits are orbits with no secular perturbations in the inclination, argument of pericentre, and eccentricity [55]. These orbits are periodic orbits, except for the orbital plane of precession, and are therefore called frozen. Frozen orbits are of key interest for any scientific and observational missions especially unknown bodies as, among the other applications, their good stability properties might allow a very fast process of physical characterization of the body, with all the possible implications in saving mission time and money or for safetyness in the case, for example, of an hazardous asteroid which is approaching the Earth.
The procedure followed to get to such explicit formulation and the new application for detection of initial conditions for frozen orbits, is summarized in the main steps below:

- Relegation of the polar component of the angular momentum N to obtain the relegated nodal polar variables where the conjugate momenta of the argument of nodes (i.e. the polar component of the angular momentum) is constant along the Hamiltonian flow.

- Transformation to Delaunay variables

- Normalization of the Delaunay variables which yields a reduced ordinary differential equation in two coordinates; the total angular momentum and the argument of pericentre

- Identification of frozen orbits, for fixed eccentricity, inclination and argument of perigee, as the equilibrium points of these equations i.e. where the total angular momentum about the z-axis and the argument of pericentre are constant. This final stage essentially reduces the problem of computing frozen orbits to a problem of solving a 2-D algebraic equation.

Results are shown for the Jupiter Trojan 624-Hektor, for which the spherical harmonics coefficients have been derived from a three dimensional polyhedric model of the asteroid, assuming a constant density.

4.3 The relegation of the polar component of the angular momentum N

In the context of artificial satellite theory, in general, it is needed to order the terms of the Hamiltonian H according to an asymptotic expansion in order to built a perturbation theory. The usual way to arrange the Hamiltonian for the cases in which the angular velocity of the asteroid is higher than the mean motion of the spacecraft [64](which holds, for example, for fast rotating bodies or for relatively high altitudes) is here followed. It consists in placing the full unperturbed part at zeroth order and distribute the perturbation at first and second orders. The dominant (unperturbed) part of the Hamilton function is set to be the sum of the two-body Hamiltonian H_K and the Coriolis term H_C. The perturbing potential takes into account an arbitrary number of spherical harmonic coefficients, distributed as first or second order perturbations, depending on the harmonics of the specific asteroid studied and thus providing a dynamical model based on an arbitrarily accurate approxmation of the inhomogeneous body.
The flows associated to the two components of the unperturbed Hamiltonian are used to relegate the whole system first and then to put it into normal form by means of symplectic transformations.
The Hamiltonian in (2.79) is therefore rearranged as:

$$H = H_0 + \epsilon H_1 + \frac{\epsilon^2}{2} H_2 + O(\epsilon^3), \tag{4.1}$$

where ϵ is merely an ordering, dimensionless parameter, which will be decided later on for the applications, and

$$\begin{aligned} H_0 &= H_K + H_C \\ H_1 &= U^{(1)}(r, \theta, \nu, \_, \Theta, N) \\ H_2 &= U^{(2)}(r, \theta, \nu, \_, \Theta, N) \end{aligned} \tag{4.2}$$

where:

$$\begin{aligned} H_K &:= \tfrac{1}{2}(R^2 + \tfrac{\Theta^2}{r^2}) - \tfrac{\bar{M}}{r} \\ H_C &= -\Omega N, \end{aligned} \tag{4.3}$$

and, for $s = 1,\ 2$

$$\begin{aligned} U^{(s)}(r,\theta,\nu,\_,\Theta,N) = -\tfrac{s!}{\epsilon^s}\sum_{n=1}^{\infty}\sum_{m=0}^{n}\sum_{j=-n}^{n}\sum_{t=\max\{0,j+m\}}^{\min\{n+m,n+j\}} ci^{2n+m+j-2t}\, si^{2t-m-j}\cdot \\ \cdot\tfrac{1}{r^{n+1}}\left(\mathcal{A}^{(s)}_{n,m,j,t}\cos(m\nu - j\theta) + \mathcal{B}^{(s)}_{n,m,j,t}\sin(m\nu - j\theta)\right), \end{aligned} \tag{4.4}$$

with:

$$\begin{aligned} \mathcal{A}^{(s)}_{n,m,j,t} &= \bar{\mathcal{G}}_{n,m,j,t}\left(C^{(s)}_{n,m}\cos(\tfrac{\pi}{2}(j+m)) - S^{(s)}_{n,m}\sin(\tfrac{\pi}{2}(j+m))\right) \\ \mathcal{B}^{(s)}_{n,m,j,t} &= \bar{\mathcal{G}}_{n,m,j,t}\left(C^{(s)}_{n,m}\sin(\tfrac{\pi}{2}(j+m)) + S^{(s)}_{n,m}\cos(\tfrac{\pi}{2}(j+m))\right), \end{aligned} \tag{4.5}$$

with:

$$\begin{aligned} C^{(s)}_{n,m} &= \begin{cases} C_{n,m}\ if\ the\ term\ containing\ C_{n,m}\ is\ \sim O(\epsilon^q) \\ 0 \quad otherwise \end{cases} \\ S^{(s)}_{n,m} &= \begin{cases} S_{n,m}\ if\ the\ term\ containing\ S_{n,m}\ is\ of\ \sim O(\epsilon^q) \\ 0 \quad otherwise \end{cases} \end{aligned} \tag{4.6}$$

Again ci and si as in (2.103) and $\bar{\mathcal{G}}_{n,m,j,t}$ as in (6.11).

Now, considering the case $|H_K| < |H_C|$, two different Lie transformations are performed: the relegation of the polar component of the angular momentum N first and the Delaunay normalisation then.

Definition 10 *A Lie transformation ϕ is a one-parameter family of mappings $\phi : (y, Y; \epsilon) \to (x, X)$, defined by the solution $x(y, Y; \epsilon)$ and $X(y, Y; \epsilon)$ of the Hamiltonian system*

$$\begin{cases} \frac{dx}{d\epsilon} = \frac{\partial W}{\partial X} \\ \frac{dX}{d\epsilon} = -\frac{\partial W}{\partial x} \end{cases}$$

with initial conditions $x(y, Y; 0) = y$ and $X(y, Y; 0) = Y$ and where the function

$$W(x, X; \epsilon) = \sum_{s\geq 0}\frac{\epsilon^s}{s!}W_{s+1}(x, X)$$

is the generator of the transformation.

Due to the properties of the Hamiltonian systems, the Lie transformation ϕ is a completely canonical transformation that maps a Hamiltonian

$$H(x, X; \epsilon) = \sum_{s\geq 0}\frac{\epsilon^s}{s!}H_s(x, X)$$

onto an equivalent Hamiltonian K of the form

$$K(y, Y; \epsilon) = \sum_{s \geq 0} \frac{\epsilon^s}{s!} K_s(y, Y; 0).$$

found by solving a series of homological equations:

$$[H_0; W_s] + \tilde{H}_s = K_s \quad \forall s \geq 1 \tag{4.7}$$

where the symbol [;] stands for the Poisson Brackets. In equation (4.7) the element $\tilde{H}_s$ collects the terms from the previous orders (see [53] and [27]). The relegation and the normalization algorithms (see [51] and [49] respectively) are two different methods of solving such homological equations. In particular, the relegation maps the Hamiltonian (4.1) into an equivalent one of the form:

$$K = K_0 + \sum_{s \geq 1} \frac{\epsilon^s}{s!} K_s = \sum_{s \geq 0} \frac{\epsilon^s}{s!} \left(\sum_{j=0}^{p} K_{s,p} + R_s \right) \tag{4.8}$$

with $K_0 = H_0(y, Y)$ and the coefficients $K_{s,p} \in ker(\mathcal{L}_{H_C})$, where $\mathcal{L}_{H_C}$ is the Lie derivative with respect to the Coriolis term[1].
In contrast with normalization, the term K_s may not belong to $ker(\mathcal{L}_{H_C})$ due to the presence of the residual R_s. In this resulting Hamiltonian the terms containing the variable ν will only appear in the remainder R_s. Moreover, for every order s of the Hamiltonian, the algorithm is iterated $p^{(s)}$ times (depending on the choice of the small parameter ϵ), progressively diminishing the importance of the remainder R_s, such that after $p^{(s)}$ times it results $R_s \sim O(\epsilon^3)$.
As a result the truncated system

$$K = \sum_{s \geq 0} \frac{\epsilon^s}{s!} \sum_{j=0}^{p} K_{s,p}, \tag{4.9}$$

is obtained, which represents an approximation of the starting Hamiltonian independent from ν and admits H_C as an integral.
In this section, in order to keep the generality of the analysis, the relegation is performed to the second order, arbitrary number of iterations $p^{(s)}$. In the applications section, once the parameter ϵ will be fixed, the number of iterations necessary to relegate the terms of the Hamiltonian containing ν to orders $\sim O(\epsilon^3)$ will therefore be estimated.

[1] Let $\mathcal{L}_W$ be the Lie derivative induced by the function W, then $\mathcal{L}_W$ which maps any function $f(X, x)$ into its Poisson Bracket with W, namely $f(X, x) :\rightarrow [f; W]$.
It must be noted that $\mathcal{L}_{H_C} H_K = 0$ and that $\mathcal{L}_{H_C}$ is semi-simple over a Poisson algebra of functions P.

4.3.1 Algorithm

The general relegation algorithm is briefly described here before the application to the problem. For each homological equation ($\forall s \geq 1$):

$$[H_0; W_s] + \tilde{H}_s = K_s \tag{4.10}$$

considering that, as $\mathcal{L}_{H_C}$ is semi-simple, there $\exists K_{s,0}, W_{s,0} \in P$ s.t.

$$\begin{cases} \tilde{H}_s = K_{s,0} + [W_{s,0}; H_C] \\ K_{s,0} \in Ker(\mathcal{L}_{H_C}). \end{cases} \tag{4.11}$$

Therefore (4.10) becomes:

$$[H_0; W_s] + [W_{s,0}; H_C] = K_s - K_{s,0}. \tag{4.12}$$

Thus, setting $W_s = W^*_{s,0} + W_{s,0}$, (4.12) yields:

$$[H_0; W^*_s] + [H_0 - H_C; W_{s,0}] = K_s - K_{s,0}. \tag{4.13}$$

The algorithm continues re-invoking $p^{(s)}$-times the semi-simplicity of $\mathcal{L}_{H_C}$, and finding $\forall 1 \leq p \leq p^{(s)} \quad K_{s,p}, W_{s,p} \in P$ s.t.

$$\begin{cases} [H_0 - H_C; W_{s,p-1}] = K_{s,p} + [W_{s,p}; H_C] \\ K_{s,p} \in Ker(\mathcal{L}_{H_C}) \end{cases} \tag{4.14}$$

and setting $p^{(s)}$-times $\forall 1 \leq p \leq p^{(s)} \quad W_{s,p-1} = W^*_{s,p} + W_{s,p}$.

Finally the algorithm ends at a certain iteration $p^{(s)}$ setting $W^*_{s,p^{(s)}} = 0$ and obtaining (4.13) to become:

$$K_s = \sum_{p=0}^{p^{(s)}} (K_{s,p}) + R_s \tag{4.15}$$

with $R_s := [H_0 - H_C; W_{s,p^{(s)}}]$.

Although the procedure is general, in view of the applications, only the first two homological equations will here be considered and explicitly solved.

4.3.2 Results

Following the procedure just described and [53], for the first order $s = 1$ of the Hamiltonian (4.1), it is found that:

$$\tilde{H}_{1,0} = H_1 \tag{4.16}$$

therefore, after the first iteration $p = 1$, it results:

$$\begin{aligned} K_{1,0} = -\tfrac{1}{\epsilon} \sum_{n=1}^{\infty} \sum_{j=-n}^{n} \sum_{t=\max\{0,j\}}^{\min\{n,n+j\}} & ci^{2n+j-2t} si^{2t-j} \frac{1}{r^{n+1}} \Big(\mathcal{A}^{(1)}_{n,0,j,t} \cos(-j\theta) \\ & + \mathcal{B}^{(1)}_{n,0,j,t} \sin(-j\theta) \Big). \end{aligned} \tag{4.17}$$

Moreover

$$\begin{aligned} W_{1,0} &= -\tfrac{1}{\Omega} \int (H_1 - K_{1,0}) d\nu \\ &= -\left(\tfrac{1}{\epsilon} \sum_{n=1}^{\infty} \sum_{m=1}^{n} \sum_{j=-n}^{n} \sum_{t=\max\{0,j+m\}}^{\min\{n+m,n+j\}} ci^{2n+m+j-2t} si^{2t-m-j} \left(-\frac{1}{m\Omega} \right) \frac{1}{r^{n+1}} \cdot \right. \\ &\qquad \left. \cdot \Big(\mathcal{A}^{(1)}_{n,m,j,t} \sin(m\nu - j\theta) + \mathcal{B}^{(1)}_{n,m,j,t} (-\cos(m\nu - j\theta)) \Big) \right), \end{aligned} \tag{4.18}$$

and

$$\begin{aligned} [H_K, W_{1,0}] &= R \tfrac{\partial W_{1,0}}{\partial r} + \tfrac{\Theta}{r^2} \tfrac{\partial W_{1,0}}{\partial \theta} - (\tfrac{\Theta^2}{r^3} - \tfrac{\bar{M}}{r^2}) \tfrac{\partial W_{1,0}}{\partial R} \\ &= -\tfrac{1}{\epsilon} \sum_{n=1}^{\infty} \sum_{m=1}^{n} \sum_{j=-n}^{n} \sum_{t=\max\{0,j+m\}}^{\min\{n+m,n+j\}} ci^{2n+m+j-2t} si^{2t-m-j} \left(-\frac{1}{m\Omega} \right) \left(-\frac{R}{r} \right) \cdot \\ &\qquad \cdot (-(n+1)) \tfrac{1}{r^{n+1}} \Big(\mathcal{A}^{(1)}_{n,m,j,t} \sin(m\nu - j\theta) + \mathcal{B}^{(1)}_{n,m,j,t} (-\cos(m\nu - j\theta)) \Big) \\ &\quad -\tfrac{1}{\epsilon} \sum_{n=1}^{\infty} \sum_{m=1}^{n} \sum_{j=-n}^{n} \sum_{t=\max\{0,j+m\}}^{\min\{n+m,n+j\}} ci^{2n+m+j-2t} si^{2t-m-j} \left(-\frac{1}{m\Omega} \right) \left(\frac{j\Theta}{r^2} \right) \frac{1}{r^{n+1}} \cdot \\ &\qquad \cdot \Big(\mathcal{A}^{(1)}_{n,m,j,t} \cos(m\nu - j\theta) + \mathcal{B}^{(1)}_{n,m,j,t} \sin(m\nu - j\theta) \Big), \end{aligned} \tag{4.19}$$

Then the algorithm is iterated $\forall 1 < p \leq p^{(s)}$, where at each iteration, by induction, it can be derived that:

$$K_{1,p} = 0 \tag{4.20}$$

Calling $p_{O_{max}} = 2\lfloor\frac{p-1}{2}\rfloor + 1, \quad p_{E_{max}} = 2\lfloor\frac{p}{2}\rfloor$, and:

$$\begin{aligned}
&\mathcal{S}(\hat{k}, k^*) = \sum_{k=\hat{k}}^{k^*} a_k \\
&\mathcal{S}_E(\hat{k}, k^*) = \sum_{\substack{k=\hat{k},\\ k\ even}}^{k^*} a_k, \quad \mathcal{S}'_E(\hat{k}, k^*) = \sum_{\substack{k=\hat{k},\\ k\ even}}^{k^*} a'_k, \quad \mathcal{S}''_E(\hat{k}, k^*) = \sum_{\substack{k=\hat{k},\\ k\ even}}^{k^*} a''_k \\
&\mathcal{S}_O(\hat{k}, k^*) = \sum_{\substack{k=\hat{k},\\ k\ odd}}^{k^*} a_k, \quad \mathcal{S}'_O(\hat{k}, k^*) = \sum_{\substack{k=\hat{k},\\ k\ odd}}^{k^*} a'_k, \quad \mathcal{S}''_O(\hat{k}, k^*) = \sum_{\substack{k=\hat{k},\\ k\ odd}}^{k^*} a''_k
\end{aligned} \tag{4.21}$$

Also, calling:

$$\mathcal{D} := (-1)^{p-\mathcal{S}(1,p)} \binom{p - \mathcal{S}(2,p)}{p - \mathcal{S}(1,p)} \frac{(n + p - \mathcal{S}(1,p))!}{(n + a_1)!} \tag{4.22}$$

and $\forall k$ *odd*

$$\begin{aligned}
\mathcal{O}_k := &\left(\tbinom{a_{p_{O_{max}}}}{a'_{p_{O_{max}}}} \ldots \tbinom{a_5}{a'_5} \tbinom{a_3}{a'_3}\right) \left(\tbinom{a_{p_{O_{max}}} - a'_{p_{O_{max}}}}{a''_{p_{O_{max}}}} \ldots \tbinom{a_5 - a'_5}{a''_5} \tbinom{a_3 - a'_3}{a''_3}\right) \\
&\left(\tfrac{(a_1+n+p+2\mathcal{S}_E(2,k-1)-\mathcal{S}(k,p)+a_k-a''_k+\mathcal{S}'_O(3,k-2)-\mathcal{S}''_O(3,k-2))!}{(a_1+n+p+2\mathcal{S}_E(2,k-1)-\mathcal{S}(k,p)+a'_k+\mathcal{S}'_O(3,k-2)-\mathcal{S}''_O(3,k-2))!}\right) \\
&\left(\tfrac{(a_1+n+p+\mathcal{S}_E(2,k-1)-\mathcal{S}(k,p)+a_k+\mathcal{S}_O(3,k-2)-\mathcal{S}''_O(3,k-2))!}{(a_1+n+p+\mathcal{S}_E(2,k-1)-\mathcal{S}(k,p)+a_k-a''_k+\mathcal{S}_O(3,k-2)-\mathcal{S}''_O(3,k-2))!}\right)
\end{aligned} \tag{4.23}$$

while $\forall k$ *even*

$$\begin{aligned}
\mathcal{E}_2 &:= \left(\tfrac{(p-\mathcal{S}(1,p))!}{(p-\mathcal{S}(1,p)-a_2)!}\right) \\
\mathcal{E}_k &:= \left(\tfrac{(p-a_1-2\mathcal{S}_E(2,k-2)-\mathcal{S}(k,p)-\mathcal{S}'_O(3,k-1)+a_k+1)!}{(p-a_1-2\mathcal{S}_E(2,k-2)-\mathcal{S}(k,p)-\mathcal{S}'_O(3,k-1)-1)!}\right) \quad \forall k \geq 4,\ k\ even
\end{aligned} \tag{4.24}$$

it results:

$$W_{1,p} = -\tfrac{1}{\epsilon} \sum_{n=1}^{\infty} \sum_{m=1}^{n} \sum_{j=-n}^{n} \sum_{t=\max\{0,j+m\}}^{\min\{n+m,n+j\}} ci^{2n+m+j-2t} si^{2t-m-j} \left(-\frac{1}{m\Omega}\right)^{p+1}$$

$$\sum_{a_p=0}^{1} \left(\sum_{a_{p-1}=1-\delta_{a_p,0}}^{\max\{p-(p-2),0\}} \dots \sum_{a_3=1-\delta_{a_4,0}}^{\max\{p-\mathcal{S}(4,p)-2,0\}} \sum_{a_2=1-\delta_{a_3,0}}^{\max\{p-\mathcal{S}(3,p)-1,0\}} \left(\sum_{a_1=0}^{\max\{p-\mathcal{S}(2,p),0\}} \right.\right.$$

$$\mathcal{D} \left(\sum_{a'_{p_{O_{max}}}=0}^{a_{p_{O_{max}}}} \dots \sum_{a'_5}^{a_5} \sum_{a'_3}^{a_3} \left(\sum_{a''_{p_{O_{max}}}=0}^{a_{p_{O_{max}}}-a'_{p_{O_{max}}}} \dots \sum_{a''_5=0}^{a_5-a'_5} \sum_{a''_3=0}^{a_3-a'_3} \right.\right.$$

$$\left(\mathcal{O}_{p_{O_{max}}} \cdot \dots \cdot \mathcal{O}_5 \cdot \mathcal{O}_3\right) \left(\mathcal{E}_{p_{E_{max}}} \cdot \dots \cdot \mathcal{E}_4 \mathcal{E}_2\right) \left(\tfrac{1}{r}\right)^{3(\mathcal{S}_O(3,p_{O_{max}})-\mathcal{S}'_O(3,p_{O_{max}}))}$$

$$\left(-\tfrac{1}{r}\right)^{p-a_1-\mathcal{S}_E(2,p_{E_{max}})-\mathcal{S}'_O(3,p_{O_{max}})} R^{p-a_1-2\mathcal{S}_E(2,p_{E_{max}})-\mathcal{S}'_O(3,p_{O_{max}})}$$

$$\left(\tfrac{j\Theta}{r^2}\right)^{a_1+\mathcal{S}'_O(3,p_{O_{max}})} \left(\tfrac{-\Theta^2+r\bar{M}}{r^3}\right)^{\mathcal{S}_E(2,p_{E_{max}})-\mathcal{S}_O(3,p_{O_{max}})+\mathcal{S}'_O(3,p_{O_{max}})}$$

$$\begin{aligned}
&\Theta^{2(\mathcal{S}_O(3,p_{O_{max}})-\mathcal{S}'_O(3,p_{O_{max}})-\mathcal{S}''_O(3,p_{O_{max}}))} (-r\bar{M})^{\mathcal{S}''_O(3,p_{O_{max}})} \tfrac{1}{r^{n+1}} \\
&\Big(\mathcal{A}^{(1)}_{n,m,j,t} \left(\cos(m\nu - j\theta) \cos\left(\tfrac{\pi}{2}(-(p+1) + a_1 + \mathcal{S}'_O(3,p_{O_{max}}))\right)\right. \\
&\left. - \sin(m\nu - j\theta) \sin\left(\tfrac{\pi}{2}(-(p+1) + a_1 + \mathcal{S}'_O(3,p_{O_{max}}))\right)\right) \\
&+\mathcal{B}^{(1)}_{n,m,j,t} \left(\sin(m\nu - j\theta) \cos\left(\tfrac{\pi}{2}(-(p+1) + a_1 + \mathcal{S}'_O(3,p_{O_{max}}))\right)\right. \\
&\quad \left.\left.\left.\left.\left.\left. + \cos(m\nu - j\theta) \sin\left(\tfrac{\pi}{2}(-(p+1) + a_1 + \mathcal{S}'_O(3,p_{O_{max}}))\right)\right)\right)\right)\right)\right)\right)
\end{aligned} \tag{4.25}$$

and

$$[H_K, W_{1,p}] = -\tfrac{1}{\epsilon}\sum_{n=1}^{\infty}\sum_{m=1}^{n}\sum_{j=-n}^{n}\sum_{t=\max\{0,j+m\}}^{\min\{n+m,n+j\}} ci^{2n+m+j-2t}si^{2t-m-j}$$

$$\sum_{a_{p+1}=0}^{1}\left(\sum_{a_p=1-\delta_{a_{p+1},0}}^{\max\{p+1-(p-1),0\}}\cdots\sum_{a_3=1-\delta_{a_4,0}}^{\max\{p+1-\mathcal{S}(4,p+1)-2,0\}}\sum_{a_2=1-\delta_{a_3,0}}^{\max\{p+1-\mathcal{S}(3,p+1)-1,0\}}\right.$$

$$\left(\sum_{a_1=0}^{\max\{p+1-\mathcal{S}(2,p+1),0\}}\mathcal{D}^*\left(\sum_{a'_{p_{O_{max}}+1}=0}^{a_{p_{O_{max}}+1}}\cdots\sum_{a'_5}^{a_5}\sum_{a'_3}^{a_3}\left(-\frac{1}{m\Omega}\right)^{p+1}\right.\right.$$

$$\left(\sum_{a''_{p_{O_{max}}+1}=0}^{a_{p_{O_{max}}+1}-a'_{p_{O_{max}}+1}}\cdots\sum_{a''_5=0}^{a_5-a'_5}\sum_{a''_3=0}^{a_3-a'_3}\right.$$

$$\left(\mathcal{O}^*_{p_{O_{max}}+1}\cdot\ldots\cdot\mathcal{O}^*_5\cdot\mathcal{O}^*_3\right)\left(\mathcal{E}^*_{p_{E_{max}}+1}\cdot\ldots\cdot\mathcal{E}^*_4\mathcal{E}^*_2\right)$$

$$\left(\tfrac{1}{r}\right)^{3(\mathcal{S}_O(3,p_{O_{max}}+1)-\mathcal{S}'_O(3,p_{O_{max}}+1))}$$

$$\left(-\tfrac{1}{r}\right)^{p+1-a_1-\mathcal{S}_E(2,p_{E_{max}}+1)-\mathcal{S}'_O(3,p_{O_{max}}+1)}$$

$$R^{p+1-a_1-2\mathcal{S}_E(2,p_{E_{max}}+1)-\mathcal{S}'_O(3,p_{O_{max}}+1)}$$

$$\left(\tfrac{j\Theta}{r^2}\right)^{a_1+\mathcal{S}'_O(3,p_{O_{max}}+1)}\left(\tfrac{-\Theta^2+r\bar{M}}{r^3}\right)^{\mathcal{S}_E(2,p_{E_{max}}+1)-\mathcal{S}_O(3,p_{O_{max}}+1)+\mathcal{S}'_O(3,p_{O_{max}}+1)}$$

$$\Theta^{2(\mathcal{S}_O(3,p_{O_{max}}+1)-\mathcal{S}'_O(3,p_{O_{max}}+1)-\mathcal{S}''_O(3,p_{O_{max}}+1))}(-r\bar{M})^{\mathcal{S}''_O(3,p_{O_{max}}+1)}\tfrac{1}{r^{n+1}}$$

$$\begin{aligned}&\left(\mathcal{A}^{(1)}_{n,m,j,t}\left(\cos\left(m\nu-j\theta\right)\cos\left(\tfrac{\pi}{2}(-(p+1)+a_1+\mathcal{S}'_O(3,p_{O_{max}}))\right)\right.\right.\\&\left.-\sin\left(m\nu-j\theta\right)\sin\left(\tfrac{\pi}{2}(-(p+1)+a_1+\mathcal{S}'_O(3,p_{O_{max}}))\right)\right)\\&+\mathcal{B}^{(1)}_{n,m,j,t}\left(\sin\left(m\nu-j\theta\right)\cos\left(\tfrac{\pi}{2}(-(p+1)+a_1+\mathcal{S}'_O(3,p_{O_{max}}))\right)\right.\\&\left.\left.+\cos\left(m\nu-j\theta\right)\sin\left(\tfrac{\pi}{2}(-(p+1)+a_1+\mathcal{S}'_O(3,p_{O_{max}}))\right)\right)\right)\right)\right)\end{aligned}\tag{4.26}$$

where $\mathcal{D}^*$, $\mathcal{O}^*_t$ and $\mathcal{E}^*_t$ are like the one in (6.15) (6.16) and (6.17) respectively with $p+1$ instead of p.

As

$$[H_K;\ \cdot\ ] = [\tfrac{1}{2}(R^2+\tfrac{\Theta^2}{r^2})-\tfrac{\bar{M}}{r};\ \cdot\ ] = R\tfrac{\partial\cdot}{\partial r}+\tfrac{\Theta}{r^2}\tfrac{\partial\cdot}{\partial\theta}-(\tfrac{\Theta^2}{r^3}-\tfrac{\bar{M}}{r^2})\tfrac{\partial\cdot}{\partial R}\tag{4.27}$$

at each step p the term $[H_K, W_{1,p}]$ is the sum functions that have the same order of the preceding $[H_K, W_{1,p-1}]$ but multiplied by $\frac{R}{\Omega r}$, $\frac{\Theta}{\Omega r^2}$ or $\frac{\Theta^2+r}{\Omega R r^3}$. Following [64], as $R \sim \frac{\Theta}{r}$ and as, at order zero, for the two-body problem, $\Theta \sim r^2\dot{\theta}$, for a satellite period greater than the rotational period of the asteroid (i.e. $\dot{\theta} < \Omega$), these coefficients are and therefore less than the unity over an orbit $\sim \frac{\dot{\theta}}{\Omega} < 1$. Therefore, at each step of the relegation, the transformation process reduces the magnitude of the terms of the perturbing potential which contain the angle ν. Thus, after fixing the parameter ϵ, the number of iteration $p^{(1)}$ is fixed such that $[H_K, W_{1,p^{(1)}}] \sim O(\epsilon^3)$.

The relegation of the first order is ended setting:

$$\begin{aligned} W_1 &:= \textstyle\sum_{p=0}^{p^{(1)}} W_{1,p} \\ R_1 &:= [H_K, W_{1,p^{(1)}}] \\ K_1 &:= \textstyle\sum_{p=0}^{p^{(1)}} K_{1,p} + R_1 = K_{1,0} + R_1 \end{aligned} \tag{4.28}$$

To pass to the second order $s = 2$, the evaluation of $\tilde{H}_{2,0} = H_2 + 2[H_1, W_1] + [[H_0, W_1], W_1]$ is first required, from which the expression for $K_{2,0}$ is derived (see Appendix B). In analogy with the first order, it results $K_{2,p} = 0 \ \ \forall p \geq 1$.
The relegation of the second order is ended setting:

$$\begin{aligned} W_2 &:= \textstyle\sum_{p=0}^{p^{(2)}} W_{2,p} \\ R_2 &:= [H_K, W_{2,p^{(2)}}] \\ K_2 &:= \textstyle\sum_{p=0}^{p^{(2)}} K_{2,p} + R_2 = K_{2,0} + R_2 \end{aligned} \tag{4.29}$$

where $p^{(2)}$ is chosen such that $[H_K, W_{2,p^{(2)}}] \sim O(\epsilon^3)$ which is $p^{(2)} = \lfloor \frac{p^{(1)}+1}{2} \rfloor$.

The resulting Hamiltonian $K = K_0 + \epsilon K_1 + \frac{\epsilon^2}{2} K_2$ is completely equivalent to the one in (4.1). However, as the terms $R_s, \ \ s = 1, 2$ are of order $\sim \epsilon^3$, a truncated system is considered in which such terms have been neglected. Setting:

$$\begin{aligned} \tilde{K}_0 &:= K_0 \\ \tilde{K}_1 &:= \textstyle\sum_{p=0}^{p^{(1)}} K_{1,p} = K_{1,0} \\ \tilde{K}_2 &:= \textstyle\sum_{p=0}^{p^{(2)}} K_{2,p} = K_{2,0} \end{aligned} \tag{4.30}$$

the truncated system is described by the Hamiltonian:

$$\tilde{K} = \tilde{K}_0 + \epsilon \tilde{K}_1 + \frac{\epsilon^2}{2} \tilde{K}_2 \tag{4.31}$$

where, to simplify notation, the $\tilde{}$ will be ignored. This Hamiltonian is equivalent to the one in the main problem of the artificial satellite, in which the argument of node ν is cyclic, which implies that the coriolis term $-\Omega N$ is constant and can therefore

be dropped from the Hamiltonian. A closed form Delaunay normalization can now be performed, for a further reduction of the degrees of freedom, thus yielding an integrable Hamiltonian.

It must be noted that, in complete analogy with the procedure adopted so far, the explicit formulation for every higher order $s \geq 2$ could be obtained.

4.4 Delaunay Normalization

In order to perform the Delaunay normalisation the Hamiltonian is transformed from the relegated Whittaker variables to the Delaunay coordinates. These coordinates have already been introduced in Section 2.2.5, but will here be extended by the introduction of two more conjugated variables h, and H, where h is the argument of the node. and H is the z-component of the total angular momentum, i.e. $H = G\cos I$.
Moreover, by Section 3, it is known that $N = G\cos I \quad => \quad H = G\cos I$ and $R = \frac{\bar{M}e\sin f}{G}$.

The relegated Hamiltonian (4.31) in the Delaunay coordinates takes the form:

$$J = J_0 + \epsilon J_1 + \frac{\epsilon^2}{2} J_2 \tag{4.32}$$

with:

$$\begin{aligned} J_0 &= -\tfrac{\bar{M}^2}{2L^2} \\ J_1 &= -\tfrac{1}{\epsilon}\sum_{n=1}^{\infty}\sum_{j=-n}^{n}\sum_{t=\max\{0,j\}}^{\min\{n,n+j\}} ci^{2n+j-2t} si^{2t-j} \left(\frac{(1+e\cos f)}{(a(1-e^2))}\right)^{n+1} \\ &\quad \left(\mathcal{A}^{(1)}_{n,0,j,t}\cos\left(-j(f+g)\right) + \mathcal{B}^{(1)}_{n,0,j,t}\sin\left(-j(f+g)\right)\right). \end{aligned} \tag{4.33}$$

with

$$\begin{aligned} ci &= \sqrt{\tfrac{1+\frac{H}{G}}{2}} \\ si &= \sqrt{\tfrac{1-\frac{H}{G}}{2}} \end{aligned} \tag{4.34}$$

For brevity of exposition the expression for J_2 will not be explicitly written.

4.4.1 The Normalization algorithm

The closed form normalization algorithm [49] is here adopted, which, instead of using the expansions of r and f in powers of the eccentricity, changes the independent variable from time to the true anomaly f.

Definition 11
A formal series $K'(y,Y,\epsilon)=\sum_{s=0}^{\infty}\frac{\epsilon^s}{s!}K'_s(y,Y)$ *is said to be in Delaunay normal form if the Lie derivative* $L_{K'_0}K'$ *is zero, that is* $[K'_s,K'_0]=0\ \ \forall s\geq 0$.

In our case, as $K'_0=J_0=-\frac{\bar{M}^2}{2L^2}$, the Lie derivative

$$L_{K'_0}(\cdot)=\frac{\bar{M}^2}{L^3}\frac{\partial(\cdot)}{\partial\ell}$$

therefore the new Hamiltonian (4.32) will be in normal form if and only if

$$\frac{\partial K'_1}{\partial\ell}=0\ \ and\ \ \frac{\partial K'_2}{\partial\ell}=0$$

Note that, as for the relegation for the angle ν, the normalization degenerates into an average over the mean anomaly ℓ. Moreover it will be used that:

$$\frac{df}{d\ell}=\frac{a^2\sqrt{1-e^2}}{r^2}. \tag{4.35}$$

4.4.2 Results

The explicit formula for the normalized J_1 is:

$$\begin{aligned}
K'_1=&-\tfrac{1}{\epsilon}\sum_{n=1}^{\infty}\sum_{t=\max\{0,j\}}^{\min\{n,n+j\}} ci^{2n+j-2t}si^{2t-j}\\
&\tfrac{\sqrt{1-e^2}}{a^{n+1}(1-e^2)^n}\left(\sum_{k=0}^{n-1}\binom{n-1}{k}e^k\mathcal{A}^{(1)}_{n,0,j,t}\frac{(k-1)!!}{k!!}(k+1)_{mod_2}+\right.\\
&+2(n+1)_{mod_2}\sum_{j=1}^{n}\sum_{k=0}^{n-1}\sum_{q=0}^{\lfloor\frac{j}{2}\rfloor}\sum_{v=0}^{q}\binom{n-1}{k}\binom{j}{2q}\binom{q}{v}(-1)^{q+v}\ e^k\ \mathcal{A}^{(1)}_{n,0,j,t}\cdot\\
&\cdot\ \cos(gj)\ \tfrac{((j-2q+k+2v)-1)!!}{(j-2q+k+2v)!!}\left((j-2q+k+2v)+1\right)_{mod_2}\\
&-2(n)_{mod_2}\sum_{j=1}^{n}\sum_{k=0}^{n-1}\sum_{q=0}^{\lfloor\frac{j}{2}\rfloor}\sum_{v=0}^{q}\binom{n-1}{k}\binom{j}{2q}\binom{q}{v}(-1)^{q+v}\ e^k\ \mathcal{B}^{(1)}_{n,0,j,t}\cdot\\
&\left.\cdot\ \sin(gj)\ \tfrac{((j-2q+k+2v)-1)!!}{(j-2q+k+2v)!!}\left((j-2q+k+2v)+1\right)_{mod_2}\right)
\end{aligned}\tag{4.36}$$

obtained using that, $\forall 1 \leq j \leq n$:

$$\begin{array}{l} if\ n\ even\ \ \mathcal{A}^{(1)}_{n,0,j} = \mathcal{A}^{(1)}_{n,0,-j} \\ if\ n\ odd\ \ \mathcal{A}^{(1)}_{n,0,j} = -\mathcal{A}^{(1)}_{n,0,-j} \end{array} \tag{4.37}$$

and

$$\begin{array}{l} if\ n\ even\ \ \mathcal{B}^{(1)}_{n,0,j} = \mathcal{B}^{(1)}_{n,0,-j} \\ if\ n\ odd\ \ \mathcal{B}^{(1)}_{n,0,j} = -\mathcal{B}^{(1)}_{n,0,-j} \end{array} \tag{4.38}$$

The first order generating function is obtained by:

$$W_1' = \int \frac{L^3}{(\bar{M})^2} \left(J_1 - \frac{1}{2\pi} \int_0^{2\pi} J_1 d\ell \right) d\ell \tag{4.39}$$

Finally the normalised J_2, namely

$$K_2' = \frac{1}{2\pi} \int_0^{2\pi} (J_2 + 2[J_1, W_1'] + [[J_0, W_1'], W_1']) d\ell \tag{4.40}$$

and its corresponding generating function

$$W_2' = \int \frac{L^3}{(\bar{M})^2} (J_2 - K_2') d\ell \tag{4.41}$$

have been analytically evaluated, using integration by parts, with the aid of the software Mathematica.

As a result $K' = K_0' + \epsilon K_1' + \frac{\epsilon^2}{2} K_2'$ is obtained which is the analytical formulation for the closed-form averaged (with respect to both the argument of node and the mean anomaly), second order, arbitrary degree Hamiltonian of any inhomogeneous gravitational field of a body uniformly rotating around its main axes of inertia for the case $|H_K| < |H_C|$. This two degree of freedom, integrable Hamiltonian approximates the initial system, and can now be applied to every inhomogeneous body in order to determine possible orbits useful for scientific observation missions such as frozen orbits.

4.5 Applications

The Hamiltonian obtained is of the form: $K'(L, G, H, \_, g, \_)$ thus the equations of motion are:

$$\begin{aligned} \ell'(t) &= \tfrac{\partial K'}{\partial L} \\ g'(t) &= \tfrac{\partial K'}{\partial G} \\ h'(t) &= \tfrac{\partial K'}{\partial H} \\ L'(t) &= 0 \\ G'(t) &= -\tfrac{\partial K'}{\partial g} \\ H'(t) &= 0, \end{aligned} \tag{4.42}$$

which can be derived by (4.36) and (4.40) where L and H are constants and all the other motions will only depend on $G(t)$ and $g(t)$.
As already said frozen orbit is an orbit in which the Inclination, the Eccentricity and the Argument of pericenter remains constant during the motion.
This in particular implies that such an orbit is then perfectly periodic except for the orbital plane precession.
A frozen orbit it thus described by the system:

$$\begin{aligned} \dot{e} &= \tfrac{d}{dt}\tfrac{\sqrt{L^2-G^2}}{L} = 0 \\ \dot{I} &= \tfrac{d}{dt}\arccos\tfrac{H}{G} = 0 \\ \dot{g} &= 0. \end{aligned} \tag{4.43}$$

For the properties of the Lie transformations, the "normalized" eccentricity, inclination and argument of pericenter are related to their relative "real" equivalents by the generator of the transformation (see [53]), and can thus be interpreted as a perturbed version of their real correspondents.
In the normalized variables (4.42), the system (4.43) is equivalent to:

$$\begin{aligned} \dot{G} &= 0 \\ \dot{g} &= 0. \end{aligned} \tag{4.44}$$

Thus fixing normalized eccentricity e and inclination I for the desired normalized frozen orbit, and solving the system gives:

$$\begin{aligned} \dot{G} &= 0 \\ \dot{g} &= 0 \\ e &= \tfrac{\sqrt{L^2-G^2}}{L} \\ I &= \arccos\tfrac{H}{G}, \end{aligned} \tag{4.45}$$

and the initial conditions (L_0, G_0, H_0, g_0) for normalized frozen orbits can be found. Moreover, as this all procedure is valid for the case $|H_K| < |H_C|$ such initial conditions

must satisfy:

$$\Omega H_0 > \frac{\bar{M}^2}{2L_0^2} \tag{4.46}$$

and also

$$0 < |H_0| < G_0 < L_0 \tag{4.47}$$

These resulting initial conditions can be transformed back to the initial system describing the full dynamics (see (4.1)) by the inverse of the generating functions [53], to generate an initial guess for frozen orbits around any inhomogeneous body.

4.6 An example

Setting the desired eccentricity and inclination it is thus possible to determine initial conditions which lead to frozen orbits in the truncated system. Such initial conditions are used to approximate the solutions for the secular motion of the satellite in the real system, showing a good agreement between the approximated and the real dynamics.

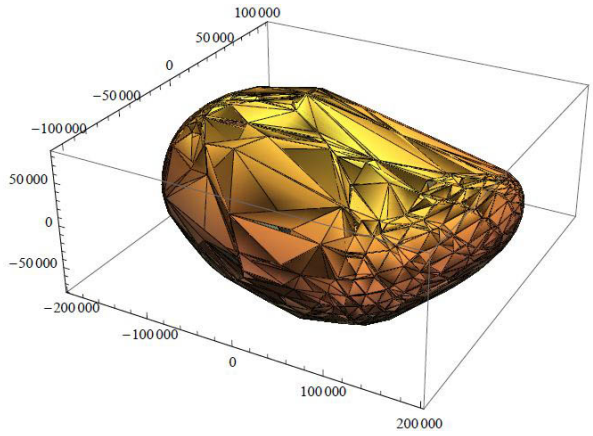

Figure 4.1: **A 3D polyhedric model of 624-Hektor, one of the main Jupiter Trojans**

An example of the application of the method is shown for the asteroid 624-Hektor, for which the spherical harmonic coefficients up to the 10^{th} order and degree (i.e.132 coefficients) are listed in the Appendix C. This coefficients have been obtained following partially the procedure described in [76] from the 1022 vertices (i.e. 2040 "simplices") 3D model of 624-Hektor represented in Fig. 4.1 and found on the *DAMIT-Database of Asteroid Models from Inversion Techniques*. The physical properties of this asteroid are summarized in the Table 4.1.

It is now needed to fix the value of ϵ to distribute the terms of the potential into the right orders of the Hamiltonian. As in this work the fast rotating case is analyzed, a

	Mass Kg	Rotational velocity rad/s	Reference Radius Km	Mean Density^2 Kg/m^3
624-Hektor	1.4×10^{19}	2.52215×10^{-4}	185	2211.12

Table 4.1: Physical properties of 624-Hektor

good candidate might be $\epsilon \sim \frac{\bar{M}^2}{\Omega L_0^3}$. This is derived from an inverse analogy with the ϵ taken in [27] for the case of an artificial satellite orbiting the Earth at low altitudes (i.e. the "slow rotation case"). In this, Palacián fixes ϵ to be the ratio between the angular velocity of the Earth, and the initial mean motion of the satellite n_0, i.e. $\epsilon = \frac{\Omega}{n_0}$, and therefore, as this work deals with the complementary case then the one examined in [27], the reciprocal ϵ is here considered. However, as the resulting frozen orbits has to be at an altitude high enough to satisfy the condition $|H_K| > |H_C|$, and trying to include an high number of spherical harmonic coefficients in the model, in the example shown the ordering parameter ϵ is set to be $\epsilon = 10^{-1}$) (i.e. semimajor axes $\sim 800km$; to apply the results found in the previous chapter, the discussion will focus on relatively high eccentricities $e \in (\frac{1}{2}, 1)$ which implies reasonable periapses radii), $p^{(1)} = 2$, $p^{(2)} = 2$ s.t. $R_1 \sim \left(\frac{\dot{\theta}}{\Omega}\right)^{p^{(1)}+1} \sim 10^{-3}$).
For this example the numerical estimation of the terms containing 624-Hektor's spherical harmonics up to order and degree 10, leads to the following distribution of the $C_{n,m}$, $S_{n,m}$ between the $C^{(1)}_{n,m}$, $C^{(2)}_{n,m}$ and the $S^{(1)}_{n,m}$, $S^{(2)}_{n,m}$ respectively:

$$
\begin{aligned}
C^{(1)}_{n,m} &= \begin{cases} C_{n,m} \; if \; (n,m) \in \{(0,0),(2,0),(2,1),(2,2)\} \\ 0 \;\; otherwise \end{cases} \\
C^{(2)}_{n,m} &= \begin{cases} C_{n,m} \; if \; (n,m) \in \{(4,0),(4,4) \\ \qquad\qquad\qquad (5,3),(5,5),(6,2),(6,6)\} \\ 0 \;\; otherwise \end{cases} \\
S^{(1)}_{n,m} &= \begin{cases} S_{n,m} \; if \; (n,m) \in \{(2,1),(2,2)\} \\ 0 \;\; otherwise \end{cases} \\
S^{(2)}_{n,m} &= \begin{cases} S_{n,m} \; if \; (n,m) \in \{(3,2),(3,3),(4,2)\} \\ 0 \;\; otherwise \end{cases}
\end{aligned}
\tag{4.48}
$$

For illustration purposes the initial conditions for (relegated and normalized) frozen orbits originating from two different eccentricity-inclination-argument of pericenter triples (E_0, I_0, g_0) have been found (see Table 4.2). In the last row of the Table, the initial semimajor axes a_0 of the resulting orbits has also been recorded.

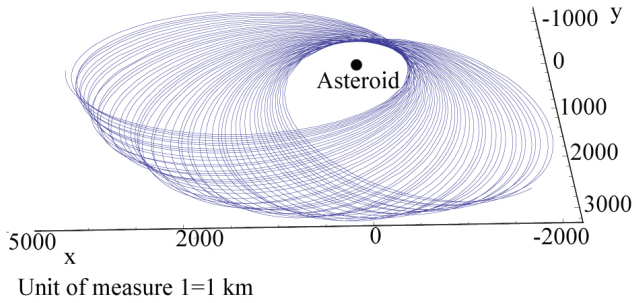

Figure 4.2: The resulting frozen orbit for $E_0 = 0.7$, $I_0 = -0.002$ and $g_0 = -\frac{\pi}{2}$ for 1 year, cartesian, inertial system of reference

	Fig. 4.2	Fig. 4.3
$I_0(rad)$	-0.002	1.1
E_0	0.7	0.85
g_0	0	$-\frac{\pi}{2}$
h_0	π	π
f_0	π	π
G_0	2.9143×10^7	3.6890×10^7
L_0	4.0264×10^7	6.1484×10^7
H_0	2.9143×10^7	1.6733×10^7
$a_0(km)$	1735.12	4045.95

Table 4.2: 624-Hektor: initial conditions for frozen orbits

The initial conditions found with this method are transformed back by canonic transformations inverse to the relegating and normalizing transformations of coordinates found before, leading to approximated initial conditions for frozen orbits in the full model. The integration of such system shows a good agreement of the dynamics between the approximated and the full system, namely a large number of initial conditions produced with the approximated model evolve, in the full system, into a frozen orbit, although some of them degenerate after some time (depending on the initial fixed eccentricity and inclination). The resulting orbits for 624-Hektor are shown in Fig. 4.2 and 4.3, in the cartesian inertial frame of reference centered in the center of mass of the inhomogeneous body (unit of measure km).

4.7 Summary

Inside the stable zone estimated in the previous chapter, the system has been modeled as a R2BP accounting the inhomogeneities of the primary. A general, analytical, closed form perturbational theory has been developed, which yields to an approximate second order Hamiltonian describing the system. An explicit formulation of such a relegated and normalized Hamiltonian is obtained, which allows the development of a method to find frozen orbits in the vicinity of the asteroid by prescribing the eccentricity,

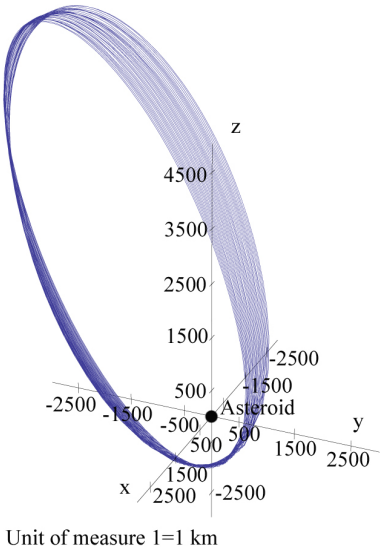

Figure 4.3: The resulting frozen orbit for $E_0 = 0.85$, $I_0 = 1.1$ and $g_0 = 0$ for 5 years, cartesian, inertial system of reference

inclination and argument of pericenter. Results, evaluated for the Trojan 624-Hektor, show two examples of frozen orbits. The first resulting orbit, found fixing an initial eccentricity $e_0 = 0.7$, inclination $I_0 = -0.002$ and argument of pericenter $g_0 = 0$ has an initial radius at pericenter of $520.536km$ which, in normalized units, is $6 \times 10^-6 < r^*(0.7) = 0.0000615179$ which means that this orbit is, in particular, contained in the range estimated in the previous chapter, see (3.70) and (3.71). Another resulting frozen orbit has been shown as well, which is not compared to the WSB estimated range as it has an high inclination and therefore the WSB estimation might not be realistic in this case. This is since the estimation of the set of stable orbits has been obtained in Chapter 3 for the value $I = 0$, and will therefore hold, by continuity for small inclinations. However, following the same methodology, different estimations should be found for different (e.g. higher) inclinations of the orbit.

Chapter 5

Lagrangian (low-thrust) circular restricted four-body model

When a spacecraft moves beyond the region defined by the WSB in Chapter 3 the perturbations due to the gravitational effects of the Sun and Jupiter dominate the dynamics. Furthermore, the effect of the inhomogeneous gravitational field of the body becomes negligible relatively to these gravitational perturbations. To complete the dynamical studies of the spacecraft beyond this region, a Sun-Planet-Trojan-spacecraft model is used. This model, known as the Lagrangian CR4BP, is analysed in this chapter. Again, it represents the dynamics of the spacecraft far from the body[1], where the influence of the two main primaries can no longer be neglected. Low thrust propulsion is included in the modelling with the objective to identify completely novel orbits both for mathematical interest as well as for potential future mission applications.

5.1 State of art

For many years trajectory designers for interplanetary missions have obtained the initial trajectory solutions in the N-body problem (e.g. the four body problem) by dividing the spacecraft's motion into several two-body models, or spheres of influence, each considering one body per time. This 'patched two-body' method, known as patched conic, is relatively straightforward, switching from the influence of one body to another. This method, also named 'spheres of influence method', breaks down when, for example, low energy trajectories [77] are considered, like those used for the WSB; in this regime, where the two bodies both influence the motion of the spacecraft with the same order of magnitude, the restricted N-body problem must be used to model the motion of the spacecraft [48]. Thus N-body dynamics offers exciting new possibilities in mission

[1] See note 2 of the Abstract

design, allowing missions to visit more targets of interest or orbits and to collect data for longer, still using less delta-V than conventionally designed missions.

The Lagrangian Coplanar CR4BP, here introduced, can be considered as one of the first generalisation of the CR3BP. It was first considered by Moulton in 1900 [78]. There exist some preliminary studies of this problem in different versions, mainly used to approximate existing symmetric or equal mass binary systems, see for example [79], [80], [81], [82], [83], [84], and [85]. Of particular relevance are the papers [86] and [87], where the latter uses a numerical approach to determine the number of equilibrium points and a linear stability analysis depending on the distribution of the masses. Most recently in [88] and [89], families of interesting simple non-symmetric periodic orbits are numerically found for two and three equal masses and for an unequal distribution of masses. Many of these papers identify the Sun-Jupiter-Trojan-spacecraft system as the main example of Lagrangian configuration in the Solar system (see also [90], [87], [91], [92], [93]) and apply their studies to such a system. However none of these authors consider that there are no asteroids in the exact L_4 or L_5 position and that they all move on tadpole orbits around such points [94], sometimes with huge oscillations even outside the orbital plane of Jupiter around the Sun.

While orbital motion under the action of a conservative gravitational potential leads to an array of problems with often complex and interesting solutions, the addition of non-conservative forces offers new avenues of investigation. In particular, the combination of natural gravitational potential and non-conservative forces lead to a rich diversity of problems associated with the existence, stability and control of families of highly non-Keplerian orbits. These orbits can potentially have a broad range of practical applications across a number of different disciplines. The use of continuous thrust can be applied in all directions including perpendicular to the flight direction, which forces the spacecraft out of a natural orbit into a displaced, non-Keplerian orbit: such kind of orbits have a wide range of potential applications. Space mission design for low-thrust spacecraft has been extensively investigated from the late 1990's. So far the two major types of low-thrust propulsion, which have been studied in this context, are solar sails and Solar Electric Propulsion SEP, the latter considered in this thesis. Research on this topic, at present, mainly focus on finding artificial equilibria as in [97], [98] and [99], on generating non-Keplerian periodic orbits using solar sails or low thrust, e.g. [100], [101], [102] and [96], on the systematic cataloguing of non-Keplerian orbits using SEP as in [103], or on analyzing the stability properties of minimum-control artificial equilibrium points as in [97] and [104], all of which are set in restricted two or three body models.

The "UK ion propulsion programme" has culminated in the availability of three thrusters of different sizes, covering the thrust $1mN$ to $300mN$ range [105], based on

the $T5$, $T6$ and UK-25 propulsion systems. This is thus the low-thrust potential capability initially assumed in this work. However the result found suggests that a shift towards micropropulsion systems (MPS) could be more appropriate for this application. As an example the Field Emission Electric Propulsion (FEEP) technology, used in the Lisa pathfinder experiment on Einstein's geodesic motion in space, which operates in the micro-Newton field covering the range from $1 \times 10^{-4} mN$ up to $0.5 \times mN$ [106], can provide a more effective propulsion system for the proposed application.

5.2 Introduction and main results

Existing literature, specifically focused on the Lagrangian CR4BP, is contemporary to the new results obtained in this thesis. This literature works are mainly focussed on determining the number of equilibrium points depending on the mass distribution of the primaries and on numerical determination of families of orbits, and the results contained in this Chapter make use of such contemporary results. So in this thesis, Chapter a new dynamical model, the Lagrangian CR4BP, is analysed for the first time, following the traditional techniques used for 2 and 3 body problems (e.g. natural equilibria, linearisation and Lyapunov stability analysis). Furthermore, in this work, the topological changes of the linearly stable zone with variations in the Trojan mass are for the first time showed and analyzed. Moreover in this work, for the first time, the low thrust perturbations are incorporated to the Lagrangian CR4BP to generate surfaces of artificial equilibria and displaced non Keplerian orbits; low thrust perturbations indeed, where thus far confined to two and three body systems. The inclusion of low thrust into the model allows the possibility to find novel, artificial, non-Keplerian orbits both for mathematical interest as well as for future discovery and scientific mission applications. Finally, as none of the previous works considers that there are no asteroids in the exact L4 or L5 position and that they all move on tadpole orbits around such points, the model here developed is here tested for a real case, i.e. considering the real tadpole orbit of the asteroid 624-Hektor around the triangular equilibrium point.
The analysis of the natural evolution of this autonomous coplanar CR4BP is thus first undertaken, which identifies eight natural equilibria, four of which are close to the asteroid. A linear stability analysis reveals that the two closest are unstable and the other two stable, when considering as primaries the Sun and two other bodies of the Solar System. Following this, the model is perturbed by the inclusion of near term low-thrust propulsion system (such as solar electric propulsion (SEP)). Assuming that the spacecraft can thrust in every direction, including perpendicular to the plane containing the three massive bodies, surfaces of artificial equilibrium points close to the smaller primary are generated, both in and out of the plane containing the celestial bodies. Low-

thrust propulsion has been previously considered only in two and three-body restricted problems. A stability analysis of these points is carried out and a stable subset of them is identified. Throughout the analysis the Sun-Jupiter-Trojan- spacecraft system is analysed, as a particular case, for conceivable masses of a hypothetical asteroid set at the libration point L_4. The different topologies of the linearly stable zone corresponding to these masses are shown. The analysis then focusses on a hypothetical asteroid, set to have the same mass of a major Jupiter Trojan: 624-Hektor. A region of bounded orbits is proved to exist, which can be maintained with a constant thrust less than $0.15mN$ for a 1000 kg spacecraft. This illustrates that, by exploiting low-thrust technologies, it would be possible to maintain an observation point more than 66% closer to the asteroid than that of a stable natural equilibrium point. Moreover, this would enable a continuous synoptic view of the hypothetical asteroid itself. The thrust required to enable close asteroid observation is determined in the simplified CR4BP model and eight resulting bounded orbits are shown. However, there are no important Trojan asteroids in or close to the L4 point of the Sun-Jupiter system. Thus a numerical investigation is performed to test the validity of the stability analysis of the model when the asteroid is moved from the exact L4 location to its actual librating orbit. The numerical simulation of the real Sun-Jupiter-Hektor-spacecraft is then undertaken. Results show a shift of the real model towards instability, i.e. the unstable zone enlarges, due to the inclusion in the real model of high perturbations. However, a zone of bounded orbits is heuristically found, in which all the orbits remain bounded within $\sim 3.5 \times 10^6$ km from the Asteroid for at least 36 Terrestrial years ($\sim$ 3 Jupiter's and 624-Hektor's revolutions around the Sun) before starting to diverge. These finite-time bounded orbits can be maintained by using a constant thrust lower than $4 \times 10^{-4}N$ without the need for any state feedback control.

5.3 Natural Equilibria

The dynamics of the massless spacecraft, whose state vector is expressed in non-dimensional cartesian coordinates $\mathbf{x} = [x, y, z]$, is described by the system (2.35), where the parameter μ, appearing on both sides of the motions, can be dropped. Note that if $m \to 0$, system (2.35) degenerates to the classical CR3BP, while if both $m \to 0$ and $M \to 0$ it becomes a R2BP. In order to find the equilibrium points of the system, the velocities $\dot{x},\ \dot{y},\ \dot{z}$ and the accelerations $\ddot{x},\ \ddot{y},\ \ddot{z}$ are set to be zero in (2.35) obtaining:

$$\begin{cases} x + L_x - \frac{(1-M)(x+\frac{1}{2})}{\sqrt{(x+\frac{1}{2})^2+(y+\frac{\sqrt{3}}{2})^2+z^2}^3} - \frac{M(x-\frac{1}{2})}{\sqrt{(x-\frac{1}{2})^2+(y+\frac{\sqrt{3}}{2})^2+z^2}^3} - \frac{mx}{\sqrt{x^2+y^2+z^2}} = 0 \\ y + L_y - \frac{(1-M)(y+\frac{\sqrt{3}}{2})}{\sqrt{(x+\frac{1}{2})^2+(y+\frac{\sqrt{3}}{2})^2+z^2}} - \frac{M(y+\frac{\sqrt{3}}{2})}{\sqrt{(x-\frac{1}{2})^2+(y+\frac{\sqrt{3}}{2})^2+z^2}} - \frac{my}{\sqrt{x^2+y^2+z^2}} = 0 \\ z - \frac{(1-M)z}{\sqrt{(x+\frac{1}{2})^2+(y+\frac{\sqrt{3}}{2})^2+z^2}} - \frac{Mz}{\sqrt{(x-\frac{1}{2})^2+(y+\frac{\sqrt{3}}{2})^2+z^2}} - \frac{mz}{\sqrt{x^2+y^2+z^2}} = 0 \end{cases} \tag{5.1}$$

As the system is in the stable Lagrangian configuration (see Chapter 2) such system admits eight solutions (see [87]), the equilibrium points $M_j,\ j = 1, ..., 8$, defined at the intersections of the three surfaces described by the equations in (5.1), see Appendix D.

Figures 5.1 and 5.2 show the behavior of the three surfaces which satisfy system (5.1) in the vicinity of the third primary; in this region such surfaces form four equilibrium points M_4, M_5, M_6 and M_7 on which this chapter is focussed. Figure 5.1 shows the three surfaces in three dimensions, while Figure 5.2 represents them for $z < 0$ plane, part a), and for $z = 0$ part b).
In particular, in these Figures, the continuous, light, meshed surfaces represent the solution of the first equation of system (5.1), the dashed, dark, meshed surfaces show the solution the second equation of (5.1), while the solution of the third equation is the plane $z = 0$, plotted in the Figures as well. As the third equation is satisfied by the plane $z = 0$, all the equilibria are bounded to stay on this plane, which, equivalently, can be seen as the degeneration of system (5.1) into a two dimensional system for $z = 0$ (see [19]).

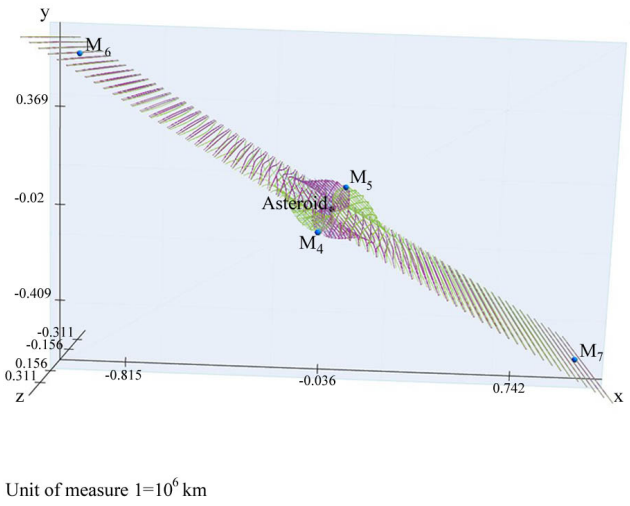

Figure 5.1: The four equilibria close to the asteroid; *spatial view*

By the stability result for unequal masses of [87], there exist a lower limit for the mass ratio $\frac{m_1}{m_1+m_2}(= 1 - M)$ such as, for all the values bigger than that, the points M_6 and M_7 are always stable, which happens, for example, when fixing the three massive bodies in the model to be the Sun and any other two objects of the Solar System. Moreover, as such ratio decreases with the increase in mass of the second primary, $\frac{m_1}{m_1+m_2}$ is fixed to be the minimal obtainable for the solar system, or, equivalently, P_2 is chosen to be Jupiter (i.e. $M = 0.000953592$, $1 - M = 0.999046$). This configuration,

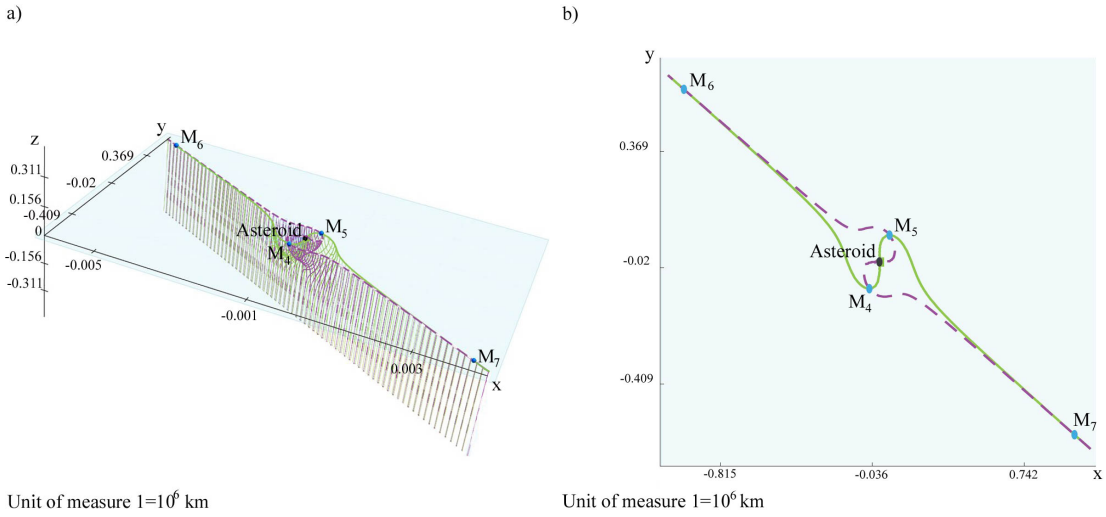

Figure 5.2: The four equilibria close to the asteroid; a) *spatial view for* $z < 0$*;* b) *Intersection with the plane* $z = 0$

in particular, satisfies the stability condition $\frac{(1-M)}{M} > 25 + 18\sqrt{2}$ that can also be rearranged as: $M < \frac{(13-9\sqrt{2})}{14}$.
The qualitative dynamics close to the asteroid does not change for different masses of the asteroid $m \in (0, M)$, in that, there are always four equilibrium points configured approximately at the same angle relative to the asteroid. However, quantitatively, as the mass increases, the equilibrium points are displaced further from the asteroid, as shown in the Figure 5.3 a) and b) where the first shows the behavior of the four equilibrium points as the mass of the asteroid increases while the second is focussed just on M_4 and M_5. Thus, it would be concluded that the only assumptions on the masses of the system should be the stability condition, which, in nondimensional units, becomes: $M < \frac{(13-9\sqrt{2})}{14}$ and that the mass of the asteroid has to be small enough such that it does not affect the motion of the other two Primaries.

5.4 Stability analysis

Hereafter, for simplicity of notation, (x_e, y_e, z_e) will indicate a generic equilibrium solution of system (5.1); moreover, for convenience, a translation to a generic equilibrium point (x_e, y_e, z_e) is performed:

$$\begin{cases} x' = x - x_e \\ y' = y - y_e \\ z' = z - z_e \end{cases} \tag{5.2}$$

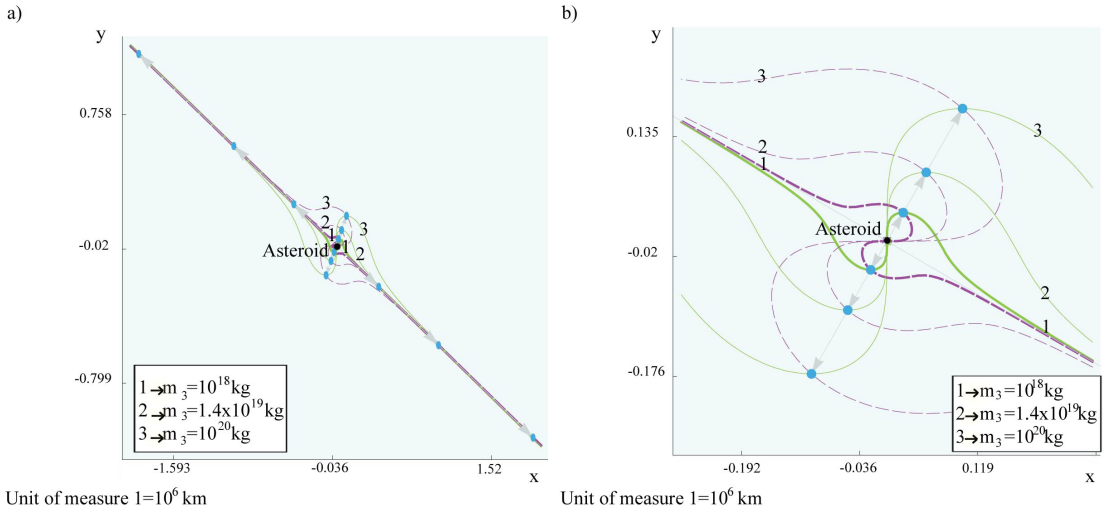

Figure 5.3: Equilibrium Points; a) $\forall m \in (0, M)$ *the two lines intersects four times in the region near the asteroid*; b) *Zoomed image*

but, to simplify notation, the indices above x', y', z' will be ignored.

Then the motion is linearized close to this generic point (x_e, y_e, z_e), obtaining

$$\begin{cases} \dot{x} = X + y \\ \dot{y} = Y - x \\ \dot{z} = Z \\ \dot{X} = Y + (\alpha - 1)x + \chi y + \delta z \\ \dot{Y} = -X + \chi x + (\beta - 1)y + \phi z \\ \dot{Z} = \delta x + \phi y + \gamma z \end{cases} \tag{5.3}$$

with

$$\begin{aligned}
\alpha &= 1 + \frac{(1-M)\left[2(x_E+\frac{1}{2})^2-(y_E+\frac{\sqrt{3}}{2})^2-{z_E}^2\right]}{\sqrt{(x_E+\frac{1}{2})^2+(y_E+\frac{\sqrt{3}}{2})^2+z_E^2}^5} + \frac{M\left[2(x_E-\frac{1}{2})^2-(y_E+\frac{\sqrt{3}}{2})^2-{z_E}^2\right]}{\sqrt{(x_E-\frac{1}{2})^2+(y_E+\frac{\sqrt{3}}{2})^2+z_E^2}^5} + \frac{m\left[2x_E^2-{y_E}^2-{z_E}^2\right]}{\sqrt{x_E^2+y_E^2+z_E^2}^5}, \\
\beta &= 1 + \frac{(1-M)\left[-(x_E+\frac{1}{2})^2+2(y_E+\frac{\sqrt{3}}{2})^2-z_E^2\right]}{\sqrt{(x_E+\frac{1}{2})^2+(y_E+\frac{\sqrt{3}}{2})^2+z_E^2}^5} + \frac{M\left[-(x_E-\frac{1}{2})^2+2(y_E+\frac{\sqrt{3}}{2})^2-z_E^2\right]}{\sqrt{(x_E-\frac{1}{2})^2+(y_E+\frac{\sqrt{3}}{2})^2+z_E^2}^5} + \frac{m\left[-x_E^2+2{y_E}^2-z_E^2\right]}{\sqrt{x_E^2+y_E^2+z_E^2}^5}, \\
\gamma &= \frac{(1-M)\left[-(x_E+\frac{1}{2})^2-(y_E+\frac{\sqrt{3}}{2})^2+2z_E^2\right]}{\sqrt{(x_E+\frac{1}{2})^2+(y_E+\frac{\sqrt{3}}{2})^2+z_E^2}^5} + \frac{M\left[-(x_E-\frac{1}{2})^2-(y_E+\frac{\sqrt{3}}{2})^2+2z_E^2\right]}{\sqrt{(x_E-\frac{1}{2})^2+(y_E+\frac{\sqrt{3}}{2})^2+z_E^2}^5} + \frac{m\left[-x_E^2-y_E^2+2z_E^2\right]}{\sqrt{x_E^2+y_E^2+z_E^2}^5}, \\
\chi &= 3\left\{\frac{(1-M)\left[(x_E+\frac{1}{2})(y_E+\frac{\sqrt{3}}{2})\right]}{\sqrt{(x_E+\frac{1}{2})^2+(y_E+\frac{\sqrt{3}}{2})^2+z_E^2}^5} + \frac{M\left[(x_E-\frac{1}{2})(y_E+\frac{\sqrt{3}}{2})\right]}{\sqrt{(x_E-\frac{1}{2})^2+(y_E+\frac{\sqrt{3}}{2})^2+z_E^2}^5} + \frac{m[x_E y_E]}{\sqrt{x_E^2+y_E^2+z_E^2}^5}\right\}, \\
\delta &= 3\left\{\frac{(1-M)\left[(x_E+\frac{1}{2})z_E\right]}{\sqrt{(x_E+\frac{1}{2})^2+(y_E+\frac{\sqrt{3}}{2})^2+z_E^2}^5} + \frac{M\left[(x_E-\frac{1}{2})z_E\right]}{\sqrt{(x_E-\frac{1}{2})^2+(y_E+\frac{\sqrt{3}}{2})^2+z_E^2}^5} + \frac{m[x_E z_E]}{\sqrt{x_E^2+y_E^2+z_E^2}^5}\right\}, \\
\phi &= 3\left\{\frac{(1-M)\left[(y_E+\frac{\sqrt{3}}{2})z_E\right]}{\sqrt{(x_E+\frac{1}{2})^2+(y_E+\frac{\sqrt{3}}{2})^2+z_E^2}^5} + \frac{M\left[(y_E+\frac{\sqrt{3}}{2})z_E\right]}{\sqrt{(x_E-\frac{1}{2})^2+(y_E+\frac{\sqrt{3}}{2})^2+z_E^2}^5} + \frac{m[y_E z_E]}{\sqrt{x_E^2+y_E^2+z_E^2}^5}\right\}.
\end{aligned} \tag{5.4}$$

which is consistent with [17].

Calling $\bar{\mathcal{A}}$ the matrix corresponding to system (5.3), namely:

$$\bar{\mathcal{A}} = \begin{pmatrix} 0 & 1 & 0 & 1 & 0 & 0 \\ -1 & 0 & 0 & 0 & 1 & 0 \\ 0 & 0 & 0 & 0 & 0 & 1 \\ \alpha - 1 & \chi & \delta & 0 & 1 & 0 \\ \chi & \beta - 1 & \phi & -1 & 0 & 0 \\ \delta & \phi & \gamma & 0 & 0 & 0 \end{pmatrix} \tag{5.5}$$

The characteristic polynomial of $\bar{\mathcal{A}}$ is

$$\begin{aligned} &\Psi^6 + (4 - \alpha - \beta - \gamma)\Psi^4 + (\alpha\beta + \alpha\gamma + \beta\gamma - \chi^2 - \delta^2 - \phi^2 - 4\gamma)\Psi^2 + (\alpha\phi^2 + \beta\delta^2 \\ &\quad + \gamma\chi^2 - \alpha\beta\gamma - 2\chi\delta\phi) = 0. \end{aligned} \tag{5.6}$$

As (5.6) is a biquadratic equation it is useful to set $\Gamma = \Psi^2$, and, observing that $(4 - \alpha - \beta - \gamma) = 2$ in (5.4), yields the monic polynomial of the third degree:

$$\begin{aligned} &\Gamma^3 + 2\Gamma^2 + (\alpha\beta + \alpha\gamma + \beta\gamma - \chi^2 - \delta^2 - \phi^2 - 4\gamma)\Gamma + (\alpha\phi^2 + \beta\delta^2 + \gamma\chi^2 - \alpha\beta\gamma \\ &\quad - 2\chi\delta\phi) = 0. \end{aligned} \tag{5.7}$$

Following the usual procedure to solve third degree polynomials, see for example, [107], it is set

$$\begin{aligned} p &= -\tfrac{4}{3} + (\alpha\beta + \alpha\gamma + \beta\gamma - \chi^2 - \delta^2 - \phi^2 - 4\gamma), \\ q &= \tfrac{16}{27} - \tfrac{2(\alpha\beta+\alpha\gamma+\beta\gamma-\chi^2-\delta^2-\phi^2-4\gamma)}{3} + (\alpha\phi^2 + \beta\delta^2 + \gamma\chi^2 - \alpha\beta\gamma - 2\chi\delta\phi), \\ \Delta &= \tfrac{q^2}{4} + \tfrac{p^3}{27}. \end{aligned} \tag{5.8}$$

Then it is well known that the three solutions $\Gamma_{1,2,3}$ of (5.7) are the only three solutions among those nine

$$\Gamma_{1,2,3} = \sqrt[3]{-\tfrac{q}{3} + \sqrt{\Delta}} + \sqrt[3]{-\tfrac{q}{3} - \sqrt{\Delta}} - \tfrac{2}{3} \tag{5.9}$$

such as

$$\left(\sqrt[3]{-\tfrac{q}{2} + \sqrt{\Delta}}\right) \cdot \left(\sqrt[3]{-\tfrac{q}{2} - \sqrt{\Delta}}\right) = -\tfrac{p}{3} \in \mathbb{R}. \tag{5.10}$$

This means that the six eigenvalues of system (5.3) will be $\Psi_k, \;\; k = 1, ..., 6$ defined as:

$$\Psi_k = \pm\sqrt{\Gamma_j} \;\; k = 1, ..., 6; \;\; j = 1, 2, 3. \tag{5.11}$$

From now on, the main primaries of the system will be considered to be the Sun and Jupiter; therefore, fixing a specific mass $m \in (0, M)$ for the hypothetical asteroid, and evaluating the eigenvalues corresponding to both the equilibrium points M_4 and

M_5, the Δ will be negative, while $\sqrt{-3p}$ will be greater than one, which, as will be shown later on, means that at least one of the three eigenvalues will have Real part non-zero, i.e. these two equilibrium points are linearly unstable and therefore nonlinearly unstable; on the other hand for both the equilibrium points M_6 and M_7, the Δ will be negative, and $\sqrt{-3p}$ will be smaller than one, which implies that all the eigenvalues will be purely imaginary, i.e. the equilibrium points are linearly stable.

5.5 The low-thrust autonomous coplanar CR4BP

The dynamics of a low-thrust spacecraft in the autonomous coplanar CR4BP is now investigated. Using SEP propulsion the spacecraft can create artificial equilibrium points in the spatial vicinity of the asteroid, suitable for observation missions. In addition, a subset of these novel equilibrium points is proved to be stable, such that the motion will remain bounded in a small region about them, with relatively low fuel requirements and without the need for a state feedback control.

Given a maximum thrust capability $\mathcal{F}_{max}$, expressed in N, and an approximate weight for the spacecraft W_s, evaluated in kg, the maximal acceleration in the non-dimensional units is given by:

$$\begin{aligned} a_{max} &= \frac{\mathcal{F}_{max}}{W_s}\frac{N}{kg} = \frac{\mathcal{F}_{max}}{W_s}\cdot\frac{m}{s^2} \\ &= \frac{\mathcal{F}_{max}}{W_s}\cdot\frac{kg}{m^2}\frac{m^3}{kg\cdot s^2} \\ &= \frac{\mathcal{F}_{max}}{W_s}\frac{d^2_{P_1/P_2}}{(m_1+m_2)}\frac{1}{\mathcal{G}}, \end{aligned} \tag{5.12}$$

where d_{P_1/P_2} means the distance in meters between the two major Primaries.
The acceleration will be indicated with $a\hat{\mathbf{n}} = a_x\bar{\mathbf{x}} + a_y\bar{\mathbf{y}} + a_z\bar{\mathbf{z}}$, where a_x, a_y, and a_z are the components of the acceleration in the x, y and z directions, $a = \sqrt{a_x^2 + a_y^2 + a_z^2}$ is the magnitude and $\hat{\mathbf{n}}$ is the direction of the acceleration itself.

Considering the actual thrust capability range between $1mN$ to $300mN$, as stated by the results of the "UK ion propulsion programme" [105], the maximal reachable thrust $\mathcal{F}_{max}$ is initially set to be $300mN$. Moreover, in order to estimate the range of possible acceleration on the spacecraft its mass is set to be $1000kg$. For the Sun-Jupiter-Asteroid-Spacecraft system, the non-dimensional value of the maximum acceleration a_{max} (corresponding to the maximal thrust $\mathcal{F}_{max} = 300mN$) will therefore be 1.36765. Moreover the acceleration has to be constant in the direction of the perturbation, namely

$$\frac{\partial}{\partial\mathbf{x}}(a\hat{\mathbf{n}}) = \frac{\partial}{\partial\mathbf{y}}(a\hat{\mathbf{n}}) = \frac{\partial}{\partial\mathbf{z}}(a\hat{\mathbf{n}}) = 0. \tag{5.13}$$

Adding low-thrust to system (2.35), it becomes:

$$\begin{cases} \ddot{x} = x + L_x + 2\dot{y} - \frac{\partial U_2(\mathbf{x})}{\partial x} + a_x \\ \ddot{y} = y + L_y - 2\dot{x} - \frac{\partial U_2(\mathbf{x})}{\partial y} + a_y \\ \ddot{z} = -\frac{\partial U_2(\mathbf{x})}{\partial z} + a_z \end{cases} \tag{5.14}$$

with $U_2(\mathbf{x})$ as in (2.36).
Again, to find the equilibrium points, the velocities $\dot{x},\ \dot{y},\ \dot{z}$ and the accelerations $\ddot{x},\ \ddot{y},\ \ddot{z}$ are set to be zero in (5.14), obtaining:

$$\begin{cases} a_x = x + L_x + \frac{\partial U_2(\mathbf{x})}{\partial x} \\ a_y = y + L_y + \frac{\partial U_2(\mathbf{x})}{\partial y} \\ a_z = \frac{\partial U_2(\mathbf{x})}{\partial z} \end{cases} \Leftrightarrow \begin{cases} a = |\nabla(\frac{(x+L_x)^2+(y+L_y)^2}{2} + U_2(\mathbf{x}))| \\ \\ \hat{\mathbf{n}} = -\frac{\nabla(\frac{(x+L_x)^2+(y+L_y)^2}{2}+U_2(\mathbf{x}))}{|\nabla(\frac{(x+L_x)^2+(y+L_y)^2}{2}+U_2(\mathbf{x}))|} \end{cases} \tag{5.15}$$

In which, the second system states that, in order to get a new equilibrium point, the acceleration on the spacecraft due to the thrusters has to be equal in magnitude (first equation) but opposite in direction (second equation) to the acceleration on the spacecraft due to the gravitational field at that point; the sign of the three components a_x, a_y and a_z will therefore be determined (and, in particular, opposite) by the respective components of the gravitational field evaluated in the point.

5.6 Stability analysis of the linearized system

Notice that, with a constant thrust, system (5.14), once linearized, is equal to the linear system in (5.3) and therefore the linear stability of the equilibrium points resulting from system (5.15) will be given by the analysis of the eigenvalues in (5.11). By the Lyapunov Stability theorem, see for example [108], in order to obtain a linearly bounded motion, the eigenvalues must have Real part less than or equal to zero. In the case examined, a non zero Real part cannot be accepted, as it would imply that either $Re(\Psi_{2k-1}) > 0$ or $Re(\Psi_{2k}) = Re(-\Psi_{2k-1}) = -Re(\Psi_{2k-1}) > 0$ for $k = 1$ *and/or* 2 *and/or* 3 , and this would lead to a *saddle* $\times$ *saddle* $\times$ *saddle*, a *saddle* $\times$ *saddle* $\times$ *center* or a *saddle* $\times$ *center* $\times$ *center* unstable equilibrium point.

Therefore, in this case, the only acceptable way to get a linearly bounded motion is with $Re(\Psi_k) = 0,\ \forall\ k = 1, ..., 6$.

Theorem 1 *If* $\Delta < 0$ *then the solutions* $\Gamma_j, \quad j = 1, 2, 3$ *of (5.7) are in* $\mathbb{R}$.

Proof:
Let be $\Delta < 0$.

From (5.9) and (5.10), and considering the fact that $\Delta < 0$, the solutions $\Gamma_j, \quad j = 1, 2, 3$ of (5.7) can be rearranged to yield the three solutions among these nine

$$\Gamma_{1,2,3} = \sqrt[3]{-\frac{q}{3} + i\sqrt{-\Delta}} + \sqrt[3]{-\frac{q}{3} - i\sqrt{-\Delta}} - \frac{2}{3} \tag{5.16}$$

that satisfy the condition:

$$\left(\sqrt[3]{-\frac{q}{2} + i\sqrt{-\Delta}}\right) \cdot \left(\sqrt[3]{-\frac{q}{2} - i\sqrt{-\Delta}}\right) = -\frac{p}{3} \in \mathbb{R}. \tag{5.17}$$

Notice that, from system (5.8),

$$\Delta < 0 \Rightarrow p < 0 \tag{5.18}$$

and that the two numbers

$$\begin{array}{l} -\frac{q}{2} + i\sqrt{-\Delta} \\ -\frac{q}{2} - i\sqrt{-\Delta} \end{array} \tag{5.19}$$

are complex conjugates (same Real part, opposite Imaginary part) such that:

$$|-\tfrac{q}{2} + i\sqrt{-\Delta}| = |-\tfrac{q}{2} - i\sqrt{-\Delta}| = \sqrt{(-\tfrac{q}{2})^2 - (\sqrt{-\Delta})^2} = \sqrt{-\tfrac{p}{3}} \in \mathbb{R}. \tag{5.20}$$

Calling

$$\theta = \begin{cases} \arctan\left(-\frac{2\sqrt{-\Delta}}{q}\right) & if \quad q < 0 \\ \arctan\left(-\frac{2\sqrt{-\Delta}}{q}\right) - \pi & if \quad q > 0 \end{cases} \tag{5.21}$$

the two numbers can be rewritten as:

$$\begin{array}{l} \sqrt{-\frac{p^3}{27}}(e^{i\theta}) \\ \sqrt{-\frac{p^3}{27}}(e^{-i\theta}) \end{array} \tag{5.22}$$

Thus, extracting the cubic root, gives:

$$\begin{array}{l} \sqrt{-\frac{p}{3}}(e^{i(\frac{\theta}{3} + \frac{2k\pi}{3})}) \\ \sqrt{-\frac{p}{3}}(e^{i(-\frac{\theta}{3} + \frac{2h\pi}{3})}) \end{array} \tag{5.23}$$

with $h, k = 0, 1, 2$.

For condition (5.17), the only couples that can be accepted are $(h = 0; k = 0)$, $(h = 2; k = 1)$ and $(h = 1; k = 2)$. This implies that the three acceptable solutions of

(5.7) can be summarized in a compact form as:

$$\begin{aligned}\Gamma_j &= \sqrt{-\tfrac{p}{3}}(e^{i(\frac{\theta}{3}+\frac{2(j-1)\pi}{3})} + e^{i(-\frac{\theta}{3}+\frac{4(j-1)\pi}{3})}) - \tfrac{2}{3} \\ &= \sqrt{-\tfrac{p}{3}}\left(\cos\left(\tfrac{\theta}{3}+\tfrac{2(j-1)\pi}{3}\right) + i\sin\left(\tfrac{\theta}{3}+\tfrac{2(j-1)\pi}{3}\right)\right) \\ &\quad +\sqrt{-\tfrac{p}{3}}\left(\cos\left(\tfrac{\theta}{3}+\tfrac{2(j-1)\pi}{3}\right) - i\sin\left(\tfrac{\theta}{3}+\tfrac{2(j-1)\pi}{3}\right)\right) - \tfrac{2}{3} \\ &= 2\sqrt{-\tfrac{p}{3}}\cos\left(\tfrac{\theta}{3}+\tfrac{2(j-1)\pi}{3}\right) - \tfrac{2}{3},\end{aligned} \tag{5.24}$$

with $j = 1, 2, 3$.

Which demonstrates that $\Delta < 0 \Rightarrow \Gamma_j \in \mathbb{R}, \quad \forall j = 1, 2, 3$.

Theorem 2 *If* $\sqrt{-3p} < 1$ *then* $\Gamma_j < 0, \quad \forall j = 1, 2, 3$.

Proof:
By (5.24) for each $j = 1, 2, 3$, Γ_j can be rewritten as

$$\Gamma_j = 2\sqrt{-\frac{p}{3}}\cos\left(\frac{\theta}{3}+\frac{2(j-1)\pi}{3}\right) - \frac{2}{3}. \tag{5.25}$$

Then, for hypothesis:

$$2\sqrt{-\tfrac{p}{3}}\cos\left(\tfrac{\theta}{3}+\tfrac{2(i-1)\pi}{3}\right) - \tfrac{2}{3} \leq 2\sqrt{-\tfrac{p}{3}} - \tfrac{2}{3} < \tfrac{2}{3} - \tfrac{2}{3} = 0 \tag{5.26}$$

Theorem 3 *If*

$$\begin{cases} \Delta < 0 \\ \sqrt{-3p} < 1 \end{cases} \tag{5.27}$$

then the six eigenvalues of system (5.3) are purely Imaginary.

Proof:
The proof of the Lemma is straight forward since the eigenvalues of (5.3) are $\Psi_k = \pm\sqrt{\Gamma_j}, \quad k = 1, ..., 6; \quad j = 1, 2, 3$. Considering the hypothesis and applying Lemma 1, indeed, yields that $\Gamma \in \mathbb{R}, \forall j = 1, 2, 3$. Then, for Lemma 2, $\Gamma_j < 0, \forall j = 1, 2, 3$, which are the two conditions that lead to the thesis of Lemma 3.

Therefore, the six eigenvalues can be rearranged in the form:

$$\Psi_k = \pm i\sqrt{-\Gamma_j}, \quad k = 1, ..., 6; \quad j = 1, 2, 3. \tag{5.28}$$

Figure 5.4 shows the spatial view of the three possible topologies of the zone that satisfies the conditions in (5.27), obtained for a realistic range for the mass of the hypothetical asteroid (i.e. from zero to the total mass of the Jupiter Trojans $\sim 6 \times 10^{20} kg$).

In particular part a) of the Figure represents the topology of the "four leaf clover" [19] for $m_3 \in [0; 1.648 \times 10^{17}[$ kg ($\Rightarrow \epsilon \in [0; 8.27632 \times 10^{-14}[$), part b) represents it for $m_3 = 1.648 \times 10^{17}$ kg ($\Rightarrow \epsilon = 8.27632 \times 10^{-14}$), and part c) for $m_3 \in]1.648 \times 10^{17}; 6 \times 10^{20}]$ kg ($\Rightarrow \epsilon \in]8.27632 \times 10^{-14}; 3.01356 \times 10^{-10}]$).
In this figure, the zone that satisfies the conditions in (5.27), is the linearly "stable zone", intersection of the zone outside the dashed, dark, meshed surfaces and that outside the continuous, light, meshed surfaces which represents the solution of the first and the second equations of system (5.27) respectively.

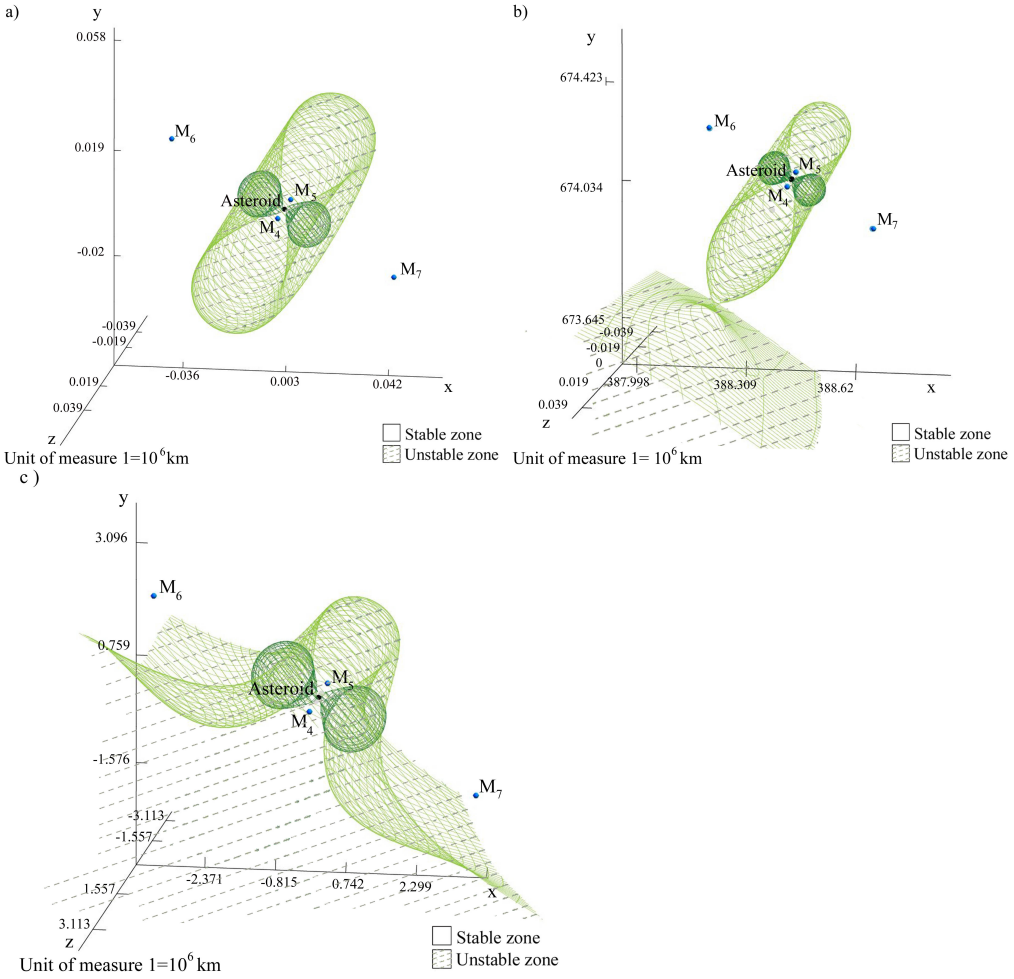

Figure 5.4: The possible topologies obtainable varying the mass of the Asteroid; *a)* $m_3 \in [0; 1.648 \times 10^{17}[$ *kg* $(\Rightarrow \epsilon \in [0; 8.27632 \times 10^{-14}[$ *). b)* $m_3 = 1.648 \times 10^{17}$ *kg* $(\Rightarrow \epsilon = 8.27632 \times 10^{-14}$ *). c)* $m_3 \in]1.648 \times 10^{17}; 6 \times 10^{20}]$ *kg* $(\Rightarrow \epsilon \in]8.27632 \times 10^{-14}; 3.01356 \times 10^{-10}]$*).*

For displaying purpose only, from now on, the mass of the Asteroid will be set to be equal to the major of the actual Trojan Asteroids, namely 624-Hektor, therefore fixing $m_3 = 1.4 \times 10^{19} kg$ (which implies $\epsilon = 7.03165 \times 10^{-12}$). Qualitatively the results for this value will be the same as for each value in the range considered, from zero to the total mass of the Jupiter Trojans.

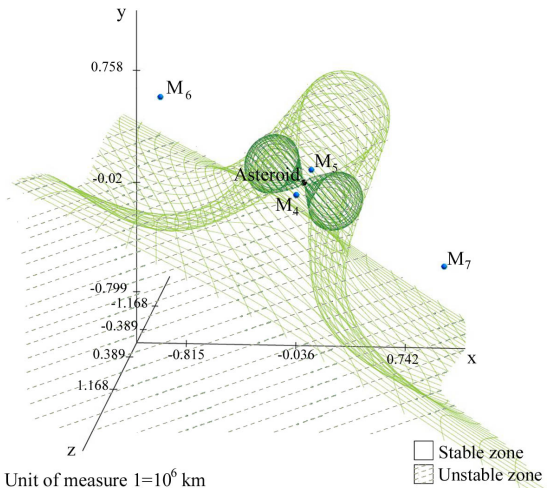

Figure 5.5: Linearly stable/unstable zones; *the three dimensional "four leaf clover",the boundary between the linearly stable and the unstable zones near the asteroid*

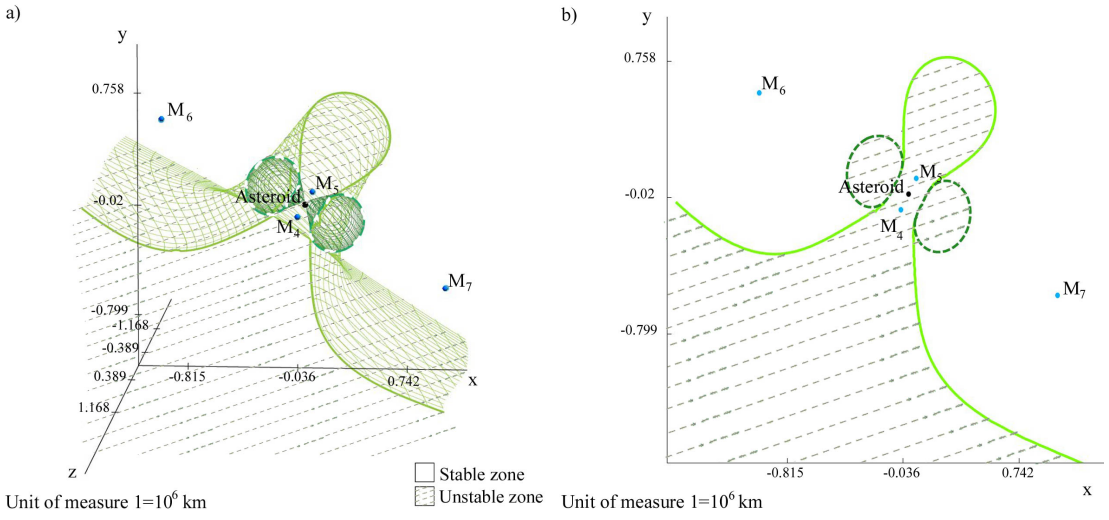

Figure 5.6: Linearly stable/unstable zones; a) *spatial view for $z < 0$;* b) *Intersection with the plane $z = 0$*

Figure 5.5 represents the spatial view of the linearly stable zone of the Sun-Jupiter-Asteroid-Spacecraft system, while, once again, Figure 5.6 represents the horizontal x/y section, part a), and its intersection with the x/y plane, part b).

Of course, there exist an upper, external limit of the linearly stable zone as represented in Figure 5.7.

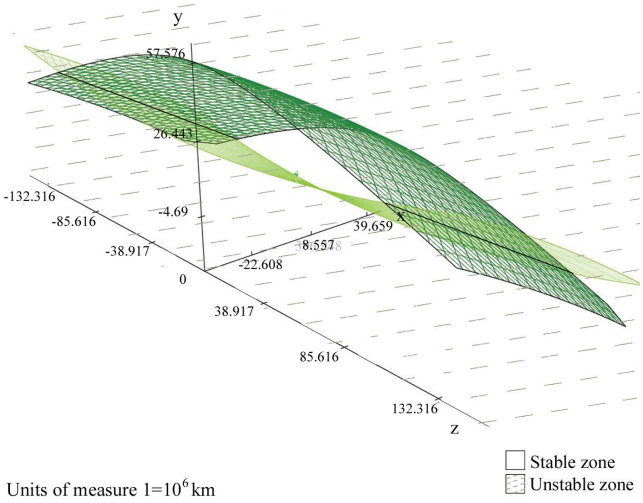

Figure 5.7: The outside boundary; *The linearly stable zone is bounded.*

In particular the first inequality of system (5.27) is verified by the points between the dashed, dark, meshed surfaces, while the second by those between the continuous, light, meshed surfaces. Thus, within the bounded area defined by the intersection of these two zones the linearized motion is stable. Once again, these zones are represented in the three dimensions, Figure 5.7, then for $z < 0$, Figure 5.8 a), and finally intersected with this plane, Figure 5.8 b).

With reference to Figure 5.4 it should be noted that the external limit is separated from the four leaf clover for small values of the mass of the asteroid, then approaches it as the mass of the Asteroid grows to $1.648 \times 10^{17} kg$, where two surfaces becomes tangent, and finally, as the mass overcomes such value, the two surfaces merge together and the lower part of the four leaf clover opens.

Moreover it was numerically evaluated that the maximum possible thrust required to overcome the lower outside boundary is about $0.7mN$ while for the upper one the thrust required is about $25mN$. However, for the system considered, the maximum thrust actually needed for this simplified model will be lower than $0.15mN$.
For the purpose of exposition, eight linearly stable artificial equilibrium points A, B, C, D, E, F, G, H are chosen, which have to fulfill three main requirements: to be generated by a thrust lower than $0.15mN$, to be at a distance from the unstable zone equal or higher than $3500km$ (far enough from the unstable zone to account for the likelihood of injection/position errors of the spacecraft), but remaining as close as possible

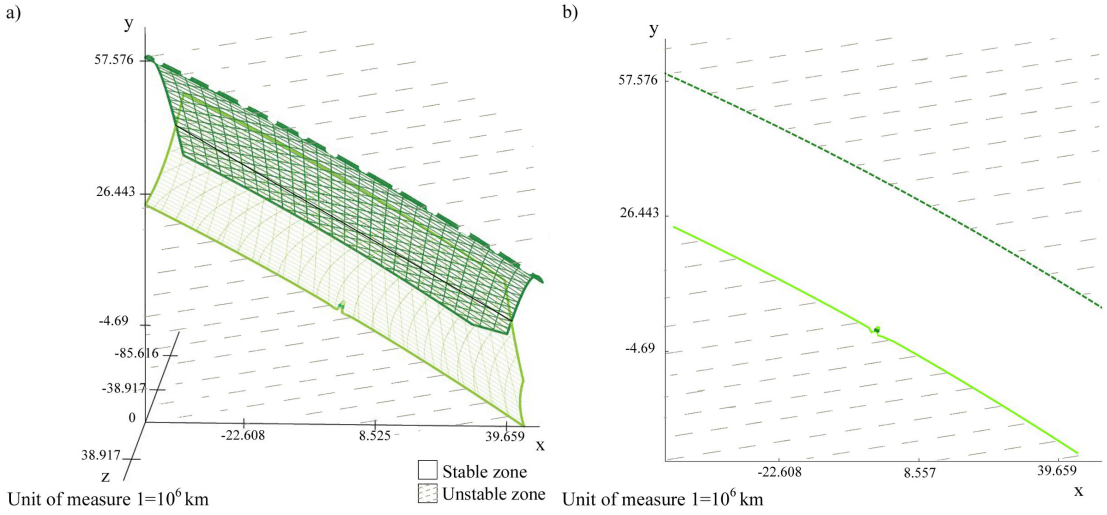

Figure 5.8: The outside boundary; a) *spatial view for* $z < 0$*;* b) *Intersection with the plane* $z = 0$

to the asteroid. Moreover the first four are taken lying on the x/y plane, while the other on the x'/z plane where x' is the tilted horizontal axis $y = -x\frac{M_{5_x} - M_{4_x}}{M_{5_y} - M_{4_y}}$, (i.e. the line passing through the asteroid and perpendicular to the segment connecting M_4 and M_5). The nondimensional coordinates of the four artificial equilibria in the x/y are:

	x	y	z
A	-0.000263408	-0.0000934038	0
B	0.0000505918	-0.000274404	0
C	0.000263592	0.0000930962	0
D	-0.0000509082	0.000274596	0

The nondimensional coordinates of the four artificial equilibrium point on the x'/z plane:

	x	y	z
E	-0.000211408	-0.866332	-0.000307
F	0.287971	0.000211592	-0.000307
G	0.287727	0.000211592	0.000307
H	-0.000211408	0.287971	0 0.000307

The eight points result to be at a distance smaller than $300000km$ from the aster-

oid (note that the distance of the stable equilibrium points from the Asteroid is about $1.16 \times 10^6 km$, more that two thirds bigger than the distance of the asteroid from the artificial equilibrium points chosen).

In this system, in non-dimensional units, the amount of thrust required to create the two artificial points in $A = (A_x; A_y; A_z)$ and in $G = (G_x; G_y; G_z)$ are evaluated; the behavior of the dynamics close to these two artificial equilibrium points, as well as their required thrust, are representative of the four points on the $z = 0$ plane, and for the four on the x'/z plane respectively, as can be seen in Figures 5.10 and 5.11, and, therefore, these points will be the only two investigated in detail.
To this end the computation of the gravitational field in both A and G is needed. For the point A it is set:

$$\begin{cases} a_x = -A_x - L_X + \frac{(1-M)(A_x+\frac{1}{2})}{\sqrt{(A_x+\frac{1}{2})^2+(A_y+\frac{\sqrt{3}}{2})^2+A_z^2}^3} + \frac{M(A_x-\frac{1}{2})}{\sqrt{(A_x-\frac{1}{2})^2+(A_y+\frac{\sqrt{3}}{2})^2+A_z^2}^3} + \frac{mA_x}{\sqrt{A_x^2+A_y^2+A_z^2}^3} \\ \quad = 0.000233755 \\ a_y = -A_y - L_y + \frac{(1-M)(A_y+\frac{\sqrt{3}}{2})}{\sqrt{(A_x+\frac{1}{2})^2+(A_y+\frac{\sqrt{3}}{2})^2+A_z^2}^3} + \frac{M(A_y+\frac{\sqrt{3}}{2})}{\sqrt{(A_x-\frac{1}{2})^2+(A_y+\frac{\sqrt{3}}{2})^2+A_z^2}^3} + \frac{mA_y}{\sqrt{A_x^2+A_y^2+A_z^2}^3} \\ \quad = 0.000521729 \\ a_z = \frac{(1-M)A_z}{\sqrt{(A_x+\frac{1}{2})^2+(A_y+\frac{\sqrt{3}}{2})^2+A_z^2}^3} + \frac{MA_z}{\sqrt{(A_x-\frac{1}{2})^2+(A_y-\frac{\sqrt{3}}{2})^2+A_z^2}^3} + \frac{mA_z}{\sqrt{A_x^2+A_y^2+A_z^2}^3} \\ \quad = 0 \end{cases} \tag{5.29}$$

which yields to $a = \sqrt{a_x^2 + a_y^2 + a_z^2} = 0.000571701$ corresponding approximately to a force of $0.125406mN$; the same evaluation for the point G leads to $(a_x, a_y, a_z) = (0.0000240703, -0.00001415, 0.00034275)$ which is $a = \sqrt{a_x^2 + a_y^2 + a_z^2} = 0.000343885$ corresponding approximately to a force of $0.075433mN$.

These thrusts are represented respectively by the two "tube shaped", meshed surfaces in Figures 5.9, 5.10 and 5.11; the first thrust is approximately the same required to create the other three equilibrium points lying on the x/y plane (B, C, and D), while the other is approximately the same required to create artificial equilibrium points set on the x'/z plane (E, F, and H). Figure 5.10 a) and b) represents the horizontal x/y section and the intersection with the x/y plane of Figure 5.9.
As the four leaf clover is tilted with respect to the system of reference, it is also useful, in terms of visual presentation, to section and intersect it with the vertical plane x'/z as shown in Figure 5.11 a) and b) respectively.
Note that, the eight points in Figures 5.9, 5.10 and 5.11 lie $3500km$ outside the linearly unstable zone, although it is not easy to visualize.

Moreover, parts b) of Figures 5.10 and 5.11 show the projections, on the respective planes, of the directions of the thrust required to counterbalance the gravitational field creating artificial equilibrium points.

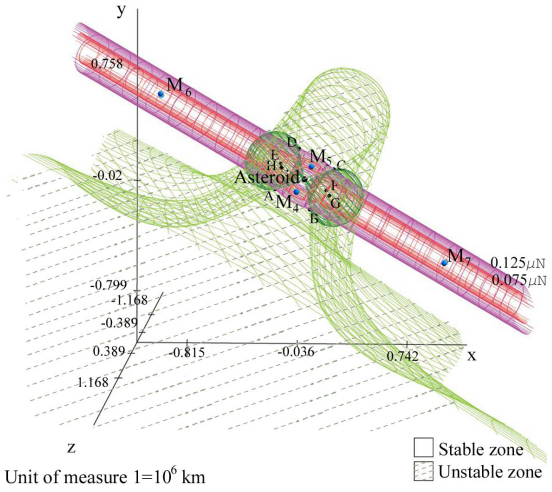

Figure 5.9: Adding the low-thrust; *eight artificial equilibrium points are created in the linearly stable zone using a thrust lower than* 1.5×10^{-4}

5.7 Integrating the linearized motion

Theorem 4 *For a linear system of the form:*

$$\begin{cases} \dot{\mathtt{x}} = \bar{\mathcal{A}}\mathtt{x} \\ \mathtt{x}(t_0) = \mathtt{x}_0 \end{cases} \tag{5.30}$$

where $\mathtt{x} \in \mathbb{R}^6$ *and*
$\bar{\mathcal{A}} \in \mathcal{L}(\mathbb{R}^6) := \{$ *linear operators* $\bar{\mathcal{A}} : \mathbb{R}^6 \to \mathbb{R}^6$, *with real coefficients* $\}$, *if* $\bar{\mathcal{A}}$ *has three couples of eigenvalues complex conjugated* $\lambda, \lambda^*; \nu, \nu^*; \varphi, \varphi^* \in \mathbb{C}$, *where the complex conjugated is indicated by the* *, *such that:*

$$\begin{aligned} \lambda &= \lambda_{_R} + i\lambda_{_I}, \\ \nu &= \nu_{_R} + i\nu_{_I}, \\ \varphi &= \varphi_{_R} + i\varphi_{_I}, \end{aligned} \tag{5.31}$$

where $\lambda_R = Re(\lambda)$ *and* $\lambda_I = Im(\lambda)$ *and* $\lambda_{_I}, \nu_{_I}, \varphi_{_I} \neq 0$; *then there exist a base of vectors* $\{\bar{\mathbf{u}}_1, \bar{\mathbf{w}}_1, \bar{\mathbf{u}}_3, \bar{\mathbf{w}}_3, \bar{\mathbf{u}}_5, \bar{\mathbf{w}}_5\}$, *with* $\bar{\mathbf{u}}_{2j-1}, \bar{\mathbf{w}}_{2j-1} \in \mathbb{R}^6 \quad \forall j = 1, 2, 3$, *and where* $\bar{\mathbf{f}}_{2j-1} = \bar{\mathbf{u}}_{2j-1} + i\bar{\mathbf{w}}_{2j-1}$, $j = 1, 2, 3$ *are the eigenvectors of system (5.30), such that, in*

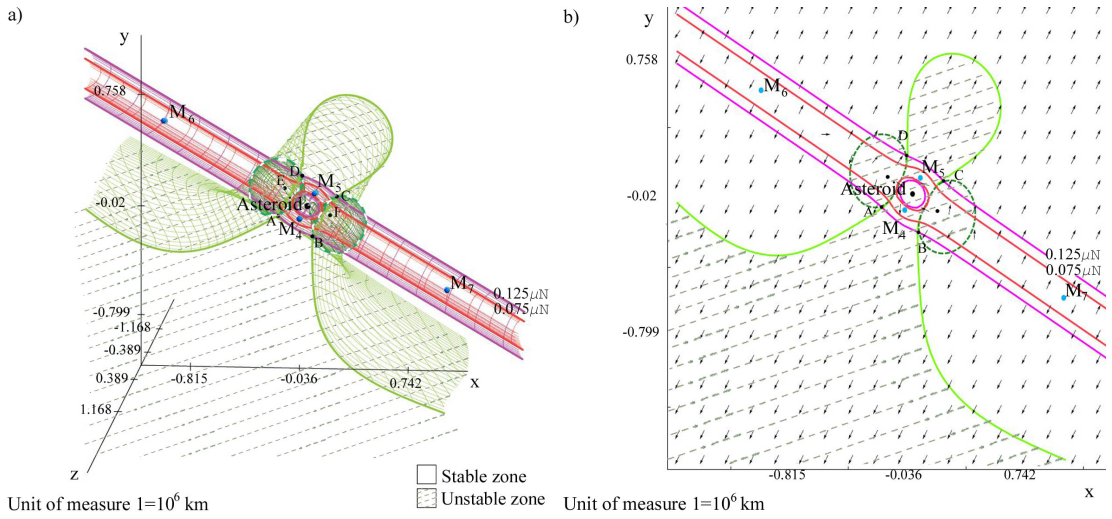

Figure 5.10: Adding the low-thrust; a) *spatial view for $z < 0$;;* b) *Intersection with the plane $z = 0$ and projection on this plane of the direction of the thrust required*

this basis, the solution $\beth(t) = [\xi_1(t), \xi_2(t), \psi_1(t), \psi_2(t), \zeta_1(t), \zeta_2(t)]^T$ of the problem is:

$$\begin{cases} \xi_1(t) = e^{\lambda_R t}\left(\cos(\lambda_{_I} t)\xi_1^0 + \sin(\lambda_{_I} t)\xi_2^0\right) \\ \xi_2(t) = e^{\lambda_R t}\left(\cos(\lambda_{_I} t)\xi_2^0 - \sin(\lambda_{_I} t)\xi_1^0\right) \\ \psi_1(t) = e^{\nu_R t}\left(\cos(\nu_{_I} t)\psi_1^0 + \sin(\nu_{_I} t)\psi_2^0\right) \\ \psi_2(t) = e^{\nu_R t}\left(\cos(\nu_{_I} t)\psi_2^0 - \sin(\nu_{_I} t)\psi_1^0\right) \\ \zeta_1(t) = e^{\varphi_R t}\left(\cos(\varphi_{_I} t)\zeta_1^0 + \sin(\varphi_{_I} t)\zeta_2^0\right) \\ \zeta_2(t) = e^{\varphi_R t}\left(\cos(\varphi_I t)\zeta_2^0 - \sin(\varphi_{_I} t)\zeta_1^0\right) \end{cases} \tag{5.32}$$

And therefore the solution $\mathtt{x}(t) = [x(t), y(t), z(t), X(t), Y(t), Z(t)]^T$ of system (5.30) will be $\mathtt{x}(t) = \mathcal{N}\beth(t)$ where $\mathcal{N}$ is the matrix which provide the expression of the original coordinates $\mathtt{x} = [x, y, z, X, Y, Z]^T$ in terms of the new one, $\beth = [\xi_1, \xi_2, \psi_1, \psi_2, \zeta_1, \zeta_2]^T$, i.e. is the matrix of the change of coordinates.

Proof:
The proof of this theorem is given in Appendix E.

For the theorem above it is enough to find the eigenvectors of the system, and its solutions will be automatically obtained; moreover it will also provide the matrix $\mathcal{N}$ of the change of coordinates, as will be shown later on.

The eigenvalues of the system will be the six vectors $\bar{\mathbf{f}}_j = \bar{\mathbf{u}}_j + i\bar{\mathbf{w}}_j \in \mathbb{C}^6, \quad j = 1, ..., 6$ which solve

$$\bar{\mathcal{A}}\bar{\mathbf{f}}_j = \Psi_j \bar{\mathbf{f}}_j, \quad j = 1, ..., 6. \tag{5.33}$$

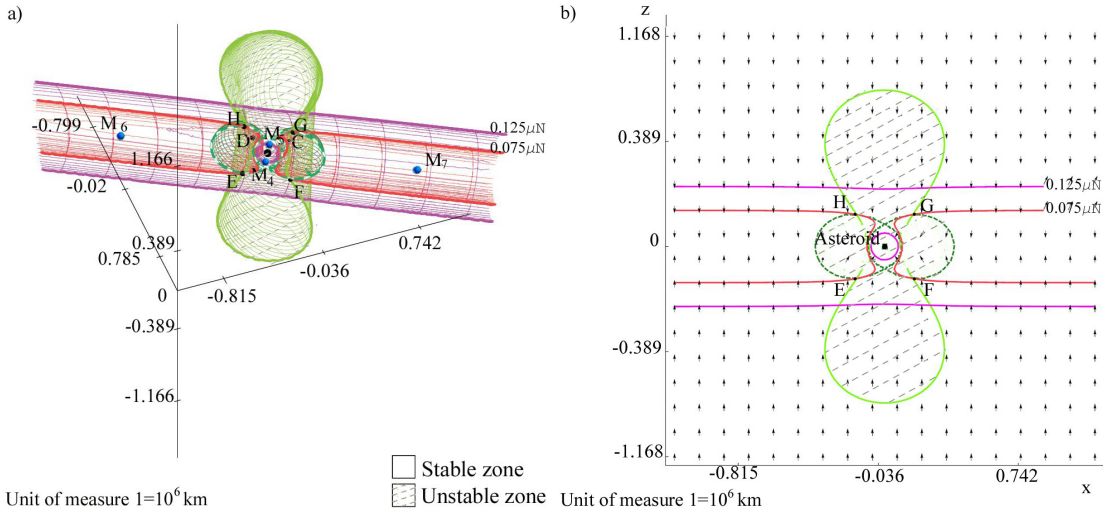

Figure 5.11: Adding the low-thrust; a) x'/z *section of the spatial view;* b) *Intersection with the plane* x'/z *and projection on this plane of the direction of the thrust required*

As the six eigenvalues are three couples of complex conjugated numbers, the eigenvectors must be three couples of complex conjugated vectors, namely $\bar{\mathbf{f}}_{2j} = \bar{\mathbf{u}}_{2j} + i\bar{\mathbf{w}}_{2j} = \bar{\mathbf{u}}_{2j-1} - i\bar{\mathbf{w}}_{2j-1} = \bar{\mathbf{f}}^*_{2j-1}, \quad \forall j = 1, 2, 3$. This, in particular implies that it is sufficient to find three of the six eigenvectors, i.e. $\bar{\mathbf{f}}_1$, $\bar{\mathbf{f}}_3$ and $\bar{\mathbf{f}}_5$. Moreover, in the case considered in this work, the eigenvalues have null Real part (i.e. are purely imaginary), and can therefore be stated in a simpler form.

Therefore, to simplify notation, hereafter the eigenvectors of the system will be:

$$\begin{aligned} \Psi_1 &= \lambda i, \\ \Psi_2 &= -\lambda i, \\ \Psi_3 &= \nu i, \\ \Psi_4 &= -\nu i, \\ \Psi_5 &= \varphi i, \\ \Psi_6 &= -\varphi i. \end{aligned} \tag{5.34}$$

A few algebraic manipulations of (5.33) lead to the determination of the coefficients $\bar{u}_{k,j} \quad k = 1, 3, 5 \quad j = 1, ..., 6$ of the three eigenvectors corresponding to the eigenvalues $\lambda i, \nu i, \varphi i$ respectively; these coefficients are listed in the Appendix F.
Note that, to be consistent with the notation used in [17] it is sufficient to invert the

relation:

$$\begin{aligned}
\bar{u}_{1,4} &= -u_{1,2} + u_{1,4} & \bar{u}_{1,5} &= u_{1,1} + u_{1,5} \\
\bar{w}_{1,4} &= -w_{1,2} + w_{1,4} & \bar{w}_{1,5} &= w_{1,1} + w_{1,5} \\
\bar{u}_{3,4} &= -u_{3,2} + u_{3,4} & \bar{u}_{3,5} &= u_{3,1} + u_{3,5} \\
\bar{w}_{3,4} &= -w_{3,2} + w_{3,4} & \bar{w}_{3,5} &= w_{3,1} + w_{3,5} \\
\bar{u}_{5,4} &= -u_{5,2} + u_{5,4} & \bar{u}_{5,5} &= u_{5,1} + u_{5,5} \\
\bar{w}_{5,4} &= -w_{5,2} + w_{5,4} & \bar{w}_{5,5} &= w_{5,1} + w_{5,5}.
\end{aligned} \tag{5.35}$$

Then the matrix $\mathcal{N} = \left(\mathcal{N}_{j,k}\right)_{\substack{j=1,\dots,6 \\ k=1,\dots,6}}$ of the change of coordinates will be given by

$$\mathcal{N}_{j,k} = \begin{cases} \bar{u}_{k,j} \text{ if } k \text{ odd} \\ \bar{w}_{k-1,j} \text{ if } k \text{ even} \end{cases} \tag{5.36}$$

Applying the transformation of coordinates $\mathcal{N}^{-1}$ on $\mathtt{x} = [x, y, z, X, Y, Z]^T$, yields the new coordinates $\beth = [\xi_1, \xi_2, \psi_1, \psi_2, \zeta_1, \zeta_2]^T$, namely:

$$\beth = \mathcal{N}^{-1}\mathtt{x}. \tag{5.37}$$

The transformation $\mathcal{N}^{-1}$ is then performed on the system (5.3) to find it's expression in the new coordinates:

$$\dot{\beth} = \mathcal{N}^{-1}\dot{\mathtt{x}} = \mathcal{N}^{-1}\bar{\mathcal{A}}\,\mathtt{x} = \mathcal{N}^{-1}\bar{\mathcal{A}}\,\mathcal{N}\,\beth. \tag{5.38}$$

Such a system can be rewritten as:

$$\dot{\beth} = \mathcal{A}'\,\beth \quad with \quad \mathcal{A}' = \mathcal{N}^{-1}\bar{\mathcal{A}}\,\mathcal{N} \tag{5.39}$$

with

$$\mathcal{A}' = \begin{pmatrix} 0 & \lambda & 0 & 0 & 0 & 0 \\ -\lambda & 0 & 0 & 0 & 0 & 0 \\ 0 & 0 & 0 & \nu & 0 & 0 \\ 0 & 0 & -\nu & 0 & 0 & 0 \\ 0 & 0 & 0 & 0 & 0 & \varphi \\ 0 & 0 & 0 & 0 & -\varphi & 0 \end{pmatrix} \tag{5.40}$$

whose solutions are

$$\begin{cases} \xi_1(t) = \cos(\lambda t)\xi_1^0 + \sin(\lambda t)\xi_2^0 \\ \xi_2(t) = \cos(\lambda t)\xi_2^0 - \sin(\lambda t)\xi_1^0 \\ \psi_1(t) = \cos(\nu t)\psi_1^0 + \sin(\nu t)\psi_2^0 \\ \psi_2(t) = \cos(\nu t)\psi_2^0 - \sin(\nu t)\psi_1^0 \\ \zeta_1(t) = \cos(\varphi t)\zeta_1^0 + \sin(\varphi t)\zeta_2^0 \\ \zeta_2(t) = \cos(\varphi t)\zeta_2^0 - \sin(\varphi t)\zeta_1^0 \end{cases} \tag{5.41}$$

Therefore the solution of system (5.14), given by $\mathtt{x}(t) = \mathcal{N}\beth(t)$, are:

$$\begin{cases} x(t) = \mathcal{N}_{1,1}\xi_1(t) + \mathcal{N}_{1,2}\xi_2(t) + \mathcal{N}_{1,3}\psi_1(t) + \mathcal{N}_{1,4}\psi_2(t) + \mathcal{N}_{1,5}\zeta_1(t) + \mathcal{N}_{1,6}\zeta_2(t) \\ \quad = \bar{u}_{1,1}\xi_1(t) + \bar{w}_{1,1}\xi_2(t) + \bar{u}_{3,1}\psi_1(t) + \bar{w}_{3,1}\psi_2(t) + \bar{u}_{5,1}\zeta_1(t) + \bar{w}_{5,1}\zeta_2(t) \\ y(t) = \mathcal{N}_{2,1}\xi_1(t) + \mathcal{N}_{2,2}\xi_2(t) + \mathcal{N}_{2,3}\psi_1(t) + \mathcal{N}_{2,4}\psi_2(t) + \mathcal{N}_{2,5}\zeta_1(t) + \mathcal{N}_{2,6}\zeta_2(t) \\ \quad = \bar{u}_{1,2}\xi_1(t) + \bar{w}_{1,2}\xi_2(t) + \bar{u}_{3,2}\psi_1(t) + \bar{w}_{3,2}\psi_2(t) + \bar{u}_{5,2}\zeta_1(t) + \bar{w}_{5,2}\zeta_2(t) \\ z(t) = \mathcal{N}_{3,1}\xi_1(t) + \mathcal{N}_{3,2}\xi_2(t) + \mathcal{N}_{3,3}\psi_1(t) + \mathcal{N}_{3,4}\psi_2(t) + \mathcal{N}_{3,5}\zeta_1(t) + \mathcal{N}_{3,6}\zeta_2(t) \\ \quad = \bar{u}_{1,3}\xi_1(t) + \bar{w}_{1,3}\xi_2(t) + \bar{u}_{3,3}\psi_1(t) + \bar{w}_{3,3}\psi_2(t) + \bar{u}_{5,3}\zeta_1(t) + \bar{w}_{5,3}\zeta_2(t). \end{cases} \tag{5.42}$$

Notice that, evaluating

$$\mathtt{x}(0) = [x(0), y(0), z(0), X(0), Y(0), Z(0)]^T = [x(0), y(0), z(0), \dot{x}(0) - y(0), \dot{y}(0) + x(0), \dot{z}(0)]^T,$$

as expected, yields:

$$\begin{pmatrix} x(0) \\ y(0) \\ z(0) \\ X(0) \\ Y(0) \\ Z(0) \end{pmatrix} = \mathcal{N} \begin{pmatrix} \xi_1^0 \\ \xi_2^0 \\ \psi_1^0 \\ \psi_2^0 \\ \zeta_1^0 \\ \zeta_2^0 \end{pmatrix} \tag{5.43}$$

which is equal to (5.37) evaluated at $t = 0$.

Recall that these resulting orbits, solutions of the linearized system, are expressed in the system of reference translated to the artificial equilibrium point x_e, y_e, z_e (see (5.2)) such that they must be translated back to the position of the asteroid.

As the behaviors of the linear solution in (5.42), in the vicinity of the points A and G, is qualitatively the same as the other six artificial equilibria, the dynamics starting sufficiently close to these two points is shown, for the Sun-Jupiter-Trojan-Spacecraft system, where the asteroid has the same mass of 624-Hektor, in Figures 5.12 and 5.13.

In these Figures, the x/y, x/z projections of the solution of the linearized system are represented by the dark, continuous lines. As expected, after 12 Jovian years ($\sim$ 150 Earth years), they are still close to the respective starting points.
The dashed projection of the $3500km$ spherical domains around the points are also plotted in the Figures.

Notice that, if the perturbation (the position error) on the z axis was null, the orbit starting close to the point A would qualitatively degenerate to the two dimensional case analyzed in [19].

5.8 Integrating the full nonlinear system

The next step to illustrate the nonlinear stability of the linearly stable artificial equilibria identified in the previous section, is to perform a numerical integration of the full nonlinear system in their vicinity. To this end, recalling system (5.14), the behavior of

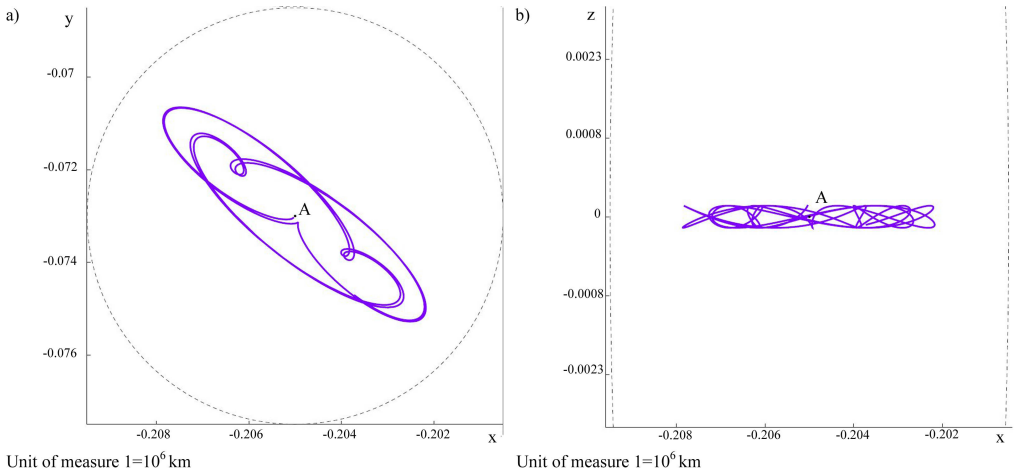

Figure 5.12: The solution of the linearized system in the vicinity of the point A after 12 Jovian years; *a) x/y projection; b) x/z projection*

a spacecraft starting sufficiently close to the points A and G is investigated.
Recalling the evaluation of the thrust needed to create artificial equilibrium points in A and G stated in Section 5, a numerical integration with Mathematica using a Runge-Kutta method is performed, starting sufficiently close to the initial points. The dark, continuous lines in Figures 5.14 and 5.15 are the x/y and x/z projections of the numerical solutions close to A and G respectively, evaluated for a null initial velocity. Once again the solutions are represented for the first 12 Jovian years and the dashed projection of the $3500km$ spherical domains around the points appears in the Figures as well. Notice that the divergence between the analytical integration of the linearized system in Fig. 5.12 and 5.13 and the numerical integration of the full system increases with the time, (i.e. the orbits starts to diverge approximately after 70 terrestrial years), but their bounded behavior, the relevant feature on which the result is focussed, holds despite the non linear terms introduced in the system. As a result of the application of the same method on the points B, C, D, H, E, and F, other six orbits are obtained, which, starting sufficiently close to the respective point with null initial velocity, will remain bounded around it. In particular, for approximately 150 Earth years, the motion starting close to each of the eight points, remains within the round domain, $3500km$ radius, outside the unstable zone. Moreover the orbits obtained can be divided into four similarly-behaving couples (A/C, B/D, H/F and G/E, in which, the two elements of the last two couples perfectly mirror each other), where, in particular, the motion starting close to B or D or that starting close to H or F remains bounded within an area much smaller than $3500km$. Furthermore, looking at their behaviors it is clear that care must be taken to the choice of the initial conditions as there is a trade-off between the amplitude of the oscillations about the initial point (in the z direction)

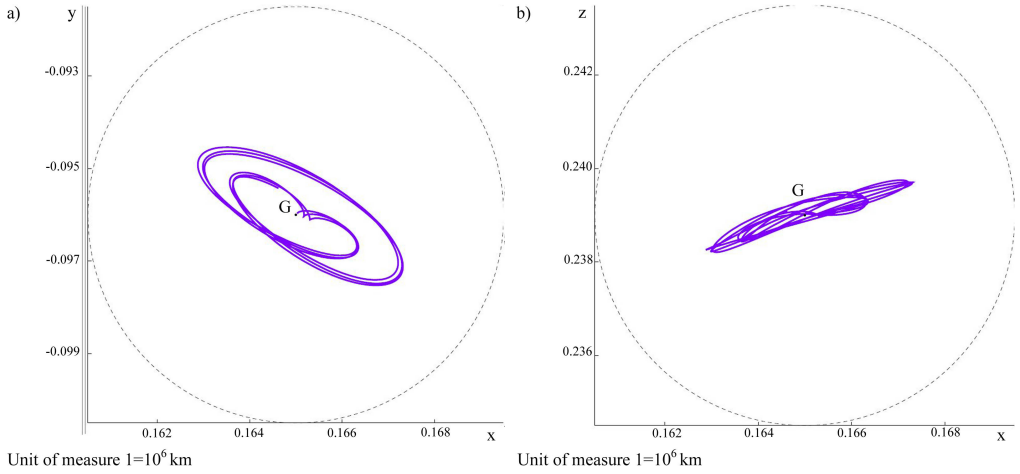

Figure 5.13: The solution of the linearized system in the vicinity of the point G after 12 Jovian years; *a) x/y projection; b) x/z projection*

and the fuel required, i.e. fuel can be saved at the expense of larger oscillations.

5.9 The numerical simulation of the real system

As there are no actual Jupiter Trojans in or close to L_4 a numerical simulation was required in order to test the results found analytically in the simplified model. The actual orbits of Jupiter and 624-Hektor were derived by interpolating their daily observed position and velocity vectors (found in the JPL Small Bodies Database). In this real model the orbit of Jupiter is elliptic, and its velocity of revolution is no longer constant. Fortunately the resulting effects on the system are minimal due to the low eccentricity of Jupiter's real orbit. On the other hand all the tadpole orbits of the main Jupiter Trojans are inclined up to 20 degrees with respect to the plane containing Jupiter's orbit around the Sun. Thus, as the x/y plane of the system of reference used is set to be the one containing the three massive planets, the change in inclination of this plane will greatly affect the change of velocity of the system $\dot{\omega}$ (in the theoretical model $\dot{\omega} = 0$) therefore representing the main difference between the two models.
The eight artificial equilibria chosen in Section 5.7, which are bounded in the simplified model, in the real model result to be unstable, quickly diverging from 624-Hektor. The x/y projections of their orbits are shown in Figure 5.16 for a period of around 36 years ($\sim$ 3 revolutions of Jupiter(and of 624-Hektor) around the Sun).
The numerical integration of many other artificial equilibrium points was then undertaken. Results highlight a shift of the model towards instability, i.e. an enlargement of the unstable zone. This result is expected considering the perturbations added in the

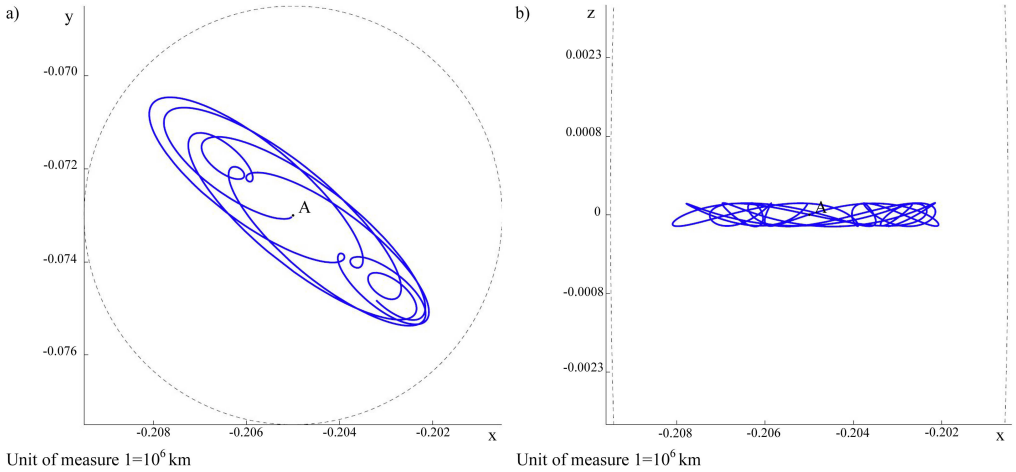

Figure 5.14: The solution of the full nonlinear system in the vicinity of the point A after 12 Jovian years; *a) x/y projection; b) x/z projection*

real model.

However, a zone of finite-time bounded orbits was heuristically found, in which all the orbits remain bounded within $\sim 3.5 \times 10^6$ km from the Asteroid for at least 36 Terrestrial years before starting to diverge. In this zone two artificial equilibria A' and G' were chosen, lying on the line connecting the Asteroid with the points A and G respectively, at a distance of 2.5 and 2.3 times their distance from the Asteroid. These artificial equilibria can be generated with a thrust lower then $4 \times 10^{-4} N$(still well within the feasible range), kept constant during the motion. The x/y projection of the resulting orbits, for ~ 3 revolution of Jupiter around the Sun, is shown in Figure 5.17 a) and b). It must be noted that, due to the x/y projection, the second orbit seems to spiral around the Asteroid but instead is displaced spatially.

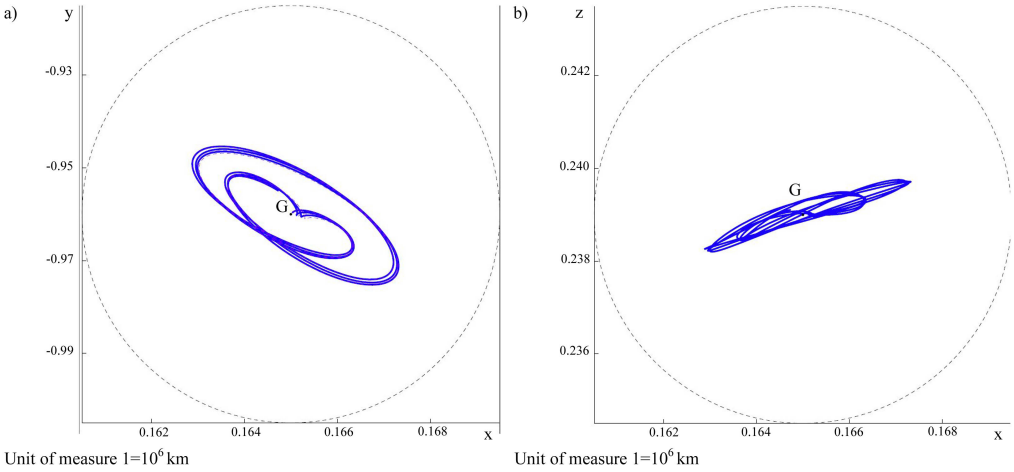

Figure 5.15: The solution of the full nonlinear system in the vicinity of the point G after 12 Jovian years; *a) x/y projection; b) x/z projection*

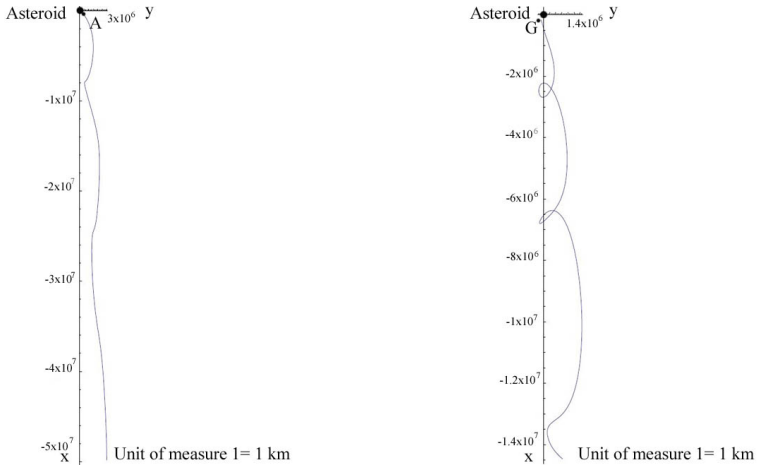

Figure 5.16: The unstable zone of the model enlarges and the eight artificial equilibria above become unstable; a) *The orbit generating from the point A in the real system*; b) *The orbit generating from the point G in the real system*

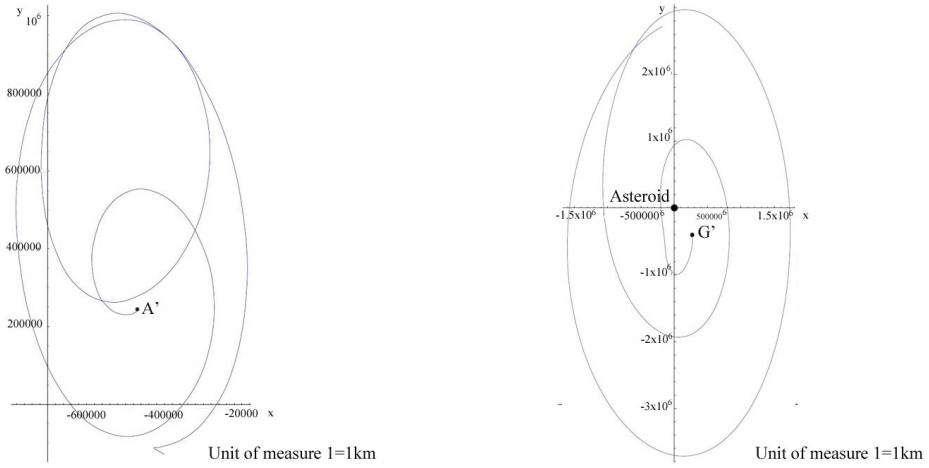

Figure 5.17: Two orbits of the finite-time bounded zone of the real case after 3 Jovian years; a) *The starting point A' is set on the line connecting A and 624-Hektor at a distance of* 544903 *km from the Asteroid*; b) *The starting point G' is set on the line connecting G and 624-Hektor at a distance of* 711477 *km from the Asteroid*

Thus the simplified model studied in this chapter can give some indications of where weakly unstable solutions about a real Trojan may exist. Moreover it is clear that the perturbations due to a nonconstant velocity of revolution and the inclination of the tadpole orbits of the main Trojans must be taken into account when analysing stability.

5.10 Summary

A low thrust autonomous coplanar CR4BP, with the primaries set in the Lagrangian equilateral triangle configuration, has been formulated for both the purpose of mathematical interest as well as to investigate potential applications in the Sun-Jupiter-Asteroid-Spacecraft system. The analyses of the natural evolution of the system was performed, for a range of conceivable masses of a hypothetical asteroid set at the libration point L_4, which revealed eight natural equilibrium points, four of which are close to the asteroid. Of these, a linear stability analysis revealed that the two closest are unstable and the other two stable, when considering as primaries the Sun and two other bodies of the solar system.

Adding a low-thrust propulsion system to the spacecraft, which can thrust in every direction, including perpendicular to the plane containing the three massive bodies, a region of stable artificial equilibrium points close to the asteroid was created. As the "UK ion propulsion programme" has culminated in the availability of three thrusters of different sizes, covering the thrust $1mN$ to $300mN$ range [105], based on the $T5$, $T6$ and UK-25 propulsion systems, the assumed low-thrust potential for the spacecraft was initially based on current capability. Moreover completely novel, bounded orbits

were proved to exist in the spatial vicinity of the asteroid which can be maintained with a constant thrust lower than the 0.1% of the maximum thrust capability, oriented in a fixed direction. Such result suggests that a shift towards micro propulsion systems (MPS) could be more appropriate for this application. Therefore, the Field Emission Electric Propulsion (FEEP) technology, used in the Lisa pathfinder experiment on Einstein's geodesic motion in space, which operates in the micro-Newton field covering the range from $1 \times 10^{-4} mN$ up to $0.5mN$ [106], may provide a more effective propulsion system for the proposed application.

This chapter illustrates that by exploiting low-thrust, it would be possible to maintain strategic observation points, more than 66% closer to the hypothetical asteroid than the stable natural equilibrium points. This would enable a continuous synoptic view of the hypothetical asteroid itself.

A numerical simulation of the system was then performed, based on the real observations of the orbits of Jupiter and the 624-Hektor Trojan Asteroid to test the result when the asteroid is moving on its real tadpole orbit instead of remaining fixed in L_4. Results show a shift of the real model towards instability, i.e. the unstable zone enlarges, due to the inclusion in the real model of high perturbations.

However, numerical integration highlights a zone of finite-time bounded orbits for the real model, in which the orbits remain bounded within $\sim 3.5 \times 10^6 km$ from the Asteroid for at least 36 Terrestrial years($\sim$ 3 Jupiter's and 624-Hektor's revolutions around the Sun) before starting to escape. These finite-time bounded orbits can be maintained by using a constant thrust lower than $4 \times 10^{-4} N$ without the need for any state feedback control.

Chapter 6

Conclusions

The dynamics of a massless spacecraft around an inhomogeneous Trojan body, in a system composed of three primaries lying at the vertexes of an equilateral triangle, with their mutual positions fixed over the course of the motion, has been investigated. Two possible dynamical models have been identified as suitable to represent and study the system, depending on the distance from the primary. In the close vicinity of the Trojan object, the motion was assumed to be dominated by this sole body, perturbed by the inhomogeneities of the gravitational field due to its shape/density irregularities. In this zone the dynamics was thus modeled using the perturbed Restricted Two Body Problem, in which an arbitrary number of harmonics of the body were taken into account.
Far from the asteroid (but still close enough to the body for scientific and observational purposes), where the gravitational influence of the other two primaries is far greater than the influence of the inhomogeneities of the body, the model adopted was the Lagrangian Circular Restricted Four Body Problem (CR4BP). Low-thrust propulsion perturbations were incorporated into this model.
The validity range of the two models was discussed and estimated as an application of a Weak Stability Boundary theory.
Interesting natural orbits (e.g. frozen orbits) close to the body and new families of artificial, non-Keplerian orbits, which could be exploited for science and commercial applications, were identified. Results where shown for the Sun-Jupiter-Trojan-spacecraft system, with particular emphasis on the asteroid 624-Hektor, a major Jupiter Trojan.

***

The concept of Weak Stability boundary was first introduced, with both its classical, algorithmic definitions. A completely new, analytical definition was then formulated, which enabled to study the topology of the set of the stable orbits of which the WSB is,

by definition, the frontier. In particular it was demonstrated that the set of the stable orbits is a bounded set formed by, at most, a countable disjoint union of open intervals plus, at most, a countable set of points. Moreover, for each fixed initial eccentricity of the orbit, a radius r^* was proven to exist, such that all the orbits generated by a smaller radius are stable. This radius provides an estimation from the below of the WSB as no points of such set can be found below r^*. However this same estimation is also an estimation of the stable zone around the asteroid. For the Jupiter Trojan 624-Hektor, for the case $e_0 > \frac{1}{2}$, analytical and numerical estimations of r^* were evaluated. This estimations were used as the estimation of the range of validity for the application of the two dynamical models proposed.
Following the definition of stability used for the WSB theory developed in Chapter 3 (see Definition 5), an orbit was defined as stable by monitoring its distance from the target asteroid and the sign of the Keplerian energy after a circle around the body. Thus estimating the variations of all the coordinates describing the motion of the spacecraft around the asteroid, it was possible to identify the set of initial conditions leading to stable orbits. In particular, for 624-Hektor, it was found that, starting with an initial eccentricity of the osculating ellipse $e_0 \in [0.557958; 0.952042]$ and a semimajor axes $a_0 < 13160km$, after completing a circle around the asteroid, the eccentricity would remain bounded within the range $e \in [0.54; 0.97]$, with a semimajor axes $a < 13420km$.

This was thus the boundary of the stable zone around the asteroid within which the dynamics was investigated as a R2BP with an inhomogeneous gravitational field. The case where the angular velocity of the asteroid is larger than the mean motion of the spacecraft was analysed. An analytical theory in closed form in terms of the eccentricity, inclination and mean anomaly of the spacecraft was presented. This is of second order with respect to a small parameter and of arbitrary degree in the expansion of the gravitational field of the body in terms of the zonal and tesseral harmonic coefficients. Two different, canonical Lie-Deprit transformations were built, together with their corresponding suitable changes of coordinates, with the aim of reducing the initial non-integrable Hamiltonian system into an integrable Hamiltonian plus a negligible remainder of higher order in the small parameter. The first was the relegation of the action conjugate to the argument of the node while the latter was a Delaunay normalisation, to average the Hamiltonian with respect to the mean anomaly of the spacecraft's orbit. An explicit analytical formulation for the averaged, second order, Hamiltonian of any inhomogeneous gravitational field was derived in closed form. A method for determining initial conditions for frozen orbits solving a 2-D algebraic equation, after prescribing the desired inclination and eccentricity of the orbit, was then presented as an application. This could be useful for the dynamical analysis of both natural and artificial satellites around any body with an inhomogeneous gravitational field.

Two examples of frozen orbits were shown, found for the Trojan 624-Hektor, in accordance with the previous stability range estimation. The former had an initial inclination close to zero while the latter with an high inclination $I_0 = 1.1$. The initial conditions of both these orbits were taken in the estimated stable set, although the validity of the estimation might deteriorate for high inclinations regimes. Moreover, as the perturbational theory is valid for the cases in which the angular velocity of the asteroid is higher than the mean motion of the spacecraft, which holds, for example, for fast rotating bodies or for relatively high altitudes, both the resulting orbits had to fulfill such altitude requirements. For the low inclined orbit the initial eccentricity was fixed to $e_0 = 0.7$ and the initial semimajor axes to $a_0 \sim 1735km$, while for the other $e_0 = 0,85$ and $a_0 \sim 4045km$. Furthermore it must be noted that the spherical harmonics of 624-Hektor couldn't be found in previous literature. A method for obtaining these coefficients from a three dimensional polyhedric model of the asteroid, assuming a constant density was thus developed.

To complete the dynamical studies of the spacecraft beyond the stable region, the autonomous Lagrangian CR4BP was used. In this outer region the perturbations due to the gravitational effects of the Sun and Jupiter dominate the dynamics and the effect of the inhomogeneous gravitational field of the body becomes negligible compared to them. The natural dynamics of this model was first investigated, which, for the stable equilateral triangle configuration (e.g. considering the Sun and any other two objects of the Solar System), was shown to have 8 equilibrium points. The study then focussed on the four equilibria close to the asteroid. A linear stability analysis of them revealed the two closer to the body to be unstable while the other two to be linearly stable. Different topologies for the linearly stable zone were investigated, for different conceivable masses for the asteroid. The system was then perturbed by the inclusion of low thrust propulsion. Surfaces of artificial equilibrium points were generated in the spatial vicinity of the asteroid. The low thrust necessary to create surfaces of artificial equilibrium points in this zone was estimated for a $1000kg$ spacecraft, for the simplified model in which the asteroid is fixed at the exact L_4 position. A zone of stable orbits was shown to exist, for the Sun-Jupiter-Trojan-spacecraft system, considering a fixed hypothetical asteroid with the same mass of 624-Hektor. As an example eight orbits around artificial equilibria, in and out the plane containing the three primaries, were shown, which, starting at a distance of approximately $\sim 21000km$ remain bounded outside the unstable zone in a round domain, $3500km$ radius, for at least 150 years. These orbits can be maintained with a constant thrust lower than $0.15mN$ without the need for any state feedback control. A numerical simulation of the system was then performed, based on the real observations of the orbits of Jupiter and the 624-Hektor Trojan Asteroid to test the result when the asteroid is moving on its real tadpole orbit instead of remaining fixed in L_4, the main perturbation introduced being the non zero

z-velocity of the plane containing the three bodies. In this real case a zone of finite-time bounded orbits was found, in which all the orbits remain bounded within $3.5 \times 10^6 km$ from the Asteroid for at least 36 years before starting to diverge. These finite-time bounded orbits can be maintained by using a constant thrust lower than $0.4mN$ without the need for any state feedback control.

Bibliography

[1] Lagrange J.L.C.:'Essai sur le Probléme des Trois Corps', Ouvres, vol.6, pp.272-292, Gauthier-Villars, Paris (1772)

[2] Connors, M., Wiegert, P., Veillet. C.:'Earth's Trojan asteroid', Nature 475, pp.481483 (2011), doi:10.1038/nature10233

[3] Wright, A.:'Planetary science: The Trojan is out there' Nature Physics, 7, 592, doi:10.1038/nphys2061 (2011)

[4] Rivkin, A.S., Emery, J., Barucci, A., Bell, J.F., Bottke, W.F., Dotto, E., Gold, R., Lisse, C., Licandro, J., Prockter, L., Hibbits, C., Paul, M., Springmann, A., Yang, B.: 'The Trojan Asteroids: Keys to Many Locks', SBAG Community White Papers (2009)

[5] Various Authors:'New Frontiers in the Solar System: An Integrated Exploration Strategy', Space Studies Board of National Research Council p.417, Washington, DC: National Academy Press (2002)

[6] Cremaschi, F., Topputo F., Sangiovanni G., vasile M.:'Low Thrust Interplanetary Transfers through invariant manyfolds and evolutionary neurocontrol', XVIII CONGRESSO NAZIONALE AIDAA (2005)

[7] Circi C. Teofilatto P.:'On the Dynamics of Weak Stability Boundary Lunar Transfers' Cel. Mech and Dyn. Astr., Vol. 79, N. 1, pp. 41-72, DOI: 10.1023/A:1011153610564 (2001)

[8] Belbruno, E.:'Capture Dynamics and Chaotic Motions in Celestial Mechanics: With Applications to the Construction of Low Energy Transfers', Princeton University Press (2004)

[9] García, F., Gómez, G.: 'A note on weak stability boundaries', Celest. Mech. Dyn. Astr., Vol.97, pp. 87-10 (2007)

[10] Ceccaroni, M., Biggs, J. D., Biasco, L.: 'Analytic estimates and topological properties of the weak stability boundary', Celest. Mech. Dyn. Astr., Vol.114, pp.124 DOI 10.1007/s10569-012-9419-x (2012)

[11] Ceccaroni, M., Biggs, J. D., Biasco, L.: 'Some Analytic Estimates of the Weak Stability Boundary', New Trends in Astrodynamics and Applications VI, New York. (2011)

[12] Ceccaroni, M., Biggs, J. D., Biasco, L.: 'The Weak Stability Boundary in the Sun-Jupiter-Trojan-spacecraft four body problem', New Trends in Astrodynamics and Applications VI, New York. (2011)

[13] Ceccaroni, M., Biggs, J. : 'Analytic perturbative theories in highly inhomogeneous gravitational fields', Icarus (in press) http://dx.doi.org/10.1016/j.icarus.2013.01.007 (2013)

[14] Ceccaroni, M., Biscani, F., Biggs, J. D.: : 'Analytical method for perturbed frozen orbit around an Asteroid in highly inhomogeneous gravitational fields: a first approach', Solar System Research (in press) (2012)

[15] Ceccaroni, M., Biscani, F., Biggs, J. D.: : 'Analytical Perturbative method for frozen orbits around the asteroid 433-Eros', IAC2010 - International Astronautical Congress - Naples (2012)

[16] Ceccaroni, M., Biscani, F., Biggs, J. D.: : 'Analytical method for perturbed frozen orbits around an Asteroid in highly inhomogeneous gravitational fields',Analytical methods for celestial mechanics, St.Petersburg (2012)

[17] Ceccaroni, M., Biggs, J. D.:'Low-thrust propulsion in a coplanar circular restricted four body problem', Celestial Mechanics and Dynamical Astronomy, Volume 112, Issue 2 (2012), pp. 191-219. DOI: 10.1007/s10569-011-9391-x. (2011)

[18] Ceccaroni, M., Biggs, J. D.:'Nonlinearly stable equilibria in the Sun-Jupiter-Trojan-Spacecraft four body problem', IAC2011 - International Astronautical Congress - Cape Town (2011)

[19] Ceccaroni, M., Biggs, J.:'Extension of low-thrust propulsion to the Autonomous Coplanar Circular Restricted Four Body Problem with application to future Trojan Asteroid missions', in 61^{st} International Astronautical Congress, IAC-10-1.1.3, Prague (2010)

[20] Ambrosetti, A., Prodi, G.:'A Primer of Nonlinear Analysis', pp. 153-159. Cambridge University Press, Cambridge (1993)

[21] Gascheau, M.:'Examen d'une classe d'equations differentielles et application a un cas particulier du probleme des trois corps', Compt. Rend. 16, Princeton (1843)

[22] Deprit, A., Deprit-Bartholome, A.:'Stability of the triangular Lagrangian points', Astronomical Journal, Vol.72, pp. 173 (1967)

[23] Erdi, B., Forgács-Dajka, E., Nagy, I., Rajnai, R.:'A parametric study of stability and resonances around L4 in the elliptic restricted three-body problem', Celest. Mech. Dyn. Astr., Vol. 104, pp. 145-158 (2009)

[24] Schwarz, R., Süli, ., Dvorak,R., Pilat-Lohinger, E.:'Stability of Trojan planets in multi-planetary systems Stability of Trojan planets in different dynamical systems', Celest. Mech. Dyn. Astr., Vol. 104, num.1-2, pp. 69-84 (2009)

[25] Celletti, A.; Chierchia, L.:' KAM stability and celestial mechanics.' Mem. Amer. Math. Soc. 187 , no. 878(2007)

[26] Whittaker, E.T.:' A treatise on the analytical dynamics of particles and rigid bodies; with an introduction to the problem of three bodies', Cambrige University Press (1917)

[27] Palacian, J.:'Closed Form normalization of perturbed two-body problems', Cambrige Chaos, Solitons and Fractals (2002)

[28] Abramowitz, M. and Stegun.,I. A.:' Handbook of Mathematical Functions with Formulas, Graps, and Mathematical Tables', National Bureau Of Standards, Washington (1965)

[29] Hofmann-Wellenhof, B., Moritz, H.:'Physical Geodesy', Springer Wien NewYork (1967)

[30] Wigner, E.D.:'Group Theory and it's application to the Quantum Mechanics of Atomic Spectra', New York, Academic Press (1959)

[31] Belbruno, E., Miller, J.:'Sun-perturbed earth-to-moon transfers with a ballistic capture', Journal of Guidance, Control, and Dynamics, vol. 16, n.4, pp.770-775 (1993)

[32] Belbruno, E.:'Lunar capture orbits. a method of constructing earth-moon trajectories and the lunar gas mission', Proceedings of AIAA/DGLR/JSASS, pp. 87-1054 (1987)

[33] Belbruno, E.:'Examples of the Nonlinear Dynamics of Ballistic Capture and Escape in the EarthMoon System', AIAA paper, pp. 90-2896 (1990)

[34] Topputo, F.:'Low-Thrust Non-Keplerian Orbits: Analysis, Design, and Control', PhD Thesis, Politecnico di Milano (2007)

[35] Koon, W.S., Lo, M.W., Marsden, J.E. , Ross, S.D.:'Low Energy Transfer to the Moon ', Celest. Mech. Dyn. Astr., Vol.81, pp. 63-73 (2001)

[36] Gómez, G., Jorba, A., Masdemont, J. J., Simó, C:'Study of the Transfer from the Earth to a Halo Orbit Around the Equilibrium Point L_1 ', Celest. Mech. Dyn. Astr., Vol.56, N.4 pp. 541-562 (1993)

[37] Romagnoli, D., Circi, C.:'Earth.Moon Weak Stability Boundaries in the restricted three and four body problem', Celest. Mech. Dyn. Astr., Vol.103, pp. 79-103 (2009)

[38] Mingotti, G., Topputo, F., and Bernelli-Zazzera, F. :'Low-energy, low-thrust transfers to the Moon', Celest. Mech. Dyn. Astr., Vol.105, pp. 61-74 (2009)

[39] Topputo, F., Belbruno, E.: 'Computation of weak stability boundaries: Sun.Jupiter system', Celest. Mech. Dyn. Astr., Vol.105, pp. 3-17 (2009)

[40] Carrico, J.P., Belbruno, E.:'Calculation of weak stability boundary ballistic lunar transfer trajectories', American Institute of Aeronautics and Astronautics (2006)

[41] Bello-Mora, M., Graziani, F., Teofilatto, P., Circi, C., Porfilio, M., Hechler, M.:'A Systematic Analysis on Weak Stability Boundary Transfers to the Moon', Paper IAF-00-A.6.03, Proceedings of the International Astronautical Conference (2000)

[42] Belbruno, E.'Fast Resonance Shifting as a Mechanism of Dynamical Instability Illustrated by Comets and the CHE Trajectories', Annals of the New York Academy of Sciences, Vol. 822, pp.195226 (1997)

[43] Gómez, G., Koon, W. S., Lo, M. W., Marsden, J. E., Masdemont, J., Ross, S. D.:' Connecting orbits and invariant manifolds in the spatial restricted three-body problem.', Nonlinearity, Vol.17 (5), pp. 1571-1606 (2004)

[44] Schoenmaekers, J., Horas, D. and Pulido, J.A.: 'SMART-1: with Solar Electric Propulsion to the Moon', 16th International Symposium on Space Flight Dynamics, Pasadena, California, 37 December (2001)

[45] Jehn, R., Campagnola, S., García, D., Kemble, S.: 'Low-thrust approach and gravitational capture at Mercury', Proc. of the 18th Int. Symp. on Space Flight Dynamics, 487492, (2004)

[46] Topputo, F., Belbruno, E., Gidea,M.:'Resonant motion, ballistic escape, and their applications in astrodynamics', Science Direct (2008)

[47] Belbruno, E.:'Structure of the Weak Stability Boundary III' Science Mission Directorate , NASA AISR annual report Mission Extension Using Extensive Trajectories and Autonomous Control (2008)

[48] Koon, W.S., Lo, M., Marsden, J.E., Ross., S.D.:'Dynamical Systems, the Three-Body Problem and Space Mission Design', pp. 123-130. Marsden Books, London (2008)

[49] Deprit, A.:'Delaunay Normalizations', Celestial Mechanics and Dynamical Astronomy, 26, 9-21, (1982)

[50] San-Juan, J.F., Abad, A., Scheeres, D.J., Lara, M.:'A First Order Analytical Solution for Spacecraft Motion about (433) Eros', AIAA, Astrodynamics Specialist Conference, California (2002)

[51] Deprit, A., Palacian, J., Deprit, E.:'The Relegation Algorithm', Celest. Mech. Dyn. Astr., Vol. 79, pp. 157-182 (2001)

[52] Palacián, J.:' 1992, Teoría del Satélite Artificial: Armónicos Teserales y su Relegación Mediante Simplificaciones Algebraicas," Doctoral Dissertation Universidad de Zaragoza, Spain (1992)

[53] Deprit, A.:'Canonical transformations depending on a small parameter', Celest. Mech. Dyn. Astr., Vol. 1, pp. 12-30 (1969)

[54] Palacián,J.F.:'Dynamics of a satellite orbiting a planet with an inhomogeneous gravitational field', Celestial Mech. Dyn. Astr., Vol. 98, pp.219249 DOI 10.1007/s10569-007-9078-5 (2007)

[55] Brouwer, D.:'Solution of the Problem of the Artificial Satellite Without Drag' Astronomical Journal, 64 (1959)

[56] Kozai, Y.: 'Mean values of cosine functions in elliptic motion'. Astron. J. Vol. 67, pp. 446461 (1962)

[57] Coffey, S., Deprit, A.: Third-order solution to the main problem in satellite theory. J Guidance ControlDynamics 5, 366371 (1982)

[58] Deprit, A.: The elimination of the parallax in satellite theory. Celest. Mech. 24, 111153 (1981)

[59] Coffey, S., Deprit, A., Deprit, E.: Frozen orbits for satellites close to an Earth-like planet. Celest. Mech. 59, 37 72 (1994)

[60] Carnelli, Gálvez:'ESA's Don Quijote Mission: an Opportunity for the Investigation of an Artificial Impact Crater on an Asteroid, in Proceedings of the 25th International Symposium on Space Technology and Science, Kanazawa, Japan, (2006) Paper ISTS 2006-k-26.

[61] Deprit, A.:'The main problem of artificial satellite theory for small and moderate eccentricities', Celestial Mechanics and Dynamical Astronomy, 2, 166-206, (1970)

[62] Abad, A., Elipe A., Tresaco E.:'Analytical Model to Find Frozen Orbits for a Lunar Orbiter', Journal of Guidance, Control and Dynamics, 32, 888-898, (2009)

[63] San-Jaun J. F., Abad, A., Lara, M., Scheeres, D. J.,:'First-order analytic solution for Spacecraft about (433) EROS.', Journal of Guidance, Control and Dynamics, vol. 27, No. 2, pp. 290-293, (2004)

[64] Segerman, A. M., Coffey, S.L., :'An analytical theory for tesseral gravitational harmonics., Celestial Mechanics and Dynamical Astronomy, vol. 76, 139-156, (2000)

[65] Lara, M.: Repeat ground track orbits of the Earth tesseral problem as bifurcations of the equatorial family of periodic orbits. Celest. Mech. Dyn. Astron. 86, 143162 (2003)

[66] Lara, M., Elipe, A.: Periodic orbits around geostationary positions. Celest. Mech. Dyn. Astron. 82, 285 299 (2002)

[67] Fahnestock, E., Scheeres, D.,:'Dynamical Characterization and Stabilization of Large Gravity-Tractor Designs', Journal of Guidance, Control, and Dynamics, 31, 501-521, (2008)

[68] Lara, M., Scheeres :'Stability bounds for three-dimensional motion close to asteroids', AAS/AIAA Space Flight Mechanics Meeting (2002)

[69] Kaula, W.T.: Theory of Satellite Geodesy Blaisdell Publishing Company, Waltham, MA (1966)

[70] Métris, G., Exertier, P., Bourdon, Y., Barlier, F.: Long period variations of the motion of a satellite due to nonresonant tesseral harmonics of a gravity potential. Celest. Mech. Dyn. Astron. 57, 175188 (1993)

[71] Scheeres, D. J. Marzari, F. Tomasella, L. Vanzani, V.,:'ROSETTA mission: satellite orbits around a cometary nucleus', Planetary and Space Science, 46, 649-671, (1998)

[72] Scheeres, D., Guman, M., Villac, B.: Stabillity analysis of planetary satellite orbiters: application to the europa orbiter. J. Guid. Control Dyn. 24, 778787 (2001)

[73] San-Juan, J., Lara, M., Ferrer, S.: Phase space structure around oblate planetary satellites. J. Guid. Control Dyn. 29, 113120 (2006)

[74] Paskowitz, M., Scheeres, D.: Design of science orbits about planetary satellites: application to Europa. J. Guid. Control Dyn. 29, 11471158 (2006)

[75] Lara, M., Palacin, J.F., Yanguas, P. et al.: Analytical theory for spacecraft motion about Mercury. Acta Astron. 66, 10221038 (2010)

[76] Jamet, O., Thomas, E.:'A linear algorithm for computing the spherical harmonic coefficients of the gravitational potential from a constant density polyhedron', Proc. Second International GOCE User Workshop "GOCE, The Geoid and Oceanography", ESA-ESRIN, Frascati, Italy, 8-10 March 2004 (ESA SP-569, June 2004)

[77] Lo, M.,W.:'Invariant Manifolds and the Interplanetary Superhighway', Proc. Appl. Math. Mech., Vol 7, Issue 1, DOI 10.1002/pamm.200700573 (2007)

[78] Moulton F.R.:'On a class of particular solutions of the problem of four bodies', Trans. of the American Math. Soc, 1, pp. 17-29 (1900)

[79] Simò, C.:'Relative equilibrium solutions in the four body problem', Celest. Mech. Dyn. Astr., Vol. 18, No. 2, pp. 165-184 (1978)

[80] Leandro, E. S. G.: On the central configurations of the planar restricted four body problem. J. Differential Equations 226, 323-351 (2006)

[81] Pedersen, P. : Librationspunkte im restringierten vierkoer-perproblem. Dan. Mat. Fys. Medd. 1-80 (1944)

[82] Kloppenborg, B., Stencel, R., Monnier, J.D., Schaefer, G., Zhao, M., Baron, F., McAlister, H., Brummelaar, T.T., Che, X., Farrington, C., Pedretti, E., Sallave-Goldfinger, P. J., Sturmann, J., Sturmann, L., Thureau, N., Turner, N., Carroll, S. M.: 'Infrared images of the transiting disk in the ϵ Aurigae system', pp.870-872., Nature Letters, 464, London (2010)

[83] Melita, M.D., Licandro, J., Jones, D.C., Williams, I.P.: 'Physical properties and orbital stability of the Trojan asteroids', Icarus, 195, pp. 686-697 (2008)

[84] Van Hamme, W., Wilson, R.E.:'The restricted four-body problem and epsilon Aurigae',The Astroph. J., 306, pp. 33-36 (1986)

[85] Schwarz, R., Suli, A., Dvorak, R. :'Dynamics of possible Trojan planets in binary systems', Mon. Not. R. Astron. Soc., 398, pp. 2085-2090 (2009)

[86] Alvarez-Ramirez, M., Vidal, C.:'Dynamical aspects of an equilateral restricted four-body prob- lem', pp. 1-23. Mathematical Problems in Engineering, Cambridge (2009)

[87] Baltagiannis, A.N., Papadakis K.E.: 'Equilibrium Points and Their Stability In The Restricted Four Body Problem', International Journal of Bifurcation and Chaos, World Scientific Publishing Company, accepted (2011)

[88] Baltagiannis, A. N., Papadakis, K. E.:'Families of periodic orbits in the restricted four-body problem', Astrophys Space Sci, DOI No: 10.1007/s10509-011-0778-7 (2011)

[89] Burgos-García, J., Delgado, J.:'Periodic orbits in the restricted four-body problem with two equal masses', Accepted for publication in Astrophysics and Space Science

[90] Dvorak, R., Schwarz R., Lhotka Ch.:'On the dynamics of Trojan planets in extra-solar planetary systems', International Astronomical Union (2008)

[91] Marzari F., Scholl, H., Murray, C., Lagerkvist, C.:'Origin and Evolution of Trojan Asteroids', Asteroid III (2002)

[92] Steves, B.A., Roy, A.E., Bell, M.:'Some special solutions of the four body problem - II. From Caledonia to Copenaghen', Planet. Space Sci., Vol. 46, No. 11-12, pp. 1475-1486 (1998)

[93] Steves, B.A., Roy, A.E., Bell, M.:'Some special restricted four-body problems I. Modelling the Caledonian problem', Planet. Space Sci., Vol. 46, No. 11-12, pp. 1465-1474 (1998)

[94] Marzari F.:'Puzzling Neptune Trojans', Science , Vol. 313, no. 5786, pp. 451-452 (2006)

[95] Dusek, H.,M.: 'Optimal station keeping at collinear points', Progress in Astronautics and Aeronautics, 17, 37-44, 1966.

[96] McKay, R., Macdonald, M., Biggs, J., McInnes, C.R.: 'Survey of Highly Non-Keplerian Orbits With Low-Thrust Propulsion', J. Guid. Contr. Dynam., Vol.34 no 3, pp. 645-666 (2011)

[97] Morimoto, K., Yamakawa, M.Y., Uesugi, H.:'Artificial Equilibrium Points in the Low-Thrust Restricted Three-Body Problem', J. Guid. Contr. Dynam., Vol. 30, No. 5, pp. 1563-1568 (2007)

[98] McInnes, C. R., McDonald, A. J., John, F. L., MacDonald, E. W.: 'Solar sail parking in restricted three-body systems', Journal of Guidance, Control, and Dynamics, Vol. 17, N. 2, pp. 399-406 (1994)

[99] Baig, S., McInnes, C.R.:'Artificial Three Body Equilibria for Hybrid Low-Thrust Propulsion', J. Guid. Contr. Dynam., Vol. 31, No. 6, pp. 1644-1655 (2008)

[100] Morimoto, K., Yamakawa, M. Y., Uesugi, H.: 'Periodic Orbits with Low-Thrust Propulsion in the Restricted Three-Body Problem', Journal of Guidance, Control, and Dynamics, Vol. 29, N. 5, pp. 1131-1139 (2006)

[101] Waters, T., McInnes, C. R.: 'Periodic orbits above the ecliptic plane in the solar sail restricted 3-body problem', Journal of Guidance, Control, and Dynamics, Vol. 30, N. 3, pp. 687-693 (2007)

[102] Baig, S., McInnes, C.R.:'Artificial halo orbits for low-thrust propulsion spacecraft', Celest. Mech. Dyn. Astr., Vol. 104, No. 4, pp. 321-335 (2009)

[103] McKay, R., Macdonald, M., Bosquillon de Frescheville, F., Vasile, M., McInnes, C.R., Biggs, J.:' Non-Keplerian Orbits Using Low Thrust, High ISP Propulsion Systems', 60th International Astronautical Congress (2009)

[104] Bombardelli C., Pelaez, J.: 'On the stability of artificial equilibrium points in the circular restricted three-body problem', Cele. Mech. and Dyn. Astr, Online First

[105] Fearn, D.G., Crookham, C.:'The development of ion propulsion in the UK: a historical prespective', Proceedings of the 29^{th} IEPC, Princeton (2005)

[106] Nicolini, D.:'LISA Pathfinder Field Emission Thruster System Development Program', Proceedings of the 30^{th} International Electric Propulsion Conference, Florence, (2007)

[107] Artin, M.:'Algebra', Prentice Hall, pp. 543-547 (1991)

[108] Arnold, V. A., Kozolov, V. V, Neishtadt, A. I.:'Mathematical aspects of classical and celestial mechanics. (Dynamical systems. III)', Springer-Verlag (2006)

Appendix A

A second approach for deriving the gravitational potential expressed using the Whittaker Nodal-Polar variables, is here provided. The procedure is undertaken using Wigner's rotation theorem for non scaled spherical harmonics.

Definition 12 *The non scaled spherical harmonics $Y_n^m(\delta,\lambda)$ are the angular portion of the solution to Laplace's equation in spherical coordinates where azimuthal symmetry is not present, which can be expressed as*

$$Y_n^m(\delta,\lambda) := P_n^m(\sin\delta)e^{\imath m\lambda} \tag{6.1}$$

Getting Back to the formulation of the potential in (2.86) the addition formula for non scaled spherical harmonics [29] is applied:

$$P_n(\cos\psi) = \Re\left[\sum_{m=0}^{n}(-1)^m(2-\delta_{0,m})Y_n^{-m}(\delta,\lambda)Y_n^m(\delta',\lambda')\right] \tag{6.2}$$

Thus obtaining:

$$\begin{aligned}
U(r,\delta,\lambda)) &= -\tfrac{\mathcal{G}}{r}\int_V\sum_{n=0}^{\infty}\left(\frac{r'}{r}\right)^n\Re\left[\sum_{m=0}^{n}(-1)^m(2-\delta_{0,m})Y_n^{-m}(\delta,\lambda)Y_n^m(\delta',\lambda')\right]\cdot \\
&\quad\cdot\rho(\mathbf{r}')dV \\
&= -\tfrac{\bar{M}}{r}\sum_{n=0}^{\infty}\Re\left[\sum_{m=0}^{n}(-1)^m\left(\frac{\alpha}{r}\right)^n Y_n^{-m}(\delta,\lambda)\left(\frac{1}{M}\int_V\left(\frac{r'}{\alpha}\right)^n(2-\delta_{0,m})\cdot\right.\right. \\
&\quad\left.\left.\cdot Y_n^m(\delta',\lambda')\rho(\mathbf{r}')dV\right)\right] \\
&= \Re\left[-\tfrac{\bar{M}}{r}\sum_{n=0}^{\infty}\sum_{m=0}^{n}\left(\frac{\alpha}{r}\right)^n\frac{(n+m)!}{(n-m)!}Y_n^{-m}(\delta,\lambda)\left(\frac{1}{M}\int_V\left(\frac{r'}{\alpha}\right)^n(2-\delta_{0,m})\cdot\right.\right. \\
&\quad\left.\left.\cdot\tfrac{(n-m)!}{(n+m)!}P_{n,m}(\sin\delta')e^{\imath m\lambda'}\rho(\mathbf{r}')dV\right)\right] \\
&= \Re\left[-\tfrac{\bar{M}}{r}\sum_{n=0}^{\infty}\sum_{m=0}^{n}\left(\frac{\alpha}{r}\right)^n\frac{(n+m)!}{(n-m)!}Y_n^{-m}(\delta,\lambda)K_{n,m}\right],
\end{aligned} \tag{6.3}$$

where $K_{n,m} = C_{n,m} + \imath S_{n,m}$ and $C_{n,m}$ and $S_{n,m}$ are as in (2.90) [11].

Wigner's rotation theorem for non scaled spherical harmonics (see [30]) is now applied in order to get to the nodal polar variables.

Theorem 5 *$\forall n,\ m \in \mathbb{N}, n,\ m$ let be $Y_n^m(\delta, \lambda)$ the spherical harmonics expressed in terms of the latitude δ and longitude λ in a system of reference $O_{\hat{\boldsymbol{x}},\hat{\boldsymbol{y}},\hat{\boldsymbol{z}}}$. Then the expression for $Y_n^m(\delta, \lambda)$ in terms of the latitude Δ and longitude Λ in another system of reference $O_{\hat{\boldsymbol{x}},\hat{\boldsymbol{y}},\hat{\boldsymbol{z}}}$, obtained by the composition of three rotations of angles α, β and γ (around the $\hat{\boldsymbol{x}}$ axes, the rotated $\hat{\boldsymbol{z}}$, and the rotated $\hat{\boldsymbol{x}}$ axes respectively), is given by:*

$$Y_n^m(\delta, \lambda) = \sum_{j=-n}^{n} D_{j,m}^n(-\alpha, -\beta, -\gamma) Y_n^j(\Delta, \Lambda) \tag{6.4}$$

where

$$D_{j,m}^n(-\alpha, -\beta, -\gamma) = e^{\imath j(\alpha + \frac{\pi}{2})} e^{\imath m(\gamma - \frac{\pi}{2})} d_{j,m}^n(-\beta) \tag{6.5}$$

and

$$\begin{aligned} d_{j,m}^n(-\beta) &= \textstyle\sum_{t=\max\{0, j-m\}}^{\min\{n-m, n+j\}} (-1)^{m-j+3t} \frac{(n-j)!(n+m)!}{t!(n+j-t)!(n-m-t)!(m-j+t)!} \cdot \\ &\cdot \left(\cos\left(\frac{\beta}{2}\right)\right)^{2n-(m-j+2t)} \left(\sin\left(\frac{\beta}{2}\right)\right)^{m-j+2t} \end{aligned} \tag{6.6}$$

This theorem is then applied by setting the second system of reference to be the one where the spacecraft position vector is $(0, 0, r)$ therefore the three angles α, β and γ are set to be θ, I and ν, the argument of latitude, the inclination of the orbital plane and namely the right ascension of the ascending node; moreover it must be noticed that in such system of reference the new latitude Δ and longitude Λ of the spacecraft will be both equal to zero as it has been set its new position vector to be $(0, 0, r)$. Therefore

[11] $C_{n,m}$ and $S_{n,m}$ are the so called "Stokes coefficient" [29]

(6.3) becomes:

$$U(r,\delta,\lambda)) = \Re\Bigg[-\tfrac{\bar{M}}{r}\sum_{n=0}^{\infty}\sum_{m=0}^{n}\left(\frac{\alpha}{r}\right)^n\frac{(n+m)!}{(n-m)!}\sum_{j=-n}^{n}D^n_{j,-m}(-\alpha,-\beta,-\gamma)$$

$$Y^j_n(0,0)K_{n,m}\Bigg]$$

$$= \Re\left[-\tfrac{\bar{M}}{r}\sum_{n=0}^{\infty}\sum_{m=0}^{n}\left(\frac{\alpha}{r}\right)^n\frac{(n+m)!}{(n-m)!}\sum_{j=-n}^{n}D^n_{j,-m}(-\theta,-I,-\nu)Y^j_n(0,0)K_{n,m}\right]$$

$$= \Re\Bigg[-\tfrac{\bar{M}}{r}\sum_{n=0}^{\infty}\sum_{m=0}^{n}\left(\frac{\alpha}{r}\right)^n\frac{(n+m)!}{(n-m)!}\sum_{j=-n}^{n}e^{\imath(j\theta-m\nu)}e^{\imath\frac{\pi}{2}(k+m)}d^n_{j,-m}(-I)\cdot$$

$$\cdot P^j_n(0)K_{n,m}\Bigg]$$

$$= -\tfrac{\bar{M}}{r}\sum_{n=0}^{\infty}\sum_{m=0}^{n}\left(\frac{\alpha}{r}\right)^n\frac{(n+m)!}{(n-m)!}\sum_{j=-n}^{n}\sum_{\ell=\max\{0,j+m\}}^{\min\{n+m,n+j\}}(-1)^{m-j+3\ell}\cdot$$

$$\cdot\tfrac{(n-j)!(n-m)!}{\ell!(n+j-\ell)!(n+m-\ell)!(-m-j+\ell)!}\left(\cos\left(\tfrac{I}{2}\right)\right)^{2n-(-m-j+2\ell)}\left(\sin\left(\tfrac{I}{2}\right)\right)^{-m-j+2\ell}\cdot$$

$$\cdot\left((-1)^j((n+j)_{\equiv_2}-1)\,(-1)^{\frac{n-j}{2}}\,\tfrac{(n+j-1)!!}{2^{\frac{n-j}{2}}(\frac{n-j}{2})!}\right)\cdot$$

$$\cdot\left(C_{n,m}\left(\cos\left(j\theta-m\nu\right)\cos\left(\tfrac{\pi}{2}(j+m)\right)-\sin\left(j\theta-m\nu\right)\sin\left(\tfrac{\pi}{2}(j+m)\right)\right)\right.$$

$$
\begin{aligned}
&+S_{n,m}\left(-\sin\left(j\theta-m\nu\right)\cos\left(\tfrac{\pi}{2}(j+m)\right)-\cos\left(j\theta-m\nu\right)\sin\left(\tfrac{\pi}{2}(j+m)\right)\right)\Big)\\
=&-\frac{\bar{M}}{r}\sum_{n=0}^{\infty}\sum_{m=0}^{n}\left(\frac{\alpha}{r}\right)^{n}\sum_{j=-n}^{n}\sum_{\ell=\max\{0,j+m\}}^{\min\{n+m,n+j\}}(-1)^{m-j+3\ell}\cdot\\
&\cdot\tfrac{(n-j)!(n+m)!}{\ell!(n+j-\ell)!(n+m-\ell)!(-m-j+\ell)!}\left(\cos\left(\tfrac{I}{2}\right)\right)^{2n-(-m-j+2\ell)}\left(\sin\left(\tfrac{I}{2}\right)\right)^{-m-j+2\ell}\cdot\\
&\cdot(-1)^{\frac{n+j}{2}}\tfrac{1}{2^n}\tfrac{(n+j)!}{\left(\frac{n+j}{2}\right)!\left(\frac{n-j}{2}\right)!}((n+j)_{\equiv_2}-1)\tfrac{(n+m)!}{2^n\left(\frac{n-m}{2}\right)!\left(\frac{n+m}{2}\right)!}\cdot\\
&\cdot\Big(C_{n,m}\left(\cos\left(j\theta-m\nu\right)\cos\left(\tfrac{\pi}{2}(j+m)\right)-\sin\left(j\theta-m\nu\right)\sin\left(\tfrac{\pi}{2}(j+m)\right)\right)\\
&+S_{n,m}\left(-\sin\left(j\theta-m\nu\right)\cos\left(\tfrac{\pi}{2}(j+m)\right)-\cos\left(j\theta-m\nu\right)\sin\left(\tfrac{\pi}{2}(j+m)\right)\right)\Big)
\end{aligned}
\tag{6.7}
$$

The potential can therefore be rearranged as:

$$
\begin{aligned}
\bar{U}(r,\theta,\nu,\_,\Theta,N)=-\sum_{n=0}^{\infty}\sum_{m=0}^{n}\sum_{j=-n}^{n}\sum_{t=\max\{0,j+m\}}^{\min\{n+m,n+j\}}ci^{2n+m+j-2t}si^{2t-m-j}\cdot\\
\cdot\tfrac{1}{r^{n+1}}\left(\mathcal{A}_{n,m,j,t}\cos\left(m\nu-j\theta\right)+\mathcal{B}_{n,m,j,t}\sin\left(m\nu-j\theta\right)\right),
\end{aligned}
\tag{6.8}
$$

where

$$
\begin{aligned}
ci:=ci(N,\Theta)=\cos\left(\tfrac{I}{2}\right)=\sqrt{\tfrac{1+\cos I}{2}}=\sqrt{\tfrac{1+\frac{N}{\Theta}}{2}}\\
si:=si(N,\Theta)=\sin\left(\tfrac{I}{2}\right)=\sqrt{\tfrac{1-\cos I}{2}}=\sqrt{\tfrac{1-\frac{N}{\Theta}}{2}}
\end{aligned}
\tag{6.9}
$$

and:

$$
\begin{aligned}
\mathcal{A}_{n,m,j,t}=\bar{\mathcal{G}}_{n,m,j,t}\left(C_{n,m}\cos\left(\tfrac{\pi}{2}(j+m)\right)-S_{n,m}\sin\left(\tfrac{\pi}{2}(j+m)\right)\right)\\
\mathcal{B}_{n,m,j,t}=\bar{\mathcal{G}}_{n,m,j,t}\left(C_{n,m}\sin\left(\tfrac{\pi}{2}(j+m)\right)+S_{n,m}\cos\left(\tfrac{\pi}{2}(j+m)\right)\right),
\end{aligned}
\tag{6.10}
$$

and

$$
\begin{aligned}
\bar{\mathcal{G}}_{n,m,j,t}=(-1)^{m+3t-j+1}\bar{M}\alpha^{n}\tfrac{(n+m)!(n-j)!}{t!(n+j-t)!(n+m-t)!(t-m-j)!}(-1)^{\frac{n+j}{2}}\tfrac{1}{2^n}\tfrac{(n+j)!}{\left(\frac{n+j}{2}\right)!\left(\frac{n-j}{2}\right)!}\cdot\\
\cdot((n+j)_{mod_2}-1)
\end{aligned}
\tag{6.11}
$$

where α is a conventionally chosen reference radius, usually taken as the radius of the circumscribing sphere of the small body and x_{mod_y} stands for the value of x modulus y, i.e. the integer reminder of the division of x by y, and where $C_{n,m}$ and $S_{n,m}$ as in (2.90).

Appendix B

As $\tilde{H}_{2,0} = H_2 + 2[H_1, W_1] + [[H_0, W_1], W_1]$, the explicit expression for $K_{2,0}$ will be given by the sum of the three corresponding contributions from the three terms of $\tilde{H}_{2,0}$ such that $K_{2,0} = K_{2,0}^{(1)} + K_{2,0}^{(2)} + K_{2,0}^{(23)}$ where:

$$K_{2,0}^{(1)} = -\frac{2!}{\epsilon^2} \sum_{n=1}^{\infty} \sum_{j=-n}^{n} \sum_{t=\max\{0,j\}}^{\min\{n,n+j\}} ci^{2n+j-2t} si^{2t-j} \cdot \frac{1}{r^{n+1}} \left(\mathcal{A}_{n,0,j,t}^{(2)} \cos(-j\theta) + \mathcal{B}_{n,0,j,t}^{(2)} \sin(-j\theta) \right) \tag{6.12}$$

then

$$K_{2,0}^{(2)} = \frac{2}{\epsilon^2} \sum_{\bar{n}=1}^{\infty} \sum_{\bar{m}=1}^{\bar{n}} \sum_{\bar{j}=-\bar{n}}^{\bar{n}} \sum_{\bar{t}=\max\{0,\bar{j}+\bar{m}\}}^{\min\{\bar{n}+\bar{m},\bar{n}+\bar{j}\}} \sum_{p=0}^{p^{(2)}} \sum_{n=1}^{\infty} \sum_{j=-n}^{n} \sum_{t=\max\{0,j+\bar{m}\}}^{\min\{n+\bar{m},n+j\}}$$

$$ci^{2\bar{n}+\bar{m}+\bar{j}-2\bar{t}+2n+\bar{m}+j-2t} si^{2\bar{t}-\bar{m}-\bar{j}+2t-\bar{m}-j} \left(-\frac{1}{\bar{m}\omega}\right)^{p+1} \sum_{a_p=0}^{1}$$

$$\left(\sum_{a_{p-1}=1-\delta_{a_p,0}}^{\max\{p-(p-2),0\}} \cdots \sum_{a_3=1-\delta_{a_4,0}}^{\max\{p-\mathcal{S}(4,p)-2,0\}} \sum_{a_2=1-\delta_{a_3,0}}^{\max\{p-\mathcal{S}(3,p)-1,0\}} \left(\sum_{a_1=0}^{\max\{p-\mathcal{S}(2,p),0\}} \right.\right.$$

$$\mathcal{D} \left(\sum_{a'_{p_{O_{max}}}=0}^{a_{p_{O_{max}}}} \cdots \sum_{a'_5}^{a_5} \sum_{a'_3}^{a_3} \left(\sum_{a''_{p_{O_{max}}}=0}^{a_{p_{O_{max}}}-a'_{p_{O_{max}}}} \cdots \sum_{a''_5=0}^{a_5-a'_5} \sum_{a''_3=0}^{a_3-a'_3} \right.\right.$$

$$\left(\mathcal{O}_{p_{O_{max}}} \cdot \ldots \cdot \mathcal{O}_5 \cdot \mathcal{O}_3\right) \left(\mathcal{E}_{p_{E_{max}}} \cdot \ldots \cdot \mathcal{E}_4 \mathcal{E}_2\right)$$

$$\left(\frac{1}{r}\right)^{3(\mathcal{S}_O(3,p_{O_{max}})-\mathcal{S}'_O(3,p_{O_{max}}))} \left(-\frac{1}{r}\right)^{p-a_1-\mathcal{S}_E(2,p_{E_{max}})-\mathcal{S}'_O(3,p_{O_{max}})}$$

$$R^{p-a_1-2\mathcal{S}_E(2,p_{E_{max}})-\mathcal{S}'_O(3,p_{O_{max}})} \left(\frac{j\Theta}{r^2}\right)^{a_1+\mathcal{S}'_O(3,p_{O_{max}})}$$

$$\left(\frac{-\Theta^2+r\mu}{r^3}\right)^{\mathcal{S}_E(2,p_{E_{max}})-\mathcal{S}_O(3,p_{O_{max}})+\mathcal{S}'_O(3,p_{O_{max}})}$$

$$\Theta^{2(\mathcal{S}_O(3,p_{O_{max}})-\mathcal{S}'_O(3,p_{O_{max}})-\mathcal{S}''_O(3,p_{O_{max}}))} (-r\mu)^{\mathcal{S}''_O(3,p_{O_{max}})} \frac{1}{r^{\bar{n}+1+n+1}} \cdot$$

$$\cdot \left(\left(\frac{-(\bar{n}+1)}{r} \frac{p-a_1-2\mathcal{S}_E(2,p_{E_{max}})-\mathcal{S}'_O(3,p_{O_{max}})}{R} \right) \right.$$

$$\left(\frac{1}{2} \left((\mathcal{A}_{n,\bar{m},j}^{(1)} \mathcal{A}_{\bar{n},\bar{m},\bar{j}}^{(1)} + \mathcal{B}_{n,\bar{m},j}^{(1)} \mathcal{B}_{\bar{n},\bar{m},\bar{j}}^{(1)}) \cos\left(\frac{\pi}{2}(-(-(p+1)+a_1+\mathcal{S}'_O(3,p_{O_{max}})))\right) \right.\right.$$

$$\left.\left. + (\mathcal{A}_{\bar{n},\bar{m},\bar{j}}^{(1)} \mathcal{B}_{n,\bar{m},j}^{(1)} - \mathcal{A}_{n,\bar{m},j}^{(1)} \mathcal{B}_{\bar{n},\bar{m},\bar{j}}^{(1)}) \sin\left(\frac{\pi}{2}(-(-(p+1)+a_1+\mathcal{S}'_O(3,p_{O_{max}})))\right) \right) \right.$$

$$\cos(-(j-\bar{j})\theta)$$

$$+\frac{1}{2} \left((\mathcal{A}_{\bar{n},\bar{m},\bar{j}}^{(1)} \mathcal{B}_{n,\bar{m},j}^{(1)} - \mathcal{A}_{n,\bar{m},j}^{(1)} \mathcal{B}_{\bar{n},\bar{m},\bar{j}}^{(1)}) \cos\left(\frac{\pi}{2}(-(-(p+1)+a_1+\mathcal{S}'_O(3,p_{O_{max}})))\right) \right.$$

$$\left.\left. - (\mathcal{A}_{n,\bar{m},j}^{(1)} \mathcal{A}_{\bar{n},\bar{m},\bar{j}}^{(1)} + \mathcal{B}_{n,\bar{m},j}^{(1)} \mathcal{B}_{\bar{n},\bar{m},\bar{j}}^{(1)}) \sin\left(\frac{\pi}{2}(-(-(p+1)+a_1+\mathcal{S}'_O(3,p_{O_{max}})))\right) \right) \right.$$

$$\left.\left.\left.\sin(-(j-\bar{j})\theta)\right)\right)\right)$$

$$
\begin{aligned}
&+\left((-\bar{j})\tfrac{1}{\Theta}\left((a_1+\mathcal{S}'_O(3,p_{O_{max}})\right)\right.\\
&+2(\mathcal{S}_O(3,p_{O_{max}})-\mathcal{S}'_O(3,p_{O_{max}})-\mathcal{S}''_O(3,p_{O_{max}}))\tfrac{(j-2t+\bar{m})N}{2(N-\Theta)}\\
&\left.-\tfrac{(j-2t+\bar{m}+2n)N}{2(N+\Theta)}+\tfrac{2(\mathcal{S}_E(2,p_{E_{max}})-\mathcal{S}_O(3,p_{O_{max}})+\mathcal{S}'_O(3,p_{O_{max}}))\Theta^2}{\Theta^2-r\mu}\right)\Big)\\
&\Big(\tfrac{1}{2}\Big((\mathcal{A}^{(1)}_{n,\bar{m},j}\mathcal{A}^{(1)}_{\bar{n},\bar{m},\bar{j}}+\mathcal{B}^{(1)}_{n,\bar{m},j}\mathcal{B}^{(1)}_{\bar{n},\bar{m},\bar{j}})\cos\left(\tfrac{\pi}{2}(-(p+1)+a_1+\mathcal{S}'_O(3,p_{O_{max}})-1)\right)\\
&+(\mathcal{A}^{(1)}_{\bar{n},\bar{m},\bar{j}}\mathcal{B}^{(1)}_{n,\bar{m},j}-\mathcal{A}^{(1)}_{n,\bar{m},j}\mathcal{B}^{(1)}_{\bar{n},\bar{m},\bar{j}})\sin\left(\tfrac{\pi}{2}(-(p+1)+a_1+\mathcal{S}'_O(3,p_{O_{max}})-1)\right)\Big)\\
&\cos(-(j-\bar{j})\theta)\\
&+\tfrac{1}{2}\Big((\mathcal{A}^{(1)}_{\bar{n},\bar{m},\bar{j}}\mathcal{B}^{(1)}_{n,\bar{m},j}-\mathcal{A}^{(1)}_{n,\bar{m},j}\mathcal{B}^{(1)}_{\bar{n},\bar{m},\bar{j}})\cos\left(\tfrac{\pi}{2}(-(p+1)+a_1+\mathcal{S}'_O(3,p_{O_{max}})-1)\right)\\
&-(\mathcal{A}^{(1)}_{n,\bar{m},j}\mathcal{A}^{(1)}_{\bar{n},\bar{m},\bar{j}}+\mathcal{B}^{(1)}_{n,\bar{m},j}\mathcal{B}^{(1)}_{\bar{n},\bar{m},\bar{j}})\sin\left(\tfrac{\pi}{2}(-(p+1)+a_1+\mathcal{S}'_O(3,p_{O_{max}})-1)\right)\Big)\\
&\sin(-(j-\bar{j})\theta))\\
&\\
&+\left(-(-j)(-\tfrac{N(\bar{n}(1-\frac{N}{\Theta})+(\bar{j}-2\bar{t}+\bar{m}))}{\Theta^2(1-\frac{N^2}{\Theta^2})})\right)\\
&\Big(\tfrac{1}{2}\Big((\mathcal{A}^{(1)}_{n,\bar{m},j}\mathcal{A}^{(1)}_{\bar{n},\bar{m},\bar{j}}+\mathcal{B}^{(1)}_{n,\bar{m},j}\mathcal{B}^{(1)}_{\bar{n},\bar{m},\bar{j}})\cos\left(\tfrac{\pi}{2}(-(p+1)+a_1+\mathcal{S}'_O(3,p_{O_{max}}+1))\right)\\
&+(\mathcal{A}^{(1)}_{\bar{n},\bar{m},\bar{j}}\mathcal{B}^{(1)}_{n,\bar{m},j}-\mathcal{A}^{(1)}_{n,\bar{m},j}\mathcal{B}^{(1)}_{\bar{n},\bar{m},\bar{j}})\sin\left(\tfrac{\pi}{2}(-(p+1)+a_1+\mathcal{S}'_O(3,p_{O_{max}}+1))\right)\Big)\\
&\cos(-(j-\bar{j})\theta)\\
&+\tfrac{1}{2}\Big((\mathcal{A}^{(1)}_{\bar{n},\bar{m},\bar{j}}\mathcal{B}^{(1)}_{n,\bar{m},j}-\mathcal{A}^{(1)}_{n,\bar{m},j}\mathcal{B}^{(1)}_{\bar{n},\bar{m},\bar{j}})\cos\left(\tfrac{\pi}{2}(-(p+1)+a_1+\mathcal{S}'_O(3,p_{O_{max}}+1))\right)\\
&-(\mathcal{A}^{(1)}_{n,\bar{m},j}\mathcal{A}^{(1)}_{\bar{n},\bar{m},\bar{j}}+\mathcal{B}^{(1)}_{n,\bar{m},j}\mathcal{B}^{(1)}_{\bar{n},\bar{m},\bar{j}})\sin\left(\tfrac{\pi}{2}(-(p+1)+a_1+\mathcal{S}'_O(3,p_{O_{max}}+1))\right)\Big)\\
&\sin(-(j-\bar{j})\theta))\\
&\\
&+\left((\bar{m})(\tfrac{(j-2t+\bar{m})+n(1-\frac{N}{\Theta})}{\Theta(1-\frac{N^2}{\Theta^2})})\right)\\
&\Big(\tfrac{1}{2}\Big((\mathcal{A}^{(1)}_{n,\bar{m},j}\mathcal{A}^{(1)}_{\bar{n},\bar{m},\bar{j}}+\mathcal{B}^{(1)}_{n,\bar{m},j}\mathcal{B}^{(1)}_{\bar{n},\bar{m},\bar{j}})\cos\left(\tfrac{\pi}{2}(-(p+1)+a_1+\mathcal{S}'_O(3,p_{O_{max}})-1)\right)\\
&+(\mathcal{A}^{(1)}_{\bar{n},\bar{m},\bar{j}}\mathcal{B}^{(1)}_{n,\bar{m},j}-\mathcal{A}^{(1)}_{n,\bar{m},j}\mathcal{B}^{(1)}_{\bar{n},\bar{m},\bar{j}})\sin\left(\tfrac{\pi}{2}(-(p+1)+a_1+\mathcal{S}'_O(3,p_{O_{max}})-1)\right)\Big)\\
&\cos(-(j-\bar{j})\theta)\\
&+\tfrac{1}{2}\Big((\mathcal{A}^{(1)}_{\bar{n},\bar{m},\bar{j}}\mathcal{B}^{(1)}_{n,\bar{m},j}-\mathcal{A}^{(1)}_{n,\bar{m},j}\mathcal{B}^{(1)}_{\bar{n},\bar{m},\bar{j}})\cos\left(\tfrac{\pi}{2}(-(p+1)+a_1+\mathcal{S}'_O(3,p_{O_{max}})-1)\right)\\
&-(\mathcal{A}^{(1)}_{n,\bar{m},j}\mathcal{A}^{(1)}_{\bar{n},\bar{m},\bar{j}}+\mathcal{B}^{(1)}_{n,\bar{m},j}\mathcal{B}^{(1)}_{\bar{n},\bar{m},\bar{j}})\sin\left(\tfrac{\pi}{2}(-(p+1)+a_1+\mathcal{S}'_O(3,p_{O_{max}})-1)\right)\Big)\\
&\sin(-(j-\bar{j})\theta))\\
&\\
&-\left((\bar{m})(\tfrac{(\bar{j}-2\bar{t}+\bar{m})+\bar{n}(1-\frac{N}{\Theta})}{\Theta(1-\frac{N^2}{\Theta^2})})\right)\\
&\Big(\tfrac{1}{2}\Big((\mathcal{A}^{(1)}_{n,\bar{m},j}\mathcal{A}^{(1)}_{\bar{n},\bar{m},\bar{j}}+\mathcal{B}^{(1)}_{n,\bar{m},j}\mathcal{B}^{(1)}_{\bar{n},\bar{m},\bar{j}})\cos\left(\tfrac{\pi}{2}(-(p+1)+a_1+\mathcal{S}'_O(3,p_{O_{max}}+1))\right)\\
&+(\mathcal{A}^{(1)}_{\bar{n},\bar{m},\bar{j}}\mathcal{B}^{(1)}_{n,\bar{m},j}-\mathcal{A}^{(1)}_{n,\bar{m},j}\mathcal{B}^{(1)}_{\bar{n},\bar{m},\bar{j}})\sin\left(\tfrac{\pi}{2}(-(p+1)+a_1+\mathcal{S}'_O(3,p_{O_{max}}+1))\right)\Big)\\
&\cos(-(j-\bar{j})\theta)\\
&+\tfrac{1}{2}\Big((\mathcal{A}^{(1)}_{\bar{n},\bar{m},\bar{j}}\mathcal{B}^{(1)}_{n,\bar{m},j}-\mathcal{A}^{(1)}_{n,\bar{m},j}\mathcal{B}^{(1)}_{\bar{n},\bar{m},\bar{j}})\cos\left(\tfrac{\pi}{2}(-(p+1)+a_1+\mathcal{S}'_O(3,p_{O_{max}}+1))\right)\\
&-(\mathcal{A}^{(1)}_{n,\bar{m},j}\mathcal{A}^{(1)}_{\bar{n},\bar{m},\bar{j}}+\mathcal{B}^{(1)}_{n,\bar{m},j}\mathcal{B}^{(1)}_{\bar{n},\bar{m},\bar{j}})\sin\left(\tfrac{\pi}{2}(-(p+1)+a_1+\mathcal{S}'_O(3,p_{O_{max}}+1))\right)\Big)\\
&\sin(-(j-\bar{j})\theta)))
\end{aligned}
\tag{6.13}
$$

where in $\mathcal{D}$, $\mathcal{O}$ and $\mathcal{E}$ the parameter m must be substituted by $\bar{m}$.

Finally, calling, $\bar{p}_{O_{max}} = 2\lfloor\frac{\bar{p}-1}{2}\rfloor + 1, \quad \bar{p}_{E_{max}} = 2\lfloor\frac{\bar{p}}{2}\rfloor$, and:

$$\begin{aligned}
&\bar{\mathcal{S}}(\hat{k},k^*) = \sum_{\bar{k}=\hat{k}}^{k^*} \bar{a}_{\bar{k}} \\
&\bar{\mathcal{S}}_E(\hat{k},k^*) = \sum_{\substack{\bar{k}=\hat{k},\\ \bar{k}\ even}}^{k^*} \bar{a}_{\bar{k}}, \quad \bar{\mathcal{S}}'_E(\hat{k},k^*) = \sum_{\substack{\bar{k}=\hat{k},\\ \bar{k}\ even}}^{k^*} \bar{a}'_{\bar{k}}, \quad \bar{\mathcal{S}}''_E(\hat{k},k^*) = \sum_{\substack{\bar{k}=\hat{k},\\ \bar{k}\ even}}^{k^*} \bar{a}''_{\bar{k}} \\
&\bar{\mathcal{S}}_O(\hat{k},k^*) = \sum_{\substack{\bar{k}=\hat{k},\\ \bar{k}\ odd}}^{k^*} \bar{a}_{\bar{k}}, \quad \bar{\mathcal{S}}'_O(\hat{k},k^*) = \sum_{\substack{\bar{k}=\hat{k},\\ \bar{k}\ odd}}^{k^*} \bar{a}'_{\bar{k}}, \quad \bar{\mathcal{S}}''_O(\hat{k},k^*) = \sum_{\substack{\bar{k}=\hat{k},\\ \bar{k}\ odd}}^{k^*} \bar{a}''_{\bar{k}}
\end{aligned} \tag{6.14}$$

Also, calling:

$$\bar{\mathcal{D}} := (-1)^{\bar{p}-\bar{\mathcal{S}}(1,\bar{p})} \binom{\bar{p}-\bar{\mathcal{S}}(2,\bar{p})}{\bar{p}-\bar{\mathcal{S}}(1,\bar{p})} \frac{(\bar{n}+\bar{p}-\bar{\mathcal{S}}(1,\bar{p}))!}{(\bar{n}+\bar{a}_1)!} \tag{6.15}$$

and $\forall \bar{k}$ *odd*

$$\begin{aligned}
\bar{\mathcal{O}}_{\bar{k}} := &\left(\binom{\bar{a}_{\bar{p}_{O_{max}}}}{\bar{a}'_{\bar{p}_{O_{max}}}} \cdots \binom{\bar{a}_5}{\bar{a}'_5}\binom{\bar{a}_3}{\bar{a}'_3}\right)\left(\binom{\bar{a}_{\bar{p}_{O_{max}}} - \bar{a}'_{\bar{p}_{O_{max}}}}{\bar{a}''_{\bar{p}_{O_{max}}}} \cdots \binom{\bar{a}_5-\bar{a}'_5}{\bar{a}''_5}\binom{\bar{a}_3-\bar{a}'_3}{\bar{a}''_3}\right) \\
&\left(\frac{(\bar{a}_1+\bar{n}+\bar{p}+2\bar{\mathcal{S}}_E(2,\bar{k}-1)-\bar{\mathcal{S}}(\bar{k},\bar{p})+\bar{a}_{\bar{k}}-\bar{a}''_{\bar{k}}+\bar{\mathcal{S}}'_O(3,\bar{k}-2)-\bar{\mathcal{S}}''_O(3,\bar{k}-2))!}{(\bar{a}_1+\bar{n}+\bar{p}+2\bar{\mathcal{S}}_E(2,\bar{k}-1)-\bar{\mathcal{S}}(\bar{k},\bar{p})+\bar{a}'_{\bar{k}}+\bar{\mathcal{S}}'_O(3,\bar{k}-2)-\bar{\mathcal{S}}''_O(3,\bar{k}-2))!}\right) \\
&\left(\frac{(\bar{a}_1+\bar{n}+\bar{p}+\bar{\mathcal{S}}_E(2,\bar{k}-1)-\bar{\mathcal{S}}(\bar{k},\bar{p})+\bar{a}_{\bar{k}}+\bar{\mathcal{S}}_O(3,\bar{k}-2)-\bar{\mathcal{S}}''_O(3,\bar{k}-2))!}{(\bar{a}_1+\bar{n}+\bar{p}+\bar{\mathcal{S}}_E(2,\bar{k}-1)-\bar{\mathcal{S}}(\bar{k},\bar{p})+\bar{a}_{\bar{k}}-\bar{a}''_{\bar{k}}+\bar{\mathcal{S}}_O(3,\bar{k}-2)-\bar{\mathcal{S}}''_O(3,\bar{k}-2))!}\right)
\end{aligned} \tag{6.16}$$

while $\forall \bar{k}$ *even*

$$\begin{aligned}
&\bar{\mathcal{E}}_2 := \left(\frac{(\bar{p}-\bar{\mathcal{S}}(1,\bar{p}))!}{(\bar{p}-\bar{\mathcal{S}}(1,\bar{p})-\bar{a}_2)!}\right) \\
&\bar{\mathcal{E}}_{\bar{k}} := \left(\frac{(\bar{p}-\bar{a}_1-2\bar{\mathcal{S}}_E(2,\bar{k}-2)-\bar{\mathcal{S}}(\bar{k},\bar{p})-\bar{\mathcal{S}}'_O(3,\bar{k}-1)+\bar{a}_{\bar{k}}+1)!}{(\bar{p}-\bar{a}_1-2\bar{\mathcal{S}}_E(2,\bar{k}-2)-\bar{\mathcal{S}}(\bar{k},\bar{p})-\bar{\mathcal{S}}'_O(3,\bar{k}-1)-1)!}\right) \quad \forall \bar{k} \geq 4,\ \bar{k}\ even
\end{aligned} \tag{6.17}$$

yields:

$$K_{2,0}^{(3)} = \left(\tfrac{1}{\epsilon^2}\right) \sum_{p=0}^{p^{(2)}} \sum_{n=1}^{\infty} \sum_{\bar{m}=1}^{n} \sum_{j=-n}^{n} \sum_{t=\max\{0,j+\bar{m}\}}^{\min\{n+\bar{m},n+j\}} \sum_{\substack{\bar{p}=0 \\ p+\bar{p}\leq p^{(2)}}}^{\bar{p}^{(2)}} \sum_{\bar{n}=1}^{\infty} \sum_{\bar{j}=-\bar{n}}^{\bar{n}} \sum_{\bar{t}=\max\{0,\bar{j}+\bar{m}\}}^{\min\{\bar{n}+\bar{m},\bar{n}+\bar{j}\}}$$

$$(2-\delta_{p,0}) ci^{2n+\bar{m}+j-2t} si^{2t-\bar{m}-j} \left(-\tfrac{1}{\bar{m}\omega}\right)^{p} ci^{2\bar{n}+\bar{m}+\bar{j}-2\bar{t}} si^{2\bar{t}-\bar{m}-\bar{j}} \left(-\tfrac{1}{\bar{m}\omega}\right)^{\bar{p}+1}$$

$$\sum_{\bar{a}_{\bar{p}}=0}^{1} \left(\sum_{\bar{a}_{\bar{p}-1}=1-\delta_{\bar{a}_{\bar{p}},0}}^{\max\{\bar{p}-(\bar{p}-2),0\}} \cdots \sum_{\bar{a}_3=1-\delta_{\bar{a}_4,0}}^{\max\{\bar{p}-\bar{\mathcal{S}}(4,\bar{p})-2,0\}} \sum_{\bar{a}_2=1-\delta_{\bar{a}_3,0}}^{\max\{\bar{p}-\bar{\mathcal{S}}(3,\bar{p})-1,0\}} \left(\sum_{\bar{a}_1=0}^{\max\{\bar{p}-\bar{\mathcal{S}}(2,\bar{p}),0\}} \right.\right.$$

$$\sum_{a_p=0}^{1} \left(\sum_{a_{p-1}=1-\delta_{a_p,0}}^{\max\{p-(p-2),0\}} \cdots \sum_{a_3=1-\delta_{a_4,0}}^{\max\{p-\mathcal{S}(4,p)-2,0\}} \sum_{a_2=1-\delta_{a_3,0}}^{\max\{p-\mathcal{S}(3,p)-1,0\}} \left(\sum_{a_1=0}^{\max\{p-\mathcal{S}(2,p),0\}} \right.\right.$$

$$\mathcal{D} \left(\sum_{a'_{pO_{max}}=0}^{a_{pO_{max}}} \cdots \sum_{a'_5}^{a_5} \sum_{a'_3}^{a_3} \left(\sum_{a''_{pO_{max}}=0}^{a_{pO_{max}}-a'_{pO_{max}}} \cdots \sum_{a''_5=0}^{a_5-a'_5} \sum_{a''_3=0}^{a_3-a'_3} \right.\right.$$

$$\bar{\mathcal{D}} \left(\sum_{\bar{a}'_{\bar{p}O_{max}}=0}^{\bar{a}_{\bar{p}O_{max}}} \cdots \sum_{\bar{a}'_5}^{\bar{a}_5} \sum_{\bar{a}'_3}^{\bar{a}_3} \left(\sum_{\bar{a}''_{\bar{p}O_{max}}=0}^{\bar{a}_{\bar{p}O_{max}}-\bar{a}'_{\bar{p}O_{max}}} \cdots \sum_{\bar{a}''_5=0}^{\bar{a}_5-\bar{a}'_5} \sum_{\bar{a}''_3=0}^{\bar{a}_3-\bar{a}'_3} \right.\right.$$

$$\left(\mathcal{O}_{pO_{max}} \cdot \ldots \cdot \mathcal{O}_5 \cdot \mathcal{O}_3\right) \left(\mathcal{E}_{pE_{max}} \cdot \ldots \cdot \mathcal{E}_4 \mathcal{E}_2\right) \left(\tfrac{1}{r}\right)^{3(\mathcal{S}_O(3,p_{O_{max}})-\mathcal{S}'_O(3,p_{O_{max}}))}$$

$$\left(\bar{\mathcal{O}}_{\bar{p}O_{max}} \cdot \ldots \cdot \bar{\mathcal{O}}_5 \cdot \bar{\mathcal{O}}_3\right) \left(\bar{\mathcal{E}}_{\bar{p}E_{max}} \cdot \ldots \cdot \bar{\mathcal{E}}_4 \bar{\mathcal{E}}_2\right) \left(\tfrac{1}{r}\right)^{3(\bar{\mathcal{S}}_O(3,\bar{p}_{O_{max}})-\bar{\mathcal{S}}'_O(3,\bar{p}_{O_{max}}))}$$

$$\left(-\tfrac{1}{r}\right)^{p-a_1-\mathcal{S}_E(2,p_{E_{max}})-\mathcal{S}'_O(3,p_{O_{max}})} R^{p-a_1-2\mathcal{S}_E(2,p_{E_{max}})-\mathcal{S}'_O(3,p_{O_{max}})}$$

$$\left(-\tfrac{1}{r}\right)^{\bar{p}-\bar{a}_1-\bar{\mathcal{S}}_E(2,\bar{p}_{E_{max}})-\bar{\mathcal{S}}'_O(3,\bar{p}_{O_{max}})} R^{\bar{p}-\bar{a}_1-2\bar{\mathcal{S}}_E(2,\bar{p}_{E_{max}})-\bar{\mathcal{S}}'_O(3,\bar{p}_{O_{max}})}$$

$$\left(\tfrac{j\Theta}{r^2}\right)^{a_1+\mathcal{S}'_O(3,p_{O_{max}})} \left(\tfrac{-\Theta^2+r\mu}{r^3}\right)^{\mathcal{S}_E(2,p_{E_{max}})-\mathcal{S}_O(3,p_{O_{max}})+\mathcal{S}'_O(3,p_{O_{max}})}$$

$$\left(\tfrac{\bar{j}\Theta}{r^2}\right)^{\bar{a}_1+\bar{\mathcal{S}}'_O(3,\bar{p}_{O_{max}})} \left(\tfrac{-\Theta^2+r\mu}{r^3}\right)^{\bar{\mathcal{S}}_E(2,\bar{p}_{E_{max}})-\bar{\mathcal{S}}_O(3,\bar{p}_{O_{max}})+\bar{\mathcal{S}}'_O(3,\bar{p}_{O_{max}})}$$

$$\Theta^{2(\mathcal{S}_O(3,p_{O_{max}})-\mathcal{S}'_O(3,p_{O_{max}})-\mathcal{S}''_O(3,p_{O_{max}}))} (-r\mu)^{\mathcal{S}''_O(3,p_{O_{max}})} \tfrac{1}{r^{n+1}}$$

$$\Theta^{2(\bar{\mathcal{S}}_O(3,\bar{p}_{O_{max}})-\bar{\mathcal{S}}'_O(3,\bar{p}_{O_{max}})-\bar{\mathcal{S}}''_O(3,\bar{p}_{O_{max}}))} (-r\mu)^{\bar{\mathcal{S}}''_O(3,\bar{p}_{O_{max}})} \tfrac{1}{r^{\bar{n}+1}}.$$

$$
\cdot \Big(- \Big(\tfrac{r^3}{-\Theta^2 + r\mu} \tfrac{1}{r^4} \big(\big((3(\bar{\mathcal{S}}_O(3, \bar{p}_{O_{max}}) - \bar{\mathcal{S}}'_O(3, \bar{p}_{O_{max}}))) - (\bar{\mathcal{S}}''_O(3, \bar{p}_{O_{max}})) + \big(\bar{p} - \bar{a}_1 - \bar{\mathcal{S}}_E(2, \bar{p}_{E_{max}}) \\
- \bar{\mathcal{S}}'_O(3, \bar{p}_{O_{max}}) \big) + 2(\bar{a}_1 + \bar{\mathcal{S}}'_O(3, \bar{p}_{O_{max}})) + 3(\bar{\mathcal{S}}_E(2, \bar{p}_{E_{max}}) - \bar{\mathcal{S}}_O(3, \bar{p}_{O_{max}}) \\
+ \bar{\mathcal{S}}'_O(3, \bar{p}_{O_{max}}) \big) + (\bar{n} + 1) \big) \Theta^2 + \big(-(3(\bar{\mathcal{S}}_O(3, \bar{p}_{O_{max}}) - \bar{\mathcal{S}}'_O(3, \bar{p}_{O_{max}}))) + (\bar{\mathcal{S}}''_O(3, \bar{p}_{O_{max}})) \\
- (\bar{p} - \bar{a}_1 - \mathcal{S}_E(2, \bar{p}_{E_{max}}) - \bar{\mathcal{S}}'_O(3, \bar{p}_{O_{max}})) - (\bar{a}_1 + \bar{\mathcal{S}}'_O(3, \bar{p}_{O_{max}})) \\
- 2(\bar{\mathcal{S}}_E(2, \bar{p}_{E_{max}}) - \bar{\mathcal{S}}_O(3, \bar{p}_{O_{max}}) + \bar{\mathcal{S}}'_O(3, \bar{p}_{O_{max}})) - (\bar{n} + 1) \big) r\mu \big) \big) \\
\left(\tfrac{p - a_1 - 2\mathcal{S}_E(2, p_{E_{max}}) - \mathcal{S}'_O(3, p_{O_{max}})}{R} \right) \\
\Big(\tfrac{1}{2} \Big((\mathcal{A}^{(1)}_{n,\bar{m},j} \mathcal{A}^{(1)}_{\bar{n},\bar{m},\bar{j}} + \mathcal{B}^{(1)}_{n,\bar{m},j} \mathcal{B}^{(1)}_{\bar{n},\bar{m},\bar{j}}) \\
\cos\big(\tfrac{\pi}{2} ((-(p) + a_1 + \mathcal{S}'_O(3, p_{O_{max}})) - (-(\bar{p} + 1) + \bar{a}_1 + \bar{\mathcal{S}}'_O(3, \bar{p}_{O_{max}})))\big) \\
+ (\mathcal{A}^{(1)}_{\bar{n},\bar{m},\bar{j}} \mathcal{B}^{(1)}_{n,\bar{m},j} - \mathcal{A}^{(1)}_{n,\bar{m},j} \mathcal{B}^{(1)}_{\bar{n},\bar{m},\bar{j}}) \\
\sin\big(\tfrac{\pi}{2} ((-(p) + a_1 + \mathcal{S}'_O(3, p_{O_{max}})) - (-(\bar{p} + 1) + \bar{a}_1 + \bar{\mathcal{S}}'_O(3, \bar{p}_{O_{max}})))\big) \big) \\
\cos(-(j - \bar{j})\theta) \\
+ \tfrac{1}{2} \Big((\mathcal{A}^{(1)}_{\bar{n},\bar{m},\bar{j}} \mathcal{B}^{(1)}_{n,\bar{m},j} - \mathcal{A}^{(1)}_{n,\bar{m},j} \mathcal{B}^{(1)}_{\bar{n},\bar{m},\bar{j}}) \\
\cos\big(\tfrac{\pi}{2} ((-(p) + a_1 + \mathcal{S}'_O(3, p_{O_{max}})) - (-(\bar{p} + 1) + \bar{a}_1 + \bar{\mathcal{S}}'_O(3, \bar{p}_{O_{max}})))\big) \\
- (\mathcal{A}^{(1)}_{n,\bar{m},j} \mathcal{A}^{(1)}_{\bar{n},\bar{m},\bar{j}} + \mathcal{B}^{(1)}_{n,\bar{m},j} \mathcal{B}^{(1)}_{\bar{n},\bar{m},\bar{j}}) \\
\sin\big(\tfrac{\pi}{2} ((-(p) + a_1 + \mathcal{S}'_O(3, p_{O_{max}})) - (-(\bar{p} + 1) + \bar{a}_1 + \bar{\mathcal{S}}'_O(3, \bar{p}_{O_{max}})))\big) \big) \\
\sin(-(j - \bar{j})\theta) \big) \\
\\
+ \left(\tfrac{\bar{p} - \bar{a}_1 - 2\bar{\mathcal{S}}_E(2, \bar{p}_{E_{max}}) - \bar{\mathcal{S}}'_O(3, \bar{p}_{O_{max}})}{R} \right) \Big(- \Big(\tfrac{r^3}{-\Theta^2 + r\mu} \tfrac{1}{r^4} \big(\big(3\left(\mathcal{S}_O(3, p_{O_{max}}) \right) \\
- \mathcal{S}'_O(3, p_{O_{max}}) \big) \big) - (\mathcal{S}''_O(3, p_{O_{max}})) + (p - a_1 - \mathcal{S}_E(2, p_{E_{max}}) \\
- \mathcal{S}'_O(3, p_{O_{max}}) \big) + 2(a_1 + \mathcal{S}'_O(3, p_{O_{max}})) + 3\left(\mathcal{S}_E(2, p_{E_{max}}) - \mathcal{S}_O(3, p_{O_{max}}) \right) \\
+ \mathcal{S}'_O(3, p_{O_{max}}) \big) + (n + 1) \big) \Theta^2 + \big(-(3(\mathcal{S}_O(3, p_{O_{max}}) - \mathcal{S}'_O(3, p_{O_{max}}))) \\
+ (\mathcal{S}''_O(3, p_{O_{max}})) - (p - a_1 - \mathcal{S}_E(2, p_{E_{max}}) - \mathcal{S}'_O(3, p_{O_{max}})) \\
- (a_1 + \mathcal{S}'_O(3, p_{O_{max}})) - 2(\mathcal{S}_E(2, p_{E_{max}}) - \mathcal{S}_O(3, p_{O_{max}}) + \mathcal{S}'_O(3, p_{O_{max}})) \\
- (n + 1)) \, r\mu))) \\
\Big(\tfrac{1}{2} \Big((\mathcal{A}^{(1)}_{n,\bar{m},j} \mathcal{A}^{(1)}_{\bar{n},\bar{m},\bar{j}} + \mathcal{B}^{(1)}_{n,\bar{m},j} \mathcal{B}^{(1)}_{\bar{n},\bar{m},\bar{j}}) \\
\cos\big(\tfrac{\pi}{2} ((-(p) + a_1 + \mathcal{S}'_O(3, p_{O_{max}})) - (-(\bar{p} + 1) + \bar{a}_1 + \bar{\mathcal{S}}'_O(3, \bar{p}_{O_{max}})))\big) \\
+ (\mathcal{A}^{(1)}_{\bar{n},\bar{m},\bar{j}} \mathcal{B}^{(1)}_{n,\bar{m},j} - \mathcal{A}^{(1)}_{n,\bar{m},j} \mathcal{B}^{(1)}_{\bar{n},\bar{m},\bar{j}}) \\
\sin\big(\tfrac{\pi}{2} ((-(p) + a_1 + \mathcal{S}'_O(3, p_{O_{max}})) - (-(\bar{p} + 1) + \bar{a}_1 + \bar{\mathcal{S}}'_O(3, \bar{p}_{O_{max}})))\big) \big) \\
\cos(-(j - \bar{j})\theta) \\
+ \tfrac{1}{2} \Big((\mathcal{A}^{(1)}_{\bar{n},\bar{m},\bar{j}} \mathcal{B}^{(1)}_{n,\bar{m},j} - \mathcal{A}^{(1)}_{n,\bar{m},j} \mathcal{B}^{(1)}_{\bar{n},\bar{m},\bar{j}}) \\
\cos\big(\tfrac{\pi}{2} ((-(p) + a_1 + \mathcal{S}'_O(3, p_{O_{max}})) - (-(\bar{p} + 1) + \bar{a}_1 + \bar{\mathcal{S}}'_O(3, \bar{p}_{O_{max}})))\big) \\
- (\mathcal{A}^{(1)}_{n,\bar{m},j} \mathcal{A}^{(1)}_{\bar{n},\bar{m},\bar{j}} + \mathcal{B}^{(1)}_{n,\bar{m},j} \mathcal{B}^{(1)}_{\bar{n},\bar{m},\bar{j}}) \\
\sin\big(\tfrac{\pi}{2} ((-(p) + a_1 + \mathcal{S}'_O(3, p_{O_{max}})) - (-(\bar{p} + 1) + \bar{a}_1 + \bar{\mathcal{S}}'_O(3, \bar{p}_{O_{max}})))\big) \big) \\
\sin(-(j - \bar{j})\theta) \big)
$$

$$
\begin{aligned}
&-(-\bar{j})\left(\tfrac{1}{2\Theta}\left(4(\mathcal{S}_O(3,p_{O_{max}})-\mathcal{S}'_O(3,p_{O_{max}})-\mathcal{S}''_O(3,p_{O_{max}}))\right.\right.\\
&+2(a_1+\mathcal{S}'_O(3,p_{O_{max}}))+\tfrac{N(j+\bar{m}-2t)}{N-\Theta}-\tfrac{N(j+\bar{m}+2n-2t)}{N+\Theta}\\
&\left.\left.+\tfrac{4(\mathcal{S}_E(2,p_{E_{max}})-\mathcal{S}_O(3,p_{O_{max}})+\mathcal{S}'_O(3,p_{O_{max}}))\Theta}{\Theta^2-r\mu}\right)\right)\\
&\left(\tfrac{1}{2}\left((\mathcal{A}^{(1)}_{n,\bar{m},j}\mathcal{A}^{(1)}_{\bar{n},\bar{m},\bar{j}}+\mathcal{B}^{(1)}_{n,\bar{m},j}\mathcal{B}^{(1)}_{\bar{n},\bar{m},\bar{j}})\right.\right.\\
&\cos\left(\tfrac{\pi}{2}((-(p)+a_1+\mathcal{S}'_O(3,p_{O_{max}}))-(-(\bar{p}+1)+\bar{a}_1+\bar{\mathcal{S}}'_O(3,\bar{p}_{O_{max}})+1))\right)\\
&+(\mathcal{A}^{(1)}_{\bar{n},\bar{m},\bar{j}}\mathcal{B}^{(1)}_{n,\bar{m},j}-\mathcal{A}^{(1)}_{n,\bar{m},j}\mathcal{B}^{(1)}_{\bar{n},\bar{m},\bar{j}})\\
&\left.\left.\sin\left(\tfrac{\pi}{2}((-(p)+a_1+\mathcal{S}'_O(3,p_{O_{max}}))-(-(\bar{p}+1)+\bar{a}_1+\bar{\mathcal{S}}'_O(3,\bar{p}_{O_{max}})+1))\right)\right)\right.\\
&\cos(-(j-\bar{j})\theta)\\
&+\tfrac{1}{2}\left((\mathcal{A}^{(1)}_{\bar{n},\bar{m},\bar{j}}\mathcal{B}^{(1)}_{n,\bar{m},j}-\mathcal{A}^{(1)}_{n,\bar{m},j}\mathcal{B}^{(1)}_{\bar{n},\bar{m},\bar{j}})\right.\\
&\cos\left(\tfrac{\pi}{2}((-(p)+a_1+\mathcal{S}'_O(3,p_{O_{max}}))-(-(\bar{p}+1)+\bar{a}_1+\bar{\mathcal{S}}'_O(3,\bar{p}_{O_{max}})+1))\right)\\
&-(\mathcal{A}^{(1)}_{n,\bar{m},j}\mathcal{A}^{(1)}_{\bar{n},\bar{m},\bar{j}}+\mathcal{B}^{(1)}_{n,\bar{m},j}\mathcal{B}^{(1)}_{\bar{n},\bar{m},\bar{j}})\\
&\left.\left.\sin\left(\tfrac{\pi}{2}((-(p)+a_1+\mathcal{S}'_O(3,p_{O_{max}}))-(-(\bar{p}+1)+\bar{a}_1+\bar{\mathcal{S}}'_O(3,\bar{p}_{O_{max}})+1))\right)\right)\right.\\
&\sin(-(j-\bar{j})\theta))
\end{aligned}
$$

$$
\begin{aligned}
&+\left(4(\bar{\mathcal{S}}_O(3,\bar{p}_{O_{max}})-\bar{\mathcal{S}}'_O(3,\bar{p}_{O_{max}})-\bar{\mathcal{S}}''_O(3,\bar{p}_{O_{max}}))+2(\bar{a}_1+\bar{\mathcal{S}}'_O(3,\bar{p}_{O_{max}}))\right.\\
&\left.+\tfrac{N(\bar{j}+\bar{m}-2\bar{t})}{N-\Theta}-\tfrac{N(\bar{j}+\bar{m}+2\bar{n}-2\bar{t})}{N+\Theta}+\tfrac{4(\bar{\mathcal{S}}_E(2,\bar{p}_{E_{max}})-\bar{\mathcal{S}}_O(3,\bar{p}_{O_{max}})+\bar{\mathcal{S}}'_O(3,\bar{p}_{O_{max}}))\Theta}{\Theta^2-r\mu}\right)(-j)\\
&\left(\tfrac{1}{2}\left((\mathcal{A}^{(1)}_{n,\bar{m},j}\mathcal{A}^{(1)}_{\bar{n},\bar{m},\bar{j}}+\mathcal{B}^{(1)}_{n,\bar{m},j}\mathcal{B}^{(1)}_{\bar{n},\bar{m},\bar{j}})\right.\right.\\
&\cos\left(\tfrac{\pi}{2}((-(p)+a_1+\mathcal{S}'_O(3,p_{O_{max}})+1)+(-(\bar{p}+1)+\bar{a}_1+\bar{\mathcal{S}}'_O(3,\bar{p}_{O_{max}})))\right)\\
&+(\mathcal{A}^{(1)}_{\bar{n},\bar{m},\bar{j}}\mathcal{B}^{(1)}_{n,\bar{m},j}-\mathcal{A}^{(1)}_{n,\bar{m},j}\mathcal{B}^{(1)}_{\bar{n},\bar{m},\bar{j}})\\
&\left.\left.\sin\left(\tfrac{\pi}{2}((-(p)+a_1+\mathcal{S}'_O(3,p_{O_{max}})+1)+(-(\bar{p}+1)+\bar{a}_1+\bar{\mathcal{S}}'_O(3,\bar{p}_{O_{max}})))\right)\right)\right.\\
&\cos(-(j-\bar{j})\theta)\\
&+\tfrac{1}{2}\left((\mathcal{A}^{(1)}_{\bar{n},\bar{m},\bar{j}}\mathcal{B}^{(1)}_{n,\bar{m},j}-\mathcal{A}^{(1)}_{n,\bar{m},j}\mathcal{B}^{(1)}_{\bar{n},\bar{m},\bar{j}})\right.\\
&\cos\left(\tfrac{\pi}{2}((-(p)+a_1+\mathcal{S}'_O(3,p_{O_{max}})+1)+(-(\bar{p}+1)+\bar{a}_1+\bar{\mathcal{S}}'_O(3,\bar{p}_{O_{max}})))\right)\\
&-(\mathcal{A}^{(1)}_{n,\bar{m},j}\mathcal{A}^{(1)}_{\bar{n},\bar{m},\bar{j}}+\mathcal{B}^{(1)}_{n,\bar{m},j}\mathcal{B}^{(1)}_{\bar{n},\bar{m},\bar{j}})\\
&\left.\left.\sin\left(\tfrac{\pi}{2}((-(p)+a_1+\mathcal{S}'_O(3,p_{O_{max}})+1)+(-(\bar{p}+1)+\bar{a}_1+\bar{\mathcal{S}}'_O(3,\bar{p}_{O_{max}})))\right)\right)\right.\\
&\sin(-(j-\bar{j})\theta))
\end{aligned}
$$

$$
\begin{aligned}
&-(\bar{m})\left(-\tfrac{1}{N^2-\Theta^2}\left((j+\bar{m}-2t)\Theta+n(-N+\Theta)\right)\right)\\
&\left(\tfrac{1}{2}\left((\mathcal{A}^{(1)}_{n,\bar{m},j}\mathcal{A}^{(1)}_{\bar{n},\bar{m},\bar{j}}+\mathcal{B}^{(1)}_{n,\bar{m},j}\mathcal{B}^{(1)}_{\bar{n},\bar{m},\bar{j}})\right.\right.\\
&\cos\left(\tfrac{\pi}{2}((-(p)+a_1+\mathcal{S}'_O(3,p_{O_{max}}))-(-(\bar{p}+1)+\bar{a}_1+\bar{\mathcal{S}}'_O(3,\bar{p}_{O_{max}})+1))\right)\\
&+(\mathcal{A}^{(1)}_{\bar{n},\bar{m},\bar{j}}\mathcal{B}^{(1)}_{n,\bar{m},j}-\mathcal{A}^{(1)}_{n,\bar{m},j}\mathcal{B}^{(1)}_{\bar{n},\bar{m},\bar{j}})\\
&\left.\left.\sin\left(\tfrac{\pi}{2}((-(p)+a_1+\mathcal{S}'_O(3,p_{O_{max}}))-(-(\bar{p}+1)+\bar{a}_1+\bar{\mathcal{S}}'_O(3,\bar{p}_{O_{max}})+1))\right)\right)\right.\\
&\cos(-(j-\bar{j})\theta)\\
&+\tfrac{1}{2}\left((\mathcal{A}^{(1)}_{\bar{n},\bar{m},\bar{j}}\mathcal{B}^{(1)}_{n,\bar{m},j}-\mathcal{A}^{(1)}_{n,\bar{m},j}\mathcal{B}^{(1)}_{\bar{n},\bar{m},\bar{j}})\right.\\
&\cos\left(\tfrac{\pi}{2}((-(p)+a_1+\mathcal{S}'_O(3,p_{O_{max}}))-(-(\bar{p}+1)+\bar{a}_1+\bar{\mathcal{S}}'_O(3,\bar{p}_{O_{max}})+1))\right)\\
&-(\mathcal{A}^{(1)}_{n,\bar{m},j}\mathcal{A}^{(1)}_{\bar{n},\bar{m},\bar{j}}+\mathcal{B}^{(1)}_{n,\bar{m},j}\mathcal{B}^{(1)}_{\bar{n},\bar{m},\bar{j}})\\
&\left.\left.\sin\left(\tfrac{\pi}{2}((-(p)+a_1+\mathcal{S}'_O(3,p_{O_{max}}))-(-(\bar{p}+1)+\bar{a}_1+\bar{\mathcal{S}}'_O(3,\bar{p}_{O_{max}})+1))\right)\right)\right.\\
&\sin(-(j-\bar{j})\theta))
\end{aligned}
$$

$$
\begin{aligned}
&+\left(-\tfrac{1}{N^2-\Theta^2}\left((\bar{j}+\bar{m}-2\bar{t})\Theta+\bar{n}(-N+\Theta)\right)\right)(\bar{m})\\
&\left(\tfrac{1}{2}\left((\mathcal{A}^{(1)}_{n,\bar{m},j}\mathcal{A}^{(1)}_{\bar{n},\bar{m},\bar{j}}+\mathcal{B}^{(1)}_{n,\bar{m},j}\mathcal{B}^{(1)}_{\bar{n},\bar{m},\bar{j}})\right.\right.\\
&\cos\left(\tfrac{\pi}{2}((-(p)+a_1+\mathcal{S}'_O(3,p_{O_{max}})+1)+(-(\bar{p}+1)+\bar{a}_1+\bar{\mathcal{S}}'_O(3,\bar{p}_{O_{max}})))\right)\\
&+(\mathcal{A}^{(1)}_{\bar{n},\bar{m},\bar{j}}\mathcal{B}^{(1)}_{n,\bar{m},j}-\mathcal{A}^{(1)}_{n,\bar{m},j}\mathcal{B}^{(1)}_{\bar{n},\bar{m},\bar{j}})\\
&\left.\left.\sin\left(\tfrac{\pi}{2}((-(p)+a_1+\mathcal{S}'_O(3,p_{O_{max}})+1)+(-(\bar{p}+1)+\bar{a}_1+\bar{\mathcal{S}}'_O(3,\bar{p}_{O_{max}})))\right)\right)\right.\\
&\cos(-(j-\bar{j})\theta)\\
&+\tfrac{1}{2}\left((\mathcal{A}^{(1)}_{\bar{n},\bar{m},\bar{j}}\mathcal{B}^{(1)}_{n,\bar{m},j}-\mathcal{A}^{(1)}_{n,\bar{m},j}\mathcal{B}^{(1)}_{\bar{n},\bar{m},\bar{j}})\right.\\
&\cos\left(\tfrac{\pi}{2}((-(p)+a_1+\mathcal{S}'_O(3,p_{O_{max}})+1)+(-(\bar{p}+1)+\bar{a}_1+\bar{\mathcal{S}}'_O(3,\bar{p}_{O_{max}})))\right)\\
&-(\mathcal{A}^{(1)}_{n,\bar{m},j}\mathcal{A}^{(1)}_{\bar{n},\bar{m},\bar{j}}+\mathcal{B}^{(1)}_{n,\bar{m},j}\mathcal{B}^{(1)}_{\bar{n},\bar{m},\bar{j}})\\
&\left.\left.\sin\left(\tfrac{\pi}{2}((-(p)+a_1+\mathcal{S}'_O(3,p_{O_{max}})+1)+(-(\bar{p}+1)+\bar{a}_1+\bar{\mathcal{S}}'_O(3,\bar{p}_{O_{max}})))\right)\right)\right.\\
&\sin(-(j-\bar{j})\theta)))
\end{aligned}
\tag{6.18}
$$

where in $\mathcal{D}$, $\mathcal{O}$ and $\mathcal{E}$ the parameter m must be substituted by $\bar{m}$.

Appendix C

The un-normalized spherical harmonic coefficients of 624-Hektor are here listed.
This coefficients have been obtained following the procedure described in [76] from the 1022 vertices 3D model of 624-Hektor represented in Fig. 4.1 and found on the DAMIT-Database of Asteroid Models from Inversion Techniques.

$C_{0,0}$	1
$C_{1,0}$	2.33217×10^{-8}
$C_{1,1}$	-5.65245×10^{-9}
$C_{2,0}$	-0.12464
$C_{2,1}$	0.00304843
$C_{2,2}$	0.04981
$C_{3,0}$	0.00102426
$C_{3,1}$	-0.00116095
$C_{3,2}$	0.000631592
$C_{3,3}$	0.0000250782
$C_{4,0}$	0.0400541
$C_{4,1}$	-0.000166485
$C_{4,2}$	-0.00381943
$C_{4,3}$	0.0000443294
$C_{4,4}$	0.00031861
$C_{5,0}$	-0.000329525
$C_{5,1}$	0.000632048
$C_{5,2}$	-0.0000697135
$C_{5,3}$	-2.77318×10^{-7}
$C_{5,4}$	8.72067×10^{-6}
$C_{5,5}$	-2.40029×10^{-6}
$C_{6,0}$	-0.0168482
$C_{6,1}$	-0.000136802
$C_{6,2}$	0.000743635
$C_{6,3}$	-3.08661×10^{-6}
$C_{6,4}$	-0.000017396
$C_{6,5}$	4.21979×10^{-7}
$C_{6,6}$	9.05311×10^{-7}
$C_{7,0}$	0.000297055
$C_{7,1}$	-0.000304151
$C_{7,2}$	0.0000102168
$C_{7,3}$	2.96129×10^{-7}
$C_{7,4}$	-9.86927×10^{-7}
$C_{7,5}$	1.95817×10^{-7}
$C_{7,6}$	4.09629×10^{-8}
$C_{7,7}$	-1.98738×10^{-8}
$C_{8,0}$	0.00791898
$C_{8,1}$	0.000133685
$C_{8,2}$	-0.000201374
$C_{8,3}$	-7.42295×10^{-8}
$C_{8,4}$	2.38859×10^{-6}
$C_{8,5}$	-3.97459×10^{-8}
$C_{8,6}$	-3.57829×10^{-8}
$C_{8,7}$	1.709×10^{-9}
$C_{8,8}$	1.76265×10^{-9}
$C_{9,0}$	-0.000322245
$C_{9,1}$	0.000137372
$C_{9,2}$	1.04867×10^{-7}
$C_{9,3}$	-1.53402×10^{-8}
$C_{9,4}$	1.70052×10^{-7}
$C_{9,5}$	-3.13028×10^{-8}
$C_{9,6}$	-4.09551×10^{-9}
$C_{9,7}$	1.06157×10^{-9}
$C_{9,8}$	9.09409×10^{-11}
$C_{9,9}$	-5.2564×10^{-11}
$C_{10,0}$	-0.00389284
$C_{10,1}$	-0.0000890129
$C_{10,2}$	0.0000641703
$C_{10,3}$	2.22255×10^{-7}
$C_{10,4}$	-4.63008×10^{-7}
$C_{10,5}$	5.78004×10^{-9}
$C_{10,6}$	3.50487×10^{-9}
$C_{10,7}$	-1.41563×10^{-10}
$C_{10,8}$	-4.90193×10^{-11}
$C_{10,9}$	3.30995×10^{-12}
$C_{10,10}$	3.07354×10^{-12}

Table 6.1: 624-Hektor,Spherical Harmonics coefficients: $C_{n,m}$

$S_{0,0}$	0
$S_{1,0}$	0
$S_{1,1}$	-3.75818×10^{-2}
$S_{2,0}$	0
$S_{2,1}$	2.44174×10^{-3}
$S_{2,2}$	2.47263×10^{-2}
$S_{3,0}$	0
$S_{3,1}$	-1.61779×10^{-3}
$S_{3,2}$	2.44957×10^{-4}
$S_{3,3}$	1.27032×10^{-4}
$S_{4,0}$	0
$S_{4,1}$	-4.37887×10^{-4}
$S_{4,2}$	1.87272×10^{-3}
$S_{4,3}$	3.92078×10^{-5}
$S_{4,4}$	1.51864×10^{-4}
$S_{5,0}$	0
$S_{5,1}$	4.67568×10^{-4}
$S_{5,2}$	-2.27241×10^{-5}
$S_{5,3}$	-2.94281×10^{-6}
$S_{5,4}$	2.39711×10^{-6}
$S_{5,5}$	-1.13629×10^{-6}
$S_{6,0}$	0
$S_{6,1}$	8.02977×10^{-5}
$S_{6,2}$	3.61996×10^{-4}
$S_{6,3}$	-4.21205×10^{-6}
$S_{6,4}$	-8.14515×10^{-6}
$S_{6,5}$	2.18522×10^{-7}
$S_{6,6}$	4.09279×10^{-7}
$S_{7,0}$	0
$S_{7,1}$	-1.79721×10^{-4}
$S_{7,2}$	9.51647×10^{-7}
$S_{7,3}$	1.15513×10^{-7}
$S_{7,4}$	-2.35444×10^{-7}
$S_{7,5}$	1.2149×10^{-7}
$S_{7,6}$	7.08749×10^{-9}
$S_{7,7}$	-1.26457×10^{-8}
$S_{8,0}$	0
$S_{8,1}$	1.56517×10^{-6}
$S_{8,2}$	-9.9021×10^{-5}
$S_{8,3}$	5.70613×10^{-7}
$S_{8,4}$	1.1143×10^{-6}
$S_{8,5}$	-2.06789×10^{-8}
$S_{8,6}$	-1.52099×10^{-8}
$S_{8,7}$	5.73623×10^{-10}
$S_{8,8}$	7.41676×10^{-10}
$S_{9,0}$	0
$S_{9,1}$	8.23674×10^{-5}
$S_{9,2}$	1.74015×10^{-6}
$S_{9,3}$	9.50787×10^{-9}
$S_{9,4}$	2.95314×10^{-8}
$S_{9,5}$	-2.01586×10^{-8}
$S_{9,6}$	-5.53021×10^{-10}
$S_{9,7}$	7.00849×10^{-10}
$S_{9,8}$	6.69884×10^{-12}
$S_{9,9}$	-3.68673×10^{-11}
$S_{10,0}$	0
$S_{10,1}$	-1.228×10^{-5}
$S_{10,2}$	3.28695×10^{-5}
$S_{10,3}$	-5.79763×10^{-8}
$S_{10,4}$	-2.2292×10^{-7}
$S_{10,5}$	2.68899×10^{-9}
$S_{10,6}$	1.43408×10^{-9}
$S_{10,7}$	-4.5155×10^{-11}
$S_{10,8}$	-1.74772×10^{-11}
$S_{10,9}$	8.34705×10^{-13}
$S_{10,10}$	1.27466×10^{-12}

Table 6.2: 624-Hektor,Spherical Harmonics coefficients: $S_{n,m}$

Appendix D

The equilibrium points $M_j, \quad j = 1, ..., 8$ are defined at the three intersect of the surfaces that satisfy the equations of (5.1). As the third equation is clearly satisfied by the plane $z = 0$, the equilibrium points $M_j, \quad j = 1, ..., 8$, are bounded to stay on the $z = 0$ plane, which, equivalently, can be seen as the degeneration of system (5.1) into a two dimensional system, once the solution of the third equation, namely $z = 0$, is substituted in. Such system is qualitatively the same treated in [19] whose solution is shown by Figure 6.1. In particular the light, continuous curve in the figure represents the solution of the first equation of system (5.1), the dark, dashed line shows the solution of the second equation of the system and the third equation is clearly satisfied by the plane $z = 0$, plotted in all the Figure as well.

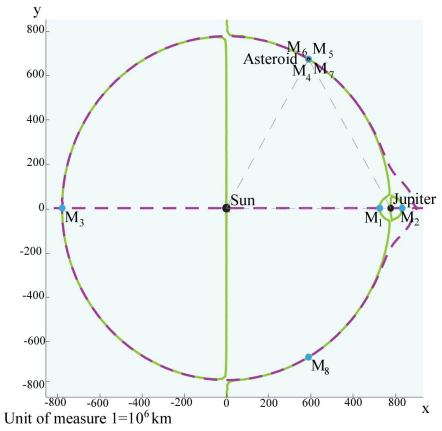

Figure 6.1: Equilibrium points; *Intersection with the plane* $z = 0$

Appendix E

Let be $\lambda, \lambda^*; \nu, \nu^*; \varphi, \varphi^* \in \mathbb{C}$ the eigenvalues of the system (5.30) and $\bar{\mathbf{f}}_j = \bar{\mathbf{u}}_j + i\bar{\mathbf{w}}_j \in \mathbb{R}^6, \quad j = 1, ..., 6$ the respective eigenvectors.

Since $\{\bar{\mathbf{u}}_1, \bar{\mathbf{w}}_1, \bar{\mathbf{u}}_3, \bar{\mathbf{w}}_3, \bar{\mathbf{u}}_5, \bar{\mathbf{w}}_5\}$ is a base of $\mathbb{R}^6$, then $\forall s \in \mathbb{R}^6$ there exist $s_1, ..., s_6 \in \mathbb{R}$ such that $s = s_1\bar{\mathbf{u}}_1 + s_2\bar{\mathbf{w}}_1 + s_3\bar{\mathbf{u}}_3 + s_4\bar{\mathbf{w}}_3 + s_5\bar{\mathbf{u}}_5 + s_6\bar{\mathbf{w}}_5$.

$$\mathcal{A}' \begin{pmatrix} s_1 \\ s_2 \\ s_3 \\ s_4 \\ s_5 \\ s_6 \end{pmatrix} = ... = s_1 \begin{pmatrix} \mathcal{A}'_{1,1} \\ \mathcal{A}'_{2,1} \\ \mathcal{A}'_{3,1} \\ \mathcal{A}'_{4,1} \\ \mathcal{A}'_{5,1} \\ \mathcal{A}'_{6,1} \end{pmatrix} + ... + s_6 \begin{pmatrix} \mathcal{A}'_{1,6} \\ \mathcal{A}'_{2,6} \\ \mathcal{A}'_{3,6} \\ \mathcal{A}'_{4,6} \\ \mathcal{A}'_{5,6} \\ \mathcal{A}'_{6,6} \end{pmatrix} \tag{6.19}$$

Then, of course, being the $\bar{\mathcal{A}}$ and $\mathcal{A}'$ the expression of the same system in two different coordinates, and being $\mathcal{N}$ the matrix of the change of coordinates, yields that (6.19) is also equal to:

$$\begin{aligned} &\bar{\mathcal{A}} \begin{pmatrix} s_1\mathcal{N}_{1,1} + s_2\mathcal{N}_{2,1} + s_3\mathcal{N}_{3,1} + s_4\mathcal{N}_{4,1} + s_5\mathcal{N}_{5,1} + s_6\mathcal{N}_{6,1} \\ s_1\mathcal{N}_{1,2} + s_2\mathcal{N}_{2,2} + s_3\mathcal{N}_{3,2} + s_4\mathcal{N}_{4,2} + s_5\mathcal{N}_{5,2} + s_6\mathcal{N}_{6,2} \\ s_1\mathcal{N}_{1,3} + s_2\mathcal{N}_{2,3} + s_3\mathcal{N}_{3,3} + s_4\mathcal{N}_{4,3} + s_5\mathcal{N}_{5,3} + s_6\mathcal{N}_{6,3} \\ s_1\mathcal{N}_{1,4} + s_2\mathcal{N}_{2,4} + s_3\mathcal{N}_{3,4} + s_4\mathcal{N}_{4,4} + s_5\mathcal{N}_{5,4} + s_6\mathcal{N}_{6,4} \\ s_1\mathcal{N}_{1,5} + s_2\mathcal{N}_{2,5} + s_3\mathcal{N}_{3,5} + s_4\mathcal{N}_{4,5} + s_5\mathcal{N}_{5,5} + s_6\mathcal{N}_{6,5} \\ s_1\mathcal{N}_{1,6} + s_2\mathcal{N}_{2,6} + s_3\mathcal{N}_{3,6} + s_4\mathcal{N}_{4,6} + s_5\mathcal{N}_{5,6} + s_6\mathcal{N}_{6,6} \end{pmatrix} \\ &= s_1\bar{\mathcal{A}} \begin{pmatrix} \mathcal{N}_{1,1} \\ \mathcal{N}_{2,1} \\ \mathcal{N}_{3,1} \\ \mathcal{N}_{5,1} \\ \mathcal{N}_{6,1} \end{pmatrix} + ... + s_6\bar{\mathcal{A}} \begin{pmatrix} \mathcal{N}_{1,6} \\ \mathcal{N}_{2,6} \\ \mathcal{N}_{3,6} \\ \mathcal{N}_{4,6} \\ \mathcal{N}_{5,6} \\ \mathcal{N}_{6,6} \end{pmatrix} \\ &= s_1 \begin{pmatrix} \bar{\mathcal{A}}(\bar{\mathbf{u}}_1)/_{\bar{\mathbf{u}}_1} \\ \bar{\mathcal{A}}(\bar{\mathbf{u}}_1)/_{\bar{\mathbf{w}}_1} \\ \bar{\mathcal{A}}(\bar{\mathbf{u}}_1)/_{\bar{\mathbf{u}}_3} \\ \bar{\mathcal{A}}(\bar{\mathbf{u}}_1)/_{\bar{\mathbf{w}}_3} \\ \bar{\mathcal{A}}(\bar{\mathbf{u}}_1)/_{\bar{\mathbf{u}}_5} \\ \bar{\mathcal{A}}(\bar{\mathbf{u}}_1)/_{\bar{\mathbf{w}}_5} \end{pmatrix} + ... + s_6 \begin{pmatrix} \bar{\mathcal{A}}(\bar{\mathbf{w}}_5)/_{\bar{\mathbf{u}}_1} \\ \bar{\mathcal{A}}(\bar{\mathbf{w}}_5)/_{\bar{\mathbf{w}}_1} \\ \bar{\mathcal{A}}(\bar{\mathbf{w}}_5)/_{\bar{\mathbf{u}}_3} \\ \bar{\mathcal{A}}(\bar{\mathbf{w}}_5)/_{\bar{\mathbf{w}}_3} \\ \bar{\mathcal{A}}(\bar{\mathbf{w}}_5)/_{\bar{\mathbf{u}}_5} \\ \bar{\mathcal{A}}(\bar{\mathbf{w}}_5)/_{\bar{\mathbf{w}}_5} \end{pmatrix} \end{aligned} \tag{6.20}$$

Where, with / it is indicated the projection, e.g. $\bar{\mathcal{A}}(\bar{\mathbf{u}}_1)/_{\bar{\mathbf{u}}_1}$ means the component of $\bar{\mathbf{u}}\bar{\mathcal{A}}(\bar{\mathbf{u}}_1)$ in the $\bar{\mathbf{u}}_1$ direction.

Equating (6.19) and (6.20) it is found that, being $\mathcal{A}' = \left(\mathcal{A}'_{j,k}\right)_{\substack{j=1,\ldots,6\\k=1,\ldots,6}}$,

$$\mathcal{A}'_{j,k} = \begin{cases} \bar{\mathcal{A}}(\bar{\mathbf{u}}_k)/_{\bar{\mathbf{u}}_j} \;\; if \;\; k,j \;\; odd \\ \bar{\mathcal{A}}(\bar{\mathbf{w}}_{k-1}/_{\bar{\mathbf{u}}_j} \;\; if \;\; k \;\; even, \; j \;\; odd \\ \bar{\mathcal{A}}(\bar{\mathbf{u}}_k)/_{\bar{\mathbf{w}}_{j-1}} \;\; if \;\; j \;\; even, \; k \;\; odd \\ \bar{\mathcal{A}}(\bar{\mathbf{w}}_{k-1})/_{\bar{\mathbf{w}}_{j-1}} \;\; if \;\; k,j \;\; even \end{cases} \tag{6.21}$$

Now, given $\bar{\mathcal{A}} \in \mathcal{L}(\mathbb{R}^6)$, let us define $\bar{\mathcal{A}}_{\mathbb{C}}$ as the "complexification" of $\bar{\mathcal{A}}$, namely, $\bar{\mathcal{A}}_{\mathbb{C}} \in \mathcal{L}(\mathbb{C}^6)$ such that $\forall \bar{\mathbf{f}} = \bar{\mathbf{u}} + i\bar{\mathbf{w}} \in \mathbb{C}^6, \;\; \bar{\mathbf{u}}, \;\; \bar{\mathbf{w}} \in \mathbb{R}^6$, $\bar{\mathcal{A}}_{\mathbb{C}}(\bar{\mathbf{f}}) := \bar{\mathcal{A}}(\bar{\mathbf{u}}) + i\bar{\mathcal{A}}(\bar{\mathbf{w}})$. Then, taking $\bar{\mathcal{A}}$ as in (5.30) and the first eigenvector $\bar{\mathbf{f}}_1 \in \mathbb{C}^6$ yields:

$$\bar{\mathcal{A}}_{\mathbb{C}}(\bar{\mathbf{f}}_1) = \bar{\mathcal{A}}(\bar{\mathbf{u}}_1) + i\bar{\mathcal{A}}(\bar{\mathbf{w}}_1) \tag{6.22}$$

But, since $\bar{\mathbf{f}}_1$ is an eigenvector of $\bar{\mathcal{A}}$, it is also true that:

$$\bar{\mathcal{A}}_{\mathbb{C}}(\bar{\mathbf{f}}_1) = \lambda\bar{\mathbf{f}}_1 = (\lambda_R + i\lambda_I)(\bar{\mathbf{u}}_1 + i\bar{\mathbf{w}}_1) = (\lambda_R\bar{\mathbf{u}}_1 - \lambda_I\bar{\mathbf{w}}_1) + i(\lambda_I\bar{\mathbf{u}}_1 + \lambda_R\bar{\mathbf{w}}_1) \tag{6.23}$$

Equaling the Real and Imaginary parts of (6.22) and (6.23) yields:

$$\begin{aligned} \bar{\mathcal{A}}(\bar{\mathbf{u}}_1) &= \lambda_R\bar{\mathbf{u}}_1 - \lambda_I\bar{\mathbf{w}}_1 \\ \bar{\mathcal{A}}(\bar{\mathbf{w}}_1) &= \lambda_R\bar{\mathbf{w}}_1 + \lambda_I\bar{\mathbf{u}}_1 \end{aligned} \tag{6.24}$$

Repeating the analogous procedure for the other eigenvectors it is finally found that:

$$\mathcal{A}' = \begin{pmatrix} \lambda_R & \lambda_I & 0 & 0 & 0 & 0 \\ -\lambda_I & \lambda_R & 0 & 0 & 0 & 0 \\ 0 & 0 & \nu_R & \nu_I & 0 & 0 \\ 0 & 0 & -\nu_I & \nu_R & 0 & 0 \\ 0 & 0 & 0 & 0 & \varphi_R & \varphi_I \\ 0 & 0 & 0 & 0 & -\varphi_I & \varphi_R \end{pmatrix} \tag{6.25}$$

Then, in this basis, the system takes the form

$$\dot{\beth}(t) = \mathcal{A}'\beth(t) \tag{6.26}$$

with $\beth(t_0) = [\xi_1^0(t), \xi_2^0(t), \psi_1^0(t), \psi_2^0(t), \zeta_1^0(t), \zeta_2^0(t)]^T$. This system is solved by

$$\beth(t) = \beth(t_0)e^{\mathcal{A}'t} \tag{6.27}$$

For the well known property of the exponential of a matrix[12] it is found that if $\mathcal{A}'$ is

[21] This property is straight forward from direct calculations once the basis in which the matrix of

as in (6.25) then $\mathcal{S} = e^{\mathcal{A}'t}$ is a block matrix (6×6) such that:

$$\mathcal{S} = e^{\mathcal{A}'t} = \begin{pmatrix} \mathcal{S}_1 & 0 & 0 \\ 0 & \mathcal{S}_2 & 0 \\ 0 & 0 & \mathcal{S}_3 \end{pmatrix} \tag{6.28}$$

with

$$\begin{aligned} \mathcal{S}_1 &= \begin{pmatrix} e^{\lambda_R t}\cos(\lambda_I t) & -e^{\lambda_R t}\sin(\lambda_I t) \\ e^{\lambda_R t}\cos(\nu_I t) & e^{\lambda_R t}\sin(\lambda_I t) \end{pmatrix} \\ \mathcal{S}_2 &= \begin{pmatrix} e^{\nu_R t}\cos(\nu_I t) & -e^{\nu_R t}\sin(\nu_I t) \\ e^{\nu_R t}\cos(\nu_I t) & e^{\nu_R t}\sin(\nu_I t) \end{pmatrix} \\ \mathcal{S}_3 &= \begin{pmatrix} e^{\varphi_R t}\cos(\varphi_I t) & -e^{\varphi_R t}\sin(\varphi_I t) \\ e^{\varphi_R t}\cos(\varphi_I t) & e^{\varphi_R t}\sin(\varphi_I t) \end{pmatrix} \end{aligned} \tag{6.29}$$

that is exactly the one in (5.32).
Finally, for how the solution has been derived, it is clear that $\mathtt{x}(t) = \mathcal{M}\beth(t)$.

the system $\mathcal{A}$ is diagonal (but with complex coefficients) is known.

Appendix F

$$\bar{u}_{1,1} = 1$$
$$\bar{w}_{1,1} = 0$$
$$\bar{u}_{1,2} = \frac{\gamma\chi-\delta\phi+\chi\lambda^2}{-\beta\gamma+\phi^2-\beta\lambda^2-\gamma\lambda^2-\lambda^4}$$
$$\bar{w}_{1,2} = \frac{-2\lambda^3-2\gamma\lambda}{-\beta\gamma+\phi^2-\beta\lambda^2-\gamma\lambda^2-\lambda^4}$$
$$\bar{u}_{1,3} = \frac{\beta\delta-\chi\phi+\delta\lambda^2}{-\beta\gamma+\phi^2-\beta\lambda^2-\gamma\lambda^2-\lambda^4}$$
$$\bar{w}_{1,3} = \frac{2\phi\lambda}{-\beta\delta\gamma+\phi^2-\beta\delta\lambda^2-\gamma\lambda^2-\lambda^4}$$
$$\bar{u}_{1,4} = -\left(\frac{\gamma\chi-\delta\phi+\chi\lambda^2}{-\beta\gamma+\phi^2-\beta\lambda^2-\gamma\lambda^2-\lambda^4}\right)$$
$$\bar{w}_{1,4} = -\left(\frac{-2\lambda^3-2\gamma\lambda}{-\beta\gamma+\phi^2-\beta\lambda^2-\gamma\Lambda^2-\lambda^4}\right)+\lambda$$
$$\bar{u}_{1,5} = 1-\lambda\ \bar{w}_{1,2}$$
$$\bar{w}_{1,5} = \lambda\ \bar{u}_{1,2}$$
$$\bar{u}_{1,6} = -\lambda\ \bar{w}_{1,3}$$
$$\bar{w}_{1,6} = \lambda\ \bar{u}_{1,3}$$

$$\bar{u}_{3,1} = 1$$
$$\bar{w}_{3,1} = 0$$
$$\bar{u}_{3,2} = \frac{-\alpha\gamma^2\chi+\gamma\chi\delta^2+\alpha\gamma\delta\phi-\delta^3\phi+(-2\alpha\gamma\chi-\gamma^2\chi+\chi\delta^2+\alpha\delta\phi+\gamma\delta\phi)\nu^2+(-\alpha\chi-2\gamma\chi+\delta\phi)\nu^4-\chi\nu^6}{\gamma^2\chi^2-2\gamma\chi\delta\phi+\delta^2\phi^2+(4\gamma^2+2\gamma\chi^2-2\chi\delta\phi)\nu^2+(8\gamma+\chi^2)\nu^4+4\nu^6}$$
$$\bar{w}_{3,2} = \frac{(2\alpha\gamma^2-2\gamma\delta^2)\nu+(4\alpha\gamma+2\gamma^2-2\delta^2)\nu^3+(2\alpha+4\gamma)\nu^5+2\nu^7}{\gamma^2\chi^2-2\gamma\chi\delta\phi+\delta^2\phi^2+(4\gamma^2+2\gamma\chi^2-2\chi\delta\phi)\nu^2+(8\gamma+\chi^2)\nu^4+4\nu^6}$$
$$\bar{u}_{3,3} = \frac{-\gamma\chi^2\delta+\alpha\gamma\chi\phi+\chi\delta^2\phi-\alpha\delta\phi^2+(-4\gamma\delta-\chi^2\delta+\alpha\chi\phi+\gamma\chi\phi-\delta\phi^2)\nu^2+(-4\delta+\chi\phi)\nu^4}{\gamma^2\chi^2-2\gamma\chi\delta\phi+\delta^2\phi^2+(4\gamma^2+2\gamma\chi^2-2\chi\delta\phi)\nu^2+(8\gamma+\chi^2)\nu^4+4\nu^6}$$
$$\bar{w}_{3,3} = \frac{(-2\alpha\gamma\phi+2\delta^2\phi)\nu+(-2\alpha\phi-2\gamma\phi)\nu^3-2\phi\nu^5}{\gamma^2\chi^2-2\gamma\chi\delta\phi+\delta^2\phi^2+(4\gamma^2+2\gamma\chi^2-2\chi\delta\phi)\nu^2+(8\gamma+\chi^2)\nu^4+4\nu^6}$$
$$\bar{u}_{3,4} = -\left(\frac{-\alpha\gamma^2\chi+\gamma\chi\delta^2+\alpha\gamma\delta\phi-\delta^3\phi+(-2\alpha\gamma\chi-\gamma^2\chi+\chi\delta^2+\alpha\delta\phi+\gamma\delta\phi)\nu^2+(-\alpha\chi-2\gamma\chi+\delta\phi)\nu^4-\chi\nu^6}{\gamma^2\chi^2-2\gamma\chi\delta\phi+\delta^2\phi^2+(4\gamma^2+2\gamma\chi^2-2\chi\delta\phi)\nu^2+(8\gamma+\chi^2)\nu^4+4\nu^6}\right)$$
$$\bar{w}_{3,4} = -\left(\frac{(2\alpha\gamma^2-2\gamma\delta^2)\nu+(4\alpha\gamma+2\gamma^2-2\delta^2)\nu^3+(2\alpha+4\gamma)\nu^5+2\nu^7}{\gamma^2\chi^2-2\gamma\chi\delta\phi+\delta^2\phi^2+(4\gamma^2+2\gamma\chi^2-2\chi\delta\phi)\nu^2+(8\gamma+\chi^2)\nu^4+4\nu^6}\right)+\nu$$
$$\bar{u}_{3,5} = 1-\nu\ \bar{w}_{3,2}$$
$$\bar{w}_{3,5} = \nu\ \bar{u}_{3,2}$$
$$\bar{u}_{3,6} = -\nu\ \bar{w}_{3,3}$$
$$\bar{w}_{3,6} = \nu\ \bar{u}_{3,3}$$

$$\bar{u}_{5,1} = 1$$
$$\bar{w}_{5,1} = 0$$
$$\bar{u}_{5,2} = \frac{(-\beta\chi\delta^2+\alpha\beta\delta\phi+\chi^2\delta\phi-\alpha\chi\phi^2+(-\chi\delta^2-4\delta\phi+\alpha\delta\phi+\beta\delta\phi-\chi\phi^2)\varphi^2+\delta\phi\varphi^4)}{\beta^2\delta^2-2\beta\chi\delta\phi+\chi^2\phi^2+(2\beta\delta^2-2\chi\delta\phi+4\phi^2)\varphi^2+\delta^2\varphi^4}$$
$$\bar{w}_{5,2} = \frac{(2\beta\delta^2-4\chi\delta\phi+2\alpha\phi^2)\varphi+(2\delta^2+2\phi^2)\varphi^3}{\beta^2\delta^2-2\beta\chi\delta\phi+\chi^2\phi^2+(2\beta\delta^2-2\chi\delta\phi+4\phi^2)\varphi^2+\delta^2\varphi^4}$$
$$\bar{u}_{5,3} = \frac{-\alpha\beta^2\delta+\beta\delta\chi^2+\alpha\beta\chi\phi-\chi^3\phi+(4\beta\delta-2\alpha\beta\delta-\beta^2\delta+\chi^2\delta-4\chi\phi+\alpha\chi\phi+\beta\chi\phi)\varphi^2}{\beta^2\delta^2-2\beta\chi\delta\phi+\chi^2\phi^2+(2\beta\delta^2-2\chi\delta\phi+4\phi^2)\varphi^2+\delta^2\varphi^4}$$
$$+\frac{(4\delta-\alpha\delta-2\beta\delta+\chi\phi)\varphi^4-\delta\varphi^6}{\beta^2\delta^2-2\beta\chi\delta\phi+\chi^2\phi^2+(2\beta\delta^2-2\chi\delta\phi+4\phi^2)\varphi^2+\delta^2\varphi^4}$$
$$\bar{w}_{5,3} = \frac{(-2\alpha\beta\phi+2\chi^2\phi)\varphi+(8\phi-2\alpha\phi-2\beta\phi)\varphi^3-2\phi\varphi^5}{\beta^2\delta^2-2\beta\chi\delta\phi+\chi^2\phi^2+(2\beta\delta^2-2\chi\delta\phi+4\phi^2)\varphi^2+\delta^2\varphi^4}$$
$$\bar{u}_{5,4} = -\left(\frac{(-\beta\chi\delta^2+\alpha\beta\delta\phi+\chi^2\delta\phi-\alpha\chi\phi^2+(-\chi\delta^2-4\delta\phi+\alpha\delta\phi+\beta\delta\phi-\chi\phi^2)\varphi^2+\delta\phi\varphi^4)}{\beta^2\delta^2-2\beta\chi\delta\phi+\chi^2\phi^2+(2\beta\delta^2-2\chi\delta\phi+4\phi^2)\varphi^2+\delta^2\varphi^4}\right)$$
$$\bar{w}_{5,4} = -\left(\frac{(2\beta\delta^2-4\chi\delta\phi+2\alpha\phi^2)\varphi+(2\delta^2+2\phi^2)\varphi^3}{\beta^2\delta^2-2\beta\chi\delta\phi+\chi^2\phi^2+(2\beta\delta^2-2\chi\delta\phi+4\phi^2)\varphi^2+\delta^2\varphi^4}\right)+\varphi$$
$$\bar{u}_{5,5} = 1-\varphi\ \bar{w}_{5,2}$$
$$\bar{w}_{5,5} = \varphi\ \bar{u}_{5,2}$$
$$\bar{u}_{5,6} = -\varphi\ \bar{w}_{5,3}$$
$$\bar{w}_{5,6} = \varphi\ \bar{u}_{5,3}$$